



**EJBCS**

**Eurasian Journal of  
Biological and Chemical Sciences  
(Eurasian J. Bio. Chem. Sci.)**

*Cilt: 7    Volume: 2    Year: 2024*

***e-ISSN 2651-5237***



# EJBCS

Eurasian Journal of Biological and Chemical Sciences

**Cilt: 7    Volume: 2    Year: 2024**

**Published Biannually**

### Corresponding Address

Gaziantep University, Faculty of Arts and Sciences, Department of Biology, Gaziantep, Turkey

E-mail: mtdogan1@gmail.com

Web: <https://www.dergipark.org.tr/ejbc>

### Editor in Chief

Prof. Dr. Muhittin DOĞAN

### Editor (Associate)

Assoc. Prof. Dr. Muhammet DOĞAN

### Editorial Board

Prof. Dr. Ali Tuncay ÖZYILMAZ	Hatay Mustafa Kemal University, Turkey
Prof. Dr. Anna PEKSA	Wrocław University, Poland
Prof. Dr. Elif LOLOĞLU	Gazi University, Turkey
Prof. Dr. Elif ÖZTETİK	Eskisehir Technical University, Turkey
Prof. Dr. Erol ATAY	Hatay Mustafa Kemal University, Turkey
Prof. Dr. Hacı Ahmet DEVECİ	Gaziantep University, Turkey
Prof. Dr. Hikmet GEÇKİL	İnönü University, Turkey
Prof. Dr. Issa SHARİFPOUR	Iranian Fisheries Research Organization, Iran
Prof. Dr. İsmet YILMAZ	İnönü University, Turkey
Prof. Dr. Osman GÜLNAZ	Cukurova University, Turkey
Prof. Dr. Osman Selçuk ALDEMİR	Adnan Menderes University, Turkey
Prof. Dr. Vladimer TSITSISHVILI	Ivane Javakhishvili Tbilisi State University, Georgia
Prof. Dr. Zeliha SELAMOĞLU	Niğde Ömer Halisdemir University, Turkey
Assoc. Prof. Dr. Demet DOĞAN	Gaziantep University, Turkey
Assoc. Prof. Dr. Gökhan NUR	Gaziantep University, Turkey
Assoc. Prof. Dr. Şenay UĞUR	Niğde Ömer Halisdemir University, Turkey
Assoc. Prof. Dr. Utku AVCI	Recep Tayyip Erdoğan University, Turkey
Assoc. Prof. Dr. Mustafa PEHLİVAN	Gaziantep University, Turkey
Dr. Ardalan PASDARAN	Shiraz University, Iran.
Dr. Eva URGEOVÁ	The University of St. Cyril and Methodius of Trnava, Slovakia

### Technical Editor

Assoc. Prof. Dr. Mustafa SEVİNDİK	Osmaniye Korkut Ata University, Turkey
-----------------------------------	--

Owner / Publisher

Muhammet DOĞAN

This journal is peer-reviewed and published twice (June, December) a year.

All responsibility of the articles belongs to the authors.

**e-ISSN 2651-5237**



# EJBCS

Eurasian Journal of Biological and Chemical Sciences

Cilt: 7      Volume: 2      Year: 2024

## Contents / İçindekiler

### Research Articles / Araştırma Makeleleri

**Development of a dynamic multiple reaction monitoring LC-APCI-MS/MS method for quantification of ten nitrosamines in ranitidine API with simple extraction approach ..... 66-75**

*Murat Emrah Maviş , Neşe Ular Çağatay , Gökçe Göksu Gürsu*

**Hatay ili Payas ilçesi zeytin bahçesi topraklarının yararlı bor içeriği ve bazı toprak özellikleri ile ilişkilerinin belirlenmesi..... 76-82**

*Mehmet Yalçın*

**Dörtüol ovası topraklarının temel özelliklerinin belirlenmesi ve yersel dağılımlarının coğrafi bilgi sistemleri (CBS) kullanılarak haritalanması ..... 83-95**

*Emine Derya Aşkiner , Necat Ağca*

**Investigation of the effects of copper hydroxide (Cu(OH)<sub>2</sub>) nanopesticide on female and male populations of a wild-type and non-target model organism, *Drosophila melanogaster* Oregon-R, by *in vivo* longevity test ..... 96-101**

*Handan Uysal*

**The potential use of *Epilobium hirsutum* L. in phytoremediation of zinc and an efficient method for *in vitro* propagation ..... 102-110**

*Nüket Akanlı Bingöl , Betül Akın , Nergiz Erdaş*

**Pyrazoline compounds containing different groups: Design, synthesis and comprehensive molecular docking studies..... 111-124**

*Halise Yalazan , Damla Koç , Seda Fandaklı , Burak Tüzün , Halit Kantekin*

**Evaluation of genetic diversity of tomato spotted wilt virus (TSWV) NSs gene region isolates at geographical level..... 125-131**

*Filiz Randa Zelyüt , Ali Karanfil*

**Impact of growth medium components on absorbance-viable cell count correlation and cell surface area of *Cereibacter sphaeroides* O.U.001 ..... 132-138**

*Kader Çakır , Gökhan Kars*

**Investigation of the effects of lycorine and galanthamine extracted from *Galanthus elwesii* on viral and parasitic targets: An *in-silico* analysis and DFT Study..... 139-150**

*Melek Gül , Ebru Batı Ay*

**Sorafenib ve Yalancı portakal ekstresi kombinasyonunun A549 hücre hatları üzerindeki *in vitro* sitotoksik ve antioksidan aktivitesi..... 151-156**

*Deniz Altun Çolak , Heval Kaya , Tuğba Atıcı*

**A hypothetical study on the structural properties of limonene compounds using semi-empirical (PM3) method with arguslab software..... 157-164**

*Özlem İşcan*

**Synthesis of waste pineapple peel cellulose based hydrogels and aerogels ..... 165-170**

*Oğuzhan Şimşek , Burcu Okutucu*

**Effect of different azinphos-ethyl and azinphos-methyl concentrations on Tetradesmus obliquus growth in culture conditions ..... 171-177**

*Elif Soylu , Bengü Temizel*

**Review Articles / Derleme Makeleleri**

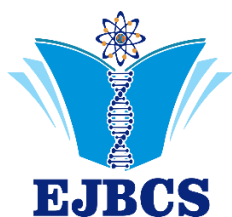
**An overview of leech saliva and cosmetic potential ..... 178-185**

*Fatma Çoruk , Sibel Kaymak , Hüseyin Ayhan , Nilufer Vural , Salih Mollahaliloğlu*

**A review on health benefits of local food products in Nigeria ..... 186-194**

*Olodu Blessing Adoh*





## Development of a dynamic multiple reaction monitoring LC-APCI-MS/MS method for quantification of ten nitrosamines in ranitidine API with simple extraction approach

Murat Emrah Mavis<sup>1</sup>, Nese Ular Cagatay\*<sup>1</sup>, Gokce Goksu Gursu<sup>1</sup>  
<sup>1</sup>Altium International Laboratuvar Cihazları A.Ş, R&D Center, Istanbul 34746, Turkey

\*Corresponding author : [nese.ular@jasem.com.tr](mailto:nese.ular@jasem.com.tr)  
Orcid No: <https://orcid.org/0000-0002-2324-3422>

Received : 26/09/2023  
Accepted : 02/06/2024

**To Cite / Atıf için:** Mavis ME, Ular Cagatay N, Goksu Gursu, G. 2024. Development of a dynamic multiple reaction monitoring LC-APCI-MS/MS method for quantification of ten nitrosamines in ranitidine API with simple extraction approach. Eurasian J Bio Chem Sci, 7(2):66-75 <https://doi.org/10.46239/ejbs.1366734>

**Abstract:** Nitrosamines (NAs) are classified as probable or possible human carcinogens by the International Agency for Research on Cancer (IARC) and the presence of these impurities has resulted in numerous drug recalls from the market. In April 2020, ranitidine which is prescribed to reduce the amount of acid secreted by the stomach has been recalled owing to contamination with NAs. In this work, a simple and sensitive method for simultaneous determination of 10 NAs were developed, utilizing atmospheric pressure chemical ionisation source coupled liquid chromatography tandem mass spectrometer (LC-APCI-MS/MS). By performing dynamic multiple reaction monitoring (dMRM) mode, 10 NAs were separated on a Poroshell HPH C18 (4.6 x 150 mm, 2.7 µm) column with gradient elution implementing mobile phase A consisting of 0.2 % formic acid in water and mobile phase B consisting of methanol in 17 min. The proposed analytical method was successfully implemented in active pharmaceutical ingredient (API) of ranitidine with a water-based extraction procedure. Good linearity with a correlation coefficient ( $R^2$ )  $\geq 0.994$  was accomplished over the concentration in range of 0.5–50 ng/mL. The limits of detection (LODs) ranged in 0.06–0.17 ng/mL and limits of quantitation (LOQs) ranged in 0.21–0.58 ng/mL of the method met thresholds of US Food and Drug Administration (US-FDA) and European Medicines Agency (EMA) for testing of NAs. The accuracy of the developed method ranged from 83.1% to 111.9 % and the percent relative standard deviation (RSD %) was  $\leq 8.9$ .

**Keywords:** N-nitrosamines, Ranitidine, Liquid chromatography, Mass spectrometry, Simultaneous determination

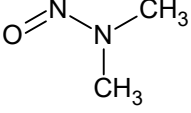
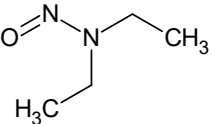
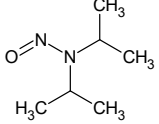
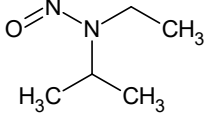
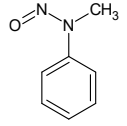
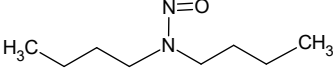
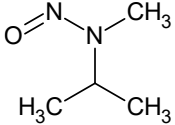
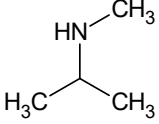
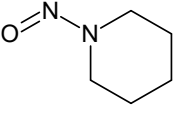
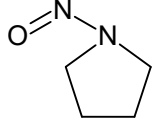
© EJBCS. All rights reserved.

### 1. Introduction

N-Nitrosamines, (NAs) which are commonly formed by the interaction of a nitrosating agent generating from either nitrite salts or nitrogen oxides with secondary, tertiary, or quaternary amines, belong to a larger group of potent carcinogens known as N-nitroso compounds (Bharate et al. 2021; Campillo et al. 2021). Therefore, the existence of NAs in pharmaceuticals is a cause of concern for patients as well as for regulatory authorities. Since July 2018, the United States Food and Drug Administration (US FDA) and the European Medicines Agency (EMA) recalled a great number of medicinal products owing to the detection of NAs above their daily acceptable limit (Wichitnithad et al. 2021). In the light of recent events in NA-contaminated medicinal products, the global concern has raised beyond angiotensin II receptor blockers (so called “sartans”) to comprise the ranitidine. Ranitidine medicines are used for decreasing the amount of acid produced by the stomach in

patients with conditions such as heartburn and gastric ulcers. On April 1, 2020, the US FDA and EMA decided to withdraw all prescription and over the counter (OTC) ranitidine drugs from the market due to the presence of N-nitrosodimethylamine (NDMA) impurity (Tuesuwan et al. 2021). There is a considerable literature on investigation into the possible root causes of the NDMA formation in ranitidine (Bharate et al. 2021; Tuesuwan et al. 2021; King et al. 2020; Yokoo et al. 2021; Aldawsari et al. 2021; Shaik et al. 2020). Moreover, regulatory authorities and research groups have developed a number of analytical methods aimed at determining accurate concentration of NA-contaminants below the US FDA and EMA interim limits of the NAs in both active pharmaceutical ingredients (APIs) and final products (FPs) using gas chromatography-mass spectrometry (GC-MS) with different analysers (single quadrupole and triple quadrupole) equipped with either a headspace (HS) system or direct injection, supercritical

**Table 1.** Molecular structures, CAS numbers and abbreviations of NAs covered in the article.

Analyte	Abbreviation	CAS Number	Molecular Structure
N-nitrosodimethylamine	NDMA	62-75-9	
N-nitrosodiethylamine	NDEA	55-18-5	
N-nitrosodiisopropylamine	DIPNA	601-77-4	
N-nitrosoethylisopropylamine	EIPNA	16339-04-1	
N-nitrosomethylphenylamine	NMPhA	614-00-6	
N-nitrosodibutylamine	NDBA	924-16-3	
N-nitrosoethylmethylamine	NMEA	10595-95-6	
N-isopropylmethylnitrosamine	NMIPA	4747-21-1	
N-nitrosopiperidine	NPIP	100-75-4	
N-nitrosopyrrolidine	NPyR	930-55-2	

fluid chromatography, LC coupled with high resolution mass spectrometer, LC-MS/MS and HPLC-UV (U.S. Food & Drug Administration 2019; Health Canada 2019; U.S. Food & Drug Administration 2018; EDQM 2019; Schmidtsdorff et al. 2019; Parra et al. 2019; Masada et al. 2019; Ngongang et al. 2015; Ngongang et al. 2015; Lim et al. 2020; Ripollés et al. 2011; AlShehri et al. 2020; Giménez-Campillo et al. 2020; Liu et al. 2021).

The aim of this study was to develop and validate a simple, robust, and sensitive dMRM-based method using LC-APCI-MS/MS for simultaneous determination of ten (Table 1) nitrosamines in API of ranitidine in combination with water-based extraction.

## 2. Materials and methods

### 2.1. Chemicals, reagents, and pharmaceutical

NDMA, NDEA (N-nitrosodiethylamine), NMBA (N-nitroso-N-methyl-4-aminobutyric acid), DIPNA (N-nitrosodiisopropylamine), NDBA (N-nitrosodibutylamine), NMPHA (N-nitrosomethylphenylamine), EIPNA (N-nitrosoethylisopropylamine), NMEA (N-nitrosoethylmethylamine), NMIPA (N-isopropylmethylnitrosamine), NPIP (N-nitrosopiperidine), NPyR (N-nitrosopyrrolidine) and NDMA-D6 were supplied by Toronto Research Chemicals (Toronto, Canada). NDBA-D18, NDEA-D10 and NMPHA-D5 were purchased from Cambridge Isotope Laboratories, Inc. (Massachusetts, USA). LC-MS grade methanol (MeOH), LC-MS grade acetonitrile (ACN) and formic acid (purity >98%) were purchased from Merck (Darmstadt, Germany). Deionized (DI) water was prepared at our laboratory using Elga Purelab (High Wycombe, United Kingdom) water purification system. The API of ranitidine (as ranitidine hydrochloride) was provided by local pharmaceutical company.

#### 2.1.1. Preparation of working solutions, standard solutions, and quality controls

The primary stock solutions of 1000 µg/mL of the ten NAs (NDMA NDEA, DIPNA, NDBA, EIPNA, NMEA, NMIPA, NPIP, NPyR and NMPHA in MeOH) were used for the preparation of intermediary stock solutions. The intermediary stock solution of NAs mix (10 µg/mL) and stable isotope-labelled standard (IS) mix composed of NDMA-D6, NDBA-D18, NDEA-D5 and NMPHA-D5 (1 µg/mL) were prepared in MeOH and stored in a freezer at -20 °C. The working mix solution of NAs was prepared by dilution with DI water at a concentration of 1 g/mL from the intermediary stock solution and stored at -20 °C. Calibration standard solutions were made by fortifying appropriate volumes of NA working mix solution to obtain ultimate concentrations of 2.5, 10, 25, 50, and 250 ng/mL in DI water, which were then used in calibrator preparation. Furthermore, quality control samples (QCs) were prepared by spiking appropriate volumes of the working mix solution

of NAs (10 g/mL) in not spiked ranitidine API to obtain QCs at concentrations of 1 and 10 ng/mL.

### 2.2. Instrumentation and chromatographic conditions

Agilent HPLC system (Agilent Technologies, Santa Clara, CA, USA) with flexible pump (G7104A), column compartment (G7116B), and autosampler (G7129C) coupled to Agilent Ultivo triple quadrupole LC/MS (6465B, Agilent Technologies, Santa Clara, CA, USA) equipped with APCI source was used for the experiments. Positive chemical ionisation in dMRM mode was used to detect NAs in MS/MS. In comparison to MRM, dMRM has a related delta retention time window (RTW) that can be turned on and off dynamically without affecting the total cycle time. It enables the instrument to only acquire MRM data during the retention time window, maximizing dwell time and improving sensitivity. The NAs were separated chromatographically using an Agilent InfinityLab Poroshell HPH C18, 4.6 x 150 mm 2.7 m (P/N 693975-702, Agilent Technologies, Santa Clara, CA, USA) analytical column maintained at 50 °C. DI water containing 0.2% formic acid (mobile phase A, pH 3) and MeOH were used to make the mobile phase (mobile phase B). The gradient elution was programmed as follows: linear elution at the flow rate of 0.4 mL/min starting at 2% mobile phase B increasing to 22% over 4 min, then converting to 66% mobile phase B at 0.6 mL/min, afterwards increasing linearly from 66% to 96% mobile phase B within 4 min at the flow rate of 0.6 mL/min, subsequently turning to 100% mobile phase B and maintaining for 3 min at 0.6 mL/min, finally equilibrating to the initial condition for 6 min. The analysis was performed in a total run time of 17 min. The injection volume was arranged as 20 µL. Following each sample injection, the needle was washed with a solvent mixture of MeOH and DI water (80:20; v/v). The autosampler's temperature was set to 8 °C. The method's mass spectrometer settings were as follows:; drying gas temperature 300 °C, drying gas flow 6 L/min, nebulizer pressure 55 psi, vaporizer temperature 350 °C, corona current 4 µA and capillary voltage 3000 V. Product ion transitions created by collision-induced dissociation (CID) of the corresponding precursor ion were used to detect NAs and ISs in MS/MS. NAs and IS dMRM transitions were studied at optimum fragmentation voltages (FV), which represented a common value for each precursor ion-product ion mass transition, and optimum collision energies (CE), which indicated a specific value for each product ion in terms of voltage (V) unit. Table 2 also shows the retention times (RTs) of NAs with a fixed RTW of 0.8 min for each analyte in dMRM mode. The analytes were quantified using calibration curves established on the calibrator concentrations, with matrix effect compensation based on the yields of the assigned ISs. Agilent MassHunter Acquisition (version 1.2), Agilent MassHunter Qualitative Analysis (version 10.0), and Agilent MassHunter Quantitative Analysis (version 10.1) software programs were used for data acquisition, qualification, and quantification, respectively.

**Table 2.** Mass transitions of analytes, ISs, RTs and MS/MS conditions

Compound Name	RT <sup>1</sup> (min.)	Precursor Ion (m/z)	Product <sup>2</sup> Ion(s) (m/z)	FV <sup>3</sup> (V)	CE <sup>2,4</sup> (V)	Polarity
NDBA	9.4	159	57/41	90	12/17	Positive
NDEA	7.7	103.1	75/47.1	80	8/15	Positive
DIPNA	8.3	131.1	89.1/43.1	60	4/10	Positive
NDMA	5.4	75	58/43	80	8/15	Positive
EIPNA	8.0	117	75/47	90	12/17	Positive
NMIPA	7.7	103.1	61/43	60	6/12	Positive
NMEA	7.0	89.1	61/43	70	9/9	Positive
NMPPhA	8.3	137	107/65.8	80	10/21	Positive
NPIP	7.8	115.1	69/41	90	12/17	Positive
NPyR	7.1	101.1	55	90	15	Positive
NDMA-D6 (IS)	5.4	81.1	64/46.1	80	12/17	Positive
NDEA-D18 (IS)	9.3	177.2	66.1	35	13	Positive
NDEA-D10 (IS)	7.7	113.1	81	45	10	Positive
NMPPhA-D5 (IS)	8.3	142.1	71	45	22	Positive

<sup>1</sup> Retention times acquired in dMRM mode

<sup>2</sup> Mass transitions as product ions are shown respectively with corresponding CE value

<sup>3</sup> FV: Fragmentor voltage

<sup>4</sup> CE: Collision energy

### 2.3. Sample preparation procedure

A 50 mg ranitidine API was weighted in a glass tube. Then, 250 µL of IS mixture was pipetted to the tube and vortex for 5 sec. Next, 2250 µL of DI water was added to the tube and agitated for 5 min. at room temperature. Following the extraction step, the solution was filtered through a 0.45 µm regenerated cellulose membrane prior to injection.

### 2.4. Quantification of NAs in prepared ranitidine API

In an HPLC vial, 100 µL of calibration standard solutions (prepared in section 2.1.1.) were transferred. Following that, 50 µL of IS mixture was added and swirled for 5 sec. Before injecting, 350 µL of DI water was added and vortexed for 5 seconds. After the injections were completed, a five-point calibration batch was established in the ranges of 0.5, 2, 5, 10, and 50 ng/mL for the quantification of NAs extracted from ranitidine API. The calibration curve was built using the peak area ratios of the standards to the assigned ISs. To achieve accurate quantification, great care was taken in assigning ISs that were not stable isotope forms of corresponding analytes. For API of ranitidine, NDEA-D10 was selected as IS for NMEA, NMIPA, NPIP and NPyR; NDBA-D18 was selected as IS for EIPNA. NDMA-D6 was assigned as IS for DIPNA (Table 3).

**Table 3.** Assigned ISs for Nas.

Compound Name	API <sup>1</sup> of ranitidine
NDBA	NDBA-D18
NDEA	NDEA-D10
DIPNA	NDMA-D6
NDMA	NDMA-D6
EIPNA	NDBA-D18
NMIPA	NDEA-D10
NMEA	NDEA-D10
NMPPhA	NMPPhA-D5
NPIP	NDEA-D10
NPyR	NDEA-D10

<sup>1</sup> API: Active pharmaceutical ingredient

## 3. Method Validation

### 3.1. System Suitability

To evaluate the system suitability before validation experiments and impurity determination, the chromatographic system was checked in terms of reproducibility. For this reason, a solution containing a mixture of the lowest level of ten NAs was prepared. The system suitability solution was injected with six replicates. The system reproducibility was assessed by the variation of peak area (RSD % <9) and retention time (RSD % <1) to indicate the precision of injections.

### 3.2. Linearity and sensitivity

The linearity of the method was determined by analysing of ten NAs at 5 calibration points in the range of 0.5-50 ng/mL. The intercept, slope, and correlation coefficient (R<sup>2</sup>) were evaluated by linear regression data analysis and fitting to a linear regression model with a weighting factor of 1/x. The correlation coefficient was ≥0.994 for all the calibration curves of NAs. For evaluation of the sensitivity of analytical method, limit of detection (LOD) and limit of quantitation (LOQ) were determined according to ICH (The International Council for Harmonisation of Technical Requirements for Pharmaceuticals for Human Use) validation of analytical procedures (CPMP/ICH/381/95), based on the standard deviations at low concentrations. Limit of detection for this method was determined from repeated analyses of neat solution at lowest concentration. The Lowest NAs concentration that could be measured with 99% confidence as 3 times the standard deviation was taken as the LOD. The experiments were repeated ten times (n=10). The correlation coefficient, LOD and LOQ for each NAs are described in Table 4.

**Table 4.** Linearity, LOD and LOQ result of NAs.

<i>Compound name</i>	<i>R</i> <sup>2</sup>	<i>LOD</i> (ng/mL)	<i>LOQ</i> (ng/mL)
<b>NDBA</b>	0.998	0.124	0.413
<b>NDEA</b>	0.998	0.065	0.210
<b>DIPNA</b>	0.994	0.076	0.254
<b>NDMA</b>	0.994	0.066	0.220
<b>EIPNA</b>	0.997	0.142	0.472
<b>NMIPA</b>	0.997	0.072	0.240
<b>NMEA</b>	0.998	0.175	0.582
<b>NMPhA</b>	0.995	0.134	0.445
<b>NPIP</b>	0.997	0.105	0.349
<b>NPYR</b>	0.998	0.092	0.308

**3.3. Accuracy and precision**

Considering the analytical range, two concentration levels of samples were used for accuracy and precision: low-level and high-level spiked samples (referred to as LLQC and HLQC). Accuracy was performed ten replicates of LLQC (1 ng/mL) and HLQC (10 ng/mL) samples. Accuracy was expressed as percentage (recovery %) of the nominal concentration. The results are summarized in Table 5. The method precision was evaluated by repeatability (intra-day) and intermediate precision (inter-day). The intra-day precision was measured by comparing the relative standard deviation (RSD %) of ten replicates of LLQC and HLQC during the same day. The inter-day precision was measured by comparing the percent relative standard deviation (RSD %) of six replicates of LLQC and HLQC on three consecutive days (Table 6).

**Table 5.** Accuracy values of NAs.

<i>Compound name</i>	<b>LLQC<sup>1</sup></b>	<b>HLQC<sup>2</sup></b>
	<i>n</i> =10 Recovery %	<i>n</i> =10 Recovery %
<b>NDBA</b>	111.9	101.5
<b>NDEA</b>	108.9	107.7
<b>DIPNA</b>	83.1	90.7
<b>NDMA</b>	104.9	101.2
<b>EIPNA</b>	85.5	88.4
<b>NMIPA</b>	110.3	101.7
<b>NMEA</b>	88.8	92.8
<b>NMPhA</b>	105.9	105.7
<b>NPIP</b>	108.7	109.5
<b>NPYR</b>	101.0	101.7

<sup>1</sup>Low-level quality control (LLQC): 1 ng/mL<sup>2</sup>High-level quality control (HLQC): 10 ng/mL**Table 6.** Intra-day and inter-day precision of NAs.

<i>Compound name</i>	<b>Intra-day assay</b>		<b>Inter-day assay</b>	
	<i>RSD</i> % ( <i>n</i> =10)		<i>RSD</i> % ( <i>n</i> =6x3)	
	<b>LLQC<sup>1</sup></b>	<b>HLQC<sup>2</sup></b>	<b>LLQC</b>	<b>HLQC</b>
<b>NDBA</b>	2.44	4.27	5.94	3.96
<b>NDEA</b>	3.31	2.41	6.22	2.14
<b>DIPNA</b>	3.44	2.95	5.74	3.44
<b>NDMA</b>	4.83	1.96	5.85	1.76
<b>EIPNA</b>	6.15	5.89	8.91	5.80
<b>NMIPA</b>	2.64	2.72	4.21	2.43
<b>NMEA</b>	5.36	4.33	8.51	5.28
<b>NMPhA</b>	2.69	5.46	7.19	5.07
<b>NPIP</b>	3.97	2.67	4.56	2.34
<b>NPYR</b>	6.84	4.78	7.39	4.13

<sup>1</sup>Low-level quality control (LLQC): 1 ng/mL<sup>2</sup>High-level quality control (HLQC): 10 ng/mL

### 3.4. Carry-over

The carry-over effect of the method was assessed by running the blank sample (MeOH) after the analysis of the highest concentration of the calibration curve. The response in the blank sample obtained after the highest concentration standard was not greater than 20% of the analyte response and not greater than 5% of the internal standard response.

### 3.5. Robustness

The robustness of the developed method was evaluated to investigate any influence on the peak retention and peak area by changing the volume of acidic additive for both of mobile phases (0.1 and 0.2 % formic acid). The results showed that the mobile phase conditions had only a slight effect on the peak retention time and all analytes were within acceptable RSD % (< 15%), indicating the robustness of the proposed method. With this in mind,  $\Delta$ RTW values of NAs were adjusted 0.8 min. in dMRM mode.

## 4. Results and discussion

The APCI source, creating high signals for all NAs, was selected as the ionization source for the determination of NAs. Scan and MS/MS spectra were acquired from direct infusion of 10  $\mu$ g/mL of each NAs and ISs (prepared in MeOH) at a flow rate of 0.3 mL/min, in positive mode with APCI. By using these solutions, MS conditions including MRM transition, drying gas temperature and flow, nebulizer pressure, vaporizer temperature, corona current and capillary voltage were individually optimized. To improve sensitivity, dMRM mode which is centred on individual retention time windows for each MRM transition was performed. The dMRM method is allowed the collection of satisfactory data points to provide an excellent quantitative accuracy with better precision. After optimizing MS/MS parameters, to identify the most suitable analytical column for separation of NAs, Poroshell HPH C18 (4.6 x 150 mm, 2.7  $\mu$ m, Agilent, USA) and Poroshell HPH C18 (2.1 x 100 mm, 1.9  $\mu$ m, Agilent, USA) were tested utilizing 100 ng/mL of NAs mixture prepared in MeOH. During the LC optimization process, different mobile phase combinations such as DI Water containing formic acid and buffers such as ammonium formate prepared at several concentrations (as mobile phase A), and ACN or MeOH (as mobile phase B) were experimented for best peak shape and peak area. Usage of an acidic content in mobile phase A (adjusted pH=3) proved to be fitted in terms of retention and separation of NAs. As the dMRM chromatogram shown in Fig. 1, Poroshell HPH C18 column ensured sufficient resolution of NAs in total run time of 17 min. Sample preparation procedure was optimized for ranitidine API sample as hydrochloride salt form. Extraction recoveries were evaluated by comparing the analyte responses observed in spiked sample (1 and 10 ng/mL). Peak shape, symmetry and baseline resolution were examined through the optimization of extraction procedures. In this context, ACN, MeOH and DI water with consisting of formic acid were tested as extraction solvents. Among these extraction solvents, DI water showed better resolution and recovery % by applying the developed

method. NDMA was detected in not spiked API of ranitidine at a concentration of 7.9 ng/mL (Fig. 2). Besides, the analysis of low level-spiked (1 ng/mL) ranitidine API were demonstrated excellent detection responses for the rest of NAs (Fig. 3).

In the literature, liquid chromatography high resolution mass spectrometry (LC-HRMS) and LC-MS/MS-API (U.S. Food & Drug Administration 2019)-based methods were developed and validated for the detection and quantitation of NDMA in ranitidine drug substance and drug product. The U.S. FDA introduced these analytical procedures for ranitidine API (LOD 0.3 ng/mL). Besides that, Lima HH et al. (2020) reported a GC-MS/MS method for quantifying NDMA and NDEA in ranitidine (LOD 0.3  $\mu$ g/kg and 0.07  $\mu$ g/kg, respectively) with solid phase extraction (SPE). AlShehri YM et al. (2020) established a method for ranitidine based on headspace solid-phase microextraction (SPME) GC-MS technique for the determination of NDMA with LOD of 1.0  $\mu$ g/L. Giménez-Campillo C et al. (2020) developed a method for the determination of nine volatile NAs in ranitidine pharmaceutical products using GC-MS in combination with dispersive liquid-liquid microextraction (DLLME) preconcentration technique. The LODs determined for all analytes in ranitidine ranged from 0.07 to 6.6 ng/g. In another literature, NDMA was measured by ESI-LC-MS/MS in ranitidine products with LOD 1.0 ng/mL. This study was demonstrated highly sensitive and selective method using a simple sample preparation procedure compared to the other methods (summarized in Table 7). U.S. FDA and EMA guidelines were taken into account to validate the performance of the developed LC-MS/MS method. The calibration curves for all NAs showed to be linearity in the analytical range 0.5-50 ng/mL with high correlation coefficients ( $R^2 \geq 0.994$ ). LOD and LOQ levels of all NAs were calculated to range between 0.06–0.17 and 0.21–0.58 ng/mL, respectively. Intra-day and inter-day precision were tested at low- and high-level quality control samples. The method proved to be definite with RSD % values-based between 1.9-6.8 % (intra-day) and 1.7–8.9% (inter-day). The recovery of all NAs in API ranitidine was within 83.-111.9 % at LLQC and HLQC.

In the literature, various sample preparation methods such as liquid-liquid extraction (LLE) (Campillo et al. 2021), solid-phase extraction (SPE) (Lim et al. 2020) and solid phase microextraction (SPME) (AlShehri et al. 2020) methods have been developed for the extraction and preconcentration of nitrosamines. Therefore, the sample preparation procedures for the analysis of nitrosamines require excess solvent consumption and time costs. Contrary to above mentioned methods, the developed method in this article is based on “extract and shoot” approach that can detect low levels of the selected nitrosamines by LC-MS/MS with simple sample preparation providing less solvent consumption. In addition, the proposed method in this paper covers ten nitrosamines compared to the limited analyte list of literature (Liu et al. 2021; Campillo et al. 2021; Lim et al. 2020; AlShehri et al. 2020).

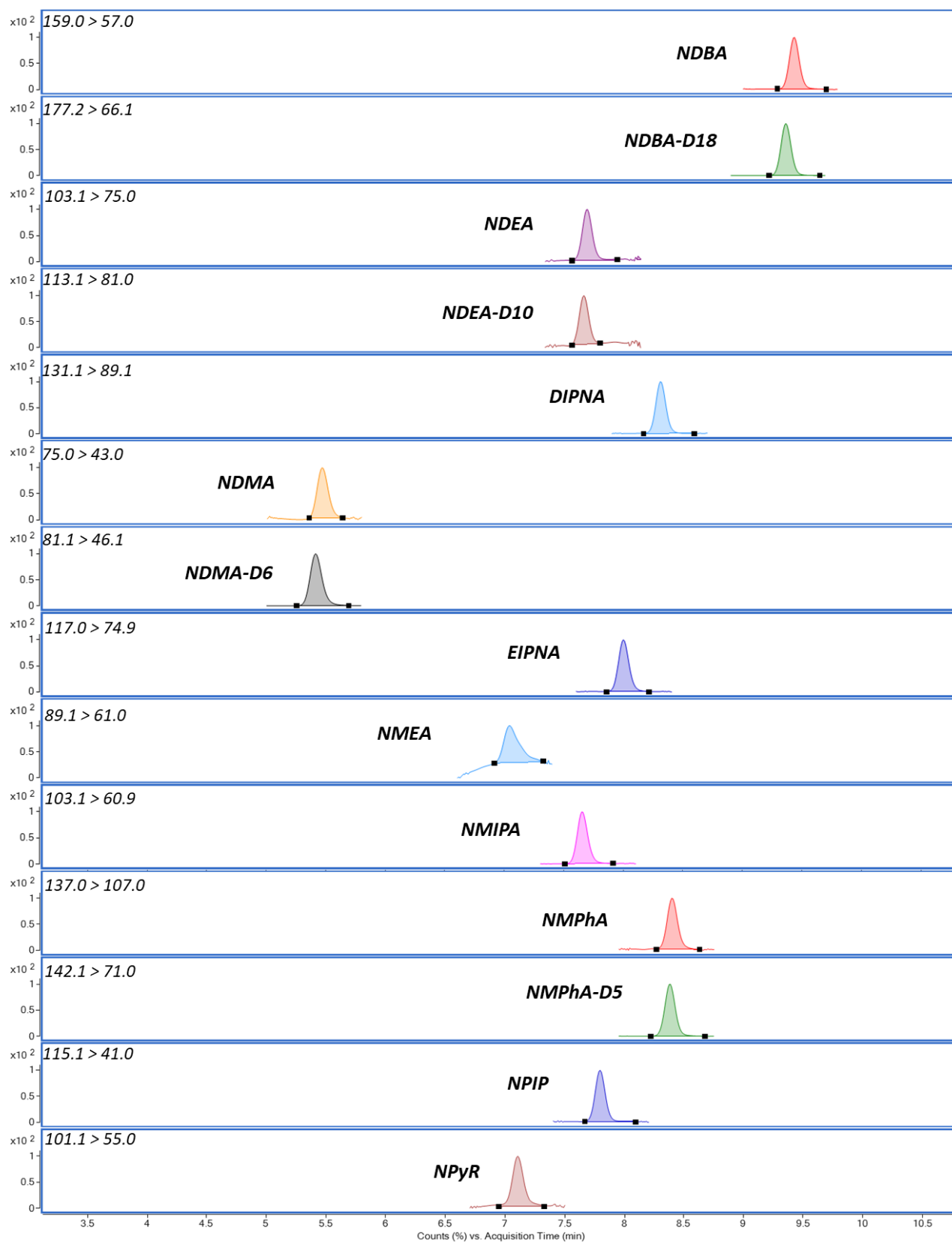


**Fig. 1.** Extracted dMRMs of NAs obtained from Poroshell HPH C18 column.

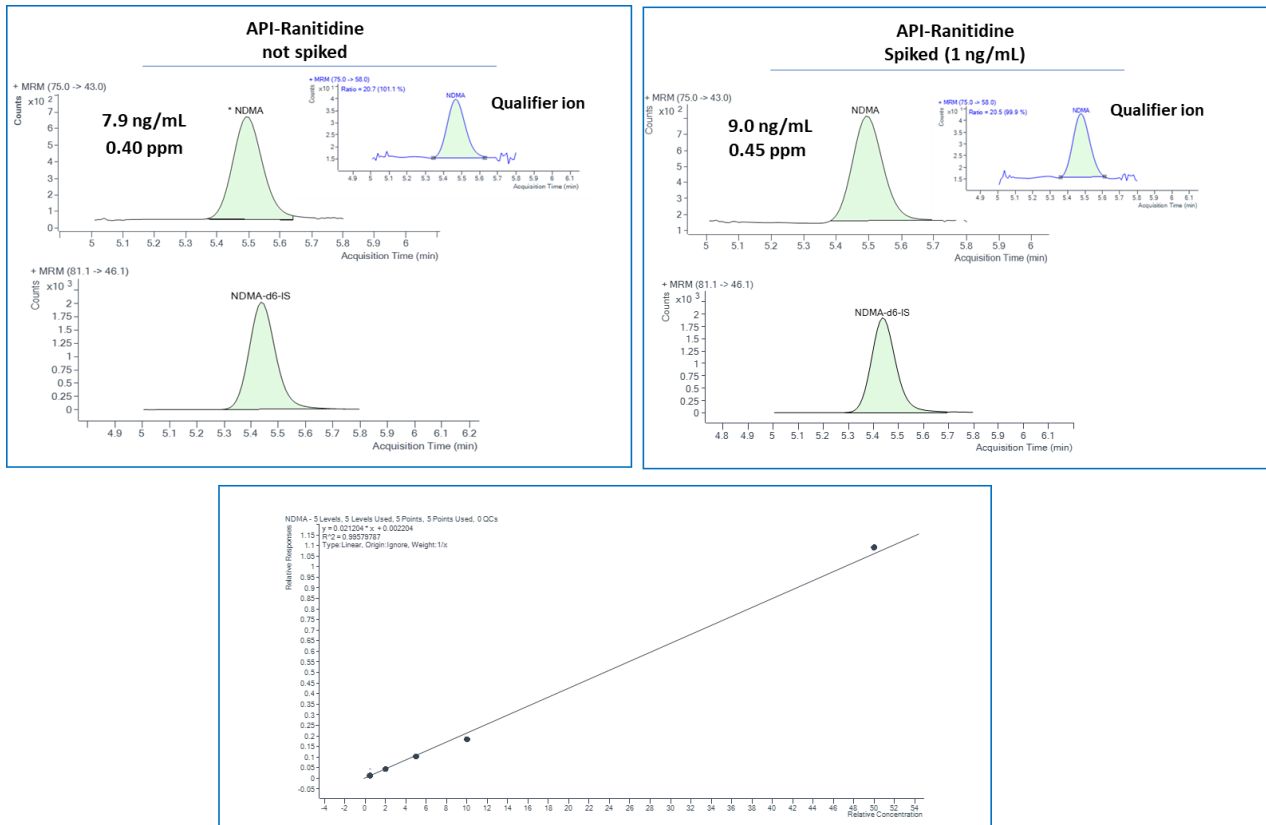


Fig. 2. The calibration curve for NDMA in not spiked and spiked (spiked with 1 ng/mL) API of ranitidine.

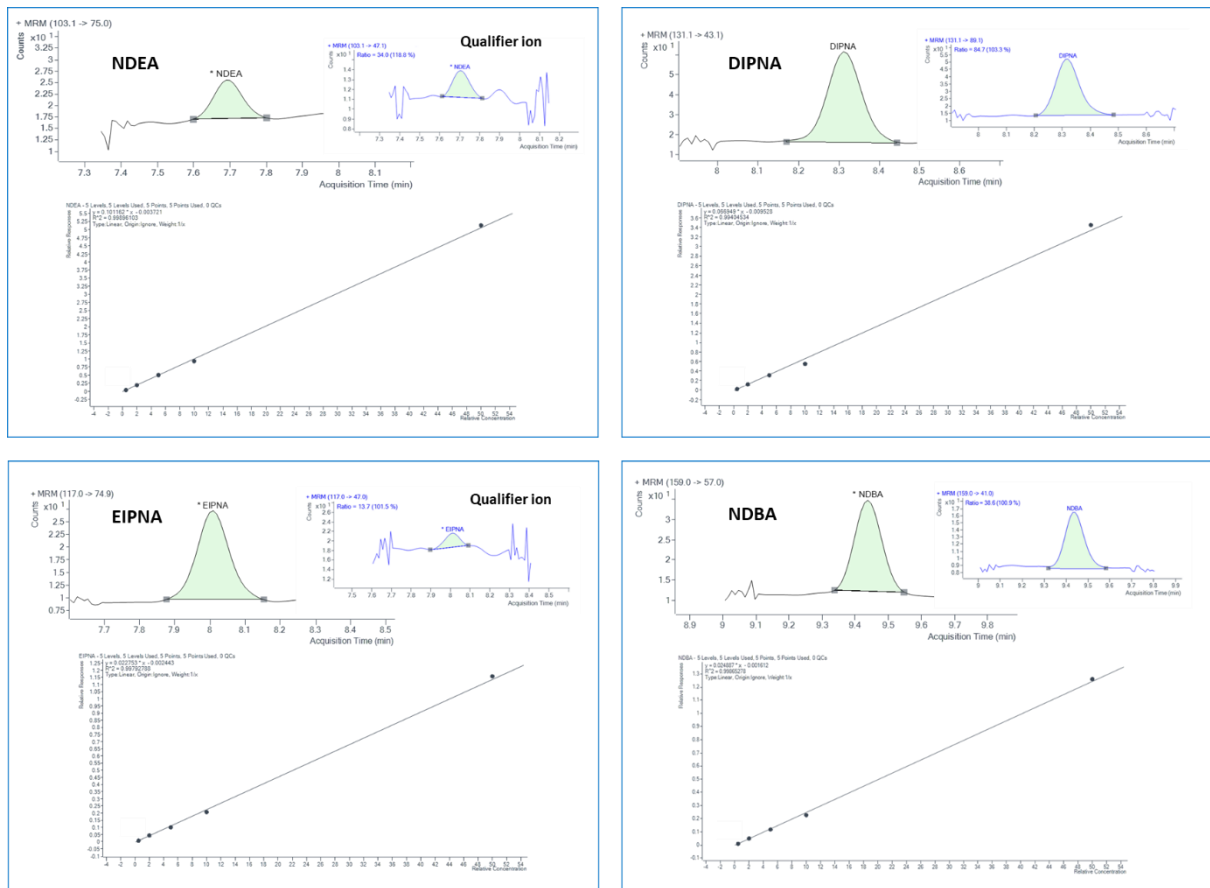


Fig. 3. The chromatograms and calibration curves of selected NAs (NDEA, DIPNA, EIPNA and NDBA) in 1 ng/mL spiked API of ranitidine.



**Table 7.** LOD values for nitrosamines to make comparison with other studies in literature.

Method	NDMA	NDEA	EIPNA	DIPN A	NDBA	NPIP	NPYR	NDPh A	NMEA	NMIP A	Ref.
LC-APCI-MS/MS <sup>a</sup>	0.066 ng/mL	0.065 ng/mL	0.142 ng/mL	0.076 ng/mL	0.124 ng/mL	0.105 ng/mL	0.092 ng/mL	0.134 ng/mL	0.175 ng/mL	0.072 ng/mL	This study
SPE-GC-MS/MS <sup>b</sup>	0.3 µg/kg	0.07 µg/kg	-	-	-	-	-	-	-	-	Lim 2020
LC-HRMS <sup>c</sup>	0.32 ng/mL	-	-	-	-	-	-	-	-	-	U.S. FDA 2019
LC-MS/MS <sup>d</sup>	0.3 ng/mL	-	-	-	-	-	-	-	-	-	U.S. FDA 2019
HS-SPME-GC-MS <sup>e</sup>	1.0 µg/L	-	-	-	-	-	-	-	-	-	AlShehri 2020
DLLME-GC-MS <sup>f</sup>	6.6 ng/g	0.29 ng/g	-	-	0.35 ng/g	0.47 ng/g	2.5 ng/g	0.07 ng/g	3.5 ng/g	-	Campillo 2021
LC-ESI-MS/MS <sup>g</sup>	1.0 ng/mL	-	-	-	-	-	-	-	-	-	Liu 2021

<sup>a</sup> LC-APCI-MS/MS: Liquid chromatography-atmospheric pressure chemical ionization-tandem mass spectrometry detection.

<sup>b</sup> SPE-GC-MS/MS: Solid phase extraction-gas chromatography-tandem mass spectrometry detection.

<sup>c</sup> LC-HRMS: Liquid chromatography-high resolution mass spectrometry detection.

<sup>d</sup> LC-MS/MS: Liquid chromatography- tandem mass spectrometry detection.

<sup>e</sup> HS-SPME-GC-MS: Headspace-solid-phase microextraction-gas chromatography mass spectrometry detection.

<sup>f</sup> DLLME-GC-MS: Dispersive liquid-liquid microextraction-gas chromatography mass spectrometry detection.

<sup>g</sup> LC-ESI-MS/MS: Liquid chromatography-electrospray ionization--tandem mass spectrometry detection.

## 5. Conclusion

In this work, an LC-APCI-MS/MS based method was developed by performing dMRM mode for the quantification of NDMA, NDEA, DIPNA, NDBA, NMPHA, EIPNA, NMEA, NMIPA, NPIP and NPYR in a single run for API of ranitidine. The dMRM significantly extended the dwell time, which provided much higher sensitivity and reproducibility than MRM. The developed method was validated with respect to the Q2(R1) ICH guidelines and ensured satisfying results of accuracy, precision, and other validation parameters. The LOQ and LOD of the proposed method were far below the US FDA and EMA interim limits of the corresponding NAs in ranitidine. This method could be modified for the simultaneous analysis of additional NAs in other type of drugs. However, the limitation is due to the fact that drugs not experienced in this study may cause unknown matrix effects over the chromatographic region which could not be compensated by the content of IS mixture. To minimize the risk of inaccuracy, future studies should address expanding the IS content placing corresponding stable isotope of target NAs.

## Declaration of interests

The authors declare that they have no known competing financial interests or personal relationships that could have appeared to influence the work reported in this paper.

## Conflict of Interest

- This manuscript has not been submitted to, nor is under review at, another journal or other publishing venue.
- The authors have no affiliation with any organization with a direct or indirect financial interest in the subject matter discussed in the manuscript.

## Contributions of the Authors to the Research

NUC, corresponding author, contributed to the research in the terms of methodology, software, investigation, writing draft, reviewing, and editing.

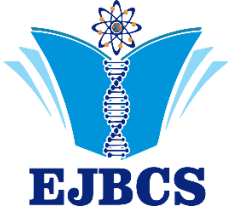
MEM contributed to the research in the terms of methodology, software, investigation, writing draft, reviewing, and editing.

GGG contributed to the research in the terms of methodology, software, investigation, writing draft reviewing, and editing.

## References

- Aldawsari FS, Alshehry YM, Alghamdi TS. 2021. N-nitrosodimethylamine (NDMA) Contamination of Ranitidine Products: A Review of Recent Findings. *J Food Drug Anal.* 29(1): 39–45.
- AlShehri YM, Alghamdi TS, Aldawsari FS. 2020. HS-SPME-GC-MS as an Alternative Method for NDMA Analysis in Ranitidine Products. *J Pharma Biomed Anal.* 191:N113582.
- Bharate SS. 2021. Critical Analysis of Drug Product Recalls due to Nitrosamine Impurities. *J Med Chem.* 64, 2923-2936.
- Campillo CG, Belda MP, Campillo N, Hernandez-Cordoba M. 2021. Development of a new methodology for the determination of N-nitrosamines impurities in ranitidine pharmaceuticals using microextraction and gas chromatography-mass spectrometry. *Talanta*, 223: 121659.
- Giménez-Campillo C, Pastor-Belda M, Campillo N, Hernández-Córdoba M, Viñas, P. 2020. Monitoring N-Nitrosamines impurities in ranitidine pharmaceuticals using microextraction and gas chromatography-mass spectrometry. *Talanta*. 121659.
- Health Canada. 2019. Impurities found in certain angiotensin II receptor blocker (ARB) products, also known as Sartans. Information update. Available at: <https://www.canada.ca/en/health-canada/services/drugs-health-products/complianceenforcement/information-health-product/drugs/angiotensin-receptor-blocker.html>. Accessed January 7, 2021.
- King FJ, Searle AD, Urquhart MW. 2020. Ranitidine- Investigations into the Root Cause for the Presence of

- N-Nitroso-N,N-dimethylamine in Ranitidine Hydrochloride Drug Substances and Associated Drug Products. *Org. Process Res. Dev.* 24:2915–2926.
- Lim HH, Oh YS, Shin HS. 2020. Determination of N-nitrosodimethylamine and N-nitrosomethylethylamine in drug substances and products of sartans, metformin and ranitidine by precipitation and solid phase extraction and gas chromatography–tandem mass spectrometry. *J Pharma Biomed Anal.* 189:113460.
- Liu J, Zhao Z, Yang X., Jin Y, Liu X, Wang C, Zhang Z. 2021. Determination of N-nitrosodimethylamine in Ranitidine Dosage Forms by ESI-LC-MS/MS; Applications for Routine Laboratory Testing. *Iran J Pharm Res.* 20 (4): 255-264.
- Masada S, Tsuji G, Arai R, Uchiyama N, Demizu Y, Tsutsumi T, Abe Y, Akiyama H, Hakamatsuka T, Izutsu K, Goda Y, Okuda H. 2019. Rapid and efficient high performance Liquid chromatography analysis of N-nitrosodimethylamine impurity in valsartan drug substance and its products. *Sci Rep.* 9:11852.
- Ngongang AD, Duy SV, Sauve S. 2015. Analysis of nine N-nitrosamines using liquid chromatography-accurate mass high resolution mass spectrometry on a Q-Exactive instrument. *Anal Methods.* 7(14):5748–5759.
- Parra MK, Josepha JF. 2019. NDMA impurity in valsartan and other pharmaceutical products: Analytical methods for the determination of N-nitrosamines *J Pharma Biomed Anal.* 164:536–549.
- Ripollés C, Pitarch E, Sancho JV, López FJ, Hernández F. 2011. Determination of eight nitrosamines in water at the ng L1 levels by liquid chromatography coupled to atmospheric pressure chemical ionization tandem mass spectrometry. *Anal Chim Acta.* 702:62e71.
- Schmidtsdorff S, Schmidt AH. 2019. Simultaneous detection of nitrosamines and other sartan-related impurities in active pharmaceutical ingredients by supercritical fluid chromatography. *J Pharma Biomed Anal.* 174:151–160.
- Shaik KM, Sarmah B, Wadekar GS, Kumar P. 2020. Regulatory Updates and Analytical Methodologies for Nitrosamine Impurities Detection in Sartans, Ranitidine, Nizatidine, and Metformin along with Sample Preparation Techniques. *Crit Rev Anal Chem.* 52(1): 53-71.
- The European Directorate for the Quality of Medicines & HealthCare (EDQM). 2019. LC-MS/MS method for LOSARTAN potassium. Test method. Available at: [https://www.edqm.eu/sites/default/files/de\\_lgl\\_losartan\\_method\\_parameters\\_nmba\\_lcms.pdf](https://www.edqm.eu/sites/default/files/de_lgl_losartan_method_parameters_nmba_lcms.pdf). Accessed January 7, 2021.
- Tuesuwan B, Vongsutilers V. 2021. Nitrosamine Contamination in Pharmaceuticals: Threat, Impact, and Control. *J Pharm Sci.* 110:3118–3128.
- U.S. Food & Drug Administration. 2018. Combined direct injection N-nitrosodimethylamine (NDMA) and N-nitrosodiethylamine (NDEA) impurity assay by GC/MS. Test method. Available at: <https://www.fda.gov/media/117807/download>. Accessed January 7, 2021.
- U.S. Food & Drug Administration. 2019. Combined N-nitrosodimethylamine (NDMA) and N-nitrosodiethylamine (NDEA) impurity assay by GC/MS-headspace. Test method. Available at: <https://www.fda.gov/media/117843/download>. Accessed January 7, 2021.
- U.S. Food & Drug Administration. 2019. GC/MS headspace method for detection of NDMA in valsartan drug substance and drug products. Test method. Available at: <https://www.fda.gov/media/115965/download>. Accessed January 7, 2021.
- U.S. Food & Drug Administration. 2019. Liquid chromatography-high resolution mass spectrometry (LC-HRMS) method for the determination of NDMA in ranitidine drug substance and drug product. Test method. Available at: <https://www.fda.gov/media/130801/download>. Accessed December 1, 2020.
- U.S. Food & Drug Administration. 2019. Liquid chromatography-tandem mass spectrometry (LC-MS/MS) method for the determination of NDMA in ranitidine drug substance and solid dosage drug product. Test method. Available at: <https://www.fda.gov/media/131868/download>. Accessed December 1, 2020.
- Wichitnithad W, Sudtanon O, Srisunak P, Cheewatanakornkool K, Nantaphol S, Rojsitthisak P. 2021. Development of a Sensitive Headspace Gas Chromatography–Mass Spectrometry Method for the Simultaneous Determination of Nitrosamines in Losartan Active Pharmaceutical Ingredients. *ACS Omega.* 6:11048–11058.
- Yokoo H, Yamamoto E, Masada S, Uchiyama N, Tsuji G, Hakamatsuka T, Demizu Y, Izutsu K, Goda Y. 2021. N-Nitrosodimethylamine (NDMA) Formation from Ranitidine Impurities: Possible Root Causes of the Presence of NDMA in Ranitidine Hydrochloride. *Chem Pharm Bulletin.* 69: 872–876.



## Hatay ili Payas ilçesi zeytin bahçesi topraklarının yararışlı bor içeriği ve bazı toprak özellikleri ile ilişkilerinin belirlenmesi

Mehmet Yalçın\*

Hatay Mustafa Kemal Üniversitesi, Toprak Bilimi ve Bitki Besleme Bölümü, Hatay/Türkiye

\*Corresponding author : myalcin@mku.edu.tr  
Orcid No: <https://orcid.org/0000-0002-1690-7681>

Received :07/03/2024  
Accepted : 22/07/2024

**To Cite / Atf için:** Yalçın M. 2024. Hatay ili Payas ilçesi zeytin bahçesi topraklarının yararışlı bor içeriği ve bazı toprak özellikleri ile ilişkilerinin belirlenmesi. Eurasian J Bio Chem Sci, 7(2):76-82 <https://doi.org/10.46239/ejbcs.1448735>

**Özet:** Bu çalışmada Hatay ili Payas ilçesi zeytin bahçelerinin bulunduğu toprakların yararlı bor içeriğinin ve bazı fiziksel ve kimyasal özelliklerinin ilişkileri araştırılmıştır. Çalışma kapsamında, zeytin bahçelerini temsil eden 14 farklı noktadan 0-30 cm ve 30-60 cm derinliklerinden 28 adet toprak örneği alınmıştır. Bu örneklerde toprakların pH, toplam tuz, bünye, kation değişim kapasitesi (KDK), kireç, organik madde ve yararlı bor içerikleri belirlenmiştir. Araştırma sonuçlarına göre, toprakların pH değerleri 7.16 ile 8.30 arasında değişirken, toplam tuz içerikleri % 0.007 ile % 0.226 arasında değişmektedir. Kil içerikleri % 7.00 ile % 43.00 arasında, kum içerikleri % 19.00 ile % 73.00 arasında ve silt içerikleri % 20.00 ile % 48.00 arasında değişmektedir. Kireç içeriği % 3.40 ile % 21.90 arasında değişirken, organik madde içeriği % 1.18 ile % 5.60 arasında değişmektedir. KDK içerikleri 10.49 ile 26.31 me/100 g arasında bulunurken, yararlı bor içerikleri ise 0.39 ile 1.06 mg/kg arasında değişmektedir. Hatay ili Payas ilçesi zeytin bahçelerinin bulunduğu topraklarının yararlı bor içeriği bakımından incelendiğinde, 0-30 cm derinlikte % 42.86'sının çok az, % 50.00'sinin az ve % 7.14'ünün yeterli düzeyde olduğu belirlenmiştir. 30-60 cm derinlikte ise % 28.57'sinin çok az, % 64.29'unun az ve % 7.14'ünün yeterli düzeyde olduğu görülmüştür. Toprakların yararlı bor içeriği ile tuz içeriği arasında pozitif bir ilişki saptanmıştır. Ayrıca, toprakların pH değeri ile kil içeriği, organik madde ve KDK arasında negatif ilişkiler gözlemlenirken, pH ile kum içeriği arasında önemli bir pozitif ilişki belirlenmiştir. Toprakların tuz içeriği ile organik madde arasında ise pozitif, kil içeriği ile kum içeriği arasında negatif bir ilişki bulunurken, kil ile organik madde ve KDK içeriği arasında pozitif ilişkiler saptanmıştır. Ayrıca, toprakların kum içeriği ile silt içeriği, organik madde ve KDK arasında negatif ilişkiler tespit edilmiştir; kum içeriği ile kireç içeriği arasında ise önemli bir pozitif ilişki bulunmuştur. Toprakların kireç ile KDK arasında negatif bir ilişki saptanmıştır. Organik madde içeriği ile KDK arasında ise pozitif bir ilişki gözlemlenmiştir. Sonuç olarak, çalışma alanı topraklarında yararlı bor içeriğinin çoğunlukla düşük seviyelerde olduğu ve bu nedenle bor gübrelemesinin gerekliliği belirlenmiştir.

**Anahtar kelimeler:** Payas toprakları, Yararışlı Bor, Fiziksel ve Kimyasal Özellikler

### *Determination of useful boron content of olive orchard soils of Payas district of Hatay province and their relationships with some soil properties*

**Abstract:** In this study, the relationships between the beneficial boron content and various physical and chemical properties of the soils in olive orchards in the Payas district of Hatay province were investigated. A total of 28 soil samples representing the study area were collected from depths of 0-30 cm and 30-60 cm, and from 14 different points. These samples were analyzed for pH, total salt content, texture, cation exchange capacity (CEC), calcium carbonate (lime), organic matter, and beneficial boron content. According to the research results, the pH values of the soils ranged from 7.16 to 8.30, while the total salt content varied between 0.007% and 0.226%. The clay content ranged from 7.00% to 43.00%, the sand content ranged from 19.00% to 73.00%, and the silt content ranged from 20.00% to 48.00%. The calcium carbonate content ranged from 3.40% to 21.90%, and the organic matter content ranged from 1.18% to 5.60%. The CEC values ranged from 10.49 to 26.31 me/100 g, while the beneficial boron content ranged from 0.39 to 1.06 mg/kg. When the beneficial boron content of the soils in olive orchards in the Payas district of Hatay province was examined, it was determined that 42.86% of the samples at a depth of 0-30 cm had very low levels, 50.00% had low levels, and 7.14% had sufficient levels. At a depth of 30-60 cm, 28.57% had very low levels, 64.29% had low levels, and 7.14% had sufficient levels. A positive relationship was found between the beneficial boron content and the salt content of the soils. Additionally, negative relationships were observed between the pH values of the soils and the clay content, organic matter, and CEC, while a significant positive relationship was found between the pH and the sand content. A positive relationship was also detected between the salt content and the organic matter of the soils. While a negative relationship was found between the clay and

sand content, positive relationships were observed between clay and organic matter, as well as clay and CEC. Furthermore, negative relationships were observed between the sand content and the silt content, organic matter, and CEC, while a significant positive relationship was found between the sand content and the calcium carbonate content. A negative relationship was identified between the calcium carbonate and CEC of the soils, while a positive relationship was observed between the organic matter content and CEC. In conclusion, it was determined that the beneficial boron content in the soils of the study area was mostly at low levels, indicating the necessity of boron fertilization.

**Keywords:** Payas soils, Available Boron, Physical and Chemical Properties

© EJBCS. All rights reserved.

## 1.Giriş

Zeytin (*Olea europae* L.), anavatanı Anadolu olan ve Akdeniz ikliminin hakim olduğu coğrafyalarda yetiştirilen önemli bir meyvedir. Dünyada 30-40 derece enlemler arasında 890 milyon zeytin ağacı bulunmaktadır ve bu ağaçların %97'si kuzey yarım kürede yer almaktadır (Tunalıoğlu ve Karahocalıgil 2004). Zeytin yetiştiriciliği M.Ö. 4000 yıllarında Anadolu'da başlamış ve buradan Akdeniz ülkelerine yayılmıştır (Topaloğlu ve Yalçın 2023). Toprakların kimyasal özellikleri, bitkisel üretimde önemli bir rol oynar. Bu nedenle toprakların kimyasal özelliklerinin korunması büyük önem taşımaktadır. Toprak pH'ı, kireç ve organik madde içeriği gibi kimyasal özellikler bitkisel üretim açısından önemli fonksiyonlara sahiptir (Esen 2019). Topraktaki bor elementinin miktarı pH'ın yanı sıra bitki çeşidi, topraktaki değişebilir iyonlar, organik madde miktarı ve toprak sıcaklığı gibi faktörlerden de etkilenir (Şimşek ve ark. 2003). Bitki besin maddelerinin topraklarda istenilen düzeyde bulunması pH, tuz, bünye, organik madde, kireç ve KDK gibi toprak faktörleri ile birlikte iklim koşullarına da bağlıdır (Sevindik ve ark. 2017). Tarımsal üretimin önemli sorunlarının başında, topraklarda çok fazla yapılan tarımsal faaliyetlerin besin elementlerinin toprakta azalmasına neden olmasıdır. Bor noksanlığı daha çok su tutma kapasitesi düşük, kum içeriği yüksek, organik madde miktarı az ve yıkanmanın çok fazla olduğu asit karakterli düşük pH'lı topraklarda ortaya çıkmaktadır. Buna ek olarak nasıl ki pH'sı düşük topraklarda bor noksanlığı görülüyorsa da topraklardaki yüksek pH ve kil içeriği fazla olan topraklarda da bor noksanlığı ortaya çıkması kaçınılmazdır (Güneş ve ark. 2017). Topraklarda önemli olayların başında tarım alanlarında gerçekleşen kuraklık ve aşırı yağış da bor alımını etkileyen faktörlerden bazılarıdır (Gürel ve ark. 2010). Hatay ilinde zeytin yetiştiriciliği önemli bir tarımsal faaliyettir. Bölgede zeytin bahçeleri topraklarının yarayışlı bor içeriği ve toprak özellikleri ile ilişkilerini inceleyen bazı çalışmalar yapılmıştır. Aynı bölgede, Yalçın (2023) tarafından yapılan çalışmada Hatay ili Arsuz ilçesi topraklarının yarayışlı bor içeriği ve bazı toprak özellikleri ile ilişkileri incelenmiştir. Çalışma sonucunda toprakların pH'sı 7.65-8.42, toplam tuz % 0.013-0.033, kil % 18.88-60.32, kum % 3.68-51.12, silt % 18.00-64.00, kireç % 0.62-28.04, organik madde % 1.68-4.09, değişebilir Na 0.07-0.93 me/100 g, değişebilir K 0.26-1.34 me/100 g ve yarayışlı bor içeriğinin ise 0.09-1.22 mg/kg arasında olduğu belirlenmiştir. Arsuz bölgesi topraklarının yarayışlı bor içeriği bakımından 0-30 cm derinlikte % 48.57'sinin çok az, % 42.86'sinin az ve % 8.57'sinin ise yeterli düzeyde olduğu saptanmıştır. Bor içeriği tüm çalışma alanı topraklarında % 91'in üzerinde az ve çok az düzeyde belirlenmiş olup

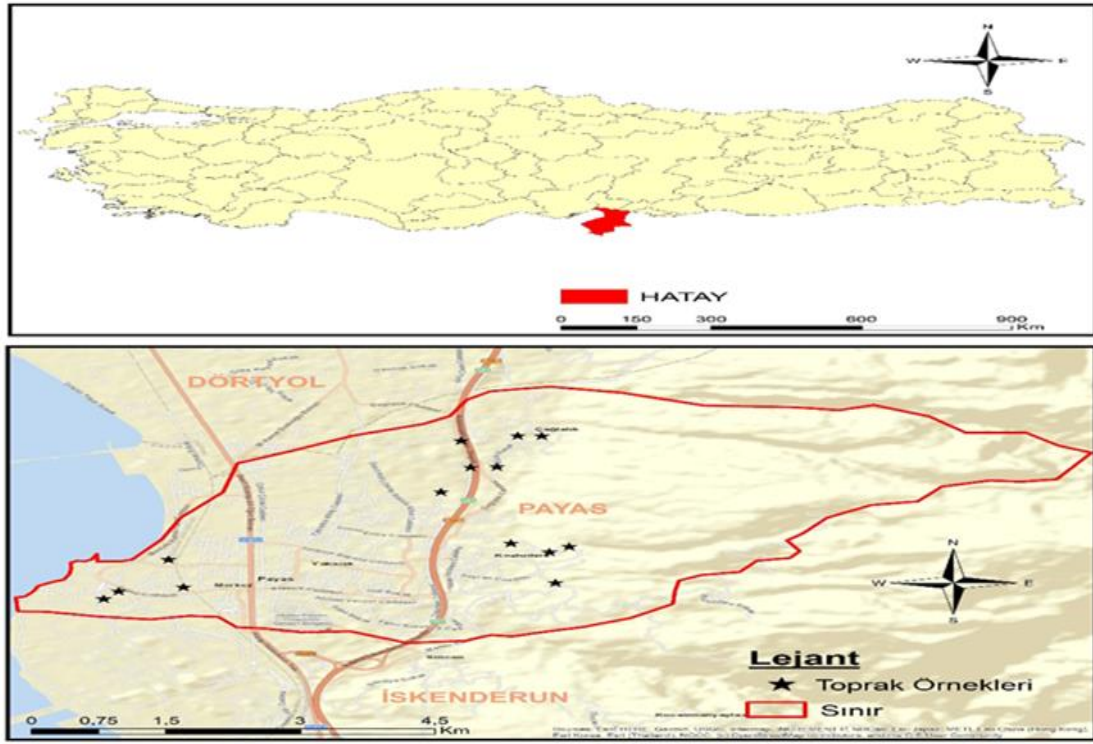
toprakların bor içeriğinin yetersiz olduğu belirlenmiştir. Açıkkel ve Yalçın (2021) tarafından yapılan çalışmada ise Hatay ili Reyhanlı-Kumlu bölgesi topraklarının yarayışlı bor içeriği ve bazı toprak özellikleri ile ilişkileri incelenmiştir. Çalışma sonucunda toprakların pH'ının 6.86-8.44, toplam tuz % 0.007-0.070, kil % 15.84-76.56, kum % 0.72-51.44, silt % 16.72-47.28, kireç % 2.71-64.23, organik madde % 0.40-2.89, KDK 26.43-91.13 me/100 g ve yarayışlı bor içeriğinin ise 0.07-1.76 mg/kg arasında değiştiği belirlenmiştir. Reyhanlı-Kumlu topraklarının yarayışlı bor içeriği bakımından 0-20 cm derinlikte % 22.50'sinin çok az, % 50.00'sinin az ve % 27.50'sinin yeterli düzeyde, 20-40 cm derinlikte ise % 37.50'sinin çok az, % 40.00'ı az ve % 22.50'si yeterli düzeyde olduğu tespit edilmiştir. Çalışma alanı topraklarında bor içeriği tüm çalışma alanı topraklarında % 77'in üzerinde az ve çok az seviyede bulunmuştur. Çimrin ve ark. (2019) Gaziantep ili Nizip ilçesi zeytin bahçeleri topraklarının bor durumunun belirlenmesini amaçlamışlardır. Araştırma sonuçlarına göre; toprakların pH içerikleri 7.93-8.44; tuz içerikleri % 0.010-0.043; kil içerikleri % 33.04-61.04; kum içerikleri % 11.68-35.36; silt içerikleri % 18.32-50.32; kireç içerikleri % 8.11-93.28 ve alınabilir bor içerikleri 0.06-1.18 ppm arasında bulunmuştur. Çalışma bölgesi toprakları bor içeriği bakımından, 0-30 cm derinlikte % 85.00'inin çok az, % 10.00'u az ve % 5.00'nin yeterli düzeyde, 30-60 cm derinlikte ise % 95.00'i çok az ve % 5.00'i az düzeyde olduğu belirlenmiştir. Toprakların alınabilir bor içerikleri ile sadece silt içeriği arasında negatif önemli bir ilişki belirlenmiştir. Diğer taraftan, toprakların tuz içeriği ile kum ve kireç içerikleri arasında negatif, kil içerikleri arasında ise pozitif önemli ilişkiler belirlenmiştir. Ayrıca, toprakların kil içerikleri ile kum, silt ve kireç içerikleri arasında negatif ve silt içeriği ile kireç içeriği arasında ise pozitif önemli ilişkiler belirlenmiştir.

Bu çalışmada, Hatay ili Payas ilçesi zeytin bahçelerinin bulunduğu topraklarının yarayışlı bor düzeyi ve bunların bazı toprak özellikleri ile ilişkileri araştırılarak bölgedeki zeytin yetiştiricilerine faydalı bilgiler sunulması ve ileride yapılacak çalışmalara ışık tutulması amaçlanmıştır.

## 2.Materyal ve Yöntem

### 2.1.Materyal

Hatay ili Payas ilçesi zeytin bahçeleri topraklarında belirlenmiş 14 ayrı nokta (Şekil 1; Tablo 1) ve 2 farklı derinlikten (0-30 ve 30-60 cm) alınan 28 adet toprak örneğinde yarayışlı B, toprakların temel kimyasal ve fiziksel özelliklerin belirlenmesi amacıyla alınan topraklar analize hazır hale getirilmiştir.



Şekil 1. Alınan toprak örneklerinin harita üzerindeki görünümü

Tablo 1. Toprak örneklerinin alındığı yerler

Toprak No	Örnek Yeri	GPS ile E/W Koordinatları	Toprak No	Örnek Yeri	GPS İle E/W Koordinatları
1	Çağlalık -1	(36.7860; 36.2419)	8	Kozludere-1	(36.7657; 36.2443)
2	Çağlalık -2	(36.7859; 36.2443)	9	Kozludere-2	(36.7641; 36.2467)
3	Çağlalık -3	(36.7850; 36.2362)	10	Kozludere-3	(36.7642; 36.2471)
4	Yakacık-1	(36.7798; 36.2372)	8	Kozludere-1	(36.7657; 36.2443)
5	Yakacık-2	(36.7790; 36.2833)	11	Sahil-1	(36.7555; 36.2019)
6	Yakacık-3	(36.7749; 36.2342)	12	Sahil-2	(36.7540; 36.2004)
7	Çağlalık-4	(36.7799; 36.2398)	13	Tütenbaca	(36.7617; 36.2069)

## 2.2.Yöntem

Toprak örneklerinde yarıyıllı bor, pH, toplam çözünebilir tuz, KDK, kireç, OM ve bünye analizleri yapılmıştır. Toprakların yarıyıllı B analizi 0.01 M mannitol + 0.01 M CaCl<sub>2</sub> ekstraktı çözeltisi kullanılarak elde edilen süzükte ICP-OES cihazı kullanılarak belirlenmiştir (Cartwright ve ark. 1983). Toplam çözülebilir tuz; saturasyon çamurunun iletkenlik aletinde ölçülen direnç değerlerinden belirlenmiş, pH ise saturasyon çamurunda pH-metre ile ölçülmüştür (Horneck ve ark. 1989). KDK, sodium asetat (1N pH: 8.2) ekstraksiyon yöntemi ile belirlenmiştir (Knudsen ve ark. 1982). Toprakların kireç (CaCO<sub>3</sub>) içerikleri Scheibler kalsimetresi aleti ile ölçülmüştür (Nelson 1982), toprakların OM içerikleri, Nelson ve Sommers (1982) tarafından bildirildiği şekilde modifiye edilmiş Walkley-Black yöntemiyle belirlenmiştir. Çalışma alanı toprakların bünye içeriği ise hidrometre yöntemi ile (Bouyoucos 1952) saptanmıştır.

## 3.Araştırma Bulgular ve Tartışma

### 3.1.Toprakların Bazı Fiziksel ve Kimyasal Özellikleri

Araştırma topraklarının pH içeriği örneklerde en düşük 7.16 iken, en yüksek pH içeriği 8.30 olarak belirlenmiştir. Toprakların 0-30 cm derinliğindeki örneklerinin ortalama pH içeriği 7.85 iken 30-60 cm derinlikteki örneklerde ise 7.78 olup iki derinlikte ortalama olarak 7.81 bulunmuştur (Topaloğlu ve Yalçın 2023). Toprak örneklerinin Eyüboğlu (1999)'ın bildirdiği sınır değerleri göre pH'ları nötr ile hafif alkalın arasında değişmekle birlikte, alınan toprakların % 17.86'sı nötr (6.5-7.5) ve % 82.14'ü ise hafif alkalın (7.5-8.5) özellikte olduğu görülmüştür (Tablo 2) (Topaloğlu ve Yalçın 2023). Bayram ve ark. (2023) Adıyaman ili antepfıstığı bahçelerinin toprak örnekleri ile verimlilik durumlarının belirlenmesi amaçladıkları çalışmada toprakların pH içeriğinin 7.10-8.07 arasında değerler belirleyerek toprakların nötr ile hafif alkalın arasında

olduğunu ortaya koyarak benzer sonuçlar bildirmişlerdir.

Çalışma alanının topraklarının tuz içeriği örneklerde en düşük % 0.007 iken, en yüksek tuz içeriği % 0.226 olarak belirlenmiştir. Toprakların 0-30 cm derinlikteki örneklerin ortalaması tuz içeriği % 0.032 iken 30-60 cm derinlikteki örneklerde ise % 0.025 olup her iki derinliğin ortalaması olarak % 0.029 olarak bulunmuştur. Toprak örneklerinin Richards 1954'in bildirdiği sınır değerlere göre toprak örneklerinin % tuz içerikleri bir nokta hariç tüm profil boyunca tuzsuz sınıfında yer aldığı belirlenmiştir (Tablo 2). Yakın bölgede yapılan çalışmada, Gökçeoğlu ve Çimrin (2022) Hatay Altınözü ilçesi zeytin (*Olea europaea L.*) ağaçlarının yaprak ve toprak örnekleri ile beslenme durumunun belirlenmesini amaçladıkları çalışmada toprakların toplam tuz içeriği yönünden benzer sonuçlar ortaya koymuştur.

Çalışma alanı topraklarının sırasıyla kil, kum ve silt miktarları en düşük % 7.00, % 19.00 ve % 20.00 iken, en yüksek kil, kum ve silt miktarları % 43.00, % 73.00 ve % 48.00 olarak belirlenmiştir. Toprakların 0-30 cm derinliğindeki ortalama kil, kum ve silt miktarları % 22.14, % 44.29 ve % 33.57 iken 30-60 cm derinlikteki örneklerde ortalama ise % 23.14, % 44.43 ve % 32.43 olup ortalama olarak % 22.64, % 44.36 ve % 33.00 bulunmuştur. Hatay ili Payas ilçesi zeytin bahçeleri toprakları Çizelge 2'de görüldüğü gibi % 42.86'sı tın, % 25.00'i killi tın, % 14.28'i kumlu tın, % 10.72'si kumlu killi tın, % 3.57'si siltli killi tın ve % 3.57'si ise kil olmak üzere 6 farklı bünye sınıfına girmiştir (Tablo 2). Bu bölgede yapılan ve Amik ovası topraklarının sınıflandırılmasının ve özelliklerinin belirlenmesi isimli çalışmada Kılıç ve ark. (2004) benzer sonuçları bildirmiştir.

**Tablo 2.** Payas bölgesi topraklarının bor içerikleri ve bazı fiziksel ve kimyasal özellikleri

No	Derinlik	pH	Tuz %	Kil %	Kum %	Silt %	Bünye Sınıfı	Kireç %	O.M. %	KDK me/100gr	B mg/kg
1	0-30	7.69	0.020	33.00	35.00	32.00	CL	11.70	5.60	23.91	0.62
	30-60	7.37	0.010	21.00	39.00	40.00	L	11.70	4.35	22.88	0.99
2	0-30	7.88	0.011	17.00	45.00	38.00	L	9.30	4.47	15.95	0.42
	30-60	7.58	0.010	21.00	41.00	38.00	L	13.20	3.39	10.49	0.57
3	0-30	7.85	0.007	27.00	43.00	30.00	CL	10.70	3.93	18.78	1.02
	30-60	7.97	0.015	23.00	49.00	28.00	SCL	12.70	2.97	18.15	0.71
4	0-30	7.80	0.012	27.00	43.00	30.00	CL	4.90	3.00	17.83	0.43
	30-60	7.64	0.011	27.00	43.00	30.00	CL	3.40	2.03	17.33	0.69
5	0-30	7.39	0.026	25.00	49.00	26.00	SCL	3.90	4.30	19.21	0.48
	30-60	7.98	0.014	25.00	47.00	28.00	SCL	4.40	3.39	18.23	0.39
6	0-30	7.84	0.026	37.00	19.00	44.00	SiCL	4.00	5.32	26.31	0.41
	30-60	7.94	0.015	43.00	19.00	38.00	C	4.00	3.87	23.63	0.43
7	0-30	8.30	0.011	7.00	73.00	20.00	SL	19.50	1.94	11.06	0.48
	30-60	8.28	0.009	13.00	67.00	20.00	SL	17.10	1.70	10.91	0.67
8	0-30	7.89	0.012	17.00	55.00	28.00	SL	7.80	4.31	21.73	0.96
	30-60	7.90	0.011	19.00	49.00	32.00	L	11.40	3.59	21.09	0.85
9	0-30	8.20	0.007	11.00	41.00	48.00	L	7.80	3.55	17.97	0.54
	30-60	7.90	0.025	15.00	51.00	34.00	L	9.90	2.27	16.48	0.73
10	0-30	8.29	0.011	9.00	55.00	36.00	SL	7.80	1.18	11.13	0.82
	30-60	7.86	0.009	11.00	49.00	40.00	L	8.30	1.42	13.17	0.48
11	0-30	8.08	0.014	23.00	43.00	34.00	L	18.80	3.19	16.23	0.64
	30-60	7.80	0.010	25.00	43.00	32.00	L	21.90	2.85	15.38	0.73
12	0-30	7.81	0.010	29.00	35.00	36.00	CL	10.70	3.77	21.09	0.39
	30-60	7.76	0.015	31.00	37.00	32.00	CL	12.70	3.65	20.79	0.44
13	0-30	7.44	0.226	25.00	43.00	32.00	L	6.90	5.31	20.16	0.97
	30-60	7.81	0.160	23.00	45.00	32.00	L	8.40	4.53	19.56	1.06
14	0-30	7.47	0.051	23.00	41.00	36.00	L	7.40	5.24	23.10	0.86
	30-60	7.16	0.043	27.00	43.00	30.00	CL	6.80	4.73	23.64	0.95
<b>Min</b>		<b>7.16</b>	<b>0.007</b>	<b>7.00</b>	<b>19.00</b>	<b>20.00</b>		<b>3.40</b>	<b>1.18</b>	<b>10.49</b>	<b>0.39</b>
<b>Max</b>		<b>8.30</b>	<b>0.226</b>	<b>43.00</b>	<b>73.00</b>	<b>48.00</b>		<b>21.90</b>	<b>5.60</b>	<b>26.31</b>	<b>1.06</b>
<b>Ort.(Av.)</b>	<b>0-30</b>	<b>7.85</b>	<b>0.032</b>	<b>22.14</b>	<b>44.29</b>	<b>33.57</b>		<b>9.37</b>	<b>3.94</b>	<b>18.89</b>	<b>0.65</b>
<b>Ort.(Av.)</b>	<b>30-60</b>	<b>7.78</b>	<b>0.025</b>	<b>23.14</b>	<b>44.43</b>	<b>32.43</b>		<b>10.42</b>	<b>3.20</b>	<b>17.98</b>	<b>0.69</b>
<b>Genel</b>	<b>Ort. (Av.)</b>	<b>7.81</b>	<b>0.029</b>	<b>22.64</b>	<b>44.36</b>	<b>33.00</b>		<b>10.31</b>	<b>3.57</b>	<b>18.44</b>	<b>0.67</b>

Araştırma topraklarının kireç içeriği örneklerde en düşük % 3.40 iken, en yüksek kireç içeriği % 21.90 olarak belirlenmiştir. Toprakların 0-30 cm derinliğindeki örneklerinin ortalama kireç içeriği % 9.37 iken 30-60 cm derinliklerde ise % 10.42 olup, iki derinlikte ortalama olarak % 9.37 bulunmuştur. Toprak örneklerinin Loeppert ve Suarez (1996)'ın bildirdiği değerlere göre kireç içerikleri kireçli ile fazla kireçli arasında değişmekle birlikte, toprakların % 21.44'ü kireçli (% 1-5), % 64.28'i orta kireçli (% 5-15) ve % 14.28'si ise fazla kireçli (% 15-25) olarak görülmüştür (Tablo 2). (Topaloğlu ve Yalçın 2023). Yakın bir bölgede yapılan çalışmada, Kılıç ve ark. (2023) Kilis ili tarım topraklarının beslenme durumunun incelenmesini amaçladıkları çalışmada toprakların kireç içerikleri yönünden % 90'ın üzerinde orta ve fazla kireçli düzeyde olduğunu benzer şekilde ortaya koymuşlardır.

Topraklarının organik madde içeriği örneklerde en düşük % 1.18 iken, en yüksek organik madde % 5.60 olarak belirlenmiştir. Toprakların 0-30 cm derinliğindeki örneklerinin ortalama organik madde % 3.94 iken 30-60 cm derinlikteki örneklerde ise % 3.20 olup iki derinlikte ortalama olarak % 3.57 bulunmuştur. Toprak örneklerinin Ülgen ve Yurtsever (1995)'in verdiği sınır değerlere göre organik maddeleri az ile çok yüksek arasında değişmekle birlikte, toprakların % 14.28'i az (% 1-2), % 17.85'i orta (% 2-3), % 32.15'i yüksek (% 3-4) ve % 35.72'si ise çok yüksek (% >4) oranda organik madde görülmüştür (Tablo 2). (Topaloğlu ve Yalçın 2023). Gökpinar ve Yalçın (2020) Hatay ili Arsuz bölgesi topraklarının pH, kireç, organik madde ve katyon değişim kapasitesi içeriklerinin belirlendiği çalışmada toprakların organik madde içeriğinin % 87'nin üzerinde az ve orta değerler olarak ortaya koyarak benzer sonuçlar bildirmişlerdir.

Topraklarının KDK içeriği örneklerde en düşük 10.49 me/100g iken, en yüksek KDK 26.31 me/100g olarak belirlenmiştir. Toprakların 0-30 cm derinliğindeki örneklerinin ortalama KDK 18.89 me/100g iken 30-60 cm derinlikteki örneklerde ise 17.98 me/100g olup iki derinlikte ortalama olarak 18.44 me/100g bulunmuştur. Toprak örneklerinin KDK değerleri içerisinde *düşük* ve *orta* sınıfta hiç örneğin olmadığı, örneklerin % 71.25'inin çok yüksek sınıfta ve % 28.75'inin yüksek sınıfta yer aldığı tespit edilmiştir (Tablo 2). Yalçın ve Çimrin (2021) Hatay ili Kırıkhan-Reyhanlı bölgesi topraklarının besin elementi durumları ve bunların bazı toprak özellikleri ile ilişkilerinin belirlendiği çalışmada toprakların KDK içeriği 16.89-42.10 me /100 g olup ortalama KDK içeriği ise 31.53 me/100 g arasında belirleyerek bulgular ile uyumlu sonuçlar ortaya koymuşlardır.

Toprakta yarayışlı Bor (B) incelendiğinde; toprak örneklerinde en düşük B içeriği 0.39 mg/kg iken, en yüksek B içeriği 1.06 mg/kg olarak bulunmuştur. Toprakların 0-30 cm örneklerin bor içeriği 0.65 mg/kg iken, 30-60 cm örneklerinin ise 0.69 mg/kg olup ortalama olarak 0.67 mg/kg olarak bulunmuştur. Wolf (1971) toprak bor sınır değerlerine göre karşılaştırıldığında bölgenin topraklarının B içeriği bakımından 0-30 cm derinlikte % 42.86'sı çok az (<0.49 mg/kg), % 50.00'sinin az (0.50-0.99 mg/kg), % 7.14'ü yeterli (1.00-2.40 mg/kg) düzeyde, 30-60 cm derinlikte ise % 28.57'si çok az (<0.49 mg/kg), % 64.29'u

az (0.50-0.99 mg/kg) ve % 7.14'ü ise yeterli (1.00-2.40 mg/kg) düzeyde olduğu belirlenmiştir (Tablo 2). Yalçın (2023) Hatay ili Arsuz ilçesi topraklarının yarayışlı bor içeriği ve bazı toprak özellikleri ile ilişkilerinin belirlendiği çalışmada toprakların yarayışlı bor içerikleri açısından % 91'in üzerinde çok az ile az değerler elde ederek benzer sonuçlar bildirmişlerdir. Benzer şekilde Kilis ilinde yapılan çalışmada da zeytin bahçelerinin B, Zn, P ve Mg bakımından önemli bitki besleme sorunlarının olduğu belirlenmiştir (Semercioğlu ve ark. 2023).

### 3.2. Yarayışlı Bor İçeriği İle Diğer Bazı Toprak Özellikleri Arasındaki İlişkiler

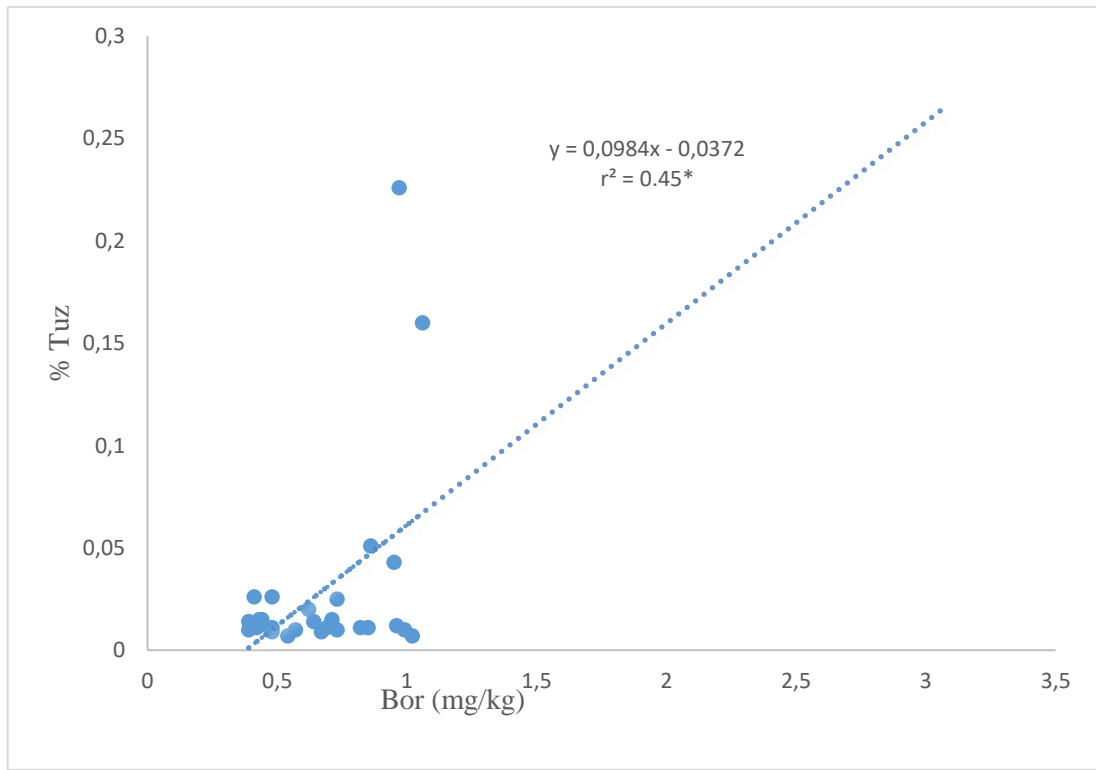
Araştırma konusu toprak özelliklerinin bazı fiziksel ve kimyasal özellikleri ile yarayışlı bor içerikleri arasındaki ilişkiler Tablo 3'de verilmiştir. Tablonun incelenmesinden de anlaşılacağı gibi yarayışlı bor ile tuz içeriği arasında (r: 0.45\*; Şekil 2) pozitif önemli ilişki belirlenmiştir. Aynı bölgede yapılan çalışmada, Özsayar ve Çimrin (2022) Hatay ili Hassa ilçesi zeytin ağaçlarının yaprak ve toprak örnekleri ile beslenme durumunun belirlenmesi isimli çalışmalarında, toprakların yarayışlı bor içeriği ile tuz içeriği arasında pozitif önemli ilişki ortaya koyarak benzer sonuçlar bildirmişlerdir. Ayrıca toprakların pH içerikleri ile kil içeriği (r:-0.44\*), organik madde (r: -60\*\*) ve KDK (r:-0.52\*\*) arasında negatif önemli ilişkiler belirlenirken, toprakların pH içeriği ile kum (r: 0.39\*) içeriği arasında ise oldukça önemli pozitif ilişkiler belirlenmiştir. Atmaca ve Nalbant (2020) Giresun ili Şebinkarahisar ilçesinde farklı topoğrafyalarda oluşmuş toprakların tarımsal özellikleri incelendikleri çalışmalarında, toprakların pH içerikleri ile organik madde içerikleri arasında negatif önemli ilişki belirlenmiş olup benzer sonuçlar bildirmiştir. Toprakları tuz içeriği ile organik madde (r: 0.42\*) arasında ise pozitif ilişki belirlenmiştir. Toprakların kil içeriği ile kum içeriği (r: -0.83\*\*) arasında negatif önemli ilişki belirlenirken, kil ile organik madde (r: 57\*\*) ve KDK içeriği arasında ise pozitif (r: 0.71\*\*) ilişkiler belirlenmiştir. Kalkancı ve ark. (2023) Gaziantep ili antepfıstığı yetiştirilen toprakların bazı verimlilik özelliklerinin belirlenmesini amaçladıkları çalışmada, toprakların kil içeriği ile kum içeriği arasında önemli negatif ilişki belirleyerek benzer sonuçlar bildirmişlerdir. Ayrıca çalışmada toprakların kum içerikleri ile silt içerikleri (r: -0.66\*\*), organik madde (r: -0.57\*\*) ve KDK (r: -0.69\*\*) aralarında negatif önemli ilişkiler belirlenirken kum içeriği ile kireç içeriği (r: 0.41\*) arasında ise pozitif önemli ilişki belirlenmiştir. Çimrin ve ark. (2018) Gaziantep ili antepfıstığı bahçeleri topraklarının bor durumunu belirledikleri çalışmada, toprakların kum içerikleri ile kireç içerikleri arasında önemli negatif ilişki belirleyerek benzer sonuçlar ortaya koymuşlardır. Aynı zamanda toprakların kireç ile KDK arasında ise negatif önemli (r: -0.46\*) ilişki belirlenmiştir. Aynı bölgede yapılan çalışmada, Yalçın ve Çimrin (2021) Hatay ili Kırıkhan-Reyhanlı bölgesi topraklarının besin elementi durumları ve bunların bazı toprak özellikleri ile ilişkilerinin belirlendiği araştırmada, toprakların kireç içeriği ile KDK içeriği arasında negatif önemli ilişki ortaya koyarak benzer sonuçlar bildirmiştir. Toprakların organik madde içeriği ile KDK (r: 0.80\*\*) arasında ise pozitif önemli ilişkiler belirlenmiştir.



**Tablo 3.** Payas bölgesi zeytin bahçesi topraklarının yarayışlı Bor ile bazı toprak özellikleri arasındaki korelasyon katsayıları (r)

	B mg/kg	pH	Tuz (%)	Kil (%)	Kum (%)	Silt (%)	Kireç (%)	OM (%)
pH	-0.30							
Tuz (%)	0.45*	-0.33						
Kil (%)	-0.16	-0.44*	0.11					
Kum (%)	0.19	0.39*	-0.06	-0.83**				
Silt (%)	-0.13	-0.10	-0.04	0.13	-0.66**			
Kireç (%)	0.08	0.34	-0.20	-0.33	0.41*	-0.29		
OM (%)	0.20	-0.60**	0.42*	0.57**	-0.57**	0.24	-0.30	
KDK(me/100gr)	0.15	-0.52**	0.19	0.71**	-0.69**	0.27	-0.46*	0.80**

\* 0.05 düzeyinde önemli, \*\*\* 0.001 düzeyinde önemli

**Şekil 2.** Toprak örneklerinin B ile tuz içerikleri arasındaki ilişki

Aynı bölgede yapılan bir çalışmada, Gökpinar ve Yalçın (2020) Hatay ili Arsuz bölgesi topraklarının pH, kireç, organik madde ve KDK içeriklerinin belirlenmesi araştırmış ve toprakların organik madde içeriği ile KDK içeriği arasında pozitif önemli ilişki ortaya koyarak benzer sonuçlar bildirmişlerdir.

#### 4.Sonuç

Hatay ili Payas ilçesi zeytin bahçesi topraklarının, pH'sı 7.16 ile 8.30 arasında değiştiğini ve genellikle nötr ve hafif alkalın olduğu belirlenmiştir. Topraklardaki toplam tuz içeriği ise % 0.007 ile % 0.226 arasında değişmektedir; ancak bir nokta dışında tüm bölge topraklarının tuzsuz sınıfa girdiği belirlenmiştir. Çalışma alanında bünye içerikleri incelendiğinde, kil, kum ve silt miktarlarının sırasıyla % 7.00 ile % 43.00, % 19.00 ile % 73.00 ve %

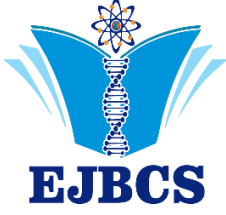
20.00 ile % 48.00 arasında değiştiği görülmüştür. Özellikle, % 68'inin tın ve killi tın sınıfında olduğu tespit edilmiştir. Kireç içeriği genel olarak % 3.40 ile % 21.90 arasında değişmektedir ve çoğunlukla orta seviyede kireçli topraklar bulunmaktadır. Organik madde içeriği ise % 1.18 ile % 5.60 arasında değişmekte olup, genellikle yüksek ve çok yüksek seviyelerde olduğu belirlenmiştir. Toprakların katyon değişim kapasitesi 10.49 ile 26.31 me/100 g arasında değişmektedir ve yarayışlı B içeriği 0.39 ile 1.06 mg/kg arasındadır; ancak çalışma alanının % 85'inden fazlasında yetersiz B içeriği bulunmaktadır. Analiz sonuçlarına göre, çalışma alanının en önemli sorunları arasında ince bünye, yetersiz drenaj, yüksek kireç içeriği ve yetersiz yarayışlı B içeriği yer almaktadır. Tuzluluk sorunu ise sadece bir noktada tespit edilmiştir. Özellikle, yetersiz B içeriği zeytin bahçesi topraklarının verimini olumsuz yönde





etkilemektedir. Bu sorunun çözümü için toprakların B içerikli gübrelere gübrenmesi gerekmektedir. Ancak, bu işlem sırasında bitki besin elementlerinin alına bilirlğini engelleyen toprak özellikleri göz önünde bulundurulmalı ve çiftçiler bilinçlendirilerek yetersiz B içeriğinin azaltılması amaçlanmalıdır.

### Kaynaklar

- Atmaca B, Nalbant H. 2020. Giresun ili Şebinkarahisar ilçesinde farklı topoğrafyalarda oluşmuş toprakların tarımsal özellikleri. Toprak Bilimi ve Bitki Besleme Dergisi 8(2):145-156.
- Açıkel K, Yalçın M. 2021. Hatay ili Reyhanlı-Kumlu bölgesi topraklarının yarayışlı bor içeriği ve bazı toprak özellikleri ile ilişkilerinin belirlenmesi. MAS Journal of Applied Sciences 6(3):551-563.
- Bayram C.A, Büyük G, Kıyas N, Uçar A. 2023. Adıyaman ili antepfıstığı bahçelerinin toprak örnekleri ile verimlilik durumlarının belirlenmesi. Mustafa Kemal Üniversitesi Tarım Bilimleri Dergisi, 28(2):308-318.
- Bouyoucos GJ. 1952. A recalibration of the hydrometer for making mechanical analysis of soil. Agro Jour. 43(9):434-438.
- Cartwright B, Tiller KG, Zarcinas BA, Spouncer LR. 1983. The chemical assessment of the boron status of soils. Aust J Soil Res. 21: 321-332.
- Çimrin KM, Yalçın M, Bozgeyik T. 2018. Gaziantep ili antepfıstığı bahçeleri topraklarının bor durumunun belirlenmesi. Ziraat Fakültesi Dergisi 13(2):18-26.
- Çimrin KM, Yalçın M, Keleş N. 2019. Gaziantep ili Nizip ilçesi zeytin bahçeleri topraklarının bor durumunun belirlenmesi. Ziraat Fakültesi Dergisi, 24(1):1-6.
- Esen M. 2019. Toprak yıkama yöntemiyle Cd ve Pb ile kirlenmiş tarımsal toprakların iyileştirilmesi. Aksaray Üni Fen Bil Ens Ç.M.A.D. Yüksek Lisans Tezi, p 77.
- Eyüboğlu F. 1999. Türkiye topraklarının verimlilik durumu. Top ve Güb Arş. Ens. Yay, Genel yayın No: 220, Teknik Yayınlar No: T.67, Ankara.
- Gökçeoğlu K, Çimrin KM. 2022. Hatay Altınözü ilçesi zeytin (*Olea europaea L.*) ağaçlarının yaprak ve toprak örnekleri ile beslenme durumunun belirlenmesi. ISPEC Journal of Agricultural Sciences 6(4): 680-697.
- Gökçınar R.C, Yalçın M. 2020. Hatay ili Arsuz bölgesi topraklarının pH, kireç, organik madde ve KDK içeriklerinin belirlenmesi. Eurasian J Bio Chem Sci. 3(1):31-37.
- Güneş A, Gezgin S, Kalınbacak K, Özcan H, Çakmak İ. 2017. Bor elementinin bitkiler için önemi. BORON, 2:108-174.
- Gürel S, Başar H, Çelik H, Ataç T. 2010. Yapaktan uygulanan borlu gübrelerin kiraz ağaçlarının gelişimi üzerine etkisi. 5. Ulusal Bitki Bes. ve Güb. Kong. Bildiri Kitabı, 15-17 Eylül 2010, Ege Üniversitesi, , 41-47, Bornova, İzmir.
- Horneck DA, Hart JM, Topper K, Koepsell B. 1989. Methods of soil analysis used in the soil testing laboratory at Oregon. State University. P 1-21. Agr. Exp. Sta. Oregon, USA.
- Kalkancı N, Şimşek T, İlikçioğlu E, Büyük G, Aslan N. 2023. Antepfıstığı yetiştirilen toprakların bazı verimlilik özelliklerinin belirlenmesi. OKÜ Fen Bil Ens Der, 6(3):2171-2182.
- Kılıç Ş, Ağca N, Yalçın M. 2004. Soils of amik plain (Turkey): properties and classification. Jour Agr. (4):291-295.
- Kılıç A, Kuzucu M, Gökçen İ.S. 2023. Kilis ili tarım topraklarının beslenme durumunun incelenmesi. Tekirdağ Ziraat Fakültesi Dergisi, 20(3): 631- 641.
- Knudsen D, Peterson GA, Pratt PF 1982. Lithium, Sodium, and Potassium. In: A.L. Page (editor). Methods of Soil Analysis Part 2. Chemical and Microbiological Properties. Second edition ASA, Inc, 9: 225-246, Wisconsin.
- Loeppert RH, Suarez DL. 1996. Carbonate and gypsum. in methods of soil analysis. Part 3. Chemical Methods, 437-474. Edited by DL. Spark. Madison, Wisconsin, USA.
- Özsayar MM, Çimrin KM. 2022. Hatay ili Hassa ilçesi zeytin ağaçlarının yaprak ve toprak örnekleri ile beslenme durumunun belirlenmesi. ISPEC, 6(1): 42-57.
- Nelson RE. 1982. Carbonate and gypsum. methods of soil analysis Part 2. chemical and microbiological properties second edition. Agronomy. No: 9 Part 2. Edition P: 191- 197.
- Nelson DW, Sommers LE. 1982. Organic matter. methods of soil analysis part 2. chemical and microbiological properties second edition. Agronomy, No: 9 Part 2. Edition P: 574- 579.
- Richards LA. 1954. Diagnosis and improvement of saline and alkali soils. USDA Handbook. 60 p.
- Semercioğlu TŞ, Kalkancı N, Kösetürkmen S, Büyük G, Aslan N. 2023. Kilis ilindeki zeytinlik alanları için toprak kalitesinin değerlendirilmesi. Mustafa Kemal Üniversitesi Tarım Bilimleri Dergisi, 28(1):211-221.
- Sevindik M, Akgül H, Pehlivan M, Selamoğlu Z. 2017. Determination of therapeutic potential of mentha longifolia ssp. longifolia. Fresen Environ Bull. 26: 4757-4763.
- Topaloğlu A, Yalçın M. 2023. Hatay ili Payas ilçesi zeytin bahçesi topraklarının pH, kireç ve organik madde içeriklerinin belirlenmesi. ISPEC. 7(2): 245-254.
- Tunalıoğlu R, Karahocagil P. 2004. Zeytinyağı ve sofralık zeytin durum tahmin: 2003- 2004. Tar. Eko. Arş. Ens. Yayın No: 118.
- Ülgen N, Yurtsever N. 1995. Türkiye gübre ve gübreleme rehberi (4. baskı). T.C. Başba. Köy Hiz. Gen. Müd. Top. ve Güb. Arş. Enst.Müd.Yay, Genel Yayın No: 209, Teknik Yayınlar No: T.66, Ankara.
- Wolf B. 1971. The determination of boron in soil extracts, plant materials, composts, manures, water and nutrient solutions. Soil Sci and Plant Ana, 2:363-374.
- Yalçın M. 2023. Hatay ili Arsuz ilçesi topraklarının yarayışlı bor içeriği ve bazı toprak özellikleri ile ilişkilerinin belirlenmesi. MAS Journal of Applied Sciences. 8(2): 222-231.
- Yalçın M, Çimrin KM. 2021. Hatay ili Kırıkhan-Reyhanlı bölgesi topraklarının besin elementi durumları ve bunların bazı toprak özellikleri ile ilişkileri. ISPEC, 5(4): 773-785.



## Dörtüyl ovası topraklarının temel özelliklerinin belirlenmesi ve yersel dağılımlarının coğrafi bilgi sistemleri (CBS) kullanılarak haritalanması

Emine Derya Aşkner<sup>1</sup> , Necat Ağca<sup>2\*</sup> 

<sup>1</sup>Tarım ve Orman İl Müdürlüğü, Afyonkarahisar, Türkiye

<sup>2</sup>Mustafa Kemal Üniversitesi, Ziraat Fakültesi, Toprak Bilimi ve Bitki Besleme Bölümü, Hatay, Türkiye

\*Corresponding author : [necagca@gmail.com](mailto:necagca@gmail.com)  
Orcid No: <https://orcid.org/0000-0003-4864-844X>

Received : 12/04/2024  
Accepted : 10/08/2024

**To Cite / Atf için:** Aşkner ED, Ağca N 2024. Dörtüyl ovası topraklarının temel özelliklerinin belirlenmesi ve yersel dağılımlarının coğrafi bilgi sistemleri (CBS) kullanılarak haritalanması. Eurasian J Bio Chem Sci, 7(2):83-95. <https://doi.org/10.46239/ejbc.1467664>

**Özet:** Bu çalışmada, Dörtüyl ovasındaki toprakların temel fiziksel ve kimyasal özellikleri belirlenmiş ve bu özelliklerin çalışma alanındaki yersel dağılım haritaları oluşturulmuştur. Çalışma alanından, alanı temsil edecek şekilde, rastgele örnekleme yöntemi kullanılarak, 0-30 cm derinlikten toplam 48 adet bozulmuş toprak örneği alınmıştır. Toprak örneklerinde; pH, elektriksel iletkenlik (EC), kireç, organik madde (OM), hava kuru nem içeriği ve bünye (tekstür) analizleri yapılmıştır. Ayrıca örnekleme noktalarının koordinatları GPS cihazı (UTM koordinat sistemine göre) ile belirlenmiştir. Toprak özelliklerine ait bütün parametrelerin tanımlayıcı istatistik analizleri hesaplanmıştır. Toprak özelliklerinin yersel değişiminin modellenmesinde jeostatistik yöntemler, haritalanmasında ise coğrafi bilgi sistemleri (CBS) kullanılmıştır. Toprak özelliklerinden pH 7.20 ile 7.78, EC 99  $\mu\text{S cm}^{-1}$  ile 997  $\mu\text{S cm}^{-1}$ , kireç % 0.57 ile % 13.17, organik madde % 0.55 ile % 8.95, nem içeriği % 1.34 ile % 9.48 arasında değişmiştir. Toprak özelliklerinin varyasyon katsayıları (VK) % 1.86 (pH) ile % 69.24 (kireç) arasında değişmiştir. Toprak özelliklerinden pH, EC, kireç ve OM için Üssel (Exponential); nem, kum ve kil için Gaussian, silt için ise Doğrusal (Linear) model en uygun yarıvaryogram modeli olarak belirlenmiştir.

**Anahtar kelimeler:** Dörtüyl ovası, kriging metodu, Coğrafi bilgi sistemleri (CBS), Toprak özellikleri

### *Determining the basic characteristics of Dörtüyl plain soils and mapping their spatial distribution using geographic information systems (GIS)*

**Abstract:** In this study, the basic physical and chemical properties of the soils in the Dörtüyl plain were determined and the spatial distribution maps of these properties in the study area were created. A total of 48 degraded soil samples were taken from the study area, from a depth of 0-30 cm, using the random sampling method to represent the area. In soil samples; pH, electrical conductivity (EC), lime, organic matter (OM), air dry moisture content and texture (texture) were analyzed. In addition, the coordinates of the sampling points were determined with a GPS device (according to the UTM coordinate system). Descriptive statistical analyzes of all parameters of the soil properties were calculated. Geostatistical methods were used to model the spatial changes in soil properties, and geographic information systems (GIS) were used to map of them. From soil characteristics, pH ranged from 7.20 to 7.78, EC ranged from 99  $\mu\text{S cm}^{-1}$  to 997  $\mu\text{S cm}^{-1}$ , lime ranged from 0.57% to 13.17%, organic matter ranged from 0.55% to 8.95%, and moisture content ranged from 1.34% to 9.48%. The coefficient of variation (VK) of soil parameters varied between 1.86% (pH) and 69.24% (lime). Exponential model for pH, EC, lime and OM; Gaussian model for for moisture, sand and clay; Linear model for silt content were determined as the most suitable semivariogram model.

**Keywords:** Dörtüyl plain, kriging method, Geographic information systems (GIS), Soil properties

#### 1. Giriş

Toprakların temel özellikleri, toprak verimliliği açısından büyük önem taşımaktadır. Bu nedenle bitkisel üretim yapılacak toprakların özelliklerinin yersel

dağılımının bilinmesi son çok önemlidir. Toprakların verimli olabilmesi için; sürdürülebilir, çevre ile uyumlu, insanlığın ve doğanın devamlılığına yönelik tarımsal faaliyetlerin benimsenmesi gerekmektedir. Toprakların verimli ve sürdürülebilirliği için

toprakların verimlilik ile ilgili özellikleri incelenmeli ve gerekli olan eksiklikler ve işlemler değerlendirilerek nasıl bir yol izlenmesi gerektiği belirlenmelidir. Bunun için de topraklardan belirli dönemlerde örnekler alınarak analiz edilmeli ve çıkan sonuçların çok yönlü olarak incelenerek; bölge iklim, toprak yapısı ve jeolojik yapı ile beraber değerlendirilmesiyle doğru bir toprak yönetim şekli belirlenmelidir.

Toprakların özellikleri derinliklerine bağlı olarak önemli ölçüde değişmektedir. Ancak bu değişim sadece derinliğe bağlı olarak değil, aynı zamanda yersel uzaklıklarda da anlamlı olarak değişmektedir. Bitkisel üretim açısından bu değişimlerin belirlenip, jeostatistiksel yöntemlerle değerlendirilmesi; tarımsal üretimde daha etkin ve daha ekonomik gübreleme ve toprağın sürdürülebilir kullanımı açısından son derece önem taşımaktadır. Günümüzde, toprak özellikleri ilgili çalışmalarda jeostatistik birçok gelişmiş ülkede üretilmekte, elde edilen veriler de toprak verimliliğini artırılmasında, gereksiz tarım kimyasallarının kullanımını önlenmesinde, toprak ve çevrenin korunması gibi konularında önemli katkılar sağlamaktadır (Hatipoğlu 2019).

Jeostatistik, ölçülen herhangi bir özelliğin yersel yapısını ve mekânsal bağımlılığını inceleyen ve sayısalılaştıran ve buradan elde edilen ilişkiyi kullanarak anılan özelliğin örneklenmemiş noktadaki değerlerini tahmin eden uygulamalı istatistiğin bir kolu olarak tanımlanmaktadır (Isaaks ve Srivastava 1989).

Coğrafi bilgi sistemleri (CBS) ise her tür coğrafi bilgiyi verimli bir şekilde elde etmek, depolamak, değiştirmek, yönetmek, analiz etmek ve görüntülemek ve haritalamak için tasarlanmış organize bir bilgisayar donanımı, yazılımı ve coğrafi veri seti olarak tanımlanmaktadır (ESRI, 2022). CBS'nin uygulanabileceği alanlar çok geniştir. Ağırlıklı olarak CBS, mekânsal planlama, devlet yöntemi, bütünleşmiş kurtarma sistemi hizmetleri, ulaşım, kaynak yönetimi, kamu hizmetleri, güvenlik ve askeri sektör, çevre, perakende, vergi gibi mekânsal verilerle çalışmanın gerekli olduğu alanlarda kullanılabilir. CBS'nin en önemli kullanım alanlarından biri de toprak özelliklerinin haritalanmasıdır (Çabuk ve ark. 2018).

Başbozkurt ve ark. (2013) tarafından "Çamgazi Toplulaştırma ve TİGH (Tarla İçi Geliştirme Hizmetleri) Projesi" kapsamında Adıyaman'ın Merkez ilçesine ait 19 köyü kapsayan alanda yapılan bir çalışmada; toprak özelliklerinin mekânsal değişim deseni belirlenmiştir. Araştırma sonuçlarına göre çalışma alanı topraklarının mekânsal bağımlılık derecelerinin genellikle orta ve yüksek düzeylerde olduğu belirlenmiştir. Ayrıca araştırmacılar, incelenen toprak özelliklerine ait yersel değişim haritaları yardımıyla çalışma alanında daha etkin toprak ve bitki

yönetim stratejilerinin belirlenmesinin mümkün olabileceğini belirtmişlerdir.

Şanlıurfa ili Halfeti İlçesi'nde yapılan bir çalışmada; toprakların bazı özellikleri ve bitki besin elementi kapsamının belirlenmesi amaçlanmıştır. Analiz sonuçlarına göre; toprakların kil bünyeli, kireçli, organik madde bakımından yetersiz olduğu belirlenmiştir (Saraçoğlu ve ark. 2014).

Akın ve Taşova (2019) tarafından yapılan bir çalışmada; İç Anadolu Bölgesi tarım topraklarının bazı özellikleri ve bitki besin element içerikleri belirlenmiş ve coğrafi bilgi sistemleri kullanılarak bunların haritaları yapılmıştır. Araştırma sonucuna göre, Topraklarının %75.9'u killi tın ve tın bünyelidir. Yine, bölge topraklarının %89.2'sini hafif alkali ve %99.4'ünü ise tuzsuz topraklar oluşturmaktadır. Topraklarının %85.5'i az ve çok az organik madde; sınıfındadır. %56.1'i ise fazla ve çok fazla kireçlidir.

Kars ve Ekberli (2019) tarafından yapılan çalışmada, Çarşamba Ovasının buğday bitkisi yetiştirilen tarım topraklarının bazı fiziksel, kimyasal özellikleri belirlenmiş ve bunların çalışma alanındaki dağılımı araştırılmıştır. Araştırma sonuçlarına göre, toprakların çoğunluğu killi tın bünyelidir. Toprakların bir çoğunluğu (%72.5'i) hafif bazik reaksiyonlu, tuzsuz ve değişik miktarlarda kireç içermekte olup, organik madde miktarlarının ise orta düzeyde belirlenmiştir.

Tepecik ve ark. (2022) tarafından Ege Üniversitesi Ziraat Fakültesi Menemen Araştırma, Uygulama ve Üretim Çiftliği arazisinde yapılan bir çalışmada; toprakların verimlilik ile ilgili özellikleri belirlenmiş ve bunların haritaları oluşturulmuştur. Araştırma sonucunda; toprakların pH değerlerinin 7.32-8.90 arasında değişim gösterdiği ve çoğunluğunun hafif bazik karakterde olduğu görülmüştür. Toprakların elektrik iletkenlikleri 586.16-2860.0  $\mu\text{S cm}^{-1}$  arasında değişirken, yaklaşık % 90'lık bölümünün kum bünyeli olduğu belirlenmiştir. Toprakların toplam karbonat içerikleri % 4.46-15.65 arasında ve kireç bakımından zengin sınıfta yer almaktadır. Toprakların organik madde içeriği % 0.05-2.97 arasında değişim göstermiş ve toprakların %60 gibi büyük bir bölümünün organik maddece fakir olduğu saptanmıştır.

Bu çalışmada, Dörtüol ovasındaki toprakların temel fiziksel ve kimyasal özellikleri belirlenmiş ve Coğrafi Bilgi Sistemleri (CBS) ile bu özelliklerin çalışma alanındaki yersel dağılım haritaları oluşturulmuştur.

## 2. Materyal ve Yöntem

### 2.1. Materyal

Çalışma alanı 36048'95" - 36051'29" kuzey enlemleri ile 36008'45" - 36010'47" doğu boylamları arasında yer almaktadır. Çalışma alanı doğudan Amanos dağları, batıdan Akdeniz, kuzeyden Erzin ve güneyden

ise Payas ilçesi ile sınırlanmış olup, yaklaşık 4000 hektarlık bir alan kaplamaktadır.

Ovanın doğusunda bunar dağlık bölgede genellikle çam ve meşeden oluşan orman ağaçları yer almaktadır. Ovanın özellikle doğu kesimlerinde, turunçgil üretiminin çok yaygın olduğu görülmektedir. Alanın ortasında bulunan Haydar dağında ise kuru tarım yapılmaktadır. Burada yetiştirilen en önemli ürünler soğan ve tahıl bitkileridir. Ovada ise sebzeçilik, pamuk, yerfıstığı ve susam üretimi giderek yaygınlaşmıştır. Dörtüol ovası aynı zamanda Türkiye'nin en önemli turunçgil üretim merkezlerinden birisidir (Doyuran 1982).

Çalışma alanında tipik Akdeniz iklimi hüküm etkindir. Çalışma alanının yer aldığı Hatay'da yıllık ortalama yağış toplamı 1161.5 mm, yıllık ortalama sıcaklık ise 18.30C'dir (Anonim 2022).

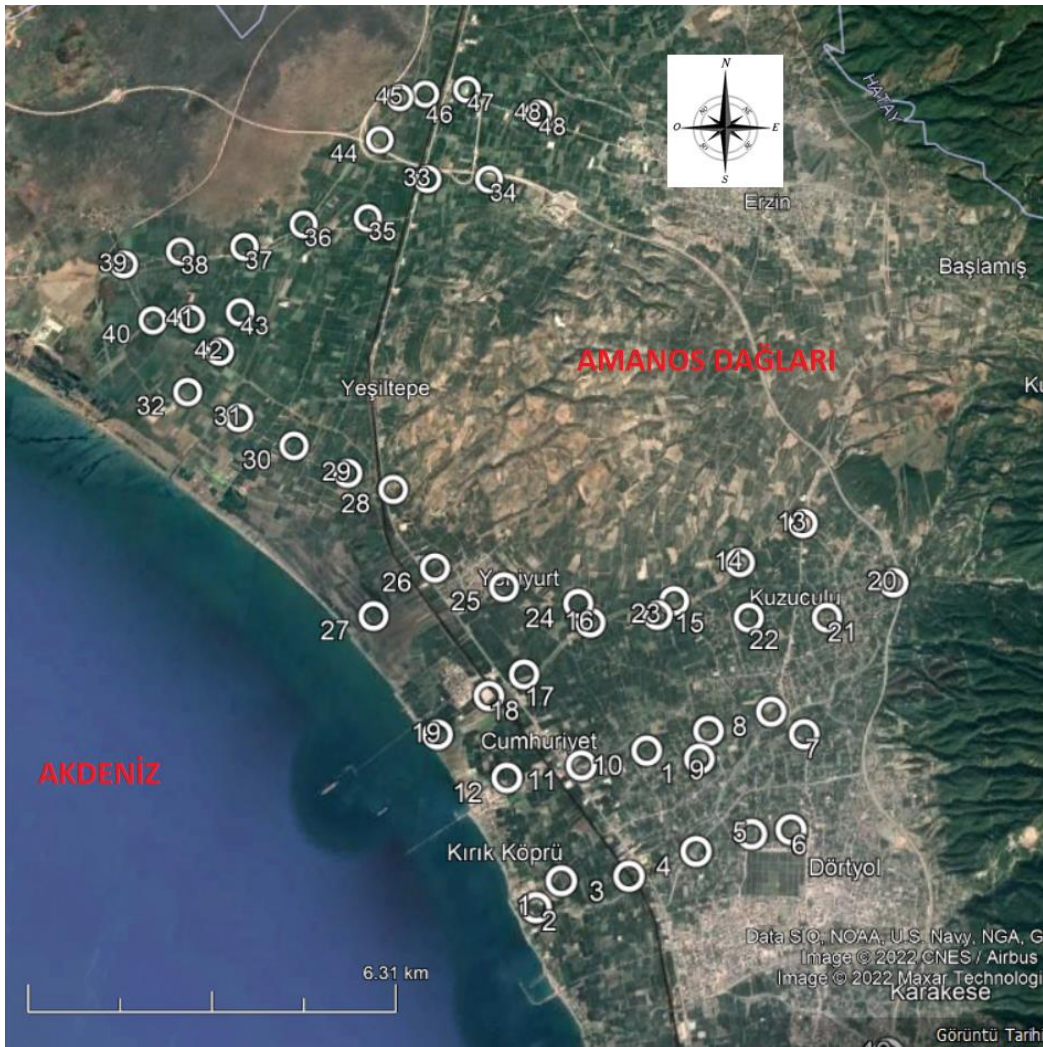
Dörtüol ovasının büyük bir kısmı alüviyal materyallerle kaplıdır. Bu alüvyonları sel suları ve akarsu çökelleri oluşturmuştur. Akarsu yataklarında daha çok çakıllı ve yer yer kumlu olan alüvyonlar yer alırken, ovanın diğer kısımlarında genellikle kumlu,

siltli ve killi materyaller bulunmaktadır. Ovadaki alüvyon materyalin kalınlığı yaklaşık 10-60 m civarında değişmektedir (Doyuran 1982). Çalışma alanının doğu sınırı boyunca yer alan, son derece geçirimli çökellerden oluşan birikinti koni kuşağı, dağlardan alana doğru akan sularının önemli bir kısmını süzmekte ve akifleri beslemektedir (Doyuran 1980).

## 2.2.Yöntem

### 2.2.1.Toprak örneklerinin alınması

Çalışma alanından 0-30 cm derinlikten toplam 48 adet bozulmuş toprak örneği alınmıştır (Şekil 1). Toprak örneklerinin alınmasında, alanı temsil edecek şekilde, rastgele örnekleme yöntemi kullanılmıştır. Yine örnekleme sırasında, her bir toprak örneğinin alındığı noktanın UTM sistemine göre coğrafi koordinatları (Magellan marka, explorer 710 model) GPS cihazı ile belirlenmiştir. Toprak örnekleme sırasında, tüm örnekleme noktalarında Turunçgil bitkisi olduğu belirlenmiştir. Alınan toprak örnekleri kurutma ve eleme işlemlerinden sonra analizler için hazır hale getirilmiştir.



Şekil 1. Çalışma alanının coğrafi konumu ve toprak örneklerinin alındığı noktalar

### 2.2.2. Toprak analizleri

Toprak örneklerinde; pH, elektriksel iletkenlik (EC), organik madde (OM), hava kuru nem içeriği, bünye ve kireç analizleri yapılmıştır. Örneklerin pH değerleri 1/2.5 toprak-su karışımında pH-metre, EC değerleri ise yine 1/2.5 toprak-su karışımında EC-metre ile belirlenmiştir (Richards 1954). Örneklerin organik madde içeriği Walkey-Black yaş yakma yöntemine (Allison 1965), kireç miktarı ise Allison ve Moode (1965)'e göre belirlenmiştir. Toprakların tane irilik dağılımı (bünye) tayini ise hidrometre yöntemine göre yapılmıştır (Bouyoucos 1951). Topraklarda belirlenen bazı fiziksel ve kimyasal özellikler, bu Tablo 1'de verilen sınır değerler ile kıyaslanarak yeterlilik durumları yorumlanmıştır.

Toprak örneklerinde; pH, elektriksel iletkenlik (EC), organik madde (OM), hava kuru nem içeriği, bünye ve kireç analizleri yapılmıştır. Örneklerin pH değerleri 1/2.5 toprak-su karışımında pH-metre, EC değerleri ise yine 1/2.5 toprak-su karışımında EC-metre ile belirlenmiştir (Richards 1954). Örneklerin organik madde içeriği Walkey-Black yaş yakma yöntemine (Allison 1965), kireç miktarı ise Allison ve Moode (1965)'e göre belirlenmiştir. Toprakların tane irilik dağılımı (bünye) tayini ise hidrometre yöntemine göre yapılmıştır (Bouyoucos 1951). Topraklarda belirlenen bazı fiziksel ve kimyasal özellikler, bu Çizelge 1'de verilen sınır değerler ile kıyaslanarak yeterlilik durumları yorumlanmıştır.

### 2.2.3. İstatistiksel ve jeostatistiksel analizler

Toprak örneklerine ait verilere; ortalama, en düşük ve en yüksek değerler, standart sapma, çarpıklık, basıklık tanımlayıcı istatistiksel analizler uygulanmıştır. Toprak özelliklerinin normal dağılım gösterip göstermediği, hem çarpıklık katsayıları hem de yapılan normalite test sonuçları (Tablo 2) yorumlanarak belirlenmiştir (Paz- González ve ark. 2000). İstatistiksel analizler Windows uyumlu SPSS 26 istatistik paket programı kullanılarak yapılmıştır.

Toprak özelliklerinin mekânsal dağılımının modellenmesinde Windows uyumlu GS<sup>+</sup> (sürüm 10) Jeostatistik programı kullanılmıştır (Gamma design 2008). Bu programda her bir her bir toprak özelliğinin en uygun yarıvariogram grafiği oluşturulmuş ve bu grafiğin parametreleri belirlenmiştir. Toprak özelliklerinin mekânsal dağılım haritalarının oluşturulmasında ise coğrafi bilgi sistemleri (CBS) kullanılmıştır. Bu kapsamda, GS<sup>+</sup> (sürüm 10) ile belirlenen yarıvariogram parametreleri kullanılmış ve her bir toprak özelliğinin dağılım haritaları ArcGis (sürüm:10.6.1.) programı ile oluşturulmuştur (Töreyn

ve ark. 2010). Bu programda ordinary kriging enterpolasyon yöntemi kullanılmıştır. Parametrelerin varyasyon katsayıları Zhou ve ark. (2010) tarafından önerilen kıstaslar kullanılmıştır. Bu kıstaslara göre varyasyon katsayısı % 10'dan düşük ise değişkenlik düzeyi düşük, % 10-100 arasında ise değişkenlik düzeyi orta ve % 100'den büyük ise değişkenlik düzeyi yüksektir.

Parametrelerin varyasyon katsayıları, bunların değişkenlik düzeylerinin belirlenmesinde kullanılmaktadır. Bu değerlendirmede Zhou ve ark. (2010) tarafından önerilen kıstaslar kullanılmıştır. Bu kıstaslara göre; varyasyon katsayısı % 10'dan düşük ise değişkenlik düzeyi düşük, % 10-100 arasında ise değişkenlik düzeyi orta, % 100'den büyük ise değişkenlik düzeyi yüksektir.

Ayrıca toprak özelliklerinin yersel bağımlılıklarının değerlendirilmesinde nugget yarıvarsın (Co) toplam varyans (Co+C)'a olan yüzde oranı kıstas olarak kullanılmıştır. Bu değerlendirme ise Cambardella ve ark. (1994)'e göre yapılmıştır. Bu oran % 25 veya daha düşük ise özelliklerdeki yersel bağımlılık kuvvetli, % 25-75 arasında ise orta ve % 75'den büyük ise zayıf olarak değerlendirilmektedir.

## 3. Bulgular ve Tartışma

### 3.1. Araştırma alanının temel toprak özellikleri

Toprakların temel özelliklerinin istatistiksel analiz sonuçları Tablo 3'de sunulmuştur. Toprak örneklerinin pH'ları 7.20 ile 7.78 arasında ve ortalama 7.52 olarak belirlenmiştir. Toprakların Toprakların reaksiyonları pH değerlerine sınıflandırıldığında (Tablo 1) ; % 45'i nötr, % 55'inin ise bazik karakterli olduğu belirlenmiştir. Karakaya ve Ağca (2022) tarafından Sarıseki ve Dört Yol arasında yapılan çalışmada da pH değerleri açısından benzer sonuçlar bulunmuştur.

Topraklarda elektriksel iletkenlik (EC) değerlerinin 99  $\mu\text{S cm}^{-1}$  ile 997  $\mu\text{S cm}^{-1}$  arasında değiştiği ve ortalama EC değerinin ise 274  $\mu\text{S cm}^{-1}$  olduğu belirlenmiştir. Toprakların EC değerleri, sınır değerler ile karşılaştırıldığında; tüm toprakların tuzsuz sınıfında yer aldığı görülmüştür. Everest ve Özcan (2018)'nin Çanakkale'nin Ezine İlçesinde, Doğan ve Erdal (2018)'nin Burdur'da, Parlak ve ark. (2008)'in Eceabat (Çanakkale)'ta ve Bayar ve ark. (2019)'un Kırşehir topraklarında yaptığı çalışmalarda benzer sonuçlar bulunmuştur.



**Tablo 1.** Toprakların verimlilik ile ilgili özellikleri için sınır değerler

Özellik	Birim	Sınır değer	Değerlendirme
pH (Ülgen ve Yurtsever 1995)	-----	<4.5	Kuvvetli asit
		4.5 – 5.5	Orta kuvvetli asit
		5.5 – 6.5	Hafif asit
		6.5 – 7.5	Nötr
		7.5 – 8.5	Bazik
		>8.5	Alkali
Elektriksel iletkenlik (EC) (Richards 1954)	$\mu\text{Scm}^{-1}$	0-4000	Tuzsuz
		4000-8000	Hafif tuzlu
		8000-16000	Orta tuzlu
		>16000	Şiddetli tuzlu
Organik madde (Ülgen ve Yurtsever 1995)	%	<1	Çok az
		1-2	Az
		2-3	Orta
		3-4	İyi
		>4	Yüksek
Kireç (Ülgen ve Yurtsever 1995)	%	<1	Az kireçli
		1-5	Kireçli
		5-15	Orta kireçli
		15-25	Fazla kireçli
		>25	Çok fazla kireçli

**Tablo 2.** Toprak özelliklerine ait normalite test sonuçları

Parametre	Kolmogorov-Smirnova			Shapiro-Wilk		
	İstatistik	Örnek Sayısı	P	İstatistik	Örnek Sayısı	P+
pH	0.067	48	0.200	0.981	48	0.622*
EC	0.142	48	0.017	0.785	48	0.000
Kireç	0.148	48	0.010	0.904	48	0.001
OM	0.229	48	0.000	0.760	48	0.000
Nem	0.124	48	0.061	0.944	48	0.024
Kum	0.101	48	0.200	0.970	48	0.258*
Silt	0.139	48	0.022	0.948	48	0.033
Kil	0.092	48	0.200	0.974	48	0.363*

\* p > 0.05 normal dağılım gösteren veriler, p < 0.05 normal dağılım göstermeyen veriler

**Tablo 3.** Araştırma konusu toprakların temel özelliklerinin tanımlayıcı analiz sonuçları

Örnek no	pH	EC ( $\mu\text{S cm}^{-1}$ )	Kireç (%)	OM (%)	Nem %	Tane irilik dağılımı (%)		
						Kum	Silt	Kil
EK	7.20	99.00	0.57	0.55	1.34	0.50	15.80	19.20
EY	7.78	997.00	13.17	8.95	9.48	56.50	56.70	64.30
Ort.	7.52	273.58	5.43	2.66	4.27	27.30	33.44	39.28
SS	0.14	147.11	3.76	1.56	1.84	14.09	10.08	10.67
VK	1.86	53.77	69.24	58.65	43.1	51.61	30.15	27.16
Çar.	-0.07	2.66	0.63	2.35	0.85	0.27	0.54	0.29
Bas.	-0.34	11.52	-0.89	6.73	0.46	-0.79	-0.65	-0.71

OM: organik madde, EK: en küçük değer, EY: en yüksek değer, Ort.: ortalama değer, SS: standart sapma, VK: varyasyon katsayısı, Çar.: çarpıklık katsayısı, Bas. : basıklık katsayısı

Toprakların kireç içerik değerleri % 0.57 ile % 13.17 arasında değişmiş olup, ortalama kireç içeriği % 5.43 olarak saptanmıştır. Toprakların kireç içerikleri, sınır değerlerine (Tablo 2) göre değerlendirildiğinde; % 4.16'sının az kireçli, % 52.08'nin kireçli ve % 43.75'nin orta kireçli olduğu saptanmıştır. Bu konuda Bingöl topraklarında yapılan bir çalışmada benzer sonuçlar bulunmuştur (Ateş ve Turan 2015).

Toprakların organik madde içeriklerinin % 0.55 ile % 8.95 arasında, ortalama ise % 2.66 olduğu belirlenmiştir. Sınır değerlerle (Tablo 2) karşılaştırıldığında; toprakların % 4.16'sı çok az, % 31.25'i az, % 39.58'i orta, % 16.67'si iyi ve % 8.33'ü ise yüksek miktarda organik madde içerdiği tespit edilmiştir. Everest ve ark. (2018) tarafından Ezine'de (Çanakkale) yapılan bir çalışmada organik madde içeriklerinin benzer dağılım gösterdiği görülmüştür. Toprakların yaklaşık %75'inde organik madde yetersiz düzeydedir. Bunun en önemli nedeni: çalışma alanında yazları sıcak ve kurak geçmesi ve bu koşullarda organik maddenin hızlı bir şekilde parçalanmasıdır.

Toprakların tane irilik dağılımları incelendiğinde; kum içeriklerinin % 0.5 ile % 56.5, silt içeriklerinin % 15.8 ile % 56.7, kil içeriklerinin ise % 19.2 ile % 64.3 (24 nolu örnek) arasında değiştiği görülmektedir. Orta ve Doğu Karadeniz Bölgesinde Özyazıcı ve ark. (2016), yaptıkları çalışmada tarım topraklarının kum içeriklerini % 1.61-91.98 arasında değişmekte olduğunu görmüşlerdir. Saygın ve ark. (2017) ise, Çataklı Çayı havzasında yaptıkları çalışmada, 0-30 cm toprak katmanında kum içeriğinin % 28.4-77.6 ve silt içeriğinin % 14.7-34.7 arasında; yüzey altı (30-60 cm) katmanında ise kum içeriğinin % 41.1-81.1 ve % silt içeriğinin 12.0-34.0 arasında değiştiğini belirlemişlerdir. Demircioğlu ve Ağca (2022), Arsuz ovası (Hatay) topraklarında yaptıkları çalışmada; toprakların kum içeriklerinin % 47.3-54.2, silt içeriklerinin 17.8-20.6 ve kil içeriklerinin ise % 31.2-33.6 arasında değiştiğini belirlemişlerdir. Toprakların nem içerikleri ise % 1.34 ile % 9.48 arasında değişmiştir (Tablo 2). Coşar ve Ağca (2023) tarafından Erzincan ovası (Hatay) topraklarının hava kuru nem içeriklerini % 2.15 ile 13.12 arasında belirlemişlerdir.

Toprakların % 45.8'i ince (kil), % 54.2'si ise orta (tın) bünyeli topraklar sınıfında yer almıştır. İnce bünyeli toprakların bünye sınıflarına bakıldığında; % 70.3'ünün kil, % 29.7'sinin ise siltli kil bünyeli oldukları görülmüştür. Yine orta bünyeli toprakların % 54.2'sinin kili tın, % 19.2'sinin siltli killi tın, % 19.2'sinin kumlu killi tın, % 3.9'unun tın, % 3.9'unun ise kumlu tın bünyeli olduğu belirlenmiştir. Bünye sınıfları incelendiğinde; çalışma alanında 7 farklı bünye sınıfı olduğu görülür. Bu kadar farklı bünye sınıfının olması; büyük olasılıkla toprakların farklı bölgelerden taşınan aluviyal ana materyal üzerinde oluşmasıdır.

Bu çalışmada toprakların temel özellikleri içerisinde en düşük varyasyon katsayısının (VK) pH değerlerinde (% 1.86), en yüksek ise kireç içeriklerinde (% 69.24) olduğu belirlenmiştir. Kireç içeriğini % 58.65 ile OM değerleri izlemiştir. Herhangi bir özelliğin VK değerleri ne kadar küçükse, o özelliğin araştırma alanındaki dağılımı da o kadar homojen olacaktır. Buna karşın VK değeri üniform (düzenli) dağılım göstermemektedir. Bu çalışmada en düşük VK'nın pH değerlerinde olması, çalışma alanında pH değerlerinin çok üniform bir şekilde dağıldığını belirtmektedir. Budak ve ark. (2018) Dicle havzasında, Tolu (2023) ise Kocaeli topraklarında yaptıkları çalışmalarda benzer şekilde en fazla homojen dağılımın pH değerlerinde olduğunu belirlemişlerdir.

### 3.2. Toprak özellikleri arasındaki ilişkiler

Toprak özellikleri arasındaki korelasyon analiz sonuçları Tablo 4'de verilmiştir.

Korelasyon katsayılarına bakıldığında; toprakların pH değerleri ile EC değerleri arasında % 1 düzeyinde negatif; kireç değerleri arasında ise %5 düzeyinde pozitif korelasyon belirlenmiştir. Tolu (2023) tarafından yapılan çalışmada da pH ile kireç arasında benzer korelasyonlar bulunmuştur. Kireç değerleri ile kum içerikleri arasında %1 düzeyinde negatif, silt içerikleri arasında ise % 5 düzeyinde pozitif korelasyon görülmüştür. Akbay ve Günel (2023) tarafından yapılan çalışmada da kireç ile kum arasında benzer sonuçlar belirlenmiştir.

Nem içerikleri ile organik madde ve kil içeriği arasında %1 düzeyinde pozitif, silt içeriği arasında %1, kum içeriği arasında ise %5 düzeyinde negatif korelasyon belirlenmiştir. Kil içerikleri ile kum ve silt içerikleri arasında ise % 1 düzeyinde negatif korelasyon hesaplanmıştır. Tolu (2023) yaptığı çalışmada kum ile kim ve silt içerikleri arasında % 1 düzeyinde önemli pozitif korelasyonlar bulunmuştur. Buna karşın, Akbay ve Günel yaptıkları bir çalışmada kil ile silt içerikleri arasında pozitif korelasyon belirlemişlerdir.

Bu çalışmada toprakların temel özellikleri içerisinde en düşük varyasyon katsayısının (VK) pH değerlerinde (% 1.86), en yüksek ise kireç içeriklerinde (% 69.24) olduğu belirlenmiştir. Kireç içeriğini % 58.65 ile OM değerleri izlemiştir. Herhangi bir özelliğin VK değerleri ne kadar küçükse, o özelliğin araştırma alanındaki dağılımı da o kadar homojen olacaktır. Buna karşın VK değeri üniform (düzenli) dağılım göstermemektedir. Bu çalışmada en düşük VK'nın pH değerlerinde olması, çalışma alanında pH değerlerinin çok üniform bir şekilde dağıldığını belirtmektedir. Budak ve ark. (2018) Dicle havzasında, Tolu (2023) yaptığı çalışmada kum ile kim ve silt içerikleri arasında % 1 düzeyinde önemli pozitif korelasyonlar bulunmuştur. Buna karşın, Akbay ve Günel yaptıkları bir çalışmada kil ile silt içerikleri arasında pozitif korelasyon belirlemişlerdir.

### 3.3. Toprak özelliklerinin yersel dağılımının modellenmesi ve haritalanması

Çalışma alanındaki toprak özelliklerinin yarıvariogram parametreleri belirlenirken, kum içeriği hariç, tüm özelliklerde bütün veriler kullanılmıştır.

Kum içeriğinde ise 3, 4 ve 45 nolu örneklerin kum içerikleri kullanılmamıştır. Toprak özellikleri için yarıvariogram modelleri belirlenirken, program tarafından, aktif ayırma uzaklığı 8466 m olarak alınmıştır. Toprak özelliklerinin yarıvariogram parametreleri Tablo 5’de, yersel dağılım haritaları ise Şekil 2’de verilmiştir.

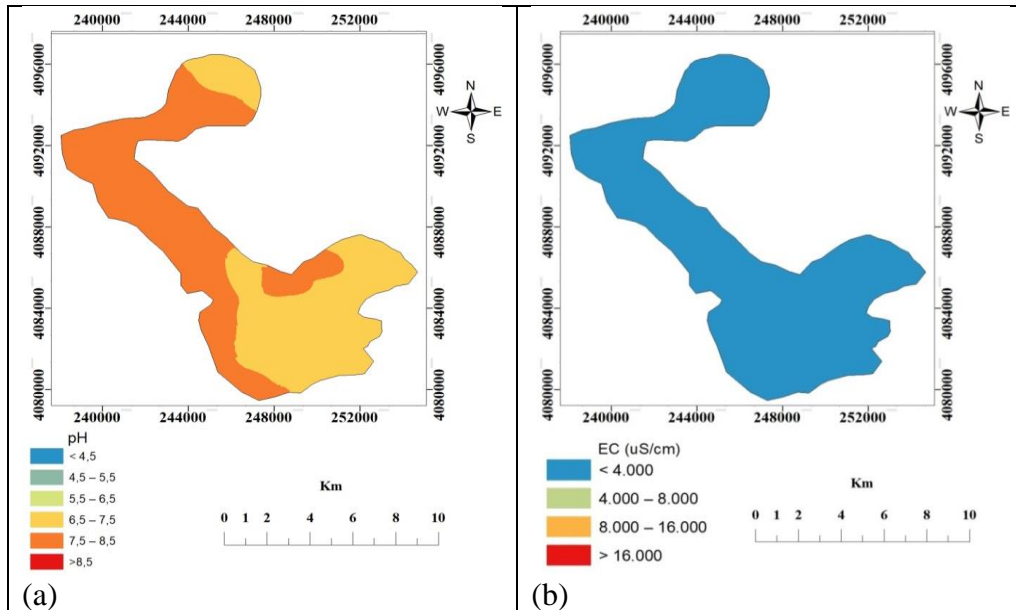
**Tablo 4.** Toprak özellikleri arasındaki korelasyon katsayıları

	pH	EC	Kireç	OM	Nem	Kum	Silt
EC	<b>-0.503**</b>						
Kireç	<b>0.309*</b>	0.104					
OM	-0.241	0.140	-0.006				
Nem	0.073	0.259	0.066	<b>0.490**</b>			
Kum	-0.125	-0.168	<b>-0.417**</b>	-0.027	<b>-0.335*</b>		
Silt	0.003	0.010	<b>0.315*</b>	-0.226	<b>-0.419**</b>	<b>-0.656**</b>	
Kil	0.162	0.211	0.255	0.249	<b>0.839**</b>	<b>-0.701**</b>	-0.079

\*\*Korelasyon %1 düzeyinde önemli, \*Korelasyon % 5 düzeyinde önemli (2-yönlü)

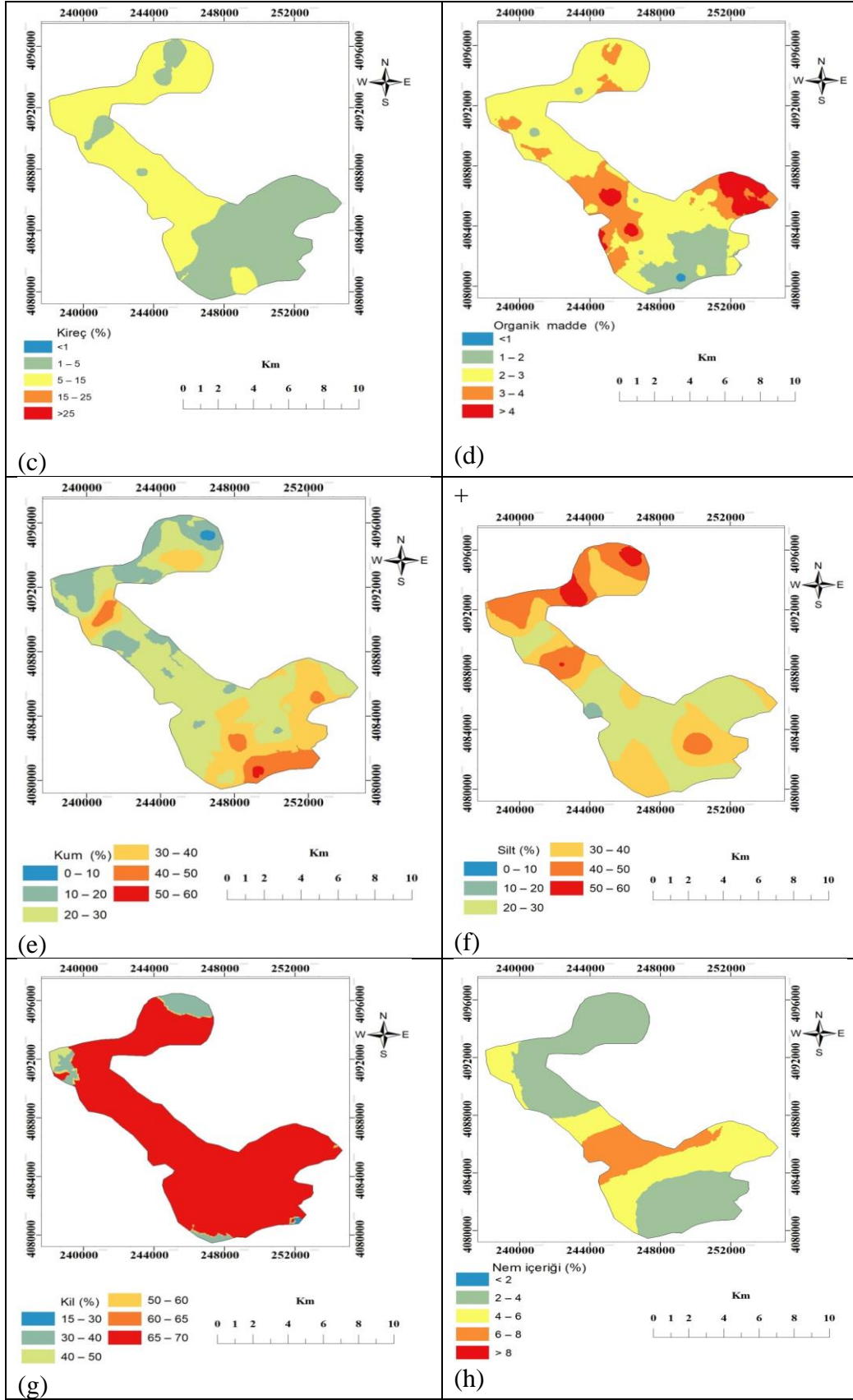
**Tablo 5.** Toprak özelliklerine ait yarıvariogram parametreleri

Özellik	Model	A <sub>0</sub> (m)	Nugget (C <sub>0</sub> )	Sill (C <sub>0</sub> +C)	(C <sub>0</sub> )/(C <sub>0</sub> +C)*100	r <sup>2</sup>
pH	Üssel	21100	0.011	0.044	25	0.459
EC	Üssel	14090	0.124	0.46	26.95	0.580
Kireç	Üssel	2480	2.360	16.56	14.25	0.748
OM	Üssel	1260	0.004	0.309	1.35	0.599
Kum	Gaussian	1260	64.00	161.50	39.62	0.383
Silt	Küresel	2620	0.100	82.600	0.12	0.499
Kil	Gaussian	13570	94.00	385.70	24.37	0.506
Nem	Gaussian	4690	0.1131	0.3112	36.34	0.845



**Şekil 2.** Toprak özelliklerinin çalışma alanındaki yersel dağılım haritaları





Şekil 2. (Devamı) Toprak özelliklerinin çalışma alanındaki yersel dağılım haritaları

Her bir toprak özelliği ve besin element içeriklerinin yersel dağılımının modellenmesi ve haritalanması aşağıda açıklanmıştır.

### 3.3.1. pH

Çarpıklık (sola çarpık) değerlerinin oldukça düşük (-0.07) olması ve normalite testlerinde (Shapiro-Wilk testi) normal dağılım göstermesi (Tablo 2) nedenleriyle, jeoistatistiksel modellemelerden önce pH verilere herhangi bir dönüşüm uygulanmamıştır. Coşar ve Ağca (2023) da Erzin ovası topraklarında pH değerlerine herhangi bir dönüşüm uygulamamışlardır. Toprakların pH değerleri için en uygun yarıvaryogram modelinin belirlenmesi için ayırma mesafeleri ise eşit bir şekilde 543 m olarak belirlenmiştir.

Toprakların pH değerleri için en uygun yarıvaryogram modeli Üssel (Exponential), yersel otokorelasyon aralığı ( $A_0$  değeri) ise 21100 m olarak saptanmıştır (Tablo 5). Isaaks ve Sriastava, (1989)'a göre; jeoistatistikte  $A_0$  (range) değeri; herhangi bir değişken için uzaysal bağımlılığın devam ettiği maksimum mesafeyi belirtmektedir. Topraklarının pH değerlerinde, Nugget/sill oranına (Tablo 5) göre, yersel bağımlılığın kuvvetli düzeydedir. Reza ve ark. (2012) yaptıkları çalışmada da pH değerlerinin güçlü yersel bağımlılık gösterdiği belirlenmiştir. Araştırma alanında en çok karşılaşılan pH değerleri 7.50 ve 8.50 arasında değişmektedir. Toprakların reaksiyonu incelendiğinde, kuzey ve güneydoğu kısımlarında nötr, orta ve batı kesimlerinde ise bazik karakterde olduğu görülmektedir (Şekil 2a).

### 3.3.2. Elektriksel iletkenlik (EC)

Toprakların EC değerleri, oldukça yüksek çarpıklık (sağa çarpık) değerlerine (2.66) sahiptir. Ayrıca normalite test (Shapiro-Wilk testi) sonuçlarına göre de normal olmayan dağılım göstermiştir (Tablo 2). Bu nednlerle, jeoistatistiksel modellemeyle başlamadan önce verilere logaritmik dönüşüm uygulanmıştır. Toprakların EC değerleri için, en uygun yarıvaryogram modelini belirlemek amacıyla ayırma mesafeleri ise eşit bir şekilde 545 m olarak belirlenmiştir. EC değerleri için en uygun yarıvaryogram modeli Üssel (Exponential),  $A_0$  değeri ise 14090 m olarak belirlenmiştir (Tablo 5). Mondal ve ark. (2020) yaptıkları bir çalışmada da; EC değerleri için en uygun modelin Üssel (Exponential) olduğunu belirlemişlerdir.

Nugget/sill oranına (Tablo 5) göre, EC değerlerine ait yersel bağımlılığın orta düzeyde olduğu belirlenmiştir. Benzer şekilde Doğan ve ark. (2020) Hatay Arsuz'da yapılan çalışmada da EC değerlerinin yersel bağımlılığının orta seviyede olduğu bulunmuştur. Buna karşın, Shit ve ark. (2016) Batı Hindistan'daki Paschim Medinipur Bölgesinde yaptıkları çalışmada

ise; EC değerleri kuvvetli yersel bağımlılık göstermiştir.

Çalışma alanı topraklarının EC değerlerinin yersel dağılımı incelendiğinde (Şekil 2b), tamamının tuzsuz olduğu ( $EC < 4000 \mu S cm^{-1}$ ) görülmektedir. Yağanoğlu ve Aydın (2017), Erzurum Hınıs'da yaptıkları çalışmada, alana ait toprak örneklerinin EC değerlerinin 310 - 810  $\mu S cm^{-1}$  arasında değiştiği, ortalama EC değerinin ise 0.45  $\mu S cm^{-1}$  olduğu ve toprakların tamamının tuzsuz olduğunu tespit etmişlerdir. Yine, Taşkın ve ark. (2018) tarafından Ankara Üniversitesi Araştırma ve Uygulama Çiftliği topraklarında yapılan bir çalışmada toprakların tamamının tuzsuz olduğu belirlenmiştir.

### 3.3.3. Kireç içerikleri

Toprakların kireç içeriklerinin, çarpıklık (sağa çarpık) değerlerinin düşük (0.63) ve normalite test sonucuna göre de normal dağılım (Tablo 2) göstermiştir. Bu nedenlerle jeoistatistiksel modelleme yapmadan önce verilere herhangi bir dönüşüm uygulanmamıştır. Toprakların kireç içeriklerinin en uygun yarıvaryogram modelini belirlemek için ayırma mesafeleri ise uniform bir şekilde 551 m olarak alınmıştır.

Kireç için en uygun yarıvaryogram modeli Üssel,  $A_0$  değeri ise 2480 m olarak belirlenmiştir (Tablo 5). Benzer şekilde, Budak ve ark. (2018) yaptıkları çalışmalarında da kireç için en uygun yarıvaryogram modelini Üssel olarak belirlemişlerdir. Buna karşın Coşar ve Ağca (2023) ise kireç için en uygun modeli Guassian olarak belirlemişlerdir. Çalışma alanı topraklarının kireç içeriklerinin kuvvetli düzeyde yersel bağımlılık gösterdiği saptanmıştır. Budak ve ark. (2018) Dicle Havzasında yaptıkları bir çalışmada ise toprakların kireç içeriklerinin orta düzeyde yersel bağımlılık gösterdiği saptanmıştır.

Çalışma alanındaki toprakların kireç dağılımı incelendiğinde (Şekil 2c), orta ve güney kısımlarının kireçli, doğu ve güneydoğu bölümlerinin orta düzeyde kireç içeriğine sahip olduğu görülmektedir. Everest ve Özcan (2018) yaptıkları çalışmada zeytin arazilerinin % 2.70'inin az kireçli, % 16.22'sinin orta kireçli, % 75.68'inin fazla kireçli ve % 5.41'inin ise çok fazla kireçli olduğunu tespit etmişlerdir. Özden ve ark. (2020), İzmir topraklarında yaptıkları çalışmada, toprakların yarısından fazlasının (% 57.17) kireçsiz ve çok az kireçli olduğunu tespit etmişlerdir.

### 3.3.4. Organik madde (OM) içerikleri

Oldukça yüksek çarpıklık (sağa çarpık) değerine (2.35) sahip olması ve normalite test sonucunda normal olmayan dağılım göstermesi (Tablo 2) gibi nedenlerle, toprakların OM içeriklerine, jeoistatistiksel modelleme yapmadan önce verilere

logaritmik dönüşüm uygulanmıştır. Toprakların organik madde içeriklerine en uygun yarıvaryogram modelinin belirlenmesi için ayırma mesafeleri ise eşit bir şekilde 575 m olarak alınmıştır. Toprakların OM içerikleri için en uygun yarıvaryogram modeli Üssel,  $A_0$  değeri ise 1260 m olarak hesaplanmıştır (Tablo 5). Reza ve ark. (2012) tarafından yapılan çalışmada da bu konuda benzer sonuçlar bulunmuştur. Çalışma alanı topraklarında organik madde içeriklerinin kuvvetli düzeyde yersel bağımlılık gösterdiği saptanmıştır. Bogunovic ve ark. (2021) tarafından yapılan bir çalışmada da organik maddenin yersel bağımlılığını kuvvetli bulmuşlardır. Araştırma alanı topraklarında OM dağılımı incelendiğinde, güney kesimlerinde çok az ve az, kuzeyin bazı kesimlerinde az ve iyi düzeyde, doğu ve orta kesimlerde iyi ve yüksek, kuzeyde ise orta seviyede organik madde içerdiği saptanmıştır (Şekil 2d). Bellitürk (2011) Uzunköprü (Edirne)'deki çalışmasında toprakların tamamının organik madde içeriklerinin yetersiz olduğu görülmüştür. Özkan ve ark. (2009) tarafından Antalya'da yapılan bir çalışmada; toprakların organik madde içeriklerinin % 0.2-6.7 arasında değiştiği ve örneklerin % 69.5'inin humusça fakir, % 27.1'inin de az humuslu sınıfta yer aldığı saptanmıştır. Erdal ve Doğan (2018) tarafından yapılan çalışmada ise organik madde içeriği toprakların % 15'inde çok az, % 55'inde az, % 26'sında orta, % 3'ünde iyi ve % 1'inde ise yüksek düzeyde olduğu belirlenmiştir.

### 3.3.5. Kum içerikleri

Toprakların kum içeriklerinin, çarpıklık (sağa çarpık) değerlerinin oldukça düşük (0.27) ve normalite testi sonucunda da normal dağılım gösterdiği (Tablo 2) belirlenmiştir. Bu nedenlerle jeostatistiksel modelleme yapmadan önce kum verilerine herhangi bir dönüşüm uygulanmamıştır. Toprakların kum içerikleri için en uygun yarıvaryogram modelinin belirlenmesi amacıyla, ayırma mesafeleri ise üniform bir şekilde 561 m olarak belirlenmiştir.

Toprakların kum içerikleri için en uygun yarıvaryogram modeli Gaussian, kum içerikleri için  $A_0$  değeri ise 1260 m olarak belirlenmiştir (Tablo 5). Kum içerikleri için en uygun yarıvaryogram modeli Bautista (2021) tarafından Spherical, Reza ve ark. (2016) tarafından ise Üssel olarak belirlenmiştir. Kum içeriklerinin, Nüket/Sil oranına göre, orta düzeyde yersel bağımlılık gösterdiği saptanmıştır. Reza ve ark. (2016) Hindistan'ın Katihar ilçesinin Kadwa Bloğunda yaptıkları çalışmada da; kum içeriğinin orta düzeyde yersel bağımlılık gösterdiği gözlenmiştir.

Çalışma alanındaki toprakların kum içerikleri genellikle kuzey ve batı kesimlerde düşükken, güneye doğru inildikçe yükseldiği görülmektedir. En

yüksek kum içeriklerine alanın güneydoğusunda rastlanmıştır. Alandaki kum içeriğinin ağırlıklı olarak % 10 ile % 40 arasında yoğunlaştığı görülmektedir (Şekil 2e).

### 3.3.6. Silt içerikleri

Çarpıklık (sağa çarpık) değerlerinin düşük (0.54) olması ve normalite test sonuçlarında normal dağılım göstermesi (Tablo 2) nedenleriyle, jeostatistiksel modellemelerden önce silt verilerine herhangi bir dönüşüm uygulanmamıştır. Toprakların silt içerikleri için, en uygun yarıvaryogram modelini belirlemek amacıyla; ayırma mesafeleri ise eşit olarak 566 m olarak alınmıştır. Silt içerikleri için en uygun yarıvaryogram modeli Küresel (Spherical),  $A_0$  değeri ise 2620 m olarak belirlenmiştir (Tablo 5). Bautista (2021) çalışmasında silt için en uygun yarıvaryogram modelini Üssel (Exponential) olarak bulmuştur.

Toprakların silt içeriklerinin nugget/silt oranına göre kuvvetli düzeyde yersel bağımlılık gösterdiği belirlenmiştir.

Çalışma alanı topraklarında silt içerikleri genellikle orta ve güneydoğu kesimlerde düşükken, kuzeye doğru gidildikçe ve yer yer güneydoğu kesimlerinde yükseldiği görülmektedir. En yüksek silt içerikleri alanın kuzeyinde rastlanmıştır. Çalışma alanındaki silt içeriğinin ağırlıklı olarak % 20 ile % 50 arasında değişiklik gösterdiği anlaşılmaktadır (Şekil 2f).

### 3.3.7. Kil içerikleri

Çalışma alanındaki topraklarda kil içeriklerinin çarpıklık (sağa çarpık) değerlerinin oldukça düşük (0.29) ve normalite testli sonuçlarında ise normal dağılım gösterdiği (Tablo 2) belirlenmiştir. Bu nedenlerle kil verilerine jeostatistiksel modelleme uygulamadan önce veriler üzerinde herhangi bir dönüşüm yapılmamıştır. Toprakların kil içeriklerine en uygun yarıvaryogram modelini belirlemek için, ayırma mesafeleri ise eşit bir şekilde 583 m olarak alınmıştır. Kil miktarları için en uygun yarıvaryogram modeli Guassian,  $A_0$  değeri 13570 m olarak belirlenmiştir (Tablo 5). Reza ve ark. (2016) çalışmalarında ise kil içeriği için Exponential yarıvaryogram modelinin en uygun olduğunu belirlemişlerdir. Toprakların kil içeriklerinin yersel bağımlılık düzeyinin kuvvetli olduğu belirlenmiştir. Benzer şekilde, Reza ve ark. (2016) yaptıkları çalışmada da kil için yersel bağımlılığı kuvvetli olarak belirlemişlerdir.

Çalışma alanındaki toprakların kil içerikleri incelendiğinde; büyük bir kısmında yüksek olduğu belirlenmiştir. Alanın kuzeydoğusunda % 30-40, kuzeybatısında % 30-50, güneyinde % 30-40 ve güneydoğu bölümünün uç kesimlerinde % 15-30 olduğu belirlenmiştir. Alanın kil içeriğinin ağırlıklı

olarak % 65 ile % 70 arasında yoğunlaştığı görülmektedir (Şekil 2g). Orta ve Doğu Karadeniz Bölgesinde Özyazıcı ve ark. (2016) yaptıkları bir araştırmada, tarım topraklarının kil içeriklerinin % 2.49-79.23 arasında değişmekte olduğunu saptamışlardır. Saygın ve ark. (2017), araştırmasında ise toprakların, 0-30 cm'deki kil içeriklerini % 7.6-46.8 arasında; yüzey altı (30-60 cm) derinlikte ise % 6.8-40.8 arasında değiştiğini belirlemişlerdir.

### 3.3.8.Hava kuru nem içerikleri

Toprakların hava kuru kuru koşullardaki nem içeriklerinin çarpıklık (sağa çarpık) değerlerinin yüksek (0.85) olması ve normalite testi sonuçlarına göre normal olmayan dağılım göstermesi (Tablo 2) nedenleriyle, jeostatistiksel modelleme yapmadan önce nem verilerine logaritmik dönüşüm uygulanmıştır. Toprakların nem için, en uygun yairvariogram modelini belirlemek için, ayırma mesafeleri ise eşit bir şekilde 577 m olarak alınmıştır. En uygun yairvariogram modeli Guassian,  $A_0$  değeri 4690 m olarak belirlenmiştir (Tablo 5). Toprakların nem içeriklerinin yersel bağımlılık düzeyinin ise orta seviyede olduğu belirlenmiştir. Çalışma alanındaki toprakların nem içeriklerinin dağılım haritasına bakıldığında, genellikle orta kesimlerde yüksekken, kuzey ve güney kesimlerinde düşük olduğu görülmektedir. Alanındaki nem içeriğinin ağırlıklı olarak % 2 ile % 6 arasında yoğunlaştığı görülmektedir (Şekil 2h).

## 4. Sonuç ve Öneriler

Bu çalışmada; Dörtöl Ovası topraklarının temel özelliklerinin durumu belirlenmiş ve bunların çalışma alanındaki yersel dağılım modellemesi yapılarak haritaları oluşturulmuştur. Çalışma alanında en homojen dağılım gösteren parametrenin pH, en az homojenlik gösteren parametrenin ise toprakların kireç içeriği olduğu saptanmıştır. Toprak parametrelerinin dağılımı ile ilgili olarak yapılan benzer çalışmaların hemen hemen tamamında da pH değerlerinin en homojen dağıldığı belirlenmiştir.

Toprakların tamamında herhangi bir tuzluluk ve alkalilik sorunu olmayıp, tamamı nötr ve bazik reaksiyonludur. Bu sonuçlar çalışma alanı topraklarında yetiştirilecek kültür bitkilerinin bu üç özellik yönünden herhangi bir problemle karşılaşmayacaklarını ortaya koymaktadır.

Toprakların % 75'inde organik madde içeriğinin yetersiz olduğu belirlenmiştir. Ancak, Amanos dağlarının yamaçlarında bulunan topraklarda organik madde içerikleri % 8.95'e kadar çıkmaktadır. Bunun en önemli nedeni, Amanos dağlarında bulunan orman

ağaçlarının bu topraklara organik madde katkısı sağlamış olmasıdır.

Toprakların bünye, organik madde ve hava kuru koşullardaki nem içerikleri incelendiğinde, aralarında önemli ilişkilerin olduğu görülmektedir (Tablo 4). Özellikle kil bünyeli toprakların hava kuru nem içeriklerinin yüksek olması, bu toprakların su tutma kapasitelerinin yüksek olduğunu göstermektedir. Yine organik madde içeriği de tutulan su miktarını önemli ölçüde yükseltmiştir. Ancak, bölge topraklarının büyük çoğunluğunda kil içeriğinin yüksek, buna karşın organik madde içeriğinin düşük olması, bu topraklarda havalanma ve su geçirgenliği sorunlarına neden olabilecektir. Bu nedenle bu alanlara, organik madde içeriğinin artırılması için, yeşil gübreleme veya fermente olmuş ahır gübre uygulaması yapılmalıdır.

jeostatistikte  $A_0$  (range) değeri; herhangi bir değişken için uzaysal bağımlılığın devam ettiği maksimum mesafeyi belirtmektedir. Diğer bir deyişle, herhangi bir parametre için  $A_0$  değerinden sonraki uzaklıklarda noktalar arasında herhangi bir yersel (uzaysal) bağımlılık bulunmamaktadır. Dolayısıyla  $A_0$  değeri aynı zamanda örnekleme uzaklığını da belirtmektedir. Çalışma alanındaki toprakların  $A_0$  değerleri 1260 m (organik madde ve kum içeriği) ile 21100 m (pH için) gibi çok geniş sınırlar arasında değişmektedir. Bu alanda bundan sonra yapılacak benzer konulardaki çalışmalarda, parametrelerin  $A_0$  değerleri dikkate alınarak, bu parametrelerin  $A_0$  değerleri gruplandırılmalı ve iki veya üç farklı örnekleme uzaklığı belirlenmelidir.

Tarımsal alanların sürdürülebilir kullanımı için toprakların; mutlak surette bu alanların toprak özelliklerinin dağılımlarını gösteren haritaların üretilmesi gerekir. Bu çalışmada üretilen haritalar üreticiler için önemli bilgiler içermektedir. Ayrıca, bu çalışmadan elde edilen bulgular bir yandan bölgede bundan sonra yapılacak olan çalışmalara ışık tutacak, diğer yandan ise Türkiye Toprak Veri Tabanına önemli katkılar sağlayacaktır.

### Teşekkür

Bu makale Mustafa Kemal Üniversitesi Bilimsel Araştırma Projeleri (BAP) Koordinatörlüğü tarafından 20.YL.038 nolu proje ile desteklenen Emine Derya Aşkner'in Yüksek Lisans Tezinden hazırlanmıştır. Maddi destekleri nedeniyle BAP koordinatörlüğüne teşekkür ederiz.

### Yazarların Katkıları

Yazarlar bu makaleye eşit oranda katkı sunmuşlardır.

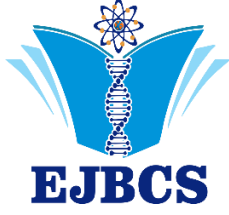
### Çıkar çatışmasının Beyanı

Bu çalışmada herhangi bir çıkar çatışması bulunmamaktadır.

**Kaynaklar**

- Akbay O, Günel H. 2023. Ergani ovasında bazı toprak özelliklerinin mekansal dağılımlarının belirlenmesinde lokal polinomal interpolasyon ve deneysel bayesyen kriging yöntemlerinin karşılaştırılması. *MAS Journal of Applied Sciences*. 8(4):654-668. doi: <http://dx.doi.org/10.5281/zenodo.8396228>
- Akın A, Taşova H. 2019. İç Anadolu Bölgesi tarım topraklarının bazı verimlilik parametrelerinin belirlenerek haritalanması. *Mediterranean Agricultural Sciences*. 32 (Özel Sayı): 1-6.
- Allison LE. 1965. Organic Carbon. C.A. Black, (ed). *Methods of soil analysis. Part 2. Agronomy Series. No. 9, ASA, Wisconsin*.
- Allison LE, Moode CD. 1965. Carbonate. C.A. Black (ed). *Methods of soil analysis. Part 2. Agronomy Series. No. 9, ASA, Wisconsin*.
- Anonim. 2022. Hatay ili iklim verileri. <https://www.mgm.gov.tr/veridegerlendirme/il-ve-ilceler-istatistik.aspx?m=HATAY> (Erişim tarihi: 17.08.2022).
- Ateş K, Turan V. 2015. Bingöl ili merkez ilçesi tarım topraklarının bazı özellikleri ve verimlilik düzeyleri. *Türk J Agric Res*. 2: 108-113.
- Bautista F. 2021. Geostatistical analysis of soil properties of the karstic sub-horizontal plain of the Yucatan Peninsula. *Tropical and Subtropical Agroecosystems*. 24: 09.
- Başbozkurt H, Öztaş Ö, Karabrahimoğlu A, Gündoğan R. 2013. Toprak özelliklerinin mekansal değişim desenlerinin jeostatistiksel yöntemlerle belirlenmesi. *Atatürk Üniv Ziraat Fak Derg* 44 (2): 169-181.
- Bayar AA A, Çınarlı M, Güven BG. 2019. Kırşehir ilindeki bazı tarım topraklarının verimlilik durumlarının belirlenmesi. *Türk Tarım ve Doğa Bilimleri Dergisi*. 6(4):636-647.
- Bellitürk K. 2011. Edirne ili Uzunköprü ilçesi tarım topraklarının beslenme durumlarının belirlenmesi. *Tekirdağ Zir Fak Dergisi*. 8(3): 8-15.
- Bouyoucos GJ. 1951. A recalibration of the hydrometer method for making mechanical analysis of soils. *Agron J*. 43:434-438.
- Budak M, Günel H, Çelik İ, Acir N, Sırrı M. 2018. Dicle Havzası toprak özelliklerinin yersel değişimlerinin jeostatistik ve coğrafi bilgi sistemleri ile belirlenmesi ve haritalanması. *Türkiye Tarımsal Araştırmalar Dergisi*. 5(2): 103-115. DOI: 10.19159/tutad.361237
- Bogunovic I, Filipovic L, Filipovic V, Pereira P. 2021. Spatial mapping of soil chemical properties using multivariate geostatistics. A study from cropland in eastern Croatia. *J Cent Eur Agric*. 22(1): 201-210
- Cambardella CA, Moorman TB, Parkin TB, Karlen DL, Novak JM, Turco RF, Konopka AE. 1994. Field-scale variability of soil properties in central Iowa soils. *Soil Sci Soc Am J*. 58: 1501-1511.
- Coşar MS, Ağca N. 2023. Erzin ovası topraklarının bazı özelliklerinin yersel dağılımlarının coğrafi bilgi sistemleri (CBS) kullanılarak haritalanması. *Çukurova J Agric Food Sci*. 38(2):179-191. doi: 10.36846/CJAIFS.2023.109
- Çabuk A, Çabuk KM, Aksoy M, Şimşek B, Güney Y, Avdan U, Uyguçgil H, Cömert R. 2018. Coğrafi bilgi sistemlerine giriş. *Anadolu Üniversitesi Yayını. Eskişehir*.
- Demircioğlu M, Ağca N. 2022. Arsuz ovası topraklarının temel özelliklerinin yersel dağılımının jeostatistiksel yöntemlerle belirlenmesi. *Osmaniye Korkut Ata Üniversitesi Fen Bilimleri Enstitüsü Dergisi*. 5(3): 1494-1513.
- Doğan A, Erdal İ. 2018. Burdur ili tahıl yetiştirilen toprakların verimlilik durumlarının belirlenmesi. *Toprak Bilimi ve Bitki Besleme Dergisi*. 6(1):39-45.
- Doğan K, Ağca N, Keçecioglu F, Benice A, Tek T. 2020. Spatial distribution of microbial activities in Arsuz plain soils (Hatay, Turkey). *Arab J Geosci*. 13:581.
- Doyuran V. 1980. Erzin - Dörtöl ovalarının hidr ojeolojisi ve yeraltı suyu işletme çalışmaları. *Orta Doğu Teknik Üniversitesi, Mühendislik Fakültesi, Jeoloji Mühendisliği Bölümü, Ankara, Doçentlik Tezi*, 88 S.
- Doyuran V. 1982. Erzin ve Dörtöl ovalarının jeolojik ve hidrojeolojik özellikleri. *Türkiye Jeoloji Kurumu Bülteni*. 25: 151-160.
- ESRI. 2022. What is GIS? *Geographic Information Systems*. [online]. [cit. 2011-03-12]. Available at: <https://www.esri.com/en-us/what-is-gis/overview> (Erişim tarihi: 08.12. 2022).
- Everest T, Özcan H. 2018. Toprak verimliliğinin değerlendirilmesinde pedo-jeolojik yaklaşım. *Türk Tarım ve Doğa Bilimleri Dergisi*. 5(4):589-603.
- Gamma Design. 2008. *Geostatistics for the Environmental Sciences*. Plainwell, Michigan USA.
- Hatipoğlu E. 2019. Bazı toprak özelliklerinin yersel değişimlerini jeostatistiksel yöntemler kullanılarak belirlenmesi. *Yüksek Lisans Tezi. Bursa Uludağ Üniversitesi Fen Bilimleri Enstitüsü, Bursa*.
- Isaaks HE, Srivastava R.M. 1989. *Applied geostatistics* Oxford University press, Inc. 561p.
- Kars N, Ekberli İ. 2019. Çarşamba Ovasının Buğday Bitkisi Altındaki Topraklarının Bazı Fiziksel ve Kimyasal Özelliklerinin İncelenmesi. *Toprak Su Dergisi*. 8 (1): 18-28.
- Mondal BP, Sekhon BS, Setia RK, Sadhukhan R. 2020. Geostatistical assessment of spatial variability of soil organic carbon under different land uses of Northwestern India. *Agric Res*. 10(3): 407-416. <https://doi.org/10.1007/s40003-020-00509-9>.
- Özden N, Uslu İ, Sökmen Ö, Metinoğlu F. 2020. İzmir ili tarım topraklarının verimlilik durumları ile mikroelement kapsamının belirlenerek haritalanması. *Toprak Su Dergisi. Özel Sayı: 31- 40*.
- Özkan CF, Arpacioğlu AE, Arı N, Demirtaş EI., Asri FÖ, 2009. Antalya bölgesinde elma yetiştirilen toprakların verimlilik durumlarının incelenmesi. *Tarım Bilimleri Araştırma Dergisi*. 2(2): 95-99.
- Özyazıcı AM, Dengiz O, Aydoğan M, Bayraklı B, Kesim E, Urla Ö, Yıldız H, Ünal E. 2016. Orta ve Doğu Karadeniz Bölgesi tarım topraklarının temel verimlilik düzeyleri ve alansal dağılımları. *Anadolu Tarım Bilimleri Dergisi*. 31: 136-148. DOI: 10.7161 ajans.2016.31.1.136-148.
- Parlak M, Fidan A, Kızılıcak İ, Koparan H. 2008. Eceabat ilçesi (Çanakkale) tarım topraklarının verimlilik durumlarının belirlenmesi. *Ankara Üniversitesi Ziraat Fakültesi, Tarım Bilimleri Dergisi*. 14 (4): 394-400.
- Reza SK, Baruah U, Sarkar D. 2012. Spatial variability of soil properties in brahmaputra plains of North-eastern India: A Geostatistical Approach. *Journal of the Indian Society of Soil Science*. 60 (2): 108-115.
- Reza SK, Nayaka DC, Chattopadhyaya TS, Mukhopadhyaya S, Singh, SK, Srinivasan R. 2016. Spatial distribution of soil physical properties of alluvial soils: a geostatistical approach. *Archives of Agronomy and Soil Science*. 62

- (7):972-981. <http://dx.doi.org/10.1080/03650340.2015.1107678>
- Richards LA. 1954. Diagnosis and improvement of saline and alkali soils. USDA Agriculture Handbook. No: 60.
- Saraçoğlu M, Sürücü A, Koşar İ, Anlağan MT, Aydoğdu M, Kara H. 2014. Şanlıurfa ili Halfeti ilçesi topraklarının bazı özellikleri ve bitki besin elementi kapsamının belirlenmesi. *Toprak Bilimi ve Bitki Besleme Dergisi*. 2 (2): 38 – 45.
- Saygın F, Gürsoy FE, Demirdağ İ, Dengiz O. 2017. Çataklı çayı havzası doğu yakasında çay tarımı yapılan toprakların fiziksel, kimyasal ve verimlilik özelliklerinin belirlenmesi. *Turk J Agric Res*. 4(2): 143-154.
- Shit KP, Bhunia SG, Maiti R. 2016. Spatial analysis of soil properties using GIS based geostatistics models. *Model. Earth Syst. Environ*. (2):107. DOI: 10.1007/s40808-016-0160-4
- Tolu B. 2023. Kocaeli-Kartepe tarım topraklarının bazı önemli özelliklerinin CBS içinde konumsal analizi. Bursa Uludağ Üniversitesi Fen Bilimleri Enstitüsü Toprak Bilimi Ve Bitki Besleme Anabilim Dalı Yüksek Lisans Tezi. Bursa, 59 S.
- Töreyan G, Özdemir İ, Kurt T.,2010. ArcGIS 10 desktop uygulama dokümanı. İşlem Coğrafi Bilgi Sistemleri Mühendislik ve Eğitim Ltd. Şti. 208 s. Ankara.
- Ülgen N, Yurtsever N. 1995. Türkiye gübre ve gübreleme rehberi (4. Baskı). TC Başbakanlık Köy Hizmetleri Genel Müdürlüğü Toprak ve Gübre Araştırma Enstitüsü Müdürlüğü Yayınları, GenelYayın No: 209, Teknik Yayınlar No: T.66, s. 209-230. Ankara.
- Yağanoğlu E, Aydın A. 2017. Erzurum İli Hınıs İlçesinde farklı bitkilerin yetiştirildiği toprakların bazı fiziksel ve kimyasal özelliklerinin araştırılması. *Atatürk Üniversitesi Ziraat Fakültesi Dergisi*. 48 (2): 125-131.
- Zhou HH, Chen YN, Li WH. 2010. Soil properties and their spatial patterninan oasis on the tarim river, northwest China. *Agric Water Manag* 97(11):1915-1922.



## Yabani tip ve hedef olmayan model bir organizmanın, *Drosophila melanogaster* Oregon-R, dişi ve erkek popülasyonlarında bakır hidroksit ( $\text{Cu}(\text{OH})_2$ ) nanopestisitine ait etkilerin *in vivo* ömür uzunluğu testi ile araştırılması

Handan Uysal\*<sup>ID</sup>

Atatürk Üniversitesi, Fen Fakültesi, Biyoloji Bölümü, Erzurum, Türkiye

\*Corresponding author : [hauysal@atauni.edu.tr](mailto:hauysal@atauni.edu.tr)  
Orcid No: <https://orcid.org/0000-0002-4290-8223>

Received : 25/04/2024  
Accepted : 10/08/2024

**To Cite / Atıf için:** Uysal H. 2024. Yabani tip ve hedef olmayan model bir organizmanın, *Drosophila melanogaster* Oregon-R, dişi ve erkek popülasyonlarında bakır hidroksit ( $\text{Cu}(\text{OH})_2$ ) nanopestisitine ait etkilerin *in vivo* ömür uzunluğu testi ile araştırılması. Eurasian J Bio Chem Sci, 7(2):96-101 <https://doi.org/10.46239/ejbc.1473449>

**Özet:** Bağ, zeytin ve turuncgil ekili bakır içeren topraklarda kullanılan bakır hidroksit (bir çeşit fungusit) inovatif bir nanopestisitir. Ancak geleneksel pestisitlerin yerini alan nanopestisitler, hedef organizmalar kadar hedef olmayan organizmaları da (omurgalı ya da omurgasız) etkileyebilmektedirler. Bu durum özellikle biyoçeşitlilik bakımından önemli bir risk faktörüdür. Bu çalışmada böyle bir riskin olup olmadığını araştırabilmek için *Drosophila melanogaster* Oregon-R'nin dişi ve erkek popülasyonlarına *in vivo* ömür uzunluğu testi uygulanmıştır. Farklı dozlarda (10, 20, 40 ve 80 ppm)  $\text{Cu}(\text{OH})_2$  nanopestisitinin kronik olarak uygulanması ile her iki popülasyonda hem maksimum hem de ortalama ömür uzunluğunun kontrol grubuna göre azaldığı görülmüştür ( $p < 0,05$ ).

**Anahtar kelimeler:** Nanoformülasyon, çevresel risk, sürdürülebilir tarım, inovatif ürün

### *Investigation of the effects of copper hydroxide ( $\text{Cu}(\text{OH})_2$ ) nanopesticide on female and male populations of a wild-type and non-target model organism, *Drosophila melanogaster* Oregon-R, by *in vivo* longevity test*

**Abstract:** Copper hydroxide (a type of fungicide) is an innovative nanopesticide used in vineyard, olive and citrus cultivated copper-containing soils. However, nanopesticides, which replace traditional pesticides, can affect non-target organisms (vertebrates or invertebrates) as well as target organisms. This situation is an important risk factor, especially in terms of biodiversity. In this study, *in vivo* longevity testing was applied to male and female populations of *Drosophila melanogaster* Oregon-R to investigate whether there is such a risk. With the chronic application of  $\text{Cu}(\text{OH})_2$  nanopesticide at different doses (10, 20, 40 and 80 ppm), it was observed that both maximum and average lifespan decreased in both populations compared to the control group ( $p < 0,05$ ).

**Keywords:** Nanoformulation, environmental risk, sustainable agriculture, innovative product

#### 1. Giriş

Nanometre (nm), gözle görülemeyen mikroskobik maddeleri ölçmek için kullanılan matematiksel bir ölçü birimi olup metrenin milyarda biridir. Nanometre ile metrenin büyüklük olarak karşılaştırması yapılırken bir bilye ile dünyanın büyüklüğü karşılaştırılmalıdır. Bir başka ifade ile nm, günlük yaşantımızda kullanılan ölçü birimleri ile karşılaştırılamayacak kadar küçük bir boyuttur. Nano parçacık ise 1-100 nanometre boyutlarındaki tek bir maddeyi ifade etmek için

kullanılmaktadır. Bu büyüklükteki parçacıklar ne çıplak gözle ne de ışık mikroskobu ile görülemezler.

1 ile 100 nanometre arasında değişen ölçülerde yapılan teknolojik çalışmalarının tümü ise nanoteknoloji olarak tanımlanmaktadır (Seaton ve Donaldson 2005). Nanoteknoloji, fonksiyonel sistemlerin kurulumu için "moleküler ölçekte mühendislik bilimi" (moleküler nanoteknoloji) olarak da tanımlanabilir. Bu bilim dalı, makro ölçekte ürünlerin imalatı için atomların



ve moleküllerin kontrolünü sağlamaktadır. Günümüzde hayatın pek çok alanında daha fonksiyonel ve küçük boyutlu ürünlerin imal edilmesi için nanoteknolojiden faydalanılmaktadır (Hanks ve ark. 2015). Nanoteknoloji disiplinler arası bir bilim dalı olup fizik, kimya, biyoloji, bilgisayar, tekstil, kozmetik, eczacılık ve tıp alanlarında nanoteknolojik gelişmeler kullanılmaktadır. Tıpta teşhis ve tedavi süreçlerinde, akıllı ilaçların geliştirilmesinde, sensör, sinyal iletimi, gösterge sistemleri ile savunma sanayinde, nanoteknolojik kumaş üretimi gibi oldukça farklı alanlarda nanoteknolojiden faydalanılmaktadır. Ayrıca altın, gümüş, çinko ve bakır gibi inorganik nanopartiküller ile de zirai alanlarda kullanılan nanopestisitler üretilmektedir (Xu ve ark. 2006). Nanopartiküller orman yangınları, buharlaşma, volkanik patlamalar, çöl tozları ve erozyon sonucu doğal yollarla çevrede bulunabilirler. Egzoz gazları, fosil yakıt kullanımı veya endüstriyel işlemler sonucunda, ayrıca ilaçlama yapılması, biyomedikal görüntüleme teknikleri ve kozmetik ürünler ile de doğaya partikül salınımı gerçekleşebilmektedir.

Dünya nüfusunun hızla artması ile birlikte çarpık kentleşme ve betonlaşmadan kaynaklanan ekilebilir tarım arazilerinin azalması açlık tehlikesine sebep olabilecek nedenlerden birisidir. Bu nedenle birim alandan alınan ürün miktarının artırılabilmesi için günümüzde hala geleneksel pestisitler kullanılmaktadır. Bu tip pestisitlerin yanlış ve fazla kullanımı ürünler üzerinde kalıntı oluşturmakta ve besin zincirine bağlı olarak diğer canlılarda da pestisit maruziyeti meydana gelebilmektedir. Sadece bu sebep bile insan ve hayvanların pestisit toksisitesine maruz kalmasına neden olmaktadır. Pestisitlere kronik olarak maruz kalınması ise kanser gibi ciddi sağlık problemlerini tetiklemektedir. Ayrıca doğal koşullarda hedef organizmalar kadar hedef olmayan organizmaların da yok olmaları ekolojik dengenin temel parametrelerinden birisi olan biyoçeşitlilik bakımından risk oluşturmaktadır (Özyurt ve ark. 2018). Nanoteknolojiden faydalanılarak hazırlanan yenilikçi nanopestisitler ise daha az aktif madde içerdikleri için günümüzde zararlılara karşı daha etkin şekilde kullanılmakta ve tercih edilmektedir (Vijayalakshmi ve ark. 2015; Ram ve ark. 2017; Raghvendra ve ark. 2021).

Nanopestisit için evrensel bir tanım bulunmamaktadır. Ancak "etken madde ve yardımcı materyalleri nano boyutta içeren pestisit" tanımı bu alanda çalışan otoriteler tarafından oldukça uygun görülmektedir (Chowdappa ve Shivakumar 2013). Nanopestisitlerin boyutları onların verimliliklerini ve hedef hücreye girebilme etkinliklerini artırmaktadır. 150nm'den küçük olan partikül büyüklüğüne sahip pestisitler hücre zarından geçerek etki alanına ulaşabilmektedir. Yüksek çözünürlük, üstün penetrasyon, kontrollü salınım, hedef odaklı pestisit olmaları ve biyolojik performanstaki artış nanopestisitlerin tercih sebeplerindedir (Kumar ve ark. 2019). Ayrıca çevre güvenliği bakımından biyolojik olarak parçalanabilen malzemelerden yapılmış olmaları da nanopestisitlerin kullanımını her geçen gün artırmaktadır. Ancak düşünebildiğimizden daha küçük boyutlu olan

nanopartiküllerin nanopestisitlerin kullanımı sırasında çevreye salınması hava yoluyla taşınmasına da sebep olabilmektedir. Bu durumda nanopestisitler yalnızca kullanıldıkları çevrede değil aynı zamanda daha uzak bölgelerde de omurgalı ve omurgasız hayvanlar, bitkiler ve insanlarda olumsuz biyoetkileşime sebebiyet verebilirler. Nanopestisitlere dayalı bir başka risk de "sürdürülebilir ekolojik denge bakımından yaşanan çevredeki toprak, su ve hava kirliliğidir (Khan ve Rizvi 2014).

Günümüzde modern insanın ihtiyaçlarına uygun ve hayatını kolaylaştıracak inovatif ürünlerin geliştirilmesi son derece önemlidir. Nanoteknoloji bunları sağlayabilecek teknolojik yaklaşımlara sahip bir bilim dalıdır. Ancak nanoteknolojik ürünlerin insan ve ekosistem bakımından pek çok sorun yaratabileceği de göz ardı edilmemelidir (Buseck ve Pósfai 1999; Kah ve ark. 2013). Çünkü Buzea ve ark. (2007)'a göre, bu teknolojiye bağlı gelişmeler ile ortamdaki nanopartiküllerin miktarı ve çeşidi artış göstermiştir. Yeni bir teknoloji olmasından dolayı da nanopartiküllerin farklı organizmalarda ne gibi zararlı etkilerinin olabileceği pek bilinmemektedir. Bu nedenle nanopartiküllerin daha az zararsız olabilmesi için nanoteknolojik ürünlerin "güvenilirlik test süreleri" son derece önemlidir. Ancak bu tip ürünlerin piyasaya sunulma sürelerinin yeterli olup olmadığı bile hala tartışmalıdır.

İnsanların nano ürünleri kullanımı ile nanopartiküller vücudumuza solunum, beslenme ve deri yoluyla girerek kana geçmekte ve pek çok organa ulaşabilmektedir. (Medina ve ark. 2007). Hatta tüm canlılar üretim aşamasında bile doğaya saçılan nanopartiküllere solunum ya da besin zinciri yoluyla maruz kalabilirler. Bu nedenle, nanopartikül içeren ürünler, günlük hayat için kullanıma sunulmadan önce dokulara karşı alerjik reaksiyon özellikleri, biyolojik uyumluluğu ve genetik açıdan toksisitesi bakımından mutlaka araştırılmalıdır. Özellikle sağlık alanında kullanılan metal nanopartiküllerin insanlarda hücre zehirlenmesine yol açtığı yapılan genetik toksisite testlerinden anlaşılmaktadır. Yine metal nanopartiküllerin insanlarda genotoksik potansiyele sahip oldukları ve nanopartiküllerin konsantrasyon artışına paralel olarak DNA hasarında artış olduğu Revell (2006) tarafından saptanmıştır. Genellikle bu tip partiküller, Patra ve Goswami (2012)'ye göre, membran proteinlerine bağlanarak onların çalışmasını engellerler ve membran geçirgenliğini bozarlar. Buna ilaveten metal nanopartiküller reaktif oksijen türlerinin (ROT) oluşumuna sebep olabilirler (Zeng ve ark. 2007). Nanomalzemelere bağlı olarak ROT oluşumu ise vücutta alerjik reaksiyonlara, otoimmün sistemde zayıflama, inflamatuvar, mutajenik ve karsinojenik etkilere yol açabilmektedir (Pfuhrer ve ark. 2013).

Sayısı ve çeşidi her geçen gün artan küresel tehditlere karşı biyoyararlılıkları bakımından nanopestisitlerin yenilenmiş etkinlikleriyle tarım alanlarında kullanılması insan ve çevre sağlığı bakımından son derece önemsenmektedir. Nanoteknoloji tabanlı bu gelişme ile şimdiye kadar bilinen pestisitlere göre daha az oranda aktif madde içeren ve kontrollü salım ile uzun süreli koruma sağlayabilen nanopestisitler günümüzde üretici için oldukça cazip hale



gelmiştir. Ancak nanopestisitler, bu yenilikçi özelliklerinden dolayı tarım alanlarında kullanılırken bazı risklere de sebep olabilirler. Bu amaçla da nanopestisitlerin öncelikle kullanıcıya, flora ve fauna üzerine risklerinin model organizmalar kullanılarak kısa süreli *in vivo* testler ile toksisite bakımından değerlendirilmesi oldukça önemlidir (Amorim ve ark. 2020). Özellikle sunulan bu çalışmada üzerinde durulan en önemli nokta, nanopestisitlerin hedef olmayan organizmalar için risk oluşturup oluşturmadığının belirlenebilmesidir ve tarım alanlarında kullanılan inorganik bakır hidroksit ( $\text{Cu}(\text{OH})_2$ ) nanopestisitinin hedef olmayan model organizmalardan birisi olan *Drosophila melanogaster* Oregon-R'nin ömür uzunluğu üzerine etkileri erkek ve dişi popülasyonlarında ayrı ayrı *in vivo* olarak araştırılmıştır.

## 2. Materyal ve Metot

### 2.1. Kullanılan Kimyasal Maddeler

Çalışmada kullanılan  $\text{Cu}(\text{OH})_2$  nanopestisiti (Cas No. 20427-59-2) molekül ağırlığı 7,56gr/mol, yoğunluğu 3,36 gr/cm<sup>3</sup>, erime noktası 80°C olan bir çeşit fungusittir ve Hefei TNJ Chemical Industry Co., Ltd. şirketinden satın alınmıştır. Stok kültürlerin ve uygulama gruplarının beslenmesi için kullanılan Standart *Drosophila* besiyerinin (SDB) içeriğini oluşturan agar agar (Cas No. 9002-18-0) ve küf inhibitörü propionik asit (Cas No. 79-09-4) ile ergin bireylerin eterizasyonu için kullanılan dietil eter (Cas No. 60-29-7) gibi kimyasal maddeler de Sigma-Aldrich Firması'ndan (St. Louis, MO, USA) temin edilmiştir.

### 2.2. Kullanılan Model Organizma ve Deney Koşulları

Uygulamalarda kullanılan *Drosophila melanogaster* Oregon-R (Diptera: Drosophilidae) kahverengi vücutlu, uzun kanatlı, yuvarlak-kırmızı gözlü herhangi bir mutant karakter taşımayan yabani tip soydur. Bu soy, Atatürk Üniversitesi, Fen Fakültesi, Biyoloji Bölümü Genetik Araştırma Laboratuvarı'nda 1988 yılından bu yana kendileştirilmiş ve genetik olarak ileri derecede homojen bir laboratuvar stoğudur. *Drosophila* stok kültürleri, %40-60 bağıl nem, 25±1°C sıcaklık ile sürekli karanlık koşulları taşıyan ısıtmalı-soğutmalı sıcaklık kabinlerinde, içinde SDB bulunan 250ml'lik şişelerde yaşatılmaktadır (Uysal ve ark. 2006). Stok kültürler her 15 günde bir taze SDB'ye aktararak yeni yavru bireyler elde edilmektedir.

### 2.3. Ömür uzunluğu deneylerinin yapılışı

Kısa süreli *in vivo* deneysel yöntemlerden birisi olan bu çalışma ile  $\text{Cu}(\text{OH})_2$  nanopestisitinin ömür uzunluğu üzerine etkisi *D. melanogaster*'in dişi ve erkek popülasyonlarında ayrı ayrı araştırılmıştır. Deneysel prosedür için öncelikle 10♀♀ X 10♂♂ çaprazlamaları yapılmış ve çaprazlamanın yapıldığı tarihten itibaren kültür şişeleri içinde pupanın görüldüğü yaklaşık 7.gün itibariyle ebeveynler ortamdan uzaklaştırılmıştır. Pupadan çıkan♀♀ ve♂♂ bireyler, 4-5 saatte bir henüz çiftleşmeden 3 gün süreyle toplanmışlardır. Böylece 1-3 günlük aynı yaşlı (72±4saatlik) 100'er birey ile kontrol ve uygulama grupları olmak üzere iki ayrı deney seti hazırlanmıştır. Kontrol grubu yalnızca SDB ile uygulama

grupları ise SDB+ suda çözülen farklı dozlarda  $\text{Cu}(\text{OH})_2$  (10, 20, 40 ve 80 ppm) ile hazırlanmıştır. Nanopestisit uygulamaları kronik olarak ve üç tekrarlı yapılmıştır.

Deneysel, her iki deney seti için eş zamanlı başlatılmıştır. Bu amaçla, önce kontrol ve uygulama gruplarına ait tüm ergin sinekler kültür şişeleri içinde 2 saat aç bırakılmıştır. Her gruba ait♀♀ ve♂♂ bireyler, haftada iki kez gerçekleştirilecek sayımların kolay yapılabilmesi için, dört ayrı gruba ayrılmış ve kültür şişelerine 25'er birey olacak şekilde konulmuştur. Uygulama ve kontrol grubuna ait tüm kültür şişeleri aynı şartlarda uygun sıcaklık kabinlerinde tutulmuş ve uygulamalar süresince besinler haftada iki kez tazelenmiştir. Birey sayıları her uygulama günü kontrol edilip ölen bireyler ortamdan uzaklaştırılmış ve yaşayan bireyler ile kronik pestisit uygulamasına devam edilmiştir. Her bir uygulama grubunda en son birey ölünceye kadar kayıtlar dikkatle tutulmuştur.

### 2.4. İstatistiksel yöntemler

Ömür uzunluğu deneylerinden elde edilen verilerle ilgili istatistiksel analizler SPSS 13.0 programı ile yapılmıştır. Kontrol ve uygulama gruplarının ömür uzunluğu ortalamaları istatistiksel olarak %5 düzeyinde Duncan testiyle karşılaştırılmıştır. Dişi ve erkek bireylerin karşılaştırılması için de bağımsız gruplara istatistiksel olarak %5 düzeyinde X<sup>2</sup> testi uygulanmıştır.

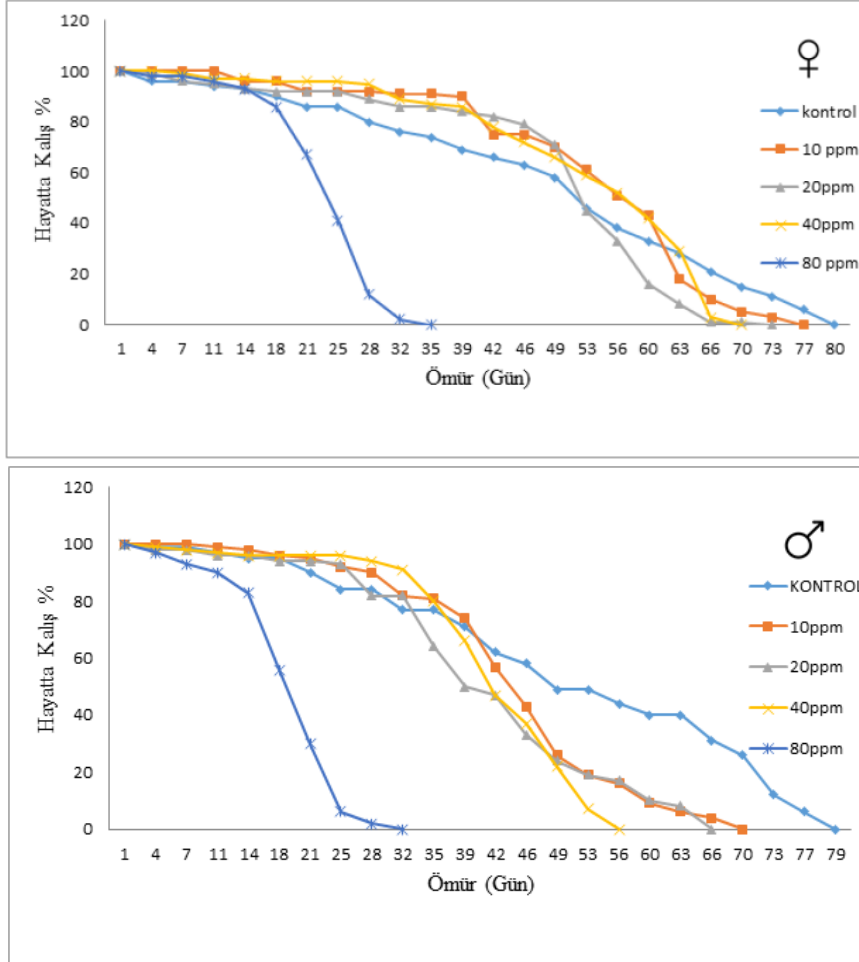
## 3. Bulgular ve Tartışma

Sunulan bu çalışmada kısa süreli *in vivo* ömür uzunluğu testi için♀♀ ve♂♂ popülasyonlarında hem maksimum ömür uzunluğu hem de ortalama ömür uzunluğu dikkate alınarak değerlendirilmiştir. Deneysel prosedürde de bahsedildiği gibi  $\text{Cu}(\text{OH})_2$  nanopestisiti suda çözünebildiği için kontrol grubu olarak yalnızca distile su ile hazırlanan SDB (1) kullanılmıştır. Maksimum ömür uzunluğu♀♀ popülasyonu için kontrol grubunda 80 gün ve♂♂ popülasyonu için de 79 gün olarak belirlenmiştir. Uygulama grubunda ise bu değerler dişi popülasyonunda 2 nolu deney grubunda 77 gün; 3 nolu deney grubunda 73 gün; 4 nolu deney grubunda 70 gün ve 5 nolu deney grubunda ise 35 gün olarak bulunmuştur (Şekil 1). Erkek popülasyonuna ait maksimum ömür uzunluğu değerleri de en düşük uygulama grubundan (2) en yüksek uygulama grubuna doğru (5) 70 günden 32 güne kadar gerilemiştir (Şekil 2). Tüm bu değerler doz artışına bağlı olarak  $\text{Cu}(\text{OH})_2$  nanopestisitinin maksimum ömür uzunluğunu kontrol grubuna göre özellikle en yüksek uygulama gruplarında (5)♀♀ popülasyonu için %43,75 ve♂♂ popülasyonu için de %40,51 oranında azalttığını göstermektedir (Tablo 1).

*D. melanogaster*'in♀♀ ve♂♂ popülasyonlarına ait ortalama ömür uzunluğu değerleri de Tablo 1'de görülmektedir.♀♀ popülasyonunda kontrol grubu (1) için ortalama ömür uzunluğu 65,87±1,43 gün iken♂♂ popülasyonunda bu değer 58,95±1,63 gündür.♀♀ popülasyonunda ortalama ömür uzunluğu değerleri,  $\text{Cu}(\text{OH})_2$  nanopestisitinin artan dozuna bağlı olarak (2, 3, 4 ve 5 nolu uygulamalar için) sırasıyla 54,33±1,45;

50,63±1,47; 53,90±1,39 ve 24,49±0,56 gün iken ♂♂ popülasyonunda aynı uygulamalar için bu değerler 45,28±1,22; 42,37±1,37; 42,61±1,01 ve 19,79±0,57 gün olarak hesaplanmıştır. Ortalama ömür uzunluğu bakımından kontrol ve uygulama grupları arasında gözlenen bu fark hem dişi hem de erkek popülasyonu için istatistiki olarak  $p<0,05$  düzeyinde önemlidir (Tablo 1). Bu çalışmada ayrıca ortalama ömür uzunluğu bakımından

regresyon düzeyleri de belirlenmiş ve dişi popülasyonu için  $R= -0,622$  ve erkek popülasyonu için de  $R= -0,655$  olarak bulunmuştur. Hem maksimum hem de ortalama ömür uzunluğu bakımından kontrol grubuna göre uygulama gruplarında gözlenen gerilemeler  $\text{Cu}(\text{OH})_2$  nanopestisitinin her iki popülasyonda da sınırlayıcı bir faktör olduğunu göstermektedir.



Şekil 1.  $\text{Cu}(\text{OH})_2$  uygulanmış *D. melanogaster*'in ♀♀ ve ♂♂ bireylerine ait ömür eğrileri

Tablo 1.  $\text{Cu}(\text{OH})_2$  uygulanmış *D. melanogaster*'in ♀♀ ve ♂♂ popülasyonlarına ait maksimum ve ortalama ömür uzunluğu değerleri ile regresyon düzeyleri

Cu(OH) <sub>2</sub> nanopestisiti								
		♀♀			♂♂			
Deney grupları	Birey sayısı	Maksimum ömür	Ortalama ömür uzunluğu±SH	Önem kontrolü(p)	Birey sayısı	Maksimum ömür	Ortalama ömür uzunluğu±SH	Önem kontrolü(p)
Distile su kontrol (1)	100	80	65,87±1,43	1-2,3,4,5* 2-5* 3-5* 4-5*	100	79	58,95±1,63	1-2,3,4,5* 2-5* 3-5* 4-5*
10 ppm (2)	100	77	54,33±1,45		100	70	45,28±1,22	
20 ppm (3)	100	73	50,63±1,47		100	66	42,37±1,37	
40 ppm (4)	100	70	53,90±1,39		100	56	42,61±1,01	
80 ppm (5)	100	35	24,49±0,56		100	32	19,79±0,57	
Regresyon düzeyi	R= -0,622				R= -0,655			

SH:Standart hata, \*  $p<0,05$  düzeyinde önemlidir.

Birleşmiş Milletler Gıda ve Tarım Örgütü (Food and Agriculture Organization/FAO), dünyada herhangi bir bölge ya da ülkede baş gösterebilecek açlığı yok etmek ve beslenme şartlarını iyileştirmek amacıyla 1943 yılında kurulmuş bir örgüttür. FAO (2018)'ya göre, pestisitlerin etkin ve yaygın şekilde uygulanmasına rağmen dünyada zirai mahsullerin % 40'a yakın kısmı bitki zararlıları ve bitkisel hastalıklardan etkilenmektedir. Bu bağlamda "Agrokimya"ya (tarım ürünlerini hammadde olarak kullanarak çeşitli kimyasal faaliyetler ile nitelik ve niceliklerini iyileştiren, aynı zamanda bitkiler için zirai ilaçlar ve gübreler üreten kimyanın alt bilim dallarından birisi) dayalı olarak artan dünya nüfusunun açlığa karşı korunabilmesi için ürün kaybının azaltılması, verimin artırılması, ekosistemlerin doğru yönetimi ve çevrenin korunabilmesi amacıyla tarımsal uygulamalarda pestisit veya gübre kullanımı gerek şart olarak görülmektedir (Das 2018). Ancak daha az ve dayanıklı aktif madde kullanılarak maliyetin azaltılması, böylece birim alandan alınan ürün miktarının artırılması, geleneksel pestisitlerin çevre üzerindeki baskısının en aza indirgenmesi ile sürdürülebilir tarım gibi bir dizi fayda agrokimyaya göre yeni nanoteknolojik gelişme ile elde edilen nanopestisitleri ön plana çıkarmaktadır (Sharon ve ark. 2010). Ticari kimyasal pestisitlere göre nanopestisitler hedef organizmalar üzerine düşük konsantrasyonlarda bile daha fazla etki göstermektedir (Kah ve ark. 2013). Son yıllarda özellikle bakır bazlı nanopestisitler toprakların çoğunda bakır bulunduğu ve diğer kimyasal pestisitlere göre daha az toksik kabul edildiklerinden dolayı oldukça yaygın şekilde kullanılmaya başlanmıştır (Kamel ve Mousa 2015). Bakır bazlı nanopestisitlerin özellikle üzüm bağı, zeytin, turuncgil, patates ve domates ekili alanlarda yaygın görülen hastalıklarla mücadelede etkili ve mükemmel koruma sağladığı da bildirilmektedir (Zhao ve ark. 2018).

Günümüzde organik ve inorganik olmak üzere üretilen ve zirai amaçlı olarak kullanılan nanopestisitlerin sayısı arttıkça bu pestisitlerin kültür bitkileri ve hedef olmayan diğer organizmalar üzerine olası etkilerinin anlaşılması insan ve çevre sağlığı açısından oldukça önemlidir (Jacques ve ark. 2017; Fojtova ve ark. 2019). Bu amaçla özellikle nanopestisitlerin biyoakümülyasyonunun belirlenebilmesi için model bir organizma olan *D.melanogaster* ve *in vivo* ömür uzunluğu testi ideal bir biyobelirteçtir.

Tablo 1'de de görüldüğü gibi uygulama gruplarında  $Cu(OH)_2$  nanopestisitinin artan dozlarda ve kronik olarak kullanımı, dişi ve erkek bireylerde biyoakümülyasyona dayalı olarak maksimum ve ortalama ömür uzunluğunu kontrol grubuna göre anlamlı derecede düşürmüştür ( $p<0,05$ ). Çünkü deneysel prosedüre göre, uygulama gruplarına ait sıcaklık, bağıl nem ve besiyeri içeriği gibi ortam şartları stabil tutulmuştur ve tek değişgenin besiyerine farklı dozlarda ilave edilen  $Cu(OH)_2$  nanopestisiti olması sebebiyle ömür uzunluğunda meydana gelen değişmeler tarafımızdan bu nanopestisite atfedilmektedir. Özellikle Şekil 1'de verilen ♀♀ ve ♂♂ popülasyonlarına ait dikkörtgensel ömür eğrileri,  $Cu(OH)_2$

nanopestisitinin sebep olduğu toplu ölümleri açıkça göstermektedir. Khan ve Rizvi (2014)'ye göre, nanopestisitler kullanıldıkları alanlarda bitkilerin yaprak ve çiçek kısımlarına akümüle olarak stomaların tıkanmasına, stigma üzerinde polen çimlenmesini engelleyen bir tabaka oluşumuna ve vasküler dokulara girerek su, besin gibi ürünlerin taşınmasına olumsuz etkilerde bulunabilirler. Nanopestisitler insan ve hayvanlar tarafından teneffüs edildiğinde de akciğerlerde alveollere kadar girebilmekte ve gaz alışverişini engelleyerek solunumu güçleştirmektedir. Özellikle tarım arazilerinde hedef olmayan omurgasız hayvanlar için de benzeri bir mekanizma ile ister doğal ortamda hava yoluyla taşınma dayalı olarak ister sunulan bu çalışmada olduğu gibi *Drosophila* popülasyonunun kronik beslenmesi ile organizma tarafından alınan nanopestisit partikülleri, vücudu ağ gibi saran tübüler yapıdaki trake sistemini tıkayarak solunum güçlüğüne bağlı toplu ölümlere sebep olabilmektedir. Şekil 1'de doz artışı ile birlikte görülen dikkörtgensel grafikler, tarafımızdan biyoakümülyasyonun göstergesi olarak kabul edilmektedir.

Popülasyon büyüklüğünü etkileyen ve popülasyonun yaşlanmasına sebep olan faktörler olarak bilinen coğrafik izolasyonlar, seleksiyon, mutasyon, göçler ya da doğum ve ölüm oranları arasında özellikle herhangi bir faktöre dayalı ölüm oranlarındaki artış, bu çalışmada olduğu gibi hem ömür uzunluğunu kısaltmakta hem de buna paralel olarak popülasyonun yaşlanmasına sebep olmaktadır. Ancak bize göre, nanopestisitler biyoakümülyasyona dayalı ölümleri tetikleyerek popülasyon yaşlanmasına neden olabileceği gibi genotoksisiteye dayalı mutasyon teorisi, proteinlerin değişikliğe uğrama teorisi ya da oksidatif stres teorisi gibi yaşlanma teorilerine bağlı olarak da günümüzde popülasyon yaşlanmasını hızlandırabilecek inovatif bir faktör olarak kabul edilebilir. Çünkü Lemire ve ark. (2013)'a göre, hücrel proteinlere bağlanabilen nanopartiküller hem membranda yer alan integral proteinlerin hem de sitoplazmada bulunan periferik proteinlerin düzgün çalışmasını engelleyerek hücre geçirgenliğinde ve hücrel taşımadaki bozulmalara sebep olabilmektedir. Zeng ve ark. (2007)'a göre de, nanopartiküller DNA'ya bağlanarak genotoksik etkisiyle hücrel ölümleri uyurabilmektedir. Ayrıca ROT'ların miktarını artırarak yine hücrel düzeyde oksidan ve antioksidanlar arasındaki dengenin bozulmasına da sebep olabilmektedir. Tüm bu mekanizmalar canlı sistemlerde tek başına çalışabildiği gibi bir ya da daha fazla mekanizma eş zamanlı olarak ömür uzunluğu üzerinde ket vurucu etki gösterebilir. Ayrıca yukarıda sayılan mekanizmalar kapsamında *Drosophila* gibi hedef olmayan herhangi bir organizmanın nanopestisitlerden etkilenmiş olması biyoçeşitlilik bakımından da sınırlandırıcı bir faktör olarak gözden uzak tutulmamalıdır (Gomes ve ark. 2019).

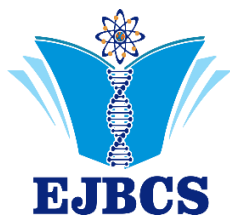
#### 4. Sonuç

Geleneksel pestisitler, amaç dışı ve doz aşımına bağlı kullanımlarından dolayı faydalı ve/veya hedef olmayan türlerin yok oluşuna, gıdalar üzerinde kalıntı oluşumuna, dirençli zararlıların gelişimine ve özellikle ilk etapta

kullanıcılarda zehirlenme etkileri ile ileri boyutlarda kanser gibi olası sağlık sorunlarına sebep olmaktadır. Tüm bu sorunların yaşanmaması için günümüzde nanoteknolojik üretim teknikleri kullanılarak çok daha az oranda aktif madde içeriğine sahip ticari nanoformülasyonlar üretilmektedir. Ancak ultraküçük boyutlara sahip olmasıyla birçok alanda başarıyla kullanılabilen nanopartiküller, bitki koruma amaçlı kullanılmadan önce farklı mutajenite, toksisite ve hatta genotoksisite testlerine tabi tutulmalıdır. Çünkü nanopestisitler yalnızca kullanıldıkları alanlardaki bitkileri değil daha uzak bölgelerdeki flora ve faunayı da etkileyebilmektedir. Bu sebeple, nanoteknoloji tabanlı ürünlerin bitki koruma amaçlı kullanımından önce ekosistemde oluşturabileceği riskler bakımından detaylı araştırılması çevre ve farklı canlı toplulukları bakımından gerek şarttır.

#### Kaynaklar

- Amorim MJB, Fernandez-Cruz ML, Hund-Rinke K, Scott-Fordsmand JJ. 2020. Environmental hazard testing of nanobiomaterials. *Environ Sci Eur*. 32: 101.
- Buseck PR, Pósfai M. 1999. Airborne minerals and related aerosol particles: effects on climate and the environment. *Proc Natl Acad Sci*. 96(7): 3372-3379.
- Buzea C, Blandino IIP, Robbie K. 2007. Nanomaterials and nanoparticles: sources and toxicity. *Biointerphases*. 2(4): 17-71.
- Chowdappa P, Shivakumar G, 2013. Nanotechnology in crop protection: Status and scope. *Pest Manag Horticult Ecosyst*. 19(2): 131-151.
- Das SK. 2018. Nanoscience in agriculture for agrochemicals. *Acta Sci Agric*. 2:1.
- FAO (Food and Agriculture Organization of the United Nations). 2018. The importance of bees and other pollinators for food and agriculture: Slovenia, Balkans.
- Fojtova D, Vasickova J, Grillo R, Bilkova Z, Simek Z, Neuwirthova N, Kah M, Hofman J. 2019. Nanoformulations can significantly affect pesticide degradation and uptake by earthworms and plants. *Environ Chem*. 16: 470-481.
- Gomes SIL, Scott-Fordsmand JJ, Campos EVR, Grillo R, Fraceto LF, Amorim MJB. 2019. On the safety of nanoformulations to non-target soil invertebrates. An atrazine case study. *Environ Sci Nano*. 6: 1950-1958.
- Hanks NA, Caruso JA, Zhang P. 2015. Assessing *Pistia stratiotes* for phytoremediation of silver nanoparticles and Ag(I) contaminated waters. *J Environ Manag*. 164: 41-45.
- Jacques MT, Oliveira JL, Campos EVR, Fraceto LF, Avila DS. 2017. Safety assessment of nanopesticides using the roundworm *Caenorhabditis elegans*. *Ecotoxicol Environ Saf*. 139: 245-253.
- Kah M, Beulke S, Tiede K, Hofmann T. 2013. Nanopesticides: state of knowledge, environmental fate, and exposure modeling. *Crit Rev Environ Sci Technol*. 43: 1823-1867.
- Kamel A, Mousa A. 2015. Nanobiofungicides: are they the next-generation of fungicides? *J Nanotechnol Mater Sci*. 2(1): 1-3.
- Khan MR, Rizvi TF. 2014. Nanotechnology: scope and application in plant disease management. *Plant Pathol J*. 13(3): 214-231.
- Kumar S, Nehra M, Dilbaghi N, Marrazza G, Hassan AA, Kim KH. 2019. Nano-based smart pesticide formulations emerging opportunities for agriculture. *J Control Release*. 294: 131-153.
- Lemire JA, Harrison JJ, Turner RJ. 2013. Antimicrobial activity of metals: mechanisms, molecular targets and applications. *Nat Rev Microbiol*. 11(6): 371-384.
- Medina C, Santos-Martinez MJ, Radomski A, Corrigan OI, Radomski MW. 2007. Nanoparticles: pharmacological and toxicological significance. *Br J Pharmacol*. 150: 552-560.
- Özyurt E, Kızılet H, Uysal H. 2018. Bio-interaction of chlordane on non-target organisms. *Commagene J Biol*. 2 (1): 48-54.
- Patra P, Goswami A. 2012. Zinc nitrate derived nano ZnO: Fungicide for disease management of horticultural crops. *Int J Innov Horticult*. 1(1):28-33.
- Pfuhler S, Elespuru R, Aardema MJ, Doak SH, Donner EM, Honma M. 2013. Genotoxicity of nanomaterials: refining strategies and tests for hazard identification. *Environ Mol Mutagen*. 54 (4): 229-268.
- Raghvendra PS, Rahul H, Geetanjali M. 2021. Nanoparticles in sustainable agriculture: An emerging opportunity. *Environ Sci Process Impacts*. 329:1234-1248.
- Ram P, Atanu B, Quang DN. 2017. Nanotechnology in sustainable agriculture: recent developments, challenges, and perspectives. *Front Microbiol*. 8: 1-13.
- Revell PA. 2006. The biological effects of nanoparticles. *Nanotechnol Percept*. 2: 283-381.
- Seaton A, Donaldson K. 2005. Nanoscience, nanotoxicology, and the need to think small. *Lancet*. 365: 923-927.
- Sharon M, Choudhary AK, Kumar R. 2010. Nanotechnology in agricultural diseases and food safety. *J Phytol* 2(4): 83-92.
- Uysal H, Şişman T, Aşkın H. 2006. *Drosophila* biyolojisi ve çaprazlama yöntemleri. Erzurum, Türkiye, Atatürk Üniversitesi Yayınları, 53 pp. ISBN:975-442-111-0.
- Xu ZP, Zeng QP, Lu GQ, Yu AB. 2006. Inorganic nanoparticles as carriers for efficient cellular delivery. *Chem Engrg Sci*. 61: 1027-1040.
- Vijayalakshmi C, Chellaram C, Kumar SL. 2015. Modern approaches of nanotechnology in agriculture-A review. *Biosci Biotechnol Res Asia*. 12(1): 327-331.
- Zeng F, Hou C, Wu SZ, Liu XX, Tong Z, Yu SN. 2007. Silver nanoparticles directly formed on natural macroporous matrix and their anti-microbial activities. *Nanotechnol*. 18:1-8.
- Zhao X, Cui H, Wang Y, Sun C, Cui B, Zeng Z. 2018. Development strategies and prospects of nano-based smart pesticide formulation. *J Agric Food Chem*. 66: 6504-6512.



## The potential use of *Epilobium hirsutum* L. in phytoremediation of zinc and an efficient method for *in vitro* propagation

Nüket Akanlı Bingöl<sup>1</sup> , Betül Akin<sup>2\*</sup> , Nergiz Erdaş<sup>3</sup> 

<sup>1</sup>Dumlupınar University, Art and Science Faculty, Department of Biology, Kütahya, Türkiye

<sup>2\*</sup>Dumlupınar University, Art and Science Faculty, Department of Biology, Kütahya, Türkiye

<sup>3</sup>Dumlupınar University, Institute Graduate Education, Department of Biology, Kütahya, Türkiye

\*Corresponding author : [betul.akin@dpu.edu.tr](mailto:betul.akin@dpu.edu.tr)  
Orcid No: <https://orcid.org/0000-0002-2325-7496>

Received : 17/09/2024  
Accepted : 13/10/2024

**To Cite / Atf için:** Akanlı Bingöl N, Akin B, Erdaş N. 2024. The potential use of *Epilobium hirsutum* L. in phytoremediation of zinc and an efficient method for *in vitro* propagation. Eurasian J Bio Chem Sci, 7(2):102-110 <https://doi.org/10.46239/ejbc.1548937>

**Abstract:** This study aimed to evaluate the capacity of *Epilobium hirsutum* L. (Onagraceae), a wetland plant, to accumulate and tolerate zinc (Zn) and its *in vitro* propagation potential. Root-shoot length, fresh weight, pigment, and protein content were analyzed in the plants grown in different Zn concentrations, including 0, 10, 20, 30, 40, 50, 75, 100, 150, and 200 mg Zn/L. In the seedlings grown at 50 and 75 mg Zn/L concentrations, a reduction in the relative root length, shoot length, and fresh weight was detected. It was found that there was a negative correlation between pigment and protein contents of *E. hirsutum* and increased Zn concentrations of solutions. On the other hand, it was determined that a considerable amount of Zn was accumulated by *E. hirsutum* in its roots (10 598 mg Zn/kg DW). In tissue culture experiments, it was found that MS medium was effective for the germination of the plant (97%). When the growth parameters of plants grown in different concentrations of Gibberellic acid were evaluated, the highest growth parameters were obtained at 50 mg/L. It has been concluded that the most successful mediums on shoot development were 1.0BAP/1.0NAA and 1.0BAP/1.0IBA. The highest number of shoots per explant was 1.0BAP/1.0NAA (3.96). The longest root length was also determined on medium with 1.0BAP/1.0IBA (0.28 cm). Regenerated shoots were transferred to different concentrations of root mediums. It was concluded that MS medium with 1.0IBA has been superior for root formation compared to other hormone concentrations.

**Keywords:** Phytoremediation, Purple loosestrife, Zinc

© EJBCS. All rights reserved.

### 1. Introduction

Heavy metal pollution in freshwater is a global environmental problem (Sabreena et al. 2022; Ali and Khan 2018, Tiwari et al. 2015). Rapid population growth, unplanned use of natural resources, and pollution caused by industrial wastes have caused a reduction in freshwater resources recently (Phillips et al. 2015; Akpor et al. 2014). With scientific studies, effective remediation techniques have been improved, such as adsorption, biosorption, remediation, and phytoremediation, using plants to remove pollution or contaminants from the environment. However, in the last decade, one of these techniques, studies on phytoremediation, has gained speed worldwide (Azubuike et al. 2016; Phillips et al. 2015; Fu and Wang 2011; Hegazy et al. 2011). One of the heavy metals, Zn, is an essential micronutrient for plants, and it is the second most common element found in living organisms after iron. However, zinc deficiency and toxicity affect plant growth. There is a

considerable difference in the tolerance of plants to zinc levels in soil. Zinc-tolerant plants have developed mechanisms to regulate excess zinc by sequestering Zn in vacuoles or forming complexes that reduce its harmful effects. Zn exists in five distinct forms in soils, including water-soluble, adsorbed, chelated, and Zn complexes (Noulas et al. 2018). The structure of more than 300 enzymes, such as superoxide dismutase, carbonic anhydrase, and polymerase, participates in carbohydrate, lipid, protein, phosphate, DNA, and RNA synthesis in plants (Nardis et al. 2018; Broadley et al. 2012). Besides, Zn promotes growth hormones and starch metabolism; it is also an essential microelement in a plant for nitrogen metabolism and seed maturation (Ackova 2018; Sharma et al. 2013; Tsonev and Lidon 2012; Cakmak 2000). However, increased anthropogenic activities and rapid industrialization caused the accumulation of Zn in the environment (Nardis et al. 2018). In this regard, the ability of plants to remove pollutants from the environment and

convert them to non-toxic forms for a sustainable environment has become increasingly important in recent years (Adki et al. 2014; Doran 2009). Plant tissue culture is a technique used to cultivate and maintain new plant tissues, cells, or organs under aseptic and controlled conditions on a nutrient medium (Sarasan et al. 2006). Compared to traditional methods, tissue culture methods appear as reliable and practical techniques for large-scale plant multiplication and conservation of plants. Plant tissue culture has broad application areas in various fields, such as environmental problems, phytoremediation, plant improvement, and secondary metabolite production. It is also a suitable tool for phytoremediation studies (Adki, Jadhav, and Bapat 2014; García-González et al. 2010; Sarasan et al. 2006). There are many wetland plants for using phytoremediation studies (Eid et al. 2021; Rodrigues et al. 2020; Schüick and Greger 2020). One of these wetland plants *Epilobium hirsutum* L. (Onagraceae), is a perennial medicinal plant popularly known as great hairy willowherb (Davis 1965). *Epilobium* species contain various flavonoids; therefore, the *E. hirsutum* plant has been used to treat benign prostatic hyperplasia (BPH) (Granica et al. 2014). Nowadays, remediation methods are frequently used to remove Zn pollution in aquatic environments. Thus, *E. hirsutum* plants accumulated very high concentrations of metals and were used to detect heavy metal pollution in wetlands (Adki, Jadhav, and Bapat 2014; Guittonny-Philippe et al. 2015). *E. hirsutum* plant is suitable for the remediation of especially Cu contaminated areas (Ghaderian and Ghotbi Ravandi 2012). Also, the biotechnological methods mentioned in our study are fundamental to reproducing and conserving the *E. hirsutum* genotype, a medicinal plant.

The objective of the present study is to reveal the usability of *E. hirsutum* in phytoremediation of Zn in hydroponic culture, to detect the response of *E. hirsutum* to Zn stress, and to develop an *in vitro* propagation protocol for the use of *in vitro* plantlets in the future phytoremediation studies. With this study, we target *E. hirsutum*, a native herbaceous plant in Turkey, and will take its place among the plants that can accumulate Zn in the literature. Considering this plant's high Zn accumulation capacity, this research will be a good sample for the possible use of wetland plants in phytoremediation studies.

## 2. Materials and Method

### 2.1. Plant Material

*E. hirsutum* capsules were collected from September to October 2016 from populations in Köprüören, Kütahya, Türkiye (39° 30' 27" N, 29° 44' 59" E). In phytoremediation experiments, the healthy seeds were sewn into pots filled with soil and placed in pools filled with water in the greenhouse until seedlings had 8-10 leaves. *E. hirsutum* seedlings were transplanted into 2.5-liter pots containing 10% Hoagland solution for acclimatization and kept in this solution for seven days.

### 2.2. Phytoremediation Experiments

To determine the maximum Zn concentration that seedlings could accumulate a high amount of Zn along with showing healthy development, *E. hirsutum* seedlings were kept in 10% Hoagland solutions (pH 6.2) containing ten different Zn concentrations (0 as a control group, 10, 20, 30, 40, 50, 75, 100, 150 and 200 mg Zn/L) for seven days. Two stock solutions, including 1000 ppm Zn solution and Hoagland solution without Zn, were prepared for the experiment. Calculated Zn stock solution amounts were added to 10% Hoagland solutions to adjust the concentrations mentioned above. At the end of the seven days, the roots of the harvested seedlings were washed with sodium-EDTA (1%) and ultra-pure water to eliminate heavy metal contamination. The relative growth parameters (RGP) were calculated as (1):

$$\text{RGP(\%)} = \frac{\text{Growth parameters in zinc solutions}}{\text{Growth parameters in control solution}} \times 100 \quad (1)$$

#### 2.2.1. Zinc Analysis

Plant samples (root, shoot, and leaf parts) were dried at 70 °C oven for 48 hours and then ground in a RETCH brand mortar grinder for Zn analysis. The dried plant parts were weighed and recorded as dry weight (DW). 0.1 g dried plant samples were digested with nitric acid and hydrogen peroxide in glass digestion tubes (Kaçar and İnal 2008). The heavy metal content of seedlings was analyzed by an Atomic Absorption Spectrometer (Analytikjena ContrAA 300, Dumlupinar University 2018) by Dumlupinar University Advanced Technologies in Design, Research, and Development, and Application Centre.

#### 2.2.2. Measurement of Protein and Chlorophyll Contents of Seedlings

The chlorophyll contents of fresh leaves were determined by crushing them in a mortar with acetone. The supernatant absorbance was read at 450, 647, and 663 nm using an Optizen POP spectrophotometer (Arnon, 1949). 0.5 g of fresh leaves were extracted with 5 mL of phosphate buffer to determine protein content. The extracts were centrifuged at 20,000 rpm for 20 min, and the absorbance of 0.1 mL supernatant sample was read at 595 nm (Bradford 1976).

### 2.3. Tissue Culture Experiments

#### 2.3.1. Sterilization of Seeds

The seeds were sterilized by adding a few drops of tween 20 to the 3% sodium hypochlorite for 10 minutes and then rinsing with sterile ultrapure water three times. Murashige and Skoog (Murashige and Skoog 1962) (MS) nutrient medium containing mineral salts, 3% sucrose, and 7 g agar were used in germination, regeneration, and rooting experiments. MS nutrient medium was sterilized in an autoclave at 121 °C and under 1.1 atm-pressure for 20 minutes. Sterilized seeds were sown in magenta vessels, left in a growth cabinet at 25 °C, and under a 16/8 hours photoperiod for 30 days.



### 2.3.2. In Vitro Germination

After 30 days of germination, *in vitro* germinated seedlings with approximately 0.3-0.5 cm shoot tips were transferred to an MS medium containing 25, 50, and 75 mg/L gibberellic acid (GA<sub>3</sub>-filter-sterilized and added to the growth medium following to autoclaving) for three weeks. After three weeks, *E. hirsutum* seedlings were transferred to MS basal medium with different combinations of 6-benzyl amino purine (BAP)/naphthalene acetic acid (NAA) and BAP/indole-3-butyric acid (IBA) for four weeks. The study used these mediums as the initiation media for *in vitro* multiplication. The regenerated shoots (about 5 cm in length) of *E. hirsutum* were excised and individually transferred to an MS root medium with various concentrations of NAA and IBA to test the rooting potential. The number of roots per shoot, root lengths, and rooting percentages were determined after four weeks after the culture initiation. Plantlets grown in tissue culture were gradually adapted to hydroponic culture.

### 2.4. Statistical Analysis

JMP6 SAS Statistical Analysis Program was used to evaluate the data obtained from this study (JMP, 2005). The experiments were conducted in three replicates containing five explants in each culture vessel. F-test and Tukey HSD multiple comparisons test (at  $p < 0.05$  level) were used to reveal the differences between different Zn concentrations and average Zn accumulation, root lengths, shoot lengths, fresh weights, chlorophyll, and protein contents of *E. hirsutum* seedlings (Kocaçalışkan and Bingöl 2017). All calculated mean values are given together with their standard deviations.

## 3. Results and Discussion (Times New Roman 10 pt, Bold)

### 3.1. Phytoremediation Experiment

A plant's tolerance to heavy metal stress can be achieved through some changes in its growth (Ackova 2018). Similarly, our research determined a significant relationship between relative growth parameters and Zn concentrations. The mean relative root lengths, shoot lengths, and fresh weights of *E. hirsutum* seedlings grown in different Zn concentrations are given in Figure 1. In this study, increasing Zn concentrations have caused a decrease in relative root and shoot lengths and fresh weights of *E. hirsutum* according to an increase in Zn concentrations from 10 to 75 mg/L in solutions, except for 10 mg/L fresh weight (86.5 to 55.4%; 79.9 to 63%; 101.5 to 34.2%, respectively) (Fig. 1).

Our data revealed a statistically significant relation between increasing Zn concentration in the solutions and root-shoot lengths and fresh weight of *E. hirsutum* compared to the control ( $p \leq 0.01$ ). While blackening and rupture were determined on the roots of the seedlings grown in solutions containing 40 mg/L and above Zn concentrations, drying and red-brown spots were also observed on the leaves. It was observed that the fresh weight of the seedlings decreased at 50 and 75 mg/L Zn concentrations. However, it was found that in all concentrations above 75 mg Zn/L (100, 150, and 200 mg Zn/L), seedlings died at the end of

the experiment. In another study related to Zn heavy metal stress, the *Lythrum salicaria* plant was shown to decrease the root-shoot length and fresh weight (Bingöl et al. 2021). A similar result has been reported by Akin et al. (2022), and they also found that increasing Zn concentrations have produced a reduction in the root length, shoot length, and fresh weight of the *E. hirsutum* plant according to the control, which made it tolerant to the Zn heavy metal by salicylic acid. Malik et al. (1970) reported that the length of roots and shoots, fresh weight, and dry weight of *Amaranthus* sp. decreased depending on the increasing Zn concentration, while the root and shoot length of the rice plant increased due to the increasing Zn concentration. Ehsan et al. (2015) investigated the effect of Zn on the *Lupinus uncinatus* plant. They found that the plant showed healthy growth in a medium containing 30  $\mu$ M Zn but showed toxic symptoms in 40  $\mu$ M Zn solution, and the plant died at 50  $\mu$ M Zn concentration. Arán et al. (2017) found that the root length and leaf number of the *Limnium laevigatum* plant decreased in parallel with the increasing Zn concentration. In their review, Bolat and Kara (2017) emphasized that depending on the increase in the Zn concentration, the plant's root and leaf development and iron and phosphorus uptake decreased significantly. Zn toxicity caused significant changes, especially in the root system of plants. Several studies have revealed that plants exposed to high metal concentrations cause changes in root morphology and develop a higher percentage of branching, especially in the metal contact area of the roots. Zn stress also causes a reduction in primary root length (Balafrej et al. 2020). Thus, the results of the studies mentioned above had similar findings to this study. As a result, excess Zn causes growth inhibition, development of chlorosis, and necrosis in the plant and inhibits cell elongation and division (Tsonev and Lidon 2012).

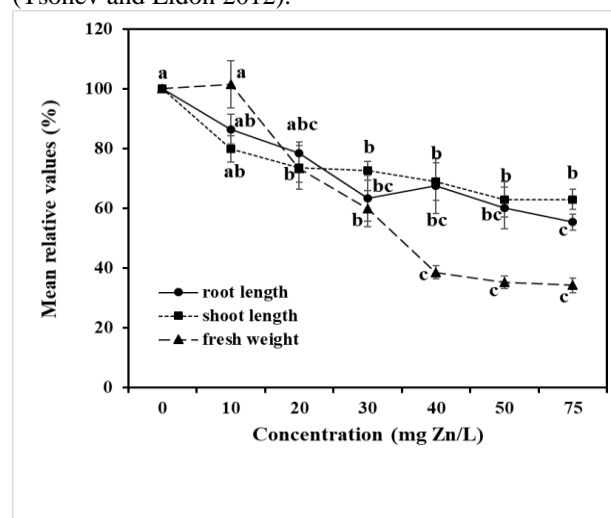


**Fig. 1** Mean relative values of root length, shoot length, and fresh weight of *E. hirsutum* at different Zn concentrations

According to the data obtained from this study, *E. hirsutum* can accumulate Zn in the whole plant under hydroponic conditions. It was determined that there was a statistically significant relation between the amount of Zn accumulated by seedlings and Zn concentrations in solutions ( $F = 11660.69$ ;  $p < 0.001$ ). The seedlings kept in 30 and 40 mg Zn/L



solutions accumulated a high amount of Zn. At the same time, the lowest Zn accumulation was calculated in solutions containing 75 mg/L Zn (Fig. 2). When all these data were evaluated, it was determined that the highest Zn concentration that the seedlings showed well-grown and accumulated more Zn was at 30 mg Zn/L ( $14\,894.90 \pm 17.11$  mg Zn/kg DW) (Fig. 2). When the Zn accumulations in three organs were compared to each other, it was determined that the roots ( $10\,598$  mg Zn/kg DW) had higher Zn accumulation than shoots ( $3\,503$  mg Zn/kg DW) and leaves ( $793.8$  mg Zn/kg DW). Zn phytotoxicity in plants can differ according to the plant type, genotype, age, environment state, and the concentration of heavy metals and other ions (Tsonev and Lidon 2012). The results obtained from phytoremediation studies with different plants show that plants can accumulate Zn in their vegetative organs, including roots, shoots, or leaves (Hesami et al. 2018; Mahdavian et al. 2017; Mazumdar and Das 2015). Doğan (2011) reported that some aquatic plants, *Alisma plantago-aquatica*, *Sagittaria sagittifolia*, *Juncus effusus*, *Lythrum salicaria*, and *Phalaris arundinacea* accumulated Pb, Cd, Zn, and Cu in their roots. Matthews et al. (2004) investigated the growth rate, Zn intake, and metal tolerance of *Eriophorum angustifolium*, *Juncus effusus*, and *Juncus articulatus* plants. Maximum Zn accumulation was  $53 \pm 28$   $\mu\text{mol/g}$  in the roots and  $43 \pm 2$   $\mu\text{mol/g}$  Zn in the leaves of the *J. effesus* plant. The plant showed some toxicity symptoms at 40 mg/L and above Zn concentrations in this research, such as necrosis and red-brown spots in leaves. Young leaves show chlorosis, the first symptom of Zn toxicity in most species (Reichman 2002). There are many studies on Zn toxicity (Al Chami et al. 2015; Mirshekali et al. 2012; Rout and Das 2003). Thus, when the accumulation results of this study were evaluated, it was understood that *E. hirsutum* has a substantial phytoremediation property.

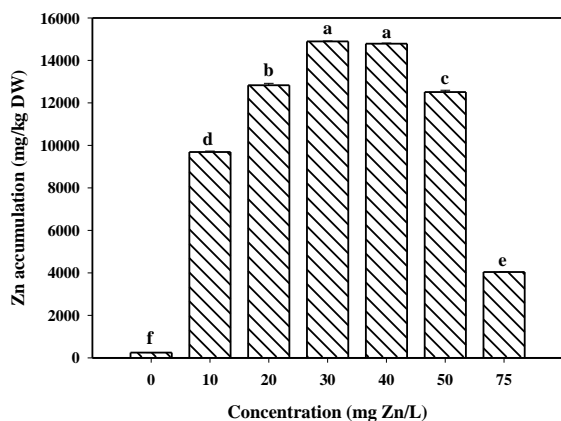


**Fig. 2** Zn accumulation (mg/kg DW) of *E. hirsutum* at concentrations of 0, 10, 20, 30, 40, 50, and 75 mg/L Zn

In this research, chlorophyll a, b, the total chlorophyll, and carotenoid amounts in leaves were studied to put forward the plant's response against Zn heavy metal. Zn toxicity has caused reductions in chlorophyll synthesis because of the

inhibition of pigment synthesis (Broadley et al. 2007). It was found that there was a statistically significant relation between the pigment contents of the seedlings and the increasing Zn concentrations (chlorophyll a  $F=3116.70$ ; chlorophyll b  $F=536.77$ ; total chlorophyll  $F=9204.30$  and total carotenoid ( $F=105147.1$ ). When photosynthetic pigments were compared in the *E. hirsutum* plant treated with Zn, it was determined that there was a significant decrease in pigment levels (Fig. 3). Consequently, total chlorophyll content decreased at excessive Zn concentrations (50 and 75 mg Zn/L). In plants, the functionality and efficiency of the photosynthetic system are hampered by Zn toxicity. Thus, the reason for reducing of chlorophyll at high Zn concentrations could be the inhibition of chlorophyll biosynthesis (Emamverdian et al. 2015; Shakya et al. 2008). Similarly, such decreases in the levels of photosynthetic pigments have been reported by other studies in many plants on exposure to heavy metals (Chandra and Kang 2016; Mirshekali et al. 2012; Shakya, Chettri, and Sawidis 2008; Vassilev et al. 2011).

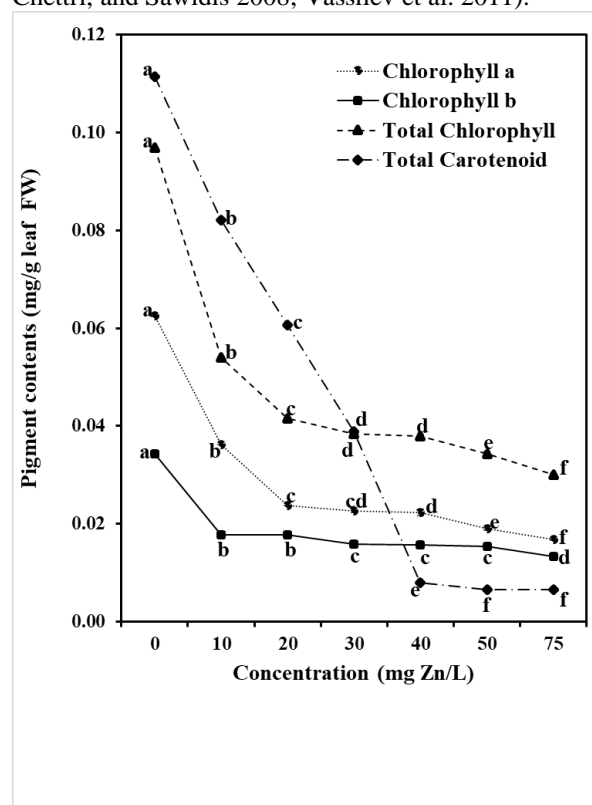


**Fig. 3** Effects of increasing Zn concentration on pigment content of *E. hirsutum*

The results showed a significant difference at the probability level ( $p < 0.001$ ) in leaf protein contents of *E. hirsutum*, which was exposed to different concentrations of Zn. The highest protein contents were found in solutions containing 10 and 20 mg Zn/L. Thus, this study calculated that plants grown at 10 mg/L Zn concentration had the highest protein content (4.39 mg/g leaf). A decrease in the amount of protein was detected at 40 mg Zn/L and above concentrations (Fig. 4). Zn is an essential component of particular proteins in all classes of enzymes, such as oxidoreductases, transferases, and hydrolases, and plays a

role as a protein cofactor (Chandra and Kang 2016; Emamverdian et al. 2015; Maret 2013; Vassilev et al. 2011). The decrease in the protein content of the plant exposed to high Zn concentrations may be due to changes in plant metabolism and plant response to heavy metal stress (Tsonev and Lidon 2012; Cakmak 2000). According to Jayasri and Suthindhiran (2017), high Zn concentration (20 mg Zn/L) negatively affected soluble proteins in *Lemna minor*. Plants respond to heavy metal stress by expressing genes that encode proteins (Chaudhary et al. 2019). Hence, from the above results, we can conclude that metal stress causes changes in plant protein content.

### 3.2. Tissue Culture Experiments

In our study, we determined the most suitable tissue culture conditions for using the *E. hirsutum* plant to detect metal toxicity and phytoremediation purposes in the future. The most crucial step of *in vitro* culture studies is selecting the appropriate tissue culture medium for the plant (Espinosa-Leal et al. 2018; Sarasan et al. 2006). This study obtained the highest (97 %  $\pm$  1.53) and fastest seed germination percentage in MS medium within  $7.7 \pm 0.26$  days. Based on the results, the MS medium was selected as the optimum medium for the germination of *E. hirsutum*. In a study by Rogers (2003), *Typha angustifolia* seeds had a 60-95% germination rate when cultured in light in liquid MS or sterile water. According to Dreger et al. (2016), it was stated that MS medium is sufficient for the germination of *Epilobium angustifolium*, and they found that the highest germination was 99% within seven days. When the results are compared with the literature data, our study is similar to these studies.

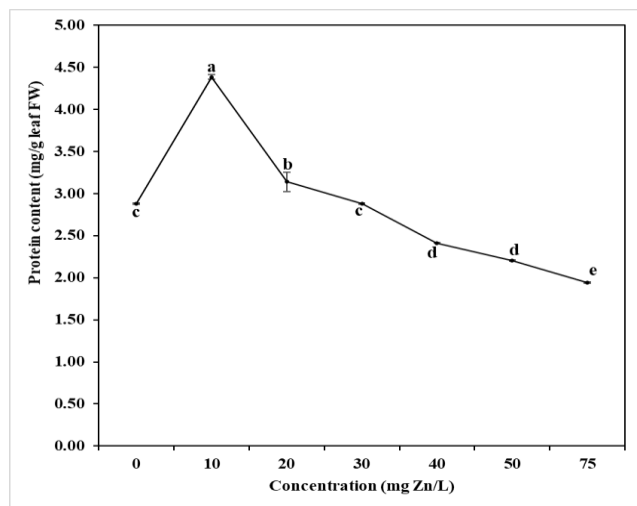


**Fig. 4** Effects of different Zn concentrations on the leaf protein content of *E. hirsutum*

*E. hirsutum* seeds germinated in the MS medium did not occur adequate growth. Therefore, seedlings were first transferred to an MS medium containing different concentrations of GA. As shown in Table 1, when the growth parameters of the seedlings grown at different concentrations of GA (25, 50, and 75 mg GA/L) were evaluated, the number of shoots per explant ( $F=4.57$ ;  $p=0.0168$ ), shoot length ( $F=53.33$ ;  $p<0.001$ ), number of

roots per shoot ( $F=24.87$ ;  $p<0.0001$ ), root length ( $F=74.76$ ;  $p<0.0001$ ), and the number of leaves per explant ( $F=29.58$ ;  $p<0.0001$ , respectively) were increased by 50 mg GA/L. However, 75 mg GA/L treatment showed an inhibitory effect on root formation (Table 1). Endogenous hormones such as gibberellin are essential in seed germination (Hilhorst and Karssen 1992; Vishal and Kumar 2018). Furthermore, it has been found that exogenous GA treatment was an effective method to break seed dormancy and promote seed germination of *Pinus massoniana* (Guangwu and Xuwen 2014). Explant development depends on plant growth regulators and tissue culture medium content. Therefore, optimization of the concentration of growth regulators is crucial for promoting *in vitro* shoot cultures (Nasution and Nasution 2019; Khan et al. 2015).

The shoot tips grown in the MS medium containing 50 mg GA/L, where *E. hirsutum* shows the best growth, were transferred to the MS medium containing different plant growth regulator concentrations, as shown in Figure 5. The shoot tip explants taken into plant tissue culture exhibited different shoot growth behaviors depending on the concentration of plant growth regulator and type. Some researchers reported that BAP had superior effects over other cytokinins (Anish et al. 2008; Gümüşçü et al. 2008). Among the plant growth regulators containing different concentrations of BAP-NAA and BAP-IBA used in this study, 1.0 BAP/1.0 NAA has shown the best response to initiate multiple shoot formation. There were no statistical differences among all types of the medium; the highest number of shoots per explant was obtained in 1.0 BAP/1.0 NAA ( $3.96 \pm 0.60$ ,  $F=1.14$ ;  $p=0.37$ ). When shoot tip explants are cultured in an MS medium containing the combination of BAP and NAA or IBA, it has been found that shoot formation is interrelated with auxin concentration. An increase in the auxin concentration resulted in a significant increase in the number of shoots per explant.

However, the results showed that the highest shoot length was obtained on medium with 1.0 BAP/0.5 NAA ( $1.46 \text{ cm} \pm 0.08$ ,  $F=2.30$ ;  $p=0.005$ ). The most extended length was also determined on medium with 1.0 BAP/1.0 IBA ( $0.28 \text{ cm} \pm 0.05$ ,  $F=8.29$ ;  $p=0.0001$ ). According to the results in Figure 5, the combination of cytokinin with auxins in the MS medium significantly impacted the shoot multiplication of *E. hirsutum*. It has been determined that the most effective treatments for the shoot development of *E. hirsutum* are 1.0 BAP/1.0 NAA and 1.0 BAP/1.0 IBA treatments. Although no studies are detailed on the *in vitro* propagation of *E. hirsutum*, some researchers mentioned the regeneration procedure of *E. hirsutum*, *E. angustifolium*, and *E. parviflorum* (Akin et al. 2022; Tâmaş et al. 2009; Turker et al. 2008; Akbudak and Babaoglu 2005; Rogers 2003). Thus, Tâmaş et al. (2009) demonstrated that shoot cultivation of *E. hirsutum* on an MS medium supplemented with antioxidative agents and polyvinyl pyrrolidone (adsorbent agent) resulted in biosynthesis of higher concentrations of polyphenolic compounds than *E. hirsutum* plants collected from nature. Badkhane et al. (2016) tested the regeneration capacity of *in vitro* explants

of *Glycyrrhiza glabra* by adding different concentrations of BA, Kinetin (Ki), NAA, and IBA growth regulators to an MS nutrient medium. Besides, they obtained the best shoot regeneration percentage and shoot formation rate in a medium containing 2 BAP/0.5 NAA when they used the node and internode explants. As a result of our study, growth regulators used in plant culture medium, and their concentrations affected the organogenesis of the plant.

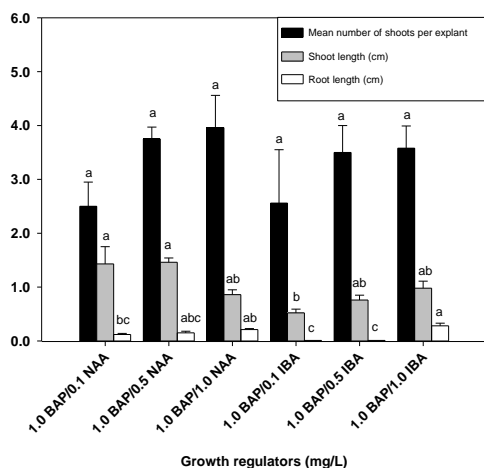


**Fig. 5** Effects of different concentrations of BAP, IBA, and NAA on shoot formation of *E. hirsutum*

**Table 1** Effect of different concentrations of GA on the shoot, root formation, and leaf number of *E. hirsutum*. According to the Tukey HSD test, mean values with the same letter are not statistically different ( $p \leq 0.01$ )

GA concentrations (mg/L)	Number of shoots/explant	Shoot length (cm)	Number of roots/shoot	Root length (cm)	Number of leaves/explant
25	1.0 ± 0.00 <sup>b*</sup>	2.1 ± 0.23 <sup>b</sup>	1.2 ± 0.32 <sup>b</sup>	0.3 ± 0.08 <sup>b</sup>	8.5 ± 0.36 <sup>b</sup>
50	1.6 ± 0.29 <sup>a</sup>	5.0 ± 0.29 <sup>a</sup>	4.0 ± 0.64 <sup>a</sup>	1.2 ± 0.10 <sup>a</sup>	10.9 ± 0.50 <sup>a</sup>
75	1.0 ± 0.00 <sup>b</sup>	2.3 ± 0.12 <sup>b</sup>	0.0 ± 0.00 <sup>c</sup>	0.0 ± 0.00 <sup>b</sup>	6.7 ± 0.27 <sup>c</sup>

Thus, 100% rooting was achieved in all root MS mediums (Table 2). *In vitro*, shoot formation may have resulted in different success levels depending upon the plant growth regulators used in the MS medium. Akın and Kocaçalışkan (2011) stated that the endemic plant *Arabis drabiformis* exhibited the best rooting at 0.5 mg IBA/L concentration. For decades, IBA was described as a ‘synthetic auxin’ most commonly used that induced root initiation and was preferred based on the results of prior studies (Akın et al. 2014; Akın and Kocaçalışkan 2011; Akın et al. 2018; Frick and Strader 2018; Kurt and Erdağ 2009; Prasad et al. 2004).

#### 4. Conclusion

Even though *E. hirsutum*, a medicinal wetland plant, can accumulate heavy metals in its organs; there are few studies on the plant's metal accumulation ability and micropropagation. This study concluded that *E. hirsutum* tolerated Zn up to 75 mg/L and accumulated more Zn at a concentration of 30 mg/L without showing any Zn toxicity symptoms. Medicinal plants have been used as sources of

The more significant influence of BAP on proliferation and multiplication was also stated by several researchers (Akın et al. 2018; Akın et al. 2014; Arab et al. 2014; Waoo et al. 2013). In our study, mediums containing 1.0 BAP/1.0 NAA and 1.0 BAP/1.0 IBA induced the highest number of green and healthy adventitious shoots. Auxins are critical plant growth regulators that are involved in the process of adventitious root development. Thus, adventitious rooting is a crucial and essential step for the vegetative propagation of plants (Sauer et al. 2013). *In vitro*, regenerated shoots of *E. hirsutum* showed different behaviors during the rooting processes. This study transferred regenerated shoots in 1.0 BAP/1.0 NAA and 1.0 BAP/1.0 IBA to varying concentrations of root mediums (0.5 NAA, 1.0 NAA, 0.5 IBA, and 1.0 IBA) to test the rooting potential. The root parameters were changed significantly with different IBA concentrations. The best rooting was obtained in the MS medium containing 1.0 mg IBA/L. However, when we compared the effects of shooting mediums (1.0 BAP/1.0 NAA or 1.0 BAP/1.0 IBA) on the rooting of seedlings, 1.0 BAP/1.0 NAA medium ( $32.9 \pm 6.71$  number of root/shoots;  $F=6.65$ ,  $p=0.002$ ) proved to be superior to 1.0 BAP/1.0 IBA ( $25.0 \pm 3.42$  number of root/shoots;  $F=0.13$ ,  $p=0.94$ , Table 2).

pharmaceutical products for many years (Akın 2020). However, tissue culture methods reported herein are powerful for selecting, multiplying, and conserving crucial medicinal plants. The possibilities of plant regeneration through tissue culture technology were investigated in this study. As a result, the *in vitro* propagation protocol (for shoot formation 1.0 BAP/1.0 NAA and root formation 1.0 IBA) and *E. hirsutum* plantlets were developed in this study. The regeneration system described here can be used in future phytoremediation studies.

**Authors’ contributions:** NB: obtaining data, editing, and writing; BA: obtaining data, experimental measurements, editing, and writing; NE: obtaining data, and experimental measurements.

#### Conflict of interest disclosure:

The authors declare that they have no conflicts of interest about the realization of this research.

**Table 2** Effect of different culture media (1.0 BAP/1.0 NAA and 1.0 BAP/1.0 IBA) and growth regulators (IBA and NAA) on rooting *in vitro* regenerated shoots after four weeks of rooting treatments. According to the Tukey HSD test, mean values with the same letter are not statistically different ( $p \leq 0.01$ )

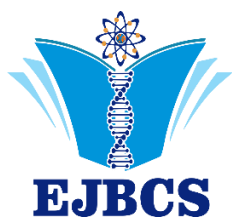
Medium (mg/L)	Growth regulators (mg/L)	Number of roots/shoots	Root length (cm)	Rooting (%)
<b>1 BAP/ 1 NAA</b>	0.5 NAA	8.17 ± 1.19 <sup>b*</sup>	0.54 ± 0.11 <sup>b</sup>	100.00
	1.0 NAA	24.7 ± 2.31 <sup>a</sup>	1.57 ± 0.24 <sup>a</sup>	100.00
	0.5 IBA	27.5 ± 2.50 <sup>a</sup>	1.22 ± 0.21 <sup>ab</sup>	100.00
	1.0 IBA	32.9 ± 6.71 <sup>a</sup>	1.13 ± 0.10 <sup>ab</sup>	100.00
Medium (mg/L)	Growth regulators (mg/L)	Number of roots/shoots	Root length (cm)	Rooting (%)
<b>1 BAP/1 IBA</b>	0.5 NAA	21.0 ± 5.67 <sup>a</sup>	0.83 ± 0.17 <sup>a</sup>	100.00
	1.0 NAA	23.8 ± 8.97 <sup>a</sup>	1.10 ± 0.28 <sup>a</sup>	100.00
	0.5 IBA	21.7 ± 1.67 <sup>a</sup>	0.88 ± 0.21 <sup>a</sup>	100.00
	1.0 IBA	25.0 ± 3.42 <sup>a</sup>	1.50 ± 0.25 <sup>a</sup>	100.00

## References

- Ackova DG. 2018. Heavy metals and their general toxicity on plants. *Plant Sci. Today* 5(1):14-18. doi.org/10.14719/pst.2018.5.1.355
- Adki VS, Jadhav JP, Bapat VA. (2014). At the cross roads of environmental pollutants and phytoremediation: A promising bio remedial approach. *J Plant Biochem Biotechnol.* 23(2):125-140. doi.org/10.1007/s13562-013-0250-6
- Akbudak MA, Babaoglu M. 2005. Callus induction in small flowered willow herb (*Epilobium parviflorum* Schreb). *J Plant Biochem Biotechnol.* 14(2):189-191. doi.org/10.1007/BF03355957
- Akın B. 2020. Tissue culture techniques of medicinal and aromatic plants: History, cultivation and micropropagation. *JSR-A* 45:253-266
- Akın B, Kocaçalışkan I. 2011. In vitro propagation of *Arabis drabiformis* Boiss. (Brassicaceae) an endemic rare species of Uludağ mountain (Bursa-Turkey). *AJB* 10(80):18356-1836. doi.org/10.5897/AJB11.2831
- Akın B, Bingöl NA, Kocacalışkan I. 2022. Zinc stress alleviation by salicylic acid in hairy willowherb (*Epilobium hirsutum* L.) under *in vitro* conditions. *Fresenius Environ Bull.* 31(03A):3735-3745
- Akın B, Çetin B, Akanlı Bingöl N. 2018. In Vitro Propagation of Wetland Medicinal Plant *Lythrum salicaria* L. *CBU Journal of Science* 14(4):369-372. doi.org/10.18466/cbayarfb.393626
- Akın B, Kocaçalışkan I, Gülerüz G. 2014. Micropropagation of *Erodium sibthorpiatum* subsp. *sibthorpiatum*, an endemic threatened species of Uludağ mountain (Bursa-Turkey). *Turk J Botany* 38(1):148-155. doi.org/10.3906/bot-1304-24
- Akpor OB, Ohiobor GO, Olaolu TD. 2014. Heavy metal pollutants in wastewater effluents: Sources, effects, and remediation. *Adv Biosci Bioeng.* 2(4):37-43. doi.org/10.11648/j.abb.20140204.11
- Al Chami Z, Amer N, Al Bitar L, Cavoski I. 2015. Potential use of *Sorghum bicolor* and *Carthamus tinctorius* in phytoremediation of nickel, lead and zinc. *Int J Environ Sci Technol.* 2(12):3957-3970. doi.org/10.1007/s13762-015-0823-0
- Ali H, Khan E. 2018. What are heavy metals? Long-standing controversy over the scientific use of the term ‘heavy metals’—proposal of a comprehensive definition. *Toxicol Environ Chem.* 100(1):6-19. doi.org/10.1080/02772248.2017.1413652
- Anish NP, Dan M, Bejoy M. 2008. Conservation using in vitro progenies of the threatened ginger-*Boesenbergia pulcherrima* (Wall.) Kuntze. *Int J Botany* 4(1):93-98. doi.org/10.3923/ijb.2008.93.98
- Arab MM, Yadollahi A, Shojaeiyan A, Shokri S, Ghoghaj SM. 2014. Effects of nutrient media, different cytokinin types and their concentrations on in vitro multiplication of G × N15 (hybrid of almond × peach) vegetative rootstock. *JGEB.* 12(2):81-87. doi.org/10.1016/j.jgeb.2014.10.001
- Arán DS, Harguinteguy CA, Fernandez-Cirelli A, Pignata, ML. 2017. Phytoextraction of Pb, Cr, Ni, and Zn using the aquatic plant *Limnium laevigatum* and its potential use in the treatment of wastewater. *Environ Sci Pollut Res.* 24(22):8295-18308. doi.org/10.1007/s11356-017-9464-9
- Arnon DI. 1949. Copper enzymes in isolated chloroplasts, polyphenoloxidase in *Beta vulgaris*. *Plant Physiol.* 24(1):1-15. doi.org/10.1104/pp.24.1.1
- Azubuike CC, Chikere CB, Okpokwasili GC. 2016. Bioremediation techniques—classification based on site of application: principles, advantages, limitations and prospects. *World J Microbiol Biotechnol.* 32(11):1-18. doi.org/10.1007/s11274-016-2137-x
- Badkhane Govt Motilal Vigyan Mahavidyalayan Y, Bajaj Govt Motilal Vigyan Mahavidyalaya A. 2016. Effect of explant sources and different concentrations of plant growth regulators on in vitro micropropagation of *Glycyrrhiza glabra* L. *Indo Am J Pharm Res.* 6:5830-5840
- Balafrej H, Bogusz D, Abidine Triqui Z el, Guedira A, Bendaou N, Smouni A, Fahr M. 2020. Zinc hyperaccumulation in plants: A review. *Plants* 9(5):562. doi.org/10.3390/plants9050562
- Bingöl NA, Akin B, Kocaçalışkan İ, Nalbantoğlu B, Meşeli O. 2021. Effect of zinc on phytoremediation potential and carbonic anhydrase and polyphenol oxidase activities of *Lythrum salicaria* L. *Turk J Botany* 45(6):553-562. doi.org/10.3906/bot-2107-52
- Bolat İ, Kara Ö. 2017. Bitki besin elementleri: Kaynakları, işlevleri, eksik ve fazlalıkları. *BAROFD* 19(1):218-228 (In Turkish).

- Bradford MM. 1976. A rapid and sensitive method for the quantitation of microgram quantities of protein utilizing the principle of protein-dye binding. *Anal Biochem.* 72:248-254. doi.org/10.1016/0003-2697(76)90527-3
- Broadley MR, White PJ, Hammond JP, Zelko I, Lux A. 2007. Zinc in plants: Tansley review. *New Phytol.* 173(4):677-702. doi.org/10.1111/j.1469-8137.2007.01996.x
- Broadley M, Brown P, Cakmak I, Rengel Z, Zhao F. 2012. Function of nutrients: micronutrients. In: Marschner P (ed) *Marschner's mineral nutrition of higher plants*, 3rd edn. Academic Press, London.
- Cakmak I. 2000. Tansley review no. 111: Possible roles of zinc in protecting plant cells from damage by reactive oxygen species. *New Phytologist* 146(2):185-205. doi.org/10.1046/j.1469-8137.2000.00630.x
- Chandra R, Kang H. 2016. Mixed heavy metal stress on photosynthesis, transpiration rate, and chlorophyll content in poplar hybrids. *Forest Sci Technol.* 12(2):55-61. doi.org/10.1080/21580103.2015.1044024
- Chaudhary M, Varshney R, Shah Nawaz M, Pandey RP. 2019. Various responses of plant proteins to heavy metal stress tolerance. *Suresh Gyan Vihar University International Journal of Environment, Science and Technology* 5(1):19-29
- Davis PH. 1965. *Flora of Turkey and the East Aegean Islands*, Vol. 1-9. University Press, Edinburgh.
- Edinburgh Univ. Press., Edinburgh.
- Doğan M. 2011. Akuatik makrofitlerde ağır metal akümülyasyonu. *Türk Bilimsel Derlemeler Dergisi* 4:33-36 (In Turkish)
- Doran PM. 2009. Application of plant tissue cultures in phytoremediation research: Incentives and limitations. *Biotechnol Bioeng.* 103(1):60-76. doi.org/10.1002/bit.22280
- Dreger M, Wegenke J, Makowiecka J, Michalik T, Wielgus K. 2016. Application of multi-shoots cultures in micropropagation of willow herb (*Chamaenerion angustifolium* (L.) Scop.). *Herba Polonica.* 62(3):28-39. doi.org/10.1515/hepo-2016-0015
- Ehsan M, Lara Viveros FM, Hernández VE, Barakat MA, Ortega AR, Maza Av, Monter Jv. 2015. Zinc and cadmium accumulation by *Lupinus uncinatus* Schldl. grown in nutrient solution. *Int J Environ Sci Technol.* 12(1):307-316. doi.org/10.1007/s13762-013-0456-0
- Eid EM, Shaltout KH, Almuqrin AH, Aloraini DA, Khedher KM, Taher MA, Alfahhan AH, Picó Y, Barcelo D. 2021. Uptake prediction of nine heavy metals by *Eichhornia crassipes* grown in irrigation canals: A biomonitoring approach. *Sci. Total Environ.* 782:146887. doi.org/10.1016/j.scitotenv.2021.146887
- Emamverdian A, Ding Y, Mokherdorran F, Xie Y. 2015. Heavy metal stress and some mechanisms of plant defense response. *Sci. World J. Article* ID 756120:1-18. doi.org/10.1155/2015/756120
- Espinosa-Leal CA, Puente-Garza CA, García-Lara S. 2018. In vitro plant tissue culture: means for production of biological active compounds. *Planta.* 248(1):1-18. doi.org/10.1007/s00425-018-2910-1
- Frick EM, Strader LC. 2018. Roles for IBA-derived auxin in plant development. *J Exp Bot.* 69(2):169-177. doi.org/10.1093/jxb/erx298
- Fu F, Wang Q. 2011. Removal of heavy metal ions from wastewaters: A review. *J Environ Manage.* 92(3):407-418. doi.org/10.1016/j.jenvman.2010.11.011
- García-González R, Quiroz K, Carrasco B, Caligari P. 2010. Plant tissue culture: Current status, opportunities and challenges. *Cienc Investig Agrar.* 37(3):5-30. doi.org/10.4067/s0718-16202010000300001
- Ghaderian SM, Ghotbi Ravandi AA. 2012. Accumulation of copper and other heavy metals by plants growing on Sarcheshmeh copper mining area, Iran. *J Geochem Explor.* 123:25-32. doi.org/10.1016/j.gexplo.2012.06.022
- Granica S, Piwowarski JP, Czerwińska ME, Kiss AK. 2014. Phytochemistry, pharmacology and traditional uses of different *Epilobium* species (Onagraceae): A review. *J Ethnopharmacol.* 156:316-346. doi.org/10.1016/j.jep.2014.08.036
- Guangwu Z, Xuwen J. 2014. Roles of gibberellin and Auxin in promoting seed germination and seedling Vigor in *Pinus massoniana*. *For Sci.* 60(2):367-373. doi.org/10.5849/forsci.12-143
- Guittonny-Philippe A, Masotti V, Rabier J, Petit ME, Malleret L, Coulomb B, Laffont-Schwob I. 2015. Biomonitoring of *epilobium hirsutum* L. health status to assess water ecotoxicity in constructed wetlands treating mixtures of contaminants. *Water (Switzerland)* 7(2):697-715. doi.org/10.3390/w7020697
- Gümüşçü A, Çöçü S, Uranbey S, Ipek A, Çalışkan M, Arslan N. 2008. In vitro micro-propagation of endangered ornamental plant-*Neotrichhatchewia isatidea* (Boiss.) Rauschert. *Afr J Biotechnol.* 7(3):234-238
- Hegazy AK, Abdel-Ghani NT, El-Chaghaby GA. 2011. Phytoremediation of industrial wastewater potentiality by *Typha domingensis*. *Int J Environ Sci Technol.* 8(3):1019-1027. doi.org/10.1007/BF03326249
- Hesami R, Salimi A, Ghaderian SM. 2018. Lead, zinc, and cadmium uptake, accumulation, and phytoremediation by plants growing around Tang-e Douzan lead-zinc mine, Iran. *Environ Sci Pollut Res.* 25(9):8701-8714. doi.org/10.1007/s11356-017-1156-y
- Hilhorst HWM, Karssen CM. 1992. Seed dormancy and germination: the role of abscisic acid and gibberellins and the importance of hormone mutants. *Plant Growth Regul.* 11(3):225-238. doi.org/10.1007/BF00024561
- Jayasri MA, Suthindhiran K. 2017. Effect of zinc and lead on the physiological and biochemical properties of aquatic plant *Lemna minor*: its potential role in phytoremediation. *Appl Water Sci.* 7(3):247-1253. doi.org/10.1007/s13201-015-0376-x
- JMP. 2005. JMP SAS statistical analysis system. Cary, North Carolina, USA.
- Kaçar B, İnal A. 2008. Bitki analizleri. Nobel Yayın Dağıtım Ltd Şti, Ankara.
- Khan N, Ahmed M, Hafiz I, Abbasi N, Ejaz S, Anjum M. 2015. Optimizing the concentrations of plant growth regulators for in vitro shoot cultures, callus induction and shoot regeneration from calluses of grapes. *Int Sci Vigne Vin.* 49(1):37-45. doi.org/10.20870/oenone.2015.49.1.95
- Kocaçalışkan İ, Bingöl AN. 2017. Biyoistatistik. Nobel Akademik Yayıncılık Eğitim danışmanlık Tic Ltd Şti, Ankara.
- Kurt S, Erdağ B. 2009. In vitro germination and axillary shoot propagation of *Centaurea zeybekii*. *Biol.* 64(1):97-101. doi.org/10.2478/s11756-009-0003-0
- Mahdavian K, Ghaderian SM, Torkzadeh-Mahani M. 2017. Accumulation and phytoremediation of Pb, Zn, and Ag by plants growing on Koshk lead-zinc mining area, Iran. *J Soils Sediments* 17(5):1310-1320. doi.org/10.1007/s11368-015-1260-x
- Malik N, Chamon A, Mondol M, Elahi S, Faiz S. 1970. Effects of different levels of zinc on growth and yield of red amaranth (*Amaranthus* sp.) and rice (*Oryza sativa*, Variety-BR49). *J Bangladesh Assoc Young Res.* 1(1):79-91. doi.org/10.3329/jbayr.v1i1.6836
- Maret W. 2013. Zinc biochemistry: From a single zinc enzyme to a key element of life. *Adv Nutr.* 4(1):2-91. doi.org/10.3945/an.112.003038

- Matthews DJ, Moran BM, Otte ML. 2004. Zinc tolerance, uptake, and accumulation in the wetland plants *Eriophorum angustifolium*, *Juncus effusus*, and *Juncus articulatus*. *Wetlands* 24(4):859-869
- Mazumdar K, Das S. 2015. Phytoremediation of Pb, Zn, Fe, and Mg with 25 wetland plant species from a paper mill contaminated site in North East India. *Environ Sci Pollut Res*. 22(1): 701-710. doi.org/10.1007/s11356-014-3377-7
- Mirshakali H, Hadi H, Amirnia R, Khodaverdiloo H, Ali H M, Hadi H, Amirnia R, Verdiloo HK. 2012. Effect of zinc toxicity on plant productivity, chlorophyll and Zn contents of sorghum (*Sorghum bicolor*) and common lambsquarter (*Chenopodium album*). *IJRR*. 2(3):247-254
- Murashige T, Skoog F. 1962. A Revised Medium for Rapid Growth and Bio Assays with Tobacco Tissue Cultures. *Physiol Plant*. 15(3):473-497. doi.org/10.1111/j.1399-3054.1962.tb08052.x
- Noulas C, Tziouvalekas M, Karyotis T. 2018. Zinc in Soils, Water and Food crops. *J Trace Elem Med Biol*. 49:252-260. doi.org/10.1016/j.jtemb.2018.02.009
- Nardis BO, Silva EB, Graziotti PH, Alleoni LRF, Melo L CA, Farnezi MMM. 2018. Availability and zinc accumulation in forage grasses grown in contaminated soil. *Int J Phytoremediation*. 20(3):205-213. doi.org/10.1080/15226514.2017.1365347
- Nasution NH, Nasution IW. 2019. The Effect of Plant Growth Regulators on Callus Induction of Mangosteen (*Garcinia mangostana* L.). *IOP Conf Ser Earth Environ Sci*. 305(1):012049. doi.org/10.1088/1755-1315/305/1/012049
- Phillips DP, Human LRD, Adams JB. 2015. Wetland plants as indicators of heavy metal contamination. *Mar Pollut Bull*. 92, 227-232. doi.org/10.1016/j.marpolbul.2014.12.038
- Prasad P, Chakradhar T, Pullaiah T. 2004. Micropropagation of *Cryptolepis buchanani* Roem. & Schult. *Taiwania*. 49:57-65. doi.org/10.6165/tai.2004.49(1).57
- Reichman SM. 2002. The Responses of Plants to Metal Toxicity: A review focusing on Copper, Manganese and Zinc. Australian Minerals and Energy Environment Foundation, Melbourne, Australia.
- Rodrigues ACD, Rocha MV de C, Lima ESA, Pinho CF de, Santos AM dos, Santos FS dos, Amaral Sobrinho NM B do. 2020. Potential of water lettuce (*Pistia stratiotes* L.) for phytoremediation: physiological responses and kinetics of zinc uptake. *Int J Phytoremediation*. 22(10):1019-1027. doi.org/10.1080/15226514.2020.1725868
- Rogers SMD. 2003. Tissue culture and wetland establishment of the freshwater monocots *Carex*, *Juncus*, *Scirpus*, and *Typha*. *In Vitro Cell Dev Biol Plant*. 39(1):1-15. doi.org/10.1079/IVP2002358
- Rout GR, Das P. 2003. Effect of metal toxicity on plant growth and metabolism: I. Zinc. *Agronomie*. 23(1):3-11. doi.org/10.1051/agro:2002073
- Sabreena Hassan S, Bhat SA, Kumar V, Ganai BA, Ameen F. 2022. Phytoremediation of heavy metals: An indispensable contrivance in green remediation technology. *Plants*. 11(9):1255. doi.org/10.3390/plants11091255.
- Sarasan V, Cripps R, Ramsay MM, Atherton C, McMichen M, Prendergast G, Rowntree JK. 2006. Conservation in vitro of threatened plants - Progress in the past decade. *In Vitro Cell Dev Biol Plant*. 42(3):206-214. doi.org/10.1079/IVP2006769
- Sauer M, Robert S, Kleine-Vehn J. 2013. Auxin: Simply complicated. *J Exp Bot*. 64(9):2565-2577. doi.org/10.1093/jxb/ert139.
- Schück M, Greger M. 2020. Screening the capacity of 34 wetland plant species to remove heavy metals from water. *Int J Environ Res Public Health*. 17(13):4623. doi.org/10.3390/ijerph17134623.
- Shakya K, Chettri MK, Sawidis T. 2008. Impact of heavy metals (copper, zinc, and lead) on the chlorophyll content of some mosses. *Arch Environ Contam Toxicol*. 54(3):412-421. doi.org/10.1007/s00244-007-9060-y
- Sharma A, Patni B, Shankhdhar D, Shankhdhar SC. 2013. Zinc - An Indispensable Micronutrient. *Physiol Mol Biol Plants*. 19(1):11-20. doi.org/10.1007/s12298-012-0139-1
- Târnaş M, Toiu I, Oniga I, Deliu C, Oltean B, Coldea G. 2009. Quantitative determination of total polyphenols and flavonoids from indigenous species of *Epilobium* of wild origin and 'in vitro' regenerated plantlets. *Contrib Bot*. 44:119-123
- Tiwari AK, de Maio M, Singh PK, Mahato MK. 2015. Evaluation of surface water quality by using GIS and a heavy metal pollution index (HPI) model in a coal mining area, India. *Bull Environ Contam Toxicol*. 95(3):304-310. doi.org/10.1007/s00128-015-1558-9
- Tsonev T, Lidon FJC. 2012. Zinc in plants - An overview. *Emir J Food Agric*. 24(4):322-333
- Turker AU, Mutlu EC, Yidirim AB. 2008. Efficient in vitro regeneration of fireweed, a medicinal plant. *Acta Physiol Plant*. 30(4):421-426. doi.org/10.1007/s11738-008-0136-8.
- Vassilev A, Nikolova A, Koleva L, Lidon F. 2011. Effects of Excess Zn on Growth and Photosynthetic Performance of Young Bean Plants. *J Phytol*. 3(6):58-62
- Vishal B, Kumar PP. 2018. Regulation of seed germination and abiotic stresses by gibberellins and abscisic acid. *Front Plant Sci*. 9:1-15. doi.org/10.3389/fpls.2018.00838
- Wao AA, Khare S, Ganguli S. 2013. In-vitro Propagation of *Datura innoxia* from nodal and shoot tip explants. *World J Environ Eng*. 1(1):1-4. doi.org/10.12691/wjee-1-1-1



## Pyrazoline compounds containing different groups: Design, synthesis and comprehensive molecular docking studies

Halise Yalazan<sup>1</sup>, Damla Koç<sup>2</sup>, Seda Fandaklı<sup>3</sup>, Burak Tüzün<sup>4</sup>, Halit Kantekin<sup>1,\*</sup>

<sup>1</sup>Karadeniz Technical University, Faculty of Sciences, Department of Chemistry, Trabzon, Turkey

<sup>2</sup>Erciyes University, Faculty of Sciences, Department of Chemistry, Kayseri, Turkey

<sup>3</sup>Artvin Çoruh University, Vocational School of Health Services, Medical Laboratory Techniques Program, Artvin, Turkey

<sup>4</sup>Sivas Cumhuriyet University, Technical Sciences Vocational School of Sivas, Plant and Animal Production Department, Sivas, Turkey

\*Corresponding author : [halit@ktu.edu.tr](mailto:halit@ktu.edu.tr)

Orcid No: <https://orcid.org/0000-0003-2625-2815>

Received : 17/07/2024

Accepted : 30/10/2024

**To Cite / Atf için:** Yalazan H, Koç D, Fandaklı S, Tüzün B . Kantekin H. 2024. Pyrazoline compounds containing different groups: Design, synthesis and comprehensive molecular docking studies. Eurasian J Bio Chem Sci, 7(2):111-124 <https://doi.org/10.46239/ejbs.1517538>

**Abstract:** In the presented study, a series of methoxylated pyrazoline compounds containing amine (Py<sub>1</sub>-NH<sub>2</sub> and Py<sub>2</sub>-NH<sub>2</sub>), tosyl (Py<sub>1</sub>-Ts and Py<sub>2</sub>-Ts), and nitrile (Py<sub>1</sub>-CN and Py<sub>2</sub>-CN) group were synthesized. The structures of these compounds were clarified (by MS, FT-IR, and NMR analysis) through the use of mass spectral (spectrometer), FT-IR (spectrophotometer), and NMR (spectrometer) data. In order to examine the chemical properties of methoxylated pyrazoline derivatives theoretically, calculations were performed on the B3LYP, HF, and M06-2x methods using the 6-31++g(d,p) basis set. In addition, molecular docking calculations were performed to examine the interactions of methoxylated pyrazoline derivatives against cancer proteins. Afterwards, ADME/T was performed to examine the effects of methoxylated pyrazoline derivatives as drugs on human metabolism. According to the Gaussian calculations, the Py<sub>1</sub>-NH<sub>2</sub> molecule is typically more active than other molecules. However, after the molecular docking calculations, the compounds' effects on cancer proteins were examined, and it was discovered that the Py<sub>1</sub>-NH<sub>2</sub> molecule had more activity overall than the others. Following a comprehensive examination of the compounds' interactions with cancer proteins, the ADME properties of the molecules were examined. According to this analysis, it would not be detrimental to use the chemicals as drugs for human metabolism.

**Keywords:** ADME/T, cancer, molecular docking, phthalonitrile, pyrazoline.

© EJBCS. All rights reserved.

### 1. Introduction

Pyrazoline derivatives, members of the heterocyclic chemical class, are intriguing substances with a wide range of biological profiles, potential applications as drugs, and synthetic adaptability (Dipankar et. al. 2011). Many experts in the realm of medicinal chemistry have researched the pyrazoline template extensively in relation to various diseases. Numerous biological actions, including antifungal, anticancer, anti-inflammatory, antituberculosis, antidepressant, antibacterial, cholinesterase, carbonic anhydrase, and antimalarial properties, have been identified for these compounds (Altıntop et. al. 2013; Çelik et. al. 2020; Kaplancıklı et. al. 2010; Kharbanda et. al. 2014; Monga et. al. 2014; Joshi et. al. 2016; Özdemir et. al. 2010; Wang et. al. 2013). In structure-activity studies on

pyrazoline-based compounds, the diversity of design substitutions to the pyrazoline ring appears to have a stupendous impact on the biological profile. It has been observed by diverse researchers that the steric and electronic properties of the substituents attached to 3,5-diaryl-4,5-dihydro-1H-pyrazole derivatives, which represent the 2-pyrazoline class, have changed (Nehra et. al. 2020). The structurally common feature of various drugs used in the clinical treatment of many diseases is the pyrazoline ring system (Fig.1) (Bhutani et. al. 2015; Kumar et. al. 2009). Pyrazoline derivatives are used in the literature as anticancer agents in the treatment of various types of cancer (Amr et. al. 2018; Ahmed et. al. 2019; Chen et. al. 2018; Kim et. al. 2017; Li et. al. 2018; Moreno et. al. 2018; Stefanos et. al. 2019; Xu et. al. 2017).



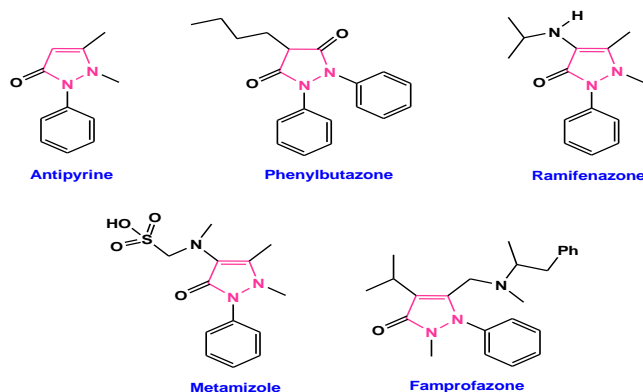


**Fig. 1.** Diverse pyrazoline-based clinically used drugs.

Cancer is a broad type of disease characterized by the uncontrolled, rapid, and pathological proliferation of abnormally transformed cells, and despite various alternative treatment methods developed for the treatment of this disease, cancer is still the second leading fatal disease after cardiovascular diseases all over the world. Lack of resistance and selectivity to chemotherapeutic agents are very important factors in the fight against cancer. Anticancer drugs used in the treatment of this disease destroy not only cancer cells but also normal cells, and this causes serious side effects. In order to prevent this situation, the synthesis of new antineoplastic agents that selectively destroy tumor cells or at least prevent their proliferation is constantly being developed by researchers (Nepali. et al. 2014; Nussbaumer et. al. 2011; Mathur et. al. 2015; Rebucci and Michiels 2013).

Theoretical calculations provide significant information on many aspects of molecules in addition to measuring their activity. Theoretical computations have become faster and more accurate with the advancement of technology. It is used to identify the active molecules, the portions of the molecules with the highest electron densities, and the active regions of the molecules using computations (Chalkha et. al. 2023; Majumdar et. al. 2022). The study used Gaussian calculations, B3LYP, HF, and M06-2x (Becke 1992; Hohenstein et. al. 2008; Vautherin and Brink 1972) methods using the 6-31++g(d,p) basis set to examine the chemical characteristics of the compounds. To contrast a molecule's action with biological materials, molecular docking calculations were conducted with breast cancer protein (PDB ID: 1JNX) (Williams et. al. 2001), liver cancer protein (PDB ID: 3WZE) (Okamoto et. al. 2015), prostate-specific membrane antigen (PDB ID: 6XXP) (Rosenfeld et. al. 2020), and colon cancer protein (PDB ID: 4UYA) (Marusiak et. al. 2016). Finally, the compounds' ADME/T calculations were performed, and their pharmacological characteristics were investigated.

In this study, syntheses, structural characterization, and in silico studies of methoxylated pyrazoline compounds containing amine (**Py<sub>1</sub>-NH<sub>2</sub>** and **Py<sub>2</sub>-NH<sub>2</sub>**), tosyl (**Py<sub>1</sub>-Ts** and **Py<sub>2</sub>-Ts**), and nitrile (**Py<sub>1</sub>-CN** and **Py<sub>2</sub>-CN**) groups were searched. The activities of these compounds against cancer proteins and their ADME properties were investigated. It was determined that the **Py<sub>1</sub>-NH<sub>2</sub>** compound showed higher activity than the other synthesized compounds.

## 2. Materials and Method

Every chemical that was utilized was of reagent-grade quality. Purchased from Sigma-Aldrich, Merck, and Fluka, phenylhydrazine, NaOH, p-tosyl chloride, potassium carbonate, and 4-nitrophthalonitrile were used exactly as directed. Purchased from Merck and Sigma Aldrich, the utilized solvents were used exactly as supplied.

All reactions were carried out in an oxygen-free, dry nitrogen environment using a Schlenk apparatus. The Perkin Elmer 1600 FT-IR Spectrophotometer was used to record infrared spectra. Chemical shifts were reported ( $\delta$ ) in the <sup>1</sup>H and <sup>13</sup>C NMR spectra recorded on a Bruker Ascent 400 MHz NMR spectrometer CDCl<sub>3</sub>, using Me<sub>4</sub>Si (tetramethylsilane) as an internal standard. A MALDI-TOF spectrometer was used to measure the mass spectra. A device known as an electrothermal was used to determine the melting points.

### 2.1. Synthesis

#### 2.1.1. Methoxylated pyrazoline derivatives bearing amine group (**Py<sub>1</sub>-NH<sub>2</sub>** and **Py<sub>2</sub>-NH<sub>2</sub>**)

Phenylhydrazine (0.54g, 5.0 mmol) was added to the solution of the appropriate chalcone-derived amine compounds (1.27g, 5.0 mmol) (**Chlcn-1**) or (1.42g, 5.0 mmol) (**Chlcn-2**) in absolute ethanol (15 mL) containing 1 g of NaOH. After heating the reaction mixture under reflux for 6–10 hours while monitoring its progress with a TLC analysis, it was allowed to cool to room temperature. The crystalline substance that had separated was filtered, then dried and cleaned with cold methanol. Hereby, the title products (**Py<sub>1</sub>-NH<sub>2</sub>** and **Py<sub>2</sub>-NH<sub>2</sub>**) were acquired as yellow solids.

##### 2.1.1.1. 2-(5-(2-methoxyphenyl)-1-phenyl-4,5-dihydro-1H-pyrazol-3-yl)benzenamine (**Py<sub>1</sub>-NH<sub>2</sub>**)

Yield: 81%. M.p: 137–139 °C. FT-IR (ATR),  $\nu_{max}$  (cm<sup>-1</sup>): 3384–3291 (NH<sub>2</sub>), 3026 (ArC–H), 2939–2844 (C–H), 1615 (C=N), 1592 (C=C), 1492–1446 (N–N), 1385, 1324, 1294, 1157, 1103, 1029, 999, 878, 736, 689. <sup>1</sup>H NMR (400 MHz,  $\delta$ , ppm, DMSO-*d*<sub>6</sub>): 7.12–6.56 (m, 13H, Ar–H), 5.52 (bs, 1H, pyrazoline-H), 3.93 (s, 3H, –OCH<sub>3</sub>), 3.93 (bs, 1H, pyrazoline-H), 3.08 (bs, 1H, pyrazoline-H). APT NMR (100 MHz,  $\delta$ , ppm, DMSO-*d*<sub>6</sub>): N=C 156.9 (C), Ar–C [155.7 (C), 147.2 (C), 150.5 (pyrazoline-C), 144.2 (C), 143.8 (C), 129.1 (CH), 129.5 (CH), 126.4 (CH), 121.1 (CH), 118.6 (CH), 117.0 (C), 115.6 (CH), 115.5 (CH), 113.7 (C), 112.7 (CH), 111.9 (CH)], 56.3 (pyrazoline-C), 56.1 (–OCH<sub>3</sub>), 43.7 (pyrazoline-C). MS (MALDI-TOF) *m/z*: Calculated: 343.42; Found: 343.51 [M]<sup>+</sup>.

##### 2.1.1.2. 3-(5-(2,5-dimethoxyphenyl)-1-phenyl-4,5-dihydro-1H-pyrazol-3-yl)benzenamine (**Py<sub>2</sub>-NH<sub>2</sub>**)

Yield: 78%. M.p: 174–176 °C. FT-IR (ATR),  $\nu_{max}$  (cm<sup>-1</sup>): 3443–3361 (NH<sub>2</sub>), 3004 (ArC–H), 2933–2834 (C–H), 1618 (C=N), 1594 (C=C), 1495–1462 (N–N), 1396, 1333, 1260, 1130, 1044, 1000, 867, 744, 687 (C–S). <sup>1</sup>H NMR (400 MHz,  $\delta$ , ppm, DMSO-*d*<sub>6</sub>): 6.45–7.18 (m, 12H, Ar–H), 5.54 (bs, 1H, pyrazoline-H), 3.86 (bs, 1H, pyrazoline-H), 3.55 (s, 3H, –OCH<sub>3</sub>), 3.40 (s, 3H, –OCH<sub>3</sub>), 2.92 (bs, 1H,

pyrazoline-H). APT NMR (100 MHz,  $\delta$ , ppm, DMSO- $d_6$ ): N=C 153.4 (C), Ar-C [150.4 (pyrazoline-C), 149.2(C), 148.7 (C), 144.8 (C), 134.8(C), 133.2(C), 130.9 (C), 129.6 (CH), 129.5 (CH), 118.7 (CH), 115.2 (CH), 114.3 (CH), 113.1 (CH), 112.9 (CH), 112.4 (CH), 111.1 (CH)], 57.9 (pyrazoline-C), 56.5 (-OCH<sub>3</sub>), 55.4 (-OCH<sub>3</sub>), 42.3 (pyrazoline-C). MS (MALDI-TOF)  $m/z$ : Calculated: 373.45; Found: 373.76 [M]<sup>+</sup>.

### 2.1.2. Methoxylated pyrazoline derivatives bearing tosyl group (Py<sub>1</sub>-Ts and Py<sub>2</sub>-Ts)

Pyrazoline-derived amine compound (0.75g, 2.17 mmol) (Py<sub>1</sub>-NH<sub>2</sub>) or (0.5g, 1.34 mmol) (Py<sub>2</sub>-NH<sub>2</sub>) was solved in pyridine (20 mL), and p-tosyl chloride (0.46g, 2.39 mmol for Py<sub>1</sub>-Ts) or (0.28g, 1.47 mmol for Py<sub>2</sub>-Ts) dissolved in pyridine (5 mL) was added dropwise in the reaction mixture for about 1 hours. This mixture was continued at -5–8 °C with stirring for 17 hours. The orange-colored reaction ingredients were added to crushed ice and acidified with concentrated HCl acid. The precipitated products were filtered, crystallized in ethanol, and dried in vacuo. Hereby, the title products (Py<sub>1</sub>-Ts and Py<sub>2</sub>-Ts) were acquired as fawn-colored solids.

#### 2.1.2.1. N-(2-(5-(2-methoxyphenyl)-1-phenyl-4,5-dihydro-1H-pyrazol-3-yl)phenyl)-4-methyl benzene sulphonamide (Py<sub>1</sub>-Ts)

Yield: 88%. M.p: 167–169 °C. FT-IR (ATR),  $\nu_{max}$  (cm<sup>-1</sup>): 3383 (N-H), 3068 (ArC-H), 2946–2842 (C-H), 1612 (C=N), 1596 (C=C), 1497–1462 (N-N), 1386, 1345–1158 (SO<sub>2</sub>, tosyl), 1042, 1000, 885, 744, 667 (C-S). <sup>1</sup>H NMR (400 MHz,  $\delta$ , ppm, CDCl<sub>3</sub>): 7.94 (t, 2H, Ar-H), 7.73 (t, 1H, Ar-H), 7.29–7.22 (m, 2H, Ar-H), 7.14 (d, 1H, Ar-H), 7.09 (d, 1H, Ar-H), 7.03 (d, 3H, Ar-H), 6.99 (s, 1H, Ar-H), 6.95 (d, 1H, Ar-H), 6.88–6.83 (m, 1H, Ar-H), 5.51 (t, 1H, pyrazoline -CH), 3.95 (s, 1H, NH), 3.93 (s, 3H, -OCH<sub>3</sub>), 3.82 (dd, 1H, pyrazoline -CH<sub>2</sub>), 3.01 (dd, 1H, pyrazoline -CH<sub>2</sub>), 2.32 (s, 3H, -CH<sub>3</sub>). <sup>13</sup>C NMR (100 MHz,  $\delta$ , ppm, CDCl<sub>3</sub>): 156.0, 148.2, 145.1, 143.6, 143.5, 141.5, 136.7, 136.4, 129.5, 128.9, 128.7, 128.4, 127.4, 126.9, 126.4, 123.9, 123.2, 120.9, 119.8, 113.1, 110.6, 57.2 (pyrazoline -CH), 55.5 (-OCH<sub>3</sub>), 42.9 (pyrazoline CH<sub>2</sub>), 21.5 (-CH<sub>3</sub>). MS (MALDI-TOF)  $m/z$ : Calculated:497.61; Found:497.45 [M]<sup>+</sup>.

#### 2.1.2.2. N-(3,4-dicyanophenyl)-N-(3-(5-(2,5-dimethoxyphenyl)-1-phenyl-4,5-dihydro-1H-pyrazol-3-yl)phenyl)-4-methylbenzenesulfonamide (Py<sub>2</sub>-Ts)

Yield: 83%. M.p: 157–159 °C. FT-IR (ATR),  $\nu_{max}$  (cm<sup>-1</sup>): 3384 (N-H), 3066 (ArC-H), 2949–2838 (C-H), 1660 (C=N), 1596 (C=C), 1497–1455 (N-N), 1386, 1345–1158 (SO<sub>2</sub>, tosyl), 1077, 1000, 919, 885, 745, 667 (C-S). <sup>1</sup>H NMR (400 MHz,  $\delta$ , ppm, CDCl<sub>3</sub>): 7.72 (t, 2H, Ar-H), 7.58 (d, 1H, Ar-H), 7.33–7.22 (m, 2H, Ar-H), 7.14 (d, 1H, Ar-H), 7.09 (d, 1H, Ar-H), 7.05–6.99 (m, 1H, Ar-H), 6.96 (s, 2H, Ar-H), 6.94 (s, 1H, Ar-H), 6.88–6.84 (m, 1H, Ar-H), 5.52 (t, 1H, pyrazoline -CH), 3.98 (s, 1H, NH), 3.93 (s, 6H, -OCH<sub>3</sub>), 3.83 (dd, 1H, pyrazoline -CH<sub>2</sub>), 3.01 (dd, 1H, pyrazoline -CH<sub>2</sub>), 2.32 (s, 3H, -CH<sub>3</sub>). <sup>13</sup>C NMR (100 MHz,  $\delta$ , ppm, CDCl<sub>3</sub>): 156.0, 148.2, 143.6, 143.5, 136.7, 136.4,

130.9, 129.5, 128.9, 128.8, 127.4, 127.2, 127.1, 126.4, 123.2, 122.9, 120.9, 119.8, 113.1, 111.4, 110.6, 57.2 (pyrazoline -CH), 55.5 (-OCH<sub>3</sub>), 54.9 (-OCH<sub>3</sub>), 42.9 (pyrazoline CH<sub>2</sub>), 21.5 (-CH<sub>3</sub>). MS (MALDI-TOF)  $m/z$ : Calculated:527.63; Found:527.67 [M]<sup>+</sup>.

### 2.1.3. Methoxylated pyrazoline derivatives bearing nitrile group (Py<sub>1</sub>-CN and Py<sub>2</sub>-CN)

Py<sub>1</sub>-Ts compound (0.5g, 1.0 mmol) or Py<sub>2</sub>-Ts compound (0.44g, 0.84 mmol) and 4-nitrophthalonitrile (0.17g, 1.0 mmol for Py<sub>1</sub>-CN) or (0.15g, 0.84 mmol for Py<sub>2</sub>-CN) were solved in dry dimethylformamide (10 mL). Following thawing, trace amounts of anhydrous K<sub>2</sub>CO<sub>3</sub> (0.41g, 3.0 mmol for Py<sub>1</sub>-CN) or (0.35g, 2.52 mmol for Py<sub>2</sub>-CN) were added to the reaction mixture. After four days at 55 °C and N<sub>2</sub> atmospheric pressure, the reaction mixture was transferred to ice and filtered. Using silica gel and column chromatography, the obtained solid product was purified. Hereby, the title products (Py<sub>1</sub>-CN and Py<sub>2</sub>-CN) were acquired as fawn-colored solids.

#### 2.1.3.1. N-(3,4-dicyanophenyl)-N-(2-(5-(2-methoxyphenyl)-1-phenyl-4,5-dihydro-1H-pyrazol-3-yl)phenyl)-4-methylbenzenesulfonamide (Py<sub>1</sub>-CN)

Yield: 48%. Column chromatography solvent: Chloroform. FT-IR (ATR),  $\nu_{max}$  (cm<sup>-1</sup>): 3073 (ArC-H), 2922–2836 (C-H), 2233 (C≡N), 1672 (C=N), 1595 (C=C), 1486–1463 (N-N), 1388, 1338–1157 (SO<sub>2</sub>, tosyl), 1090, 999, 881, 748, 691 (C-S). <sup>1</sup>H NMR (400 MHz,  $\delta$ , ppm, CDCl<sub>3</sub>): 7.96 (d, 2H, Ar-H), 7.78 (d, 2H, Ar-H), 7.31–7.28 (m, 2H, Ar-H), 7.18 (d, 2H, Ar-H), 7.11 (d, 2H, Ar-H), 7.00 (d, 2H, Ar-H), 6.97 (s, 1H, Ar-H), 6.93 (d, 1H, Ar-H), 6.87–6.82 (m, 2H, Ar-H), 5.50 (t, 1H, pyrazoline -CH), 3.92 (s, 3H, -OCH<sub>3</sub>), 3.80 (dd, 1H, pyrazoline -CH<sub>2</sub>), 3.00 (dd, 1H, pyrazoline -CH<sub>2</sub>), 2.31 (s, 3H, -CH<sub>3</sub>). <sup>13</sup>C NMR (100 MHz,  $\delta$ , ppm, CDCl<sub>3</sub>): 156.0, 148.2, 143.6, 143.5, 136.7, 136.4, 131.1, 130.9, 129.5, 129.4, 128.9, 128.7, 128.6, 128.4, 128.1, 127.7, 127.4, 126.4, 124.0, 123.2, 122.9, 121.2, 120.9, 120.8, 119.8 (C≡N), 119.1 (C≡N), 113.1, 111.4, 110.6, 107.2, 57.2 (pyrazoline -CH), 55.5 (-OCH<sub>3</sub>), (pyrazoline CH<sub>2</sub>), 21.5 (-CH<sub>3</sub>). MS (MALDI-TOF)  $m/z$ : Calculated: 623.72; Found: 646.61 [M+Na]<sup>+</sup>.

#### 2.1.3.2. N-(3,4-dicyanophenyl)-N-(3-(5-(2,5-dimethoxyphenyl)-1-phenyl-4,5-dihydro-1H-pyrazol-3-yl)phenyl)-4-methylbenzenesulfonamide (Py<sub>2</sub>-CN)

Yield: 52%. Column chromatography solvent: Chloroform. FT-IR (ATR),  $\nu_{max}$  (cm<sup>-1</sup>): 3059 (ArC-H), 2922–2835 (C-H), 2233 (C≡N), 1660 (C=N), 1595 (C=C), 1493–1462 (N-N), 1395, 1328–1158 (SO<sub>2</sub>, tosyl), 1091, 999, 875, 747, 691 (C-S). <sup>1</sup>H NMR (400 MHz,  $\delta$ , ppm, CDCl<sub>3</sub>): 7.78 (t, 2H, Ar-H), 7.62 (m, 2H, Ar-H), 7.47–7.39 (m, 2H, Ar-H), 7.12 (d, 1H, Ar-H), 7.07 (d, 2H, Ar-H), 7.05–6.98 (m, 2H, Ar-H), 6.97 (s, 2H, Ar-H), 6.92 (s, 1H, Ar-H), 6.88–6.84 (m, 1H, Ar-H), 5.51 (t, 1H, pyrazoline -CH), 3.95 (s, 6H, -OCH<sub>3</sub>), 3.85 (dd, 1H, pyrazoline -CH<sub>2</sub>), 3.03 (dd, 1H, pyrazoline -CH<sub>2</sub>), 2.30 (s, 3H, -CH<sub>3</sub>). <sup>13</sup>C NMR (100 MHz,  $\delta$ , ppm, CDCl<sub>3</sub>): 156.0, 148.3, 143.7, 143.5, 137.7, 136.4, 135.6, 134.7, 132.9, 130.9, 129.5, 129.2, 128.9, 128.1, 127.9, 127.4, 127.2, 127.1, 126.4, 123.2, 122.9, 121.6,

120.9, 120.8, 119.8 (C≡N), 119.1 (C≡N), 113.1, 111.4, 110.6, 57.2 (pyrazoline -CH), 55.5 (-OCH<sub>3</sub>), 54.9 (-OCH<sub>3</sub>), 42.9 (pyrazoline CH<sub>2</sub>), 21.5 (-CH<sub>3</sub>). MS (MALDI-TOF) *m/z*: Calculated: 653.75; Found: 676.67 [M+Na]<sup>+</sup>.

## 2.2. Theoretical methods

Theoretical computations can teach us a great deal about the chemical and biological properties of molecules. Many properties of quantum chemicals are determined by theoretical calculations (Tas et. al. 2022). The chemical behavior of the molecules is explained by the estimated parameters. Numerous programs are used to calculate molecules. Gaussian09 RevD.01 and GaussView 6.0 (Dennington et. al. 2016; Frisch et. al. 2009) are the programs in question. These programs were used to do calculations utilizing the 6-31++g(d,p) basis set using the B3LYP, HF, and M06-2x (Becke 1992), (Hohenstein et. al. 2008), (Vautherin and Brink 1972) methods. The outcome of these efforts has been the discovery of numerous quantum chemical parameters. The estimated parameters are calculated as follows, where each parameter describes a different chemical characteristic of molecules (Lakhrissi et. al. 2022; Majumdar et. al. 2022).

$$\chi = -\left(\frac{\partial E}{\partial N}\right)_{v(r)} = \frac{1}{2}(I + A) \cong -\frac{1}{2}(E_{HOMO} + E_{LUMO})$$

$$\eta = -\left(\frac{\partial^2 E}{\partial N^2}\right)_{v(r)} = \frac{1}{2}(I - A) \cong -\frac{1}{2}(E_{HOMO} - E_{LUMO})$$

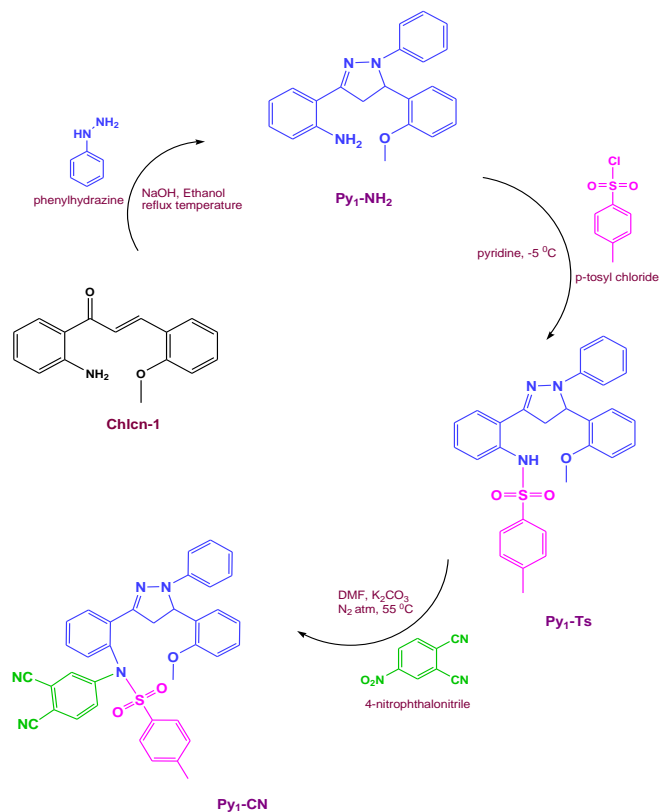
$$\sigma = 1/\eta \quad \omega = \chi^2/2\eta \quad \varepsilon = 1/\omega$$

Molecular docking calculations are performed to compare the biological activity of a molecule to that of a biological substance. Schrödinger's Maestro Molecular Modeling Platform (version 12.8a) was used to do the molecular docking computations (Schrödinger 2021-3; 2021). There are several steps involved in computation. Each step is completed in a different way. In the first phase, proteins were prepared using the protein preparation module (Schrödinger 2019-4; 2016; 2019). In this module, the protein active sites were found. After then, computations using optimized structures can be performed with the LigPrep module (Schrödinger 2021-3; 2021). Following preparation, the Glide ligand docking module was used to examine the interactions between the compounds and the cancer protein (Tüzün et. al. 2022). Every calculation was carried out with the OPLS4 technique. To evaluate the chemicals under investigation's pharmacological potential, an ADME/T (absorption, distribution, metabolism, excretion, and toxicity) study was conducted. The Qik-prop module of the Schrödinger software (Schrödinger 2021-3; 2021) was used to predict the results and interactions of molecules involved in human metabolism.

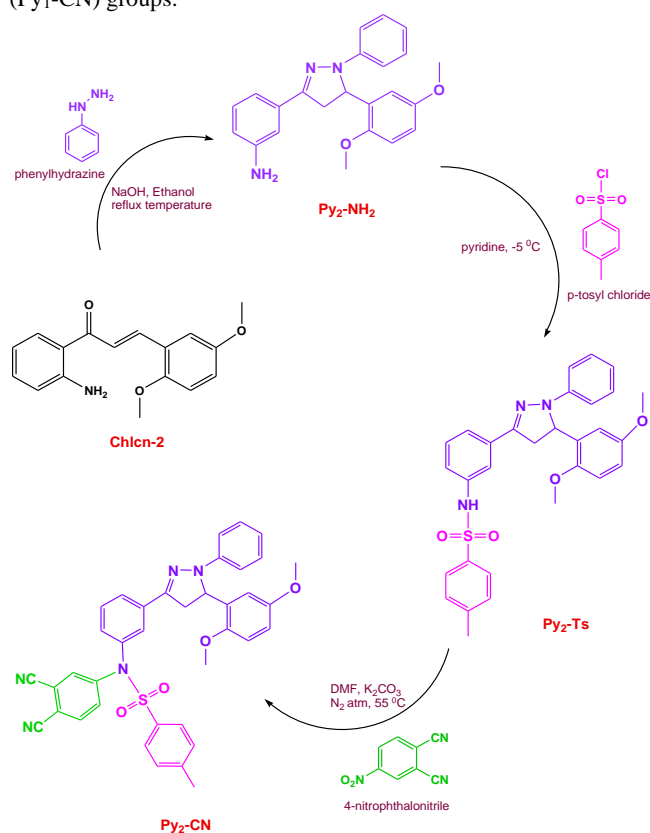
## 3. Results and Discussion

### 3.1. Characterizations of synthesized all compounds

General synthesis schemes of methoxylated pyrazoline derivatives bearing amine (**Py<sub>1</sub>-NH<sub>2</sub>** and **Py<sub>2</sub>-NH<sub>2</sub>**), tosyl (**Py<sub>1</sub>-Ts** and **Py<sub>2</sub>-Ts**), and nitrile (**Py<sub>1</sub>-CN** and **Py<sub>2</sub>-CN**) groups are given in Schemes 1 and 2.



**Scheme 1.** Synthesis scheme of methoxylated pyrazoline derivatives bearing amine (**Py<sub>1</sub>-NH<sub>2</sub>**), tosyl (**Py<sub>1</sub>-Ts**), and nitrile (**Py<sub>1</sub>-CN**) groups.



**Scheme 2.** Synthesis scheme of methoxylated pyrazoline derivatives bearing amine (**Py<sub>2</sub>-NH<sub>2</sub>**), tosyl (**Py<sub>2</sub>-Ts**), and nitrile (**Py<sub>2</sub>-CN**) groups.

These compounds' structural characterizations were carried out with the use of mass, FT-IR, and NMR spectrum data. Attained methoxylated pyrazoline derivatives bearing amine (**Py<sub>1</sub>-NH<sub>2</sub>** and **Py<sub>2</sub>-NH<sub>2</sub>**) groups have characteristic groups of NH<sub>2</sub> (amine), C=N (due to ring closure), and N-N (proves the formation of a pyrazoline ring). NH<sub>2</sub> stretching vibration was seen at 3384–3291 cm<sup>-1</sup> (for **Py<sub>1</sub>-NH<sub>2</sub>**) and 3443–3361 cm<sup>-1</sup> (for **Py<sub>2</sub>-NH<sub>2</sub>**), C=N stretching vibration was seen at 1615 cm<sup>-1</sup> (for **Py<sub>1</sub>-NH<sub>2</sub>**) and 1618 cm<sup>-1</sup> (for **Py<sub>2</sub>-NH<sub>2</sub>**), and N-N stretching vibration was seen at 1492–1446 cm<sup>-1</sup> (for **Py<sub>1</sub>-NH<sub>2</sub>**) and 1495–1462 cm<sup>-1</sup> (for **Py<sub>2</sub>-NH<sub>2</sub>**) in the FT-IR spectra. NMR spectra of methoxylated pyrazoline derivatives bearing amine (**Py<sub>1</sub>-NH<sub>2</sub>** and **Py<sub>2</sub>-NH<sub>2</sub>**) groups were recorded in DMSO-*d*<sub>6</sub> (Fig. 2). The mass spectra of **Py<sub>1</sub>-NH<sub>2</sub>** and **Py<sub>2</sub>-NH<sub>2</sub>** showed two distinct molecular ion peaks, located at *m/z*: 343.51 [M]<sup>+</sup> and 373.76 [M]<sup>+</sup>, respectively (Fig. 3). The data obtained proves the formation of methoxylated pyrazoline derivatives bearing an amine group.

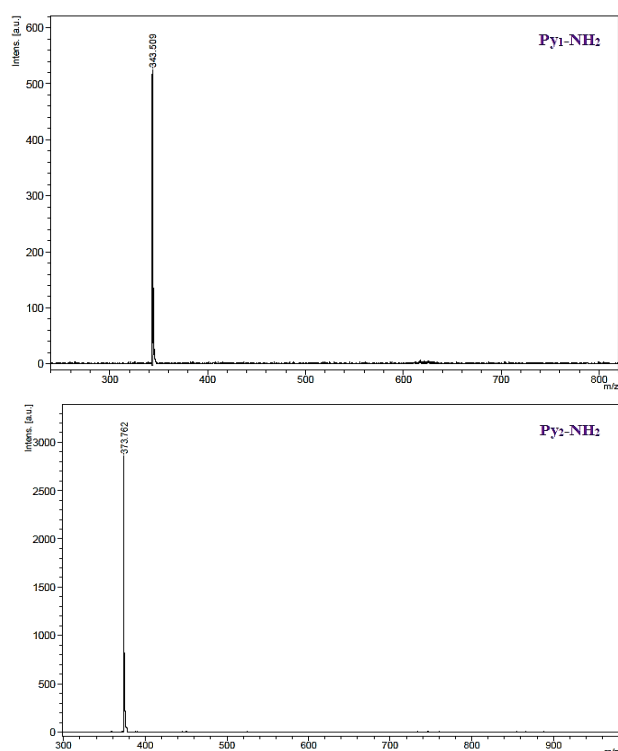


**Fig. 2.** Mass spectra of pyrazoline derivatives bearing the amine (**Py<sub>1</sub>/Py<sub>2</sub>-NH<sub>2</sub>**) group.

Obtained methoxylated pyrazoline derivatives bearing tosyl (**Py<sub>1</sub>-Ts** and **Py<sub>2</sub>-Ts**) group have characteristic groups as N-H, C=N (due to ring closure), N-N (proves the formation of pyrazoline ring), and SO<sub>2</sub> (tosyl). The FT-IR spectra showed the following: N-H stretching vibration was observed at 3383 cm<sup>-1</sup> (for **Py<sub>1</sub>-Ts**) and 3384 cm<sup>-1</sup> (for **Py<sub>2</sub>-Ts**); C=N stretching vibration was observed at 1612 cm<sup>-1</sup> (for **Py<sub>1</sub>-Ts**) and 1660 cm<sup>-1</sup> (for **Py<sub>2</sub>-Ts**); N-N stretching vibration was observed at 1497–1462 cm<sup>-1</sup> (for **Py<sub>1</sub>-Ts**) and 1497–1455 cm<sup>-1</sup> (for **Py<sub>2</sub>-Ts**); and SO<sub>2</sub> (tosyl) stretching vibration was observed at 1345–1158 cm<sup>-1</sup> (for **Py<sub>1</sub>/Py<sub>2</sub>-Ts**). Methoxylated pyrazoline derivatives with tosyl groups (**Py<sub>1</sub>-Ts** and **Py<sub>2</sub>-Ts**) were recorded in CDCl<sub>3</sub> and their

NMR spectra were obtained. Doublet of doublet (dd) characteristic peaks were observed in the <sup>1</sup>H NMR spectra at 3.82 and 3.01 ppm (for **Py<sub>1</sub>-Ts**), and 3.83 ppm and 3.01 ppm (for **Py<sub>2</sub>-Ts**). Additionally, for **Py<sub>1</sub>-Ts** and **Py<sub>2</sub>-Ts**, aromatic protons were detected at 7.94–6.83 ppm and 7.72–6.84 ppm, respectively. The molecular ion peak for **Py<sub>1</sub>-Ts** and **Py<sub>2</sub>-Ts**, respectively, were found in the mass spectra at *m/z*: 497.45 [M]<sup>+</sup> and 527.67 [M]<sup>+</sup>, as shown in Figure 4. The information gathered demonstrates the creation of derivatives of methoxylated pyrazolines with a tosyl group.

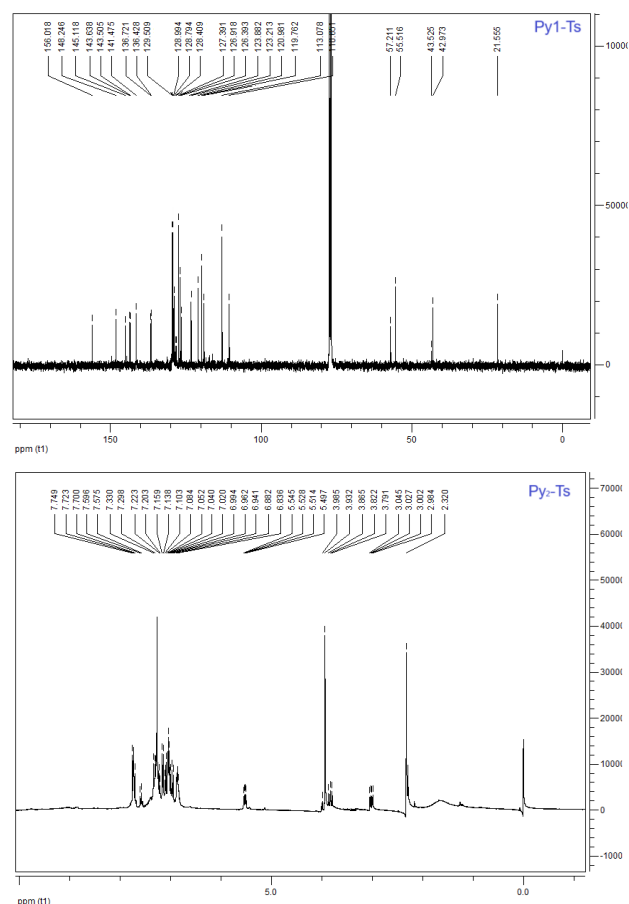


**Fig. 2.** <sup>13</sup>C NMR and <sup>1</sup>H NMR spectra of pyrazoline derivatives bearing the tosyl (**Py<sub>1</sub>/Py<sub>2</sub>-Ts**) group.

The distinctive groups of methylated pyrazoline derivatives with nitrile groups (**Py<sub>1</sub>-CN** and **Py<sub>2</sub>-CN**) are C≡N (nitrile), C=N (because of ring closure), N-N (shows that the pyrazoline ring is formed), and SO<sub>2</sub> (tosyl). In the FT-IR spectra, several stretching vibrations were observed: C≡N was observed at 2233 cm<sup>-1</sup> (for **Py<sub>1</sub>/Py<sub>2</sub>-CN**), C=N was observed at 1672 cm<sup>-1</sup> (for **Py<sub>1</sub>-CN**) and 1660 cm<sup>-1</sup> (for **Py<sub>2</sub>-CN**), N-N was observed at 1486–1463 cm<sup>-1</sup> (for **Py<sub>1</sub>-CN**) and 1493–1462 cm<sup>-1</sup> (for **Py<sub>2</sub>-CN**), and SO<sub>2</sub> (tosyl) was observed at 1338–1157 cm<sup>-1</sup> (for **Py<sub>1</sub>-CN**) and 1328–1158 cm<sup>-1</sup> (for **Py<sub>2</sub>-CN**). Methoxylated pyrazoline derivatives (**Py<sub>1</sub>-CN** and **Py<sub>2</sub>-CN**) with nitrile groups recorded their NMR spectra in CDCl<sub>3</sub>. A molecular ion peak for **Py<sub>1</sub>-CN** and **Py<sub>2</sub>-CN**, respectively, was seen in the mass spectra at *m/z*: 646.61 [M+Na]<sup>+</sup> and 676.67 [M+Na]<sup>+</sup>, respectively. The information gathered demonstrates the creation of derivatives of methoxylated pyrazolines with a nitrile group.



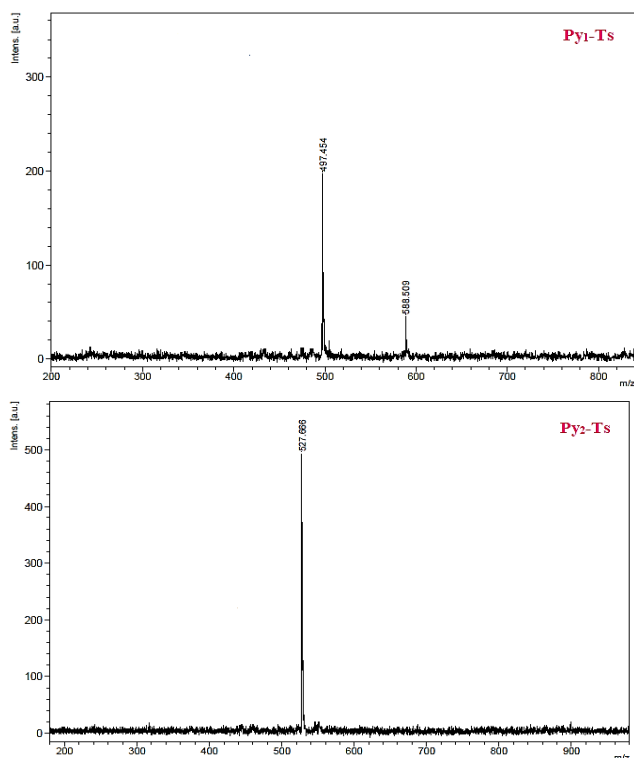


**Fig. 4.** Mass spectra of pyrazoline derivatives bearing the tosyl (Py<sub>1</sub>/Py<sub>2</sub>-Ts) group.

### 3.2. Theoretical calculations

One popular technique for comparing the activity of molecules is to perform theoretical calculations. This approach provides significant insights into the molecular features that are both chemical and biological. For this data, numerous parameters are determined (Majumdar et al. 2022). A distinct piece of information about the molecule is provided by each parameter. The Gaussian software program is used to calculate a number of quantum chemical parameters, the numerical values of which are utilized to explain the behaviors of molecules. The HOMO and LUMO parameters are more significant than the other estimated values for the molecules. The molecule with the greatest HOMO parameter numerical value is assumed to have higher activity than the other molecules since it can donate electrons more readily than the others (Majumdar et al. 2022). LUMO is an additional parameter. It is believed that the molecule with the lowest numerical expression of this characteristic has a higher activity than the other molecules because it can acquire electrons more readily than the other molecules (Lakhrissi et al. 2022). The  $\Delta E$  energy gap is the next parameter, and for highly active molecules, its numerical expression is the smallest. The electronegativity value reveals how well-suited the molecules' atoms are to luring bind electrons (Majumdar. et al. 2022). More electrons are drawn to molecules with higher electronegativity. The activity in this instance declines. Gaussian calculations yielded numerous parameters, which are included in Table 1.

When the HOMO energy values in this table are examined, it is seen that **Py<sub>1</sub>-NH<sub>2</sub>** has higher activity than other molecules as a result of the calculations made in the B3LYP

and M062X methods. Another parameter is the LUMO parameter; according to this parameter, **Py<sub>1</sub>-CN** was found to have higher activity than other molecules. Another important parameter used to compare the activities of molecules is electronegativity, which has a lower electronegativity for **Py<sub>2</sub>-NH<sub>2</sub>**. For this reason, it is seen that its activity is higher since it will interact by giving electrons more easily (Fig. 5).

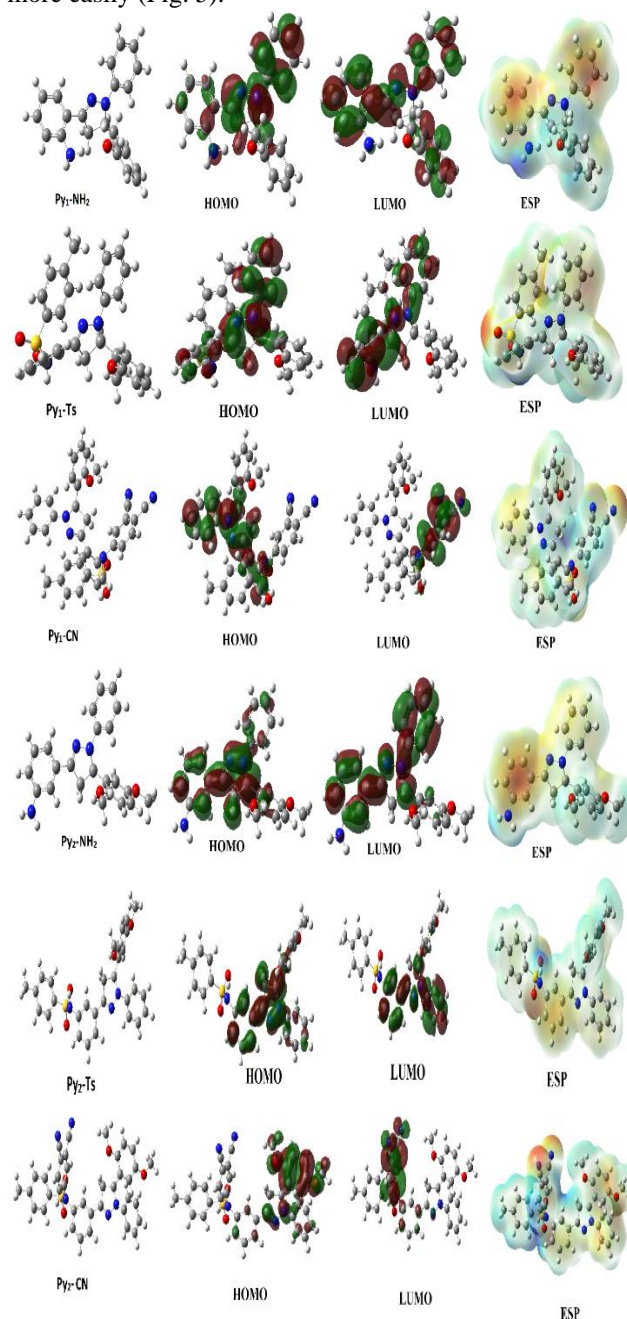


**Fig. 5.** Representations of molecules' ESP, HOMO, LUMO, and optimal structures.

Gaussian calculations are essential to elucidate the chemical properties of molecules. To further evaluate the biological activity of these molecules, another important calculation is required: molecular docking. Molecular docking studies evaluate the interactions between molecules and biological targets, usually proteins associated with human cancer cells.

This approach provides a detailed insight into how the molecule under study interacts with cancer cell proteins. The interactions include various forces such as chemical bonding, hydrogen bonding, polar and hydrophobic contacts, as well as  $\pi$ - $\pi$  and halogen interactions (Çelik et al., 2023; Tapera et al., 2022). Figures 6-9 show these molecular interactions in detail.

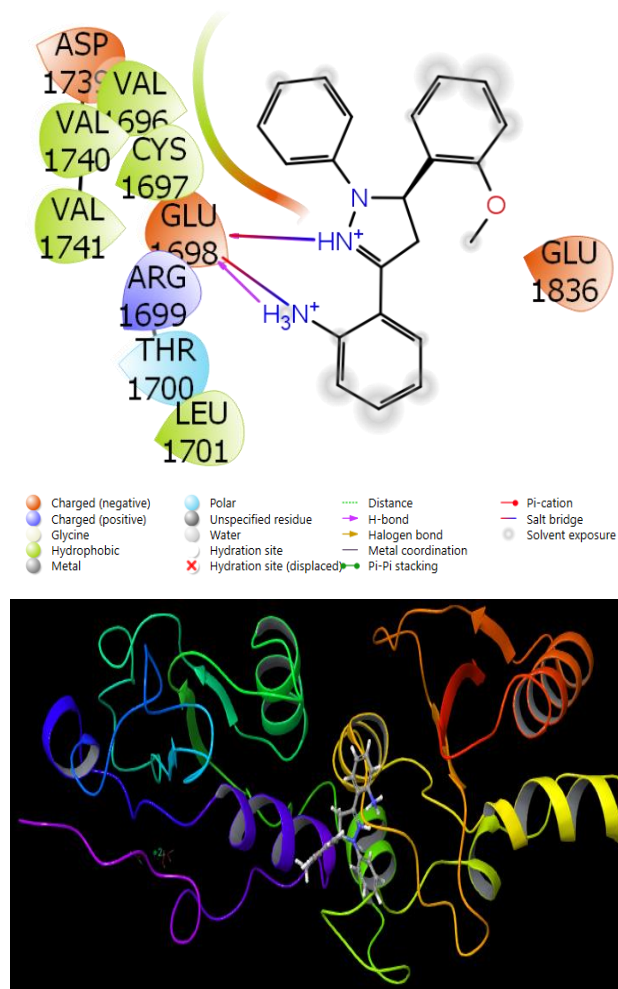


Fig. 6. Presentation interactions of  $\text{Py}_1\text{-NH}_2$  with Breast cancer

As a result of the docking calculations, when the interactions that occur between molecules and proteins are examined, in Figure 6, when the interactions that occur between  $\text{Py}_1\text{-NH}_2$  and Breast cancer are examined, it is seen that there is a salt bridge interaction between the nitrogen atom in the pyrazole ring of the  $\text{Py}_1\text{-NH}_2$  molecule and the GLU 1698 protein. In addition, it is seen that the nitrogen and hydrogen atom in the aniline ring of the  $\text{Py}_1\text{-NH}_2$  molecule make hydrogen bonds with the GLU 1698 protein. When the interactions between  $\text{Py}_1\text{-NH}_2$  and Prostate cancer are examined in figure 7, it is seen that there is a hydrogen bond interaction between the nitrogen atom in the pyrazole ring and the TRP 114 protein. When the interactions between  $\text{Py}_1\text{-NH}_2$  and Colon cancer are examined in figure 8, it is seen that there is a salt bridge interaction between the nitrogen atom in the pyrazole ring of the  $\text{Py}_1\text{-NH}_2$  molecule and the GLU 885 and ASP 1046 proteins. In addition, it is seen that there is a salt bridge

interaction between the nitrogen atom in the aniline ring attached to the central ring of the  $\text{Py}_1\text{-NH}_2$  molecule and the GLU 885 and ASP 1046 proteins. When the interactions between  $\text{Py}_2\text{-Ts}$  and Liver cancer are examined in Figure 9, it is seen that a  $\pi$ - $\pi$  interaction occurs between the benzene ring attached to the pyrazole ring in the  $\text{Py}_2\text{-Ts}$  molecule and the PHE 135 protein. It is seen that a  $\pi$ - $\pi$  interaction occurs between the toluene ring in the  $\text{Py}_2\text{-Ts}$  molecule and the TRP 296 protein. It is seen that the nitrogen atom attached to the sulfur dioxide group in the  $\text{Py}_2\text{-Ts}$  molecule forms a salt bridge with the Mg1440 and Mg 1439 atoms. The results obtained from the calculations made are given in Table 2. The most important of these parameters is the Docking Score parameter, which gives the numerical value of the chemical interactions between molecules and proteins. It is assumed that the molecule with the greatest negative numerical value of this parameter has more chemical interactions since its activity is greater than that of other molecules (Çelik et al. 2023). It should be common knowledge that when the molecule and protein interact more, the docking score parameter rises and therefore does the molecule's activity.

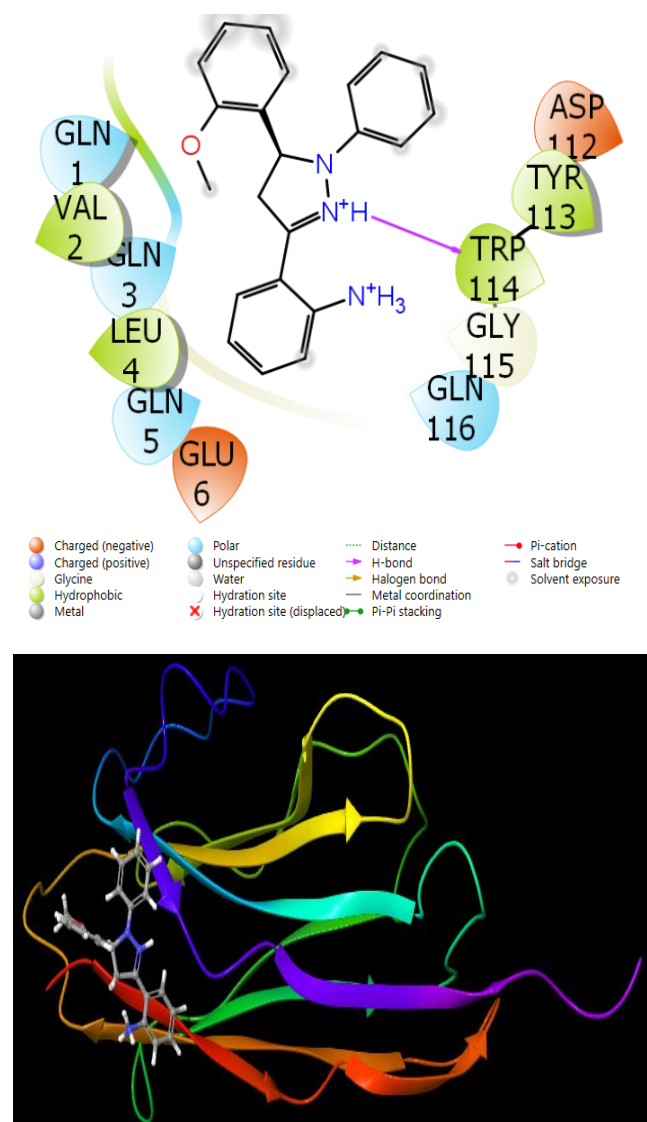


Fig. 7. Presentation interactions of  $\text{Py}_1\text{-NH}_2$  with Prostate cancer



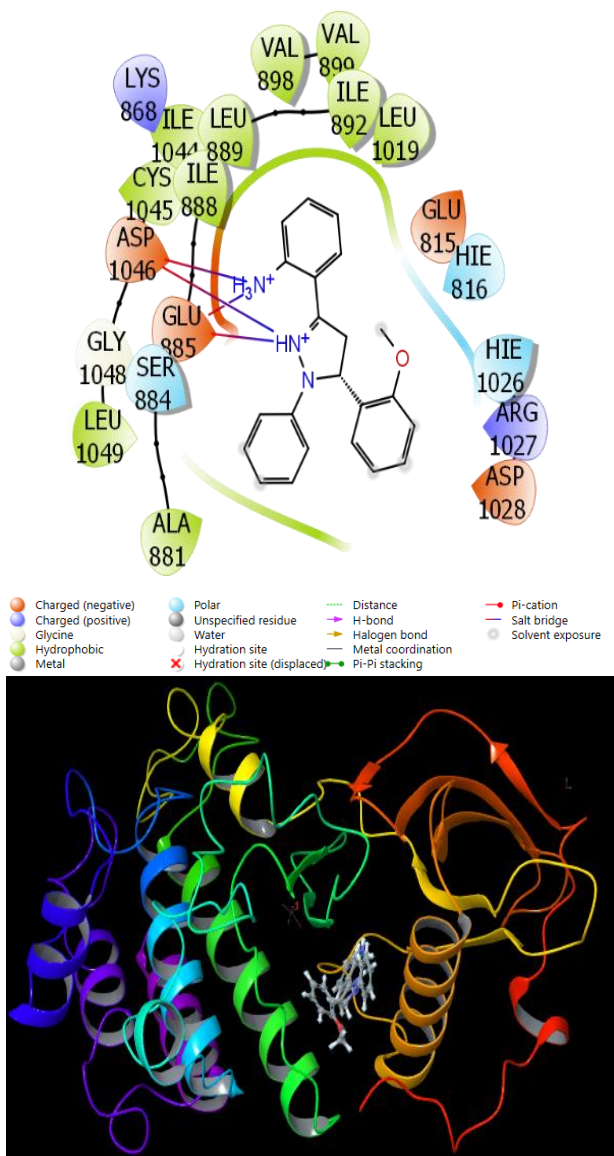


Fig. 8. Presentation interactions of  $\text{Py}_1\text{-NH}_2$  with Colon cancer

Glide ligand efficiency, glide hbond, glide evdw, and glide ecoul are additional factors in the docking computations that provide a numerical value for the chemical interactions between chemicals and proteins (Çelik et. al. 2023). Additional determined parameters include a pose resulting from the interaction of molecules with proteins; Glide emodel, Glide energy, Glide internal, and Glide posenum are the essential factors that provide numerical values for this pose (Tüzün et. al. 2022).

Comparing the activities of the studied molecules with molecular docking calculations is not sufficient by itself for the molecules to be used in human metabolism. Even if the molecules have high activity against cancer proteins, it does not allow us to comment on how they will act in human metabolism. For this, it is necessary to examine the ADME properties of molecules (Table 3).

As a result of this theoretical analysis, many parameters were obtained and these parameters are given in Table 3. The first parameter among these parameters is Solute

Molecular Weight, which requires the molecule to have a certain molecular weight.

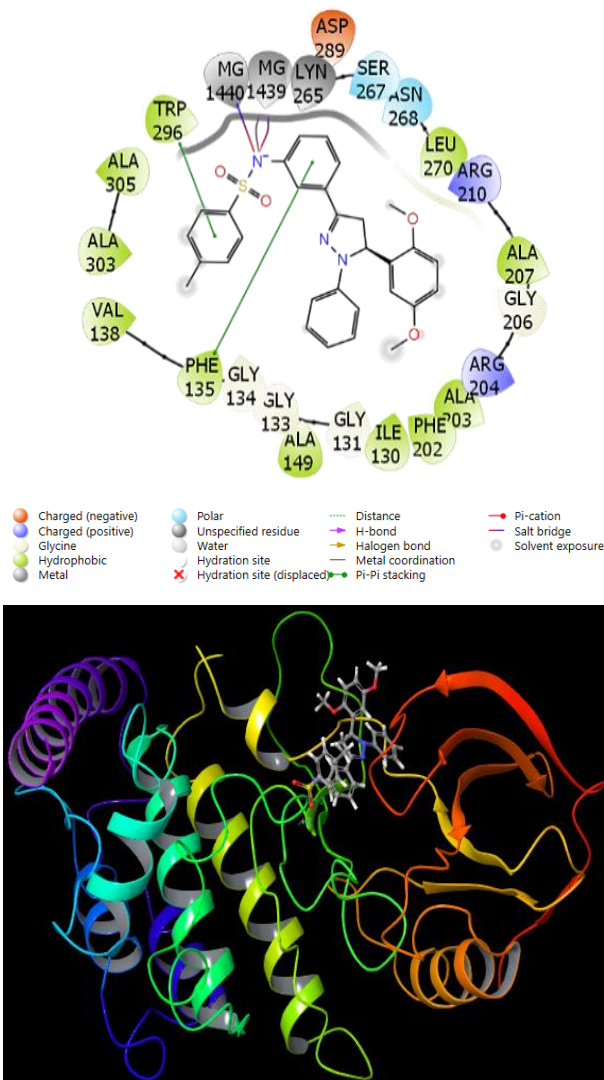


Fig. 9. Presentation interactions of  $\text{Py}_2\text{-Ts}$  with Liver cancer

Another parameter is PISA, which is also called Solute Total SASA. This parameter is  $\pi$  (carbon and attached hydrogen) component of the SASA. Another parameter is QP Polarizability, which is the parameter that predicted polarizability in cubic angstroms.

Another important parameter is QPlogHERG, which is the numerical value of the estimated  $\text{IC}_{50}$  value when the HERG K channels are blocked. The next parameter is QPPCaco, which is the Caco-2 cell permeability in the intestinal-blood barrier for inactive transport. Another parameter is QPlogBB, which is the brain-blood barrier coefficient of an orally administered drug. The next parameter is Human Oral Absorption, which predicts qualitative human oral absorption: 1, 2, or 3 for low, medium, or high.

It enables the examination of many properties of molecules, such as absorption by human metabolism, movements, and excretion by human metabolism. In ADME analysis, many biological and chemical properties of molecules are examined. At the beginning of these, many properties of molecules, such as molecular masses, dipole moments,



**Table 1.** The calculated quantum chemical parameters of molecules.

	$E_{\text{HOMO}}$	$E_{\text{LUMO}}$	$I$	$A$	$\Delta E$	$\eta$	$\mu$	$\chi$	$P\dot{I}$	$\omega$	$\varepsilon$	dipol	Energy
<b>B3LYP/6-31++g(d,p)LEVEL</b>													
Py <sub>1</sub> -NH <sub>2</sub>	-5.8091	-4.9650	5.8091	4.9650	0.8441	0.4221	2.3694	5.3871	-5.3871	34.3804	0.0291	4.0298	-29665.2437
Py <sub>1</sub> -Ts	-5.2654	-1.5663	5.2654	1.5663	3.6991	1.8496	0.5407	3.4159	-3.4159	3.1543	0.3170	4.4593	-51947.6386
Py <sub>1</sub> -CN	-3.7283	-2.3644	3.7283	2.3644	1.3638	0.6819	1.4664	3.0463	-3.0463	6.8044	0.1470	4.9789	-63236.1369
Py <sub>2</sub> -NH <sub>2</sub>	-3.8951	-1.2828	3.8951	1.2828	2.6123	1.3062	0.7656	2.5889	-2.5889	2.5657	0.3898	4.4165	-32764.1339
Py <sub>2</sub> -Ts	-3.9715	-1.5037	3.9715	1.5037	2.4678	1.2339	0.8104	2.7376	-2.7376	3.0369	0.3293	7.1815	-55046.4392
Py <sub>2</sub> -CN	-4.1481	-2.4436	4.1481	2.4436	1.7045	0.8523	1.1733	3.2959	-3.2959	6.3729	0.1569	4.7346	-66352.1260
<b>HF/6-31++g(d,p)LEVEL</b>													
Py <sub>1</sub> -NH <sub>2</sub>	-7.4274	0.9878	7.4274	-0.9878	8.4152	4.2076	0.2377	3.2198	-3.2198	1.2320	0.8117	2.5881	-29475.6565
Py <sub>1</sub> -Ts	-7.5888	0.8958	7.5888	-0.8958	8.4846	4.2423	0.2357	3.3465	-3.3465	1.3199	0.7576	4.2304	-51670.7547
Py <sub>1</sub> -CN	-7.7254	0.7908	7.7254	-0.7908	8.5161	4.2581	0.2348	3.4673	-3.4673	1.4117	0.7084	8.7016	-62907.1335
Py <sub>2</sub> -NH <sub>2</sub>	-6.8571	0.9521	6.8571	-0.9521	7.8092	3.9046	0.2561	2.9525	-2.9525	1.1163	0.8959	4.8993	-32557.4449
Py <sub>2</sub> -Ts	-6.9428	0.9236	6.9428	-0.9236	7.8663	3.9332	0.2542	3.0096	-3.0096	1.1515	0.8685	7.6145	-54752.4914
Py <sub>2</sub> -CN	-6.9373	0.6667	6.9373	-0.6667	7.6040	3.8020	0.2630	3.1353	-3.1353	1.2928	0.7735	5.3347	-65989.6125
<b>M062X/6-31++g(d,p)LEVEL</b>													
Py <sub>1</sub> -NH <sub>2</sub>	-6.2842	-0.2267	6.2842	0.2267	6.0576	3.0288	0.3302	3.2555	-3.2555	1.7495	0.5716	2.9974	-29652.5460
Py <sub>1</sub> -Ts	-6.5468	-0.6248	6.5468	0.6248	5.9221	2.9610	0.3377	3.5858	-3.5858	2.1712	0.4606	4.0107	-51929.3708
Py <sub>1</sub> -CN	-6.8426	-1.4836	6.8426	1.4836	5.3591	2.6795	0.3732	4.1631	-4.1631	3.2340	0.3092	8.3285	-63230.9218
Py <sub>2</sub> -NH <sub>2</sub>	-4.8107	-0.4150	4.8107	0.4150	4.3958	2.1979	0.4550	2.6129	-2.6129	1.5531	0.6439	2.5039	-32749.9429
Py <sub>2</sub> -Ts	-4.9604	-0.6280	4.9604	0.6280	4.3324	2.1662	0.4616	2.7942	-2.7942	1.8022	0.5549	7.0935	-55026.5510
Py <sub>2</sub> -CN	-6.8426	-1.4836	6.8426	1.4836	5.3591	2.6795	0.3732	4.1631	-4.1631	3.2340	0.3092	8.3285	-63230.9217

**Table 2.** The docking parameters of molecules against enzymes are expressed numerically

	Docking Score	Glide ligand efficiency	Glide hbond	Glide evdw	Glide ecoul	Glide emodel	Glide energy	Glide einternal	Glide posenum
<b>1JNX</b>									
<b>Py<sub>1</sub>-NH<sub>2</sub></b>	-4.29	-0.17	-0.40	-22.00	-12.02	-44.32	-34.02	3.03	45
<b>Py<sub>1</sub>-Ts</b>	-3.76	-0.10	-0.16	-26.68	-14.01	-50.70	-40.69	4.54	6
<b>Py<sub>1</sub>-CN</b>	-2.79	-0.06	0.00	-38.94	-1.57	-44.44	-40.51	1.03	216
<b>Py<sub>2</sub>-NH<sub>2</sub></b>	-3.54	-0.13	-0.55	-26.10	-4.58	-36.01	-30.68	3.89	44
<b>Py<sub>2</sub>-Ts</b>	-2.76	-0.07	-0.32	-32.78	-4.13	-43.74	-36.91	0.96	343
<b>Py<sub>2</sub>-CN</b>	-3.33	-0.07	-0.27	-32.77	-6.95	-47.39	-39.72	2.04	180
<b>6XXP</b>									
<b>Py<sub>1</sub>-NH<sub>2</sub></b>	-4.79	-0.18	0.00	-27.49	-8.00	-45.23	-35.49	2.79	67
<b>Py<sub>1</sub>-Ts</b>	-3.54	-0.10	0.00	-31.76	-7.42	-46.22	-39.18	3.97	337
<b>Py<sub>1</sub>-CN</b>	-1.39	-0.03	0.00	-28.20	-0.52	-27.26	-28.72	4.45	262
<b>Py<sub>2</sub>-NH<sub>2</sub></b>	-	-	-	-	-	-	-	-	-
<b>Py<sub>2</sub>-Ts</b>	-2.67	-0.07	-0.50	-25.17	-8.38	-37.48	-33.54	2.11	174
<b>Py<sub>2</sub>-CN</b>	-2.56	-0.05	0.00	-29.58	-6.42	-38.58	-36.00	2.53	366
<b>3WZE</b>									
<b>Py<sub>1</sub>-NH<sub>2</sub></b>	-6.08	-0.23	-0.01	-36.39	-5.32	-61.46	-41.71	0.76	234
<b>Py<sub>1</sub>-Ts</b>	-5.57	-0.15	-0.16	-33.54	-3.67	-45.73	-37.22	5.17	47
<b>Py<sub>1</sub>-CN</b>	-4.20	-0.09	0.00	-17.32	0.73	-31.08	-16.59	19.02	86
<b>Py<sub>2</sub>-NH<sub>2</sub></b>	-6.01	-0.21	-0.27	-41.31	-1.96	-56.10	-43.27	8.06	295
<b>Py<sub>2</sub>-Ts</b>	-4.15	-0.11	0.00	-51.45	0.76	-56.45	-50.69	8.25	49
<b>Py<sub>2</sub>-CN</b>	-	-	-	-	-	-	-	-	-
<b>4UYA</b>									
<b>Py<sub>1</sub>-NH<sub>2</sub></b>	-4.60	-0.18	0.00	-28.94	-0.60	-34.29	-29.54	1.35	393
<b>Py<sub>1</sub>-Ts</b>	-5.38	-0.15	0.00	-46.10	-1.61	-51.33	-47.71	11.66	89
<b>Py<sub>1</sub>-CN</b>	-5.97	-0.13	-0.32	-52.32	-3.70	-73.12	-56.01	9.78	124
<b>Py<sub>2</sub>-NH<sub>2</sub></b>	-5.63	-0.20	-0.32	-37.81	-4.28	-54.55	-42.09	4.66	359
<b>Py<sub>2</sub>-Ts</b>	-7.94	-0.21	-0.16	-44.83	-14.87	-112.10	-59.70	5.20	68
<b>Py<sub>2</sub>-CN</b>	-5.50	-0.11	-0.06	-47.84	-5.30	-68.06	-53.14	14.93	279

**Table 3.** ADME properties of molecule

	Py <sub>1</sub> -NH <sub>2</sub>	Py <sub>1</sub> -Ts	Py <sub>1</sub> -CN	Py <sub>2</sub> -NH <sub>2</sub>	Py <sub>2</sub> -Ts	Py <sub>2</sub> -CN	Reference Range
mol_MW	343	343	343	343	343	343	130-725
dipole (D)	3.0	7.4	10.6	5.3	8.0	4.7	1.0-12.5
SASA	632	759	871	671	883	1051	300-1000
FOSA	100	198	135	211	298	332	0-750
FISA	44	74	170	68	80	196	7-330
PISA	487	486	567	392	505	522	0-450
WPSA	0.0	0.0	0.5	0.0	0.4	0.6	0-175
volume (A <sup>3</sup> )	1129	1468	1776	1215	1621	1970	500-2000
donorHB	1.5	1	0	1.5	1	0	0-6
acptHB	2.75	6.25	9.25	3.5	7	10	2.0-20.0
glob (Sphere =1)	0.8	0.8	0.8	0.8	0.8	0.7	0.75-0.95
QPpolrz (A <sup>3</sup> )	42.4	54.7	65.8	44.3	60.3	72.5	13.0-70.0
QPlogPC16	12.8	16.0	19.7	13.1	17.9	22.3	4.0-18.0
QPlogPoct	17.8	23.9	28.9	19.0	26.0	30.5	8.0-35.0
QPlogPw	9.3	12.1	14.4	9.4	13.1	15.2	4.0-45.0
QPlogPo/w	5.4	5.9	5.9	5.3	6.6	6.5	-2.0-6.5
QPlogS	-6.4	-7.1	-7.7	-6.6	-8.9	-10.6	-6.5-0.5
CIQPlogS	-6.3	-8.5	-11.0	-6.6	-8.8	-11.3	-6.5-0.5
QPlogHERG	-6.6	-6.7	-7.2	-6.3	-7.9	-8.5	*
QPPCaco (nm/sec)	3757	1966	245	2256	1744	137	**
QPlogBB	0.0	-0.4	-1.6	-0.3	-0.7	-2.4	-3.0-1.2
QPPMDCK (nm/sec)	2068	1028	109	1192	907	58	**
QPlogKp	-0.4	-0.8	-2.0	-1.1	-0.7	-2.5	Kp in cm/hr
IP (ev)	8.5	8.9	8.5	8.1	8.1	7.1	7.9-10.5
EA (eV)	-0.2	0.6	1.0	0.1	0.6	1.3	-0.9-1.7
#metab	6	6	6	7	7	7	1-8
QPlogKhsa	1.0	1.2	1.0	1.1	1.4	1.3	-1.5-1.5
Human Oral Absorption	1	1	1	1	1	1	-
Percent Human Oral Absorption.	100	100	78.133	100	100	78	***
PSA	45	74	99	54	76	112	7-200
RuleOfFive	1	1	2	1	2	2	Maximum is 4
RuleOfThree	1	1	1	2	2	2	Maximum is 3
Jm	0.1	0.0	0.0	0.0	0.0	0.0	-

\*concern below -5, \*\*<25 is poor and >500 is great, \*\*\* <25% is poor and >80% is high.

volume, and the number of hydrogen bonds occurring between a molecule and a protein, are considered chemical properties (Tüzün et. al. 2022). In addition, many biological properties of molecules, such as blood-intestinal barrier and blood-brain barrier transitions in human metabolism, absorption by the skin, and orally usable properties, were investigated. In addition to these properties, the numerical values of the molecules RuleOfFive (Lipinski 2004), (Lipinski et. al. 1997), violations of Lipinski's rule of five, and RuleOfThree (Jorgensen and Duffy 2002), violations of Jorgensen's rule of three, are checked. The numerical value of these two parameters is expected to be zero, but within the desired confidence interval. On the other hand, the numerical values of the QPPCaco (nm/sec) and QPPMDCK (nm/sec) parameters were found to be quite high for some molecules. For this reason, it is thought that it may be a drug for different regions of human metabolism.

## 5. Conclusion

In the present study, in silico studies of synthesized methoxylated pyrazoline derivatives bearing amine (**Py<sub>1</sub>-NH<sub>2</sub>** and **Py<sub>2</sub>-NH<sub>2</sub>**), tosyl (**Py<sub>1</sub>-Ts** and **Py<sub>2</sub>-Ts**), and nitrile (**Py<sub>1</sub>-CN** and **Py<sub>2</sub>-CN**) groups were researched. The activities of the molecules were compared as a result of the theoretical calculations. The **Py<sub>1</sub>-NH<sub>2</sub>** molecule was shown to be usually more active than other compounds in the Gaussian calculations. But when the compounds' actions against cancer proteins were investigated following the molecular docking computations, it was found that, overall, the **Py<sub>1</sub>-NH<sub>2</sub>** molecule had more activity than the others. As a result of the calculations, the activities of the molecules were compared with the docking calculations. As a result of the calculations, the activities of the molecules were compared with the docking calculations. The **Py<sub>1</sub>-NH<sub>2</sub>** molecule was generally the most active molecule. It was observed that the **Py<sub>1</sub>-NH<sub>2</sub>** molecule had the highest activity against the 1JNX protein with a docking score value of -4.29, the **Py<sub>1</sub>-NH<sub>2</sub>** molecule had the highest activity against the 6XXP protein with a docking score value of -4.79, and the **Py<sub>1</sub>-NH<sub>2</sub>** molecule had the highest activity against the 3WZE protein with a docking score value of -6.08. In addition, the **Py<sub>2</sub>-Ts** molecule had the highest activity against the 4UYA protein with a docking score value of -7.94. After a thorough analysis of the compounds' interactions with cancer proteins, the molecules' ADME characteristics were investigated. This investigation revealed that employing the compounds as medications for human metabolism would not be harmful.

## Acknowledgements

The numerical calculations reported in this paper were fully/partially performed at TUBITAK ULAKBIM, High Performance and Grid Computing Center (TRUBA resources). This work was supported by the Scientific Research Project Fund of Sivas Cumhuriyet University (CUBAP) under the project number RGD-020.

## Authors' contributions:

HY: Conceptualization, Validation, Methodology, Investigation, Writing-Original Draft, Writing-Review&Editing, Visualization.

DK: Conceptualization, Validation, Methodology, Investigation.

SF: Conceptualization, Validation, Methodology, Investigation.

BT: Funding acquisition, Methodology, Resources, Validation, Visualization, Writing-Original Draft, Writing-Review&Editing.

HK: Funding acquisition, Methodology, Resources, Validation, Visualization, Writing-Review&Editing.

## Conflict of interest disclosure:

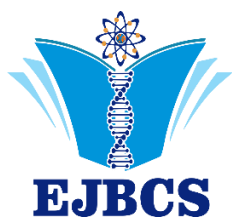
The authors declare no conflict of interest.

## References

- Ahmed NM, Youns M, Soltan MK, Said AM. 2019. Design, synthesis, molecular modelling, and biological evaluation of novel substituted pyrimidine derivatives as potential anticancer agents for hepatocellular carcinoma. *J Enzym Inhib Med Chem.* 34:1110–1120.
- Altintop MD, Özdemir A, Kaplancikli ZA, Turan-Zitouni G, Temel HE, Çiftçi GA. 2013. Synthesis and biological evaluation of some pyrazoline derivatives bearing a dithiocarbamate moiety as new cholinesterase inhibitors. *Arch Pharmazie.* 346: 189–199.
- Amr AEGE, El-Naggar M, Al-Omar MA, Elsayed EA, Abdalla MM. 2018. In vitro and in vivo anti-breast cancer activities of some synthesized pyrazolinylestran-17-one candidates. *Molecules.* 23:1572.
- Becke AD. 1992. Density-functional thermochemistry. I. The effect of the exchange-only gradient correction. *J Chem Phys.* 96(3):2155–2160.
- Bhutani R, Pathak DP, Husain A, Kapoor G, Kant R. 2015. A review on recent development of pyrazoline as a pharmacologically active molecule, *Int J Pharma Sci Res.* 6: 4113–4128.
- Chalkha M, el Hassani AA, Nakkabi A, Tüzün B, Bakhouch M, Benjelloun AT, Sfaira M, Saadi M, El Ammari L, El Yazidi M. 2023. Crystal structure, Hirshfeld surface and DFT computations, along with molecular docking investigations of a new pyrazole as a tyrosine kinase inhibitor. *J Mol Struct.* 1273:134255.
- Chen V, Zhang YL, Fan J, Ma X, Qin YJ, Zhu HL. 2018. Novel nicotinoyl pyrazoline derivatives bearing N-methyl indole moiety as antitumor agents: design, synthesis and evaluation, *Eur J Med Chem.* 156:722–737.
- Çelik G, Arslan T, Şentürk M, Ekinçi D. 2020. Synthesis and characterization of some new pyrazolines and their inhibitory potencies against carbonic anhydrases. *Arch Pharmazie.* 353:1900292.
- Çelik MS, Çetinus ŞA, Yenidünya AF, Çetinkaya S, Tüzün B. 2023. Biosorption of Rhodamine B dye from aqueous solution by *Rhus coriaria* L. plant: Equilibrium, kinetic, thermodynamic and DFT calculations. *J Mol Struct.* 1272:134158.

- Dennington R, Keith TA, Millam JM. 2016. GaussView 6.0. 16. Semichem Inc.: Shawnee Mission, KS, USA.
- Dipankar B, Hirakmoy C, Asish B, Abhijit C. 2011. 2-pyrazoline: a pharmacologically active moiety. *Int Res J Pharmaceut Appl Sci.* 1:68–80.
- Frisch MJ, Trucks GW, Schlegel HB, Scuseria GE, Robb MA, Cheeseman JR, Scalmani G, Barone V, Mennucci B, Petersson GA, Nakatsuji H, Caricato M, Li X, Hratchian HP, Izmaylov AF, Bloino J, Zheng G, Sonnenberg JL, Hada M, Ehara M, Toyota K, Fukuda R, Hasegawa J, Ishida M, Nakajima T, Honda Y, Kitao O, Nakai H, Vreven T, Montgomery JA, Peralta JE, Ogliaro F, Bearpark M, Heyd JJ, Brothers E, Kudin KN, Staroverov VN, Kobayashi R, Normand J, Raghavachari K, Raghavachari AR, Burant JC, Iyengar SS, Tomasi J, Cossi M, Rega N, Millam JM, Klene M, Knox JE, Cross JB, Bakken V, Adamo C, Jaramillo J, Gomperts R, Stratmann RE, Yazyev O, Austin AJ, Cammi R, Pomelli C, Ochterski JW, Martin RL, Morokuma K, Zakrzewski VG, Voth GA, Salvador P, Dannenberg JJ, Dapprich S, Daniels AD, Farkas O, Foresman JB, Ortiz JV, Cioslowski J, Fox DJ. 2009. Gaussian 09, revision D.01. Gaussian Inc, Wallingford CT.
- Hohenstein EG, Chill ST, Sherrill CD. 2008. Assessment of the performance of the M05–2X and M06–2X exchange-correlation functionals for noncovalent interactions in biomolecules. *J Chem Theory Comput.* 4(12):1996–2000.
- Wang HH, Qiu KM, Cui HE, Yang YS, Luo Y, Xing M, Qiu XY, Bai L.F., Zhu H.L. 2013. Synthesis, molecular docking and evaluation of thiazolyl-pyrazoline derivatives containing benzodioxole as potential anticancer agents. *Bioorg Med Chem.* 21:448–455.
- Kharbada C, Alam MS, Hamid H, Javed K, Bano S, Dhulap A, Ali Y, Nazreen S., Haider S. 2014. Synthesis and evaluation of pyrazolines bearing benzothiazole as anti-inflammatory agents. *Bioorg Med Chem.* 22: 5804–5812.
- Jorgensen WJ, Duffy EM. 2002. Prediction of drug solubility from structure. *Adv Drug Deliv Rev.* 54(3):355–366.
- Joshi SD, Dixit SR, Kirankumar MN, Aminabhavi TM, Raju KVS, Narayan R, Lherbet C, Yang KS. 2016. Synthesis, antimycobacterial screening and ligand-based molecular docking studies on novel pyrrole derivatives bearing pyrazoline, isoxazole and phenyl thiourea moieties. *Eur J Med Chem.* 107:133–152.
- Kaplancıklı ZA, Özdemir A, Turan-Zitouni G, Altıntop MD, Can DÖ. 2010. New pyrazoline derivatives and their antidepressant activity. *Eur J Med Chem.* 45: 4383–4387.
- Kim BS, Shin SY, Ahn S, Koh D, Lee YH, Lim Y. 2017. Biological evaluation of 2-pyrazolyl-1-carbothioamide derivatives against HCT116 human colorectal cancer cell lines and elucidation on QSAR and molecular binding modes. *Bioorg Med Chem.* 25: 5423–5432.
- Kumar S, Bawa S, Drabu S, Kumar R, Gupta H. 2009. Biological activities of pyrazoline derivatives -A recent development. *Recent Pat Anti-Infect Drug Discov.* 4:154–163.
- Lakhrissi Y, Rbaa M, Tuzun B, Hichar A, Ounine K, Almalki F, Hadda TB, Zarrouk A, Lakhrissi B. 2022. Synthesis, structural confirmation, antibacterial properties and bio-informatics computational analyses of new pyrrole based on 8-hydroxyquinoline. *J Mol Struct.* 1259:132683.
- Li HL, Su MM, Xu YJ, Xu C, Yang YS, Zhu HL. 2018. Design and biological evaluation of novel triaryl pyrazoline derivatives with dioxane moiety for selective BRAFV600E inhibition. *Eur J Med Chem.* 155: 725–735.
- Lipinski CA. 2004. Lead-and drug-like compounds: the rule-of-five revolution *Drug Discovery Today: Technologies,* 1(4): 337–341.
- Lipinski CA, Lombardo F, Dominy BW, Feeney PJ. 1997. Experimental and computational approaches to estimate solubility and permeability in drug discovery and development settings. *Adv Drug Deliv. Rev.* 23:3–25.
- Majumdar D, Philip JE, Tüzün B, Frontera A, Gomila RM, Roy S, Bankura K. 2022. Unravelling the Synthetic Mimic, Spectroscopic Insights, and Supramolecular Crystal Engineering of an Innovative Heteronuclear Pb (II)-Salen Cocrystal: An Integrated DFT, QTAIM/NCI Plot, NLO, Molecular Docking/PLIP, and Antibacterial Appraisal. *J Inorg Organomet Polym Mater.* 1–20.
- Majumdar D, Philip JE, Roy S, Tüzün B. 2022. Reinvigorate the synthesis, spectroscopic findings, SEM morphology investigation, and antimicrobial silhouette of contemporary Salen ligands: A comprehensive DFT landscape. *Results Chem.* 4:100574.
- Mathur G, Nain S, Sharma PK. 2015. Cancer: An Overview. *Academic Journal of Cancer Research.* 8 (1): 01-09.
- Marusiak AA, Stephenson NL, Baik H, Trotter EW, Li Y, Blyth K., Mason S, Chapman P, Puto LA, Read JA, Brassington C, Pollard HK, Philips C, Green I, Overman R, Collier M, Testoni E, Miller CJ, Hunter T, Sansom OJ, Brognard J. 2016. Recurrent MLK4 Loss-of-Function Mutations Suppress JNK Signaling to Promote Colon Tumorigenesis. *Cancer Res.* 76(3):724–735.
- Monga V, Goyal K, Steindel M, Rajani DP, Rajani S. 2014. Synthesis, and evaluation of new chalcones, derived pyrazolines and cyclohexenone derivatives as potent antimicrobial, antitubercular and antileishmanial agents. *Med Chem Res.* 23: 2019–2032.
- Moreno LM, Quiroga J, Abonia R, Ramírez-Prada J, Insuasty B. 2018. Synthesis of new 1,3,5-triazine-based 2-pyrazolines as potential anticancer agents. *Molecules.* 23:1956.
- Nehra B, Rulhania S, Jaswal S, Kumar B, Singh G, Monga V. 2020. Recent advancements in the development of bioactive pyrazoline derivatives. *Eur J Med Chem.* 205: 112666.
- Nepali K, Sharma S, Sharma M, Bedi PMS, Dhar KL. 2014. Rational approaches, design strategies, structure activity relationship and mechanistic insights for anticancer hybrids. *Eur J Med Chem.* 77:422–487.
- Nussbaumer S, Bonnabry P, Veuthey J-L, Fleury-Souverain S. 2011. Analysis of anticancer drugs: A review. *Talanta.* 85:2265–2289.
- Özdemir A, Turan-Zitouni G, Kaplancıklı ZA, Revial G, Demirci F, Işcan G. 2010. Preparation of some pyrazoline derivatives and evaluation of their antifungal activities. *J Enzym Inhib Med Chem.* 25:565–571.
- Okamoto K, Ikemori-Kawada M, Jestel A, von König K, Funahashi Y, Matsushima T, Tsuruoka A, Inoue A, Matsui J. 2015. Distinct binding mode of multikinase inhibitor lenvatinib revealed by biochemical characterization. *ACS Med Chem Lett.* 6(1):89–94.
- Rebucci M, Michiels C. 2013. Molecular aspects of cancer cell resistance to chemotherapy. *Biochem Pharmacol* 85:1219–1226.
- Rosenfeld L, Sananes A, Zur Y, Cohen S, Dhara K, Gelkop S, Zeev EB, Shahar A, Lobel L, Akabayov B, Arbely E, Papo N. 2020. Nanobodies targeting prostate-specific membrane antigen for the imaging and therapy of prostate cancer. *J Med Chem.* 63(14):7601–7615.
- Schrödinger Release 2021-3: Maestro, Schrödinger, LLC, New York, NY, 2021.
- Schrödinger Release 2019-4: Protein Preparation Wizard; Epik, Schrödinger, LLC, New York, NY, 2016; Impact, Schrödinger, LLC, New York, NY, 2016; Prime, Schrödinger, LLC, New York, NY, 2019.
- Schrödinger Release 2021-3: LigPrep, Schrödinger, LLC, New York, NY, 2021.

- Schrödinger Release 2021-3: QikProp, Schrödinger, LLC, New York, NY, 2021.
- Stefanes NM, Toigo J, Maioral MF, Jacques AV, Chiaradia-Delatorre LD, Perondi DM, Ribeiro AAB, Bigolin A, Pirath IMS, Duarte BF, Nunes RJ, Santos Silva MC. 2019. Synthesis of novel pyrazoline derivatives and the evaluation of death mechanisms involved in their antileukemic activity. *Bioorg Med Chem.* 27:375–382.
- Tas A, Tüzün B, Khalilov AN, Taslim P, Ağbektas T, Cakmak NK. 2022. In Vitro Cytotoxic Effects, In Silico Studies, Some Metabolic Enzymes Inhibition, and Vibrational Spectral Analysis of Novel  $\beta$ -Amino Alcohol Compounds. *J Mol Struct.* 1273:34282.
- Tapera M, Kekeçmuhammed H, Tüzün B, Sarıpınar E, Koçyiğit ÜM, Yıldırım E, Doğan M, Zorlu Y. 2022. Synthesis, carbonic anhydrase inhibitory activity, anticancer activity and molecular docking studies of new imidazolyl hydrazone derivatives. *J Mol Struct.* 1269 (2022): 133816.
- Tüzün B, Sayin K., Ataseven H. 2022. Could Momordica Charantia Be Effective In The Treatment of COVID19? *Cumhuriyet Science Journal.* 43(2):211–220.
- Vautherin D, Brink DM. 1972. Hartree-Fock calculations with Skyrme's interaction. I. Spherical nuclei. *Phys Rev C.* 5(3):626.
- Williams RS, Green R, Glover JN. 2001. Crystal structure of the BRCT repeat region from the breast cancer-associated protein BRCA1. *Nat Struct Mol Biol.* 8(10):838–842.
- Xu W, Pan Y, Wang H, Li H, Peng Q, Wei D, Chen C, Zheng J. 2017. Synthesis and evaluation of new pyrazoline derivatives as potential anticancer agents in HepG-2 cell line. *Molecules.* 22:467.



## Evaluation of genetic diversity of tomato spotted wilt virus (TSWV) NSs gene region isolates at geographical level

Filiz Randa-Zelyüt<sup>1,2\*</sup>, Ali Karanfil<sup>2</sup>

<sup>1</sup>Bilecik Şeyh Edebalı University, Faculty of Agriculture and Natural Sciences, Department of Plant Protection, Bilecik, Türkiye

<sup>2</sup>Bilecik Şeyh Edebalı University, Biotechnology Application and Research Centre, 11230 Gulumbe Campus, Bilecik, Türkiye

<sup>2</sup>Çanakkale Onsekiz Mart University, Faculty of Agriculture, Department of Plant Protection, Çanakkale, Türkiye

\*Corresponding author : [filizrandazelyut@yahoo.com](mailto:filizrandazelyut@yahoo.com)

Orcid No: <https://orcid.org/0000-0002-1366-4389>

Received : 27/09/2024

Accepted : 30/10/2024

**To Cite / Atf için:** Randa-Zelyüt F, Karanfil A. 2024. Evaluation of genetic diversity of tomato spotted wilt virus (TSWV) NSs gene region isolates at geographical level. Eurasian J Bio Chem Sci, 7(2):125-131. <https://doi.org/10.46239/ejbc.1557069>

**Abstract:** One of the most significant plant protection problems that adversely affect agricultural production is diseases caused by viruses, as there are no direct and rapid control methods. Tomato spotted wilt virus (TSWV), which is known to cause major losses in vegetable production and is quite common in the Mediterranean basin, is one of these viruses. In reducing the prevalence of the agent, control of vector insects and use of resistant varieties are the primary parameters. In this study, the genetic diversity of the partial Non-Structural NSs gene, which produces a putative silencing suppressor protein of TSWV, was investigated at the level of geographical populations. A total of 325 isolates were clustered from Eastern European, European Mediterranean, Asian, African, and American populations and geographic genetic diversity analyses were performed. Phylogenetic analyses revealed 2 major phylogroups (Clade I and II). Isolates reported from Asia and Africa were clustered only in Clade II, while other isolates were distributed in both groups. Haplotype network analyses revealed that the isolates had genotypes partially related to their geography. In support of these results, molecular variance analyses (AMOVA) showed that there were significant results for both proposals when applied between and within geographic groups. The findings highlight that TSWV has experienced different evolutionary processes in geographical regions, that the virus spreads along different genetic lines in regions, that local genotypes may dominate in regions and potentially adapt more quickly, and that local plant health institutions should increase regional quarantine measures and isolation strategies, and that it is important to take these genetic differences into account in order for the control to be more effective and targeted.

**Keywords:** TSWV, NSs gene, haplotype network, AMOVA

© EJBCS. All rights reserved.

### 1. Introduction

Tospoviruses (Order Bunyavirales, family Tospoviridae) are a serious threat to crop yield, costing more than \$1 billion globally (Prins and Goldbach 1998). Among these viruses, tomato spotted wilt virus (TSWV) is a significant pathogen that infects over 1000 plant species across more than 85 families, including important crops such as tomato, lettuce, and pepper (Gupta et al. 2018). However, the emergence of TSWV resistance-breaking strains that overcome the resistance genes in vegetables such as tomatoes and peppers, which are among the most produced and consumed vegetables globally, has become one of the production-limiting factors in the Mediterranean basin (Turina et al. 2012).

The TSWV viral particle, like other members of the Bunyaviridae family, is spherical and membrane-

enveloped. Genome is consists of three single-stranded RNAs (ssRNAs) named L (Large ~8.9 kb), M (Medium ~4.8 kb), and S (Small ~2.9 kb) (Turina et al. 2016). Large RNA that encodes RNA-dependent RNA polymerase (RdRp) needs to be copied onto a complementary strand before it can be read because its polarity is negative (De Haan et al. 1991). The M RNA is a double-stranded, antisense RNA that encodes proteins in the amino and carboxy-terminal regions of glycoprotein precursors (GN and GC proteins, 58 kDa and 95 kDa, respectively). These proteins are crucial for virion assembly, development, and release in the host plant (Nagata et al. 2000; Whitfield et al. 2008). The small S RNA genome is a double-sense and antisense RNA that encodes nucleoprotein (NSM 33.6 kDa) and nonstructural protein (NSs 30 kDa) from complementary RNA, which functions as a viral suppressor of RNA silencing, and both proteins play an important role



in the infection cycle (Snippe et al. 2007; Ocampo et al. 2016; Guo et al. 2017).

The global dissemination of TSWV is primarily driven by its efficient insect vector, the western flower thrips (*Frankliniella occidentalis*). This vector exhibits several traits that facilitate the virus's spread, including high fecundity, a short generation time, significant mobility, a preference for concealed environments, and a polyphagous feeding habit (Kamran et al. 2024). Furthermore, the development of resistance to multiple insecticides in *F. occidentalis* has exacerbated the spread of vectored plant viruses such as TSWV (Reitz et al. 2020). Moreover, TSWV has been reported to be present in the seeds of plants such as peppers and tomatoes with different rates of transmission (Jones 1944; Wang et al. 2022). Since TSWV infects a wide range of hosts, the symptoms it induces are quite diverse and generally cause brownish ring spots, yellowing, necrosis of several plant organs, leaf purple and curling, stunting or growth retardation, fruit deformities, necrotic spots, local lesions, and even plant death (Francki and Hatta 1981; Oetting 1991).

Plants typically employ RNA silencing as a defense mechanism against viral infections. However, plant viruses have evolved countermeasures, including the production of RNA silencing suppressors. The NSs protein of TSWV acts as an RNA silencing suppressor, playing a crucial role in facilitating the virus's infection, replication, and transmission. In this study, geographic populations were established using partial NSs gene sequences of TSWV reported from various regions of the world, including Turkey. The aim was to elucidate the genetic diversity and dispersal dynamics of this gene region within the framework of population genetics.

## 2. Materials and Method

### 2.1. Isolates and phylogenetic analyses

In this study, the nucleotide sequences of the NSs gene of TSWV, comprising 318 global isolates from various hosts and geographical regions available in GenBank (accessed on July 21, 2024), along with 7 tomato isolates obtained as part of project no. 2022-01.BŞEÜ.06-02, were analyzed. The partial nucleotide sequence of the NSs gene covers the nt sequence at position 128-851 in the small S genome (reference isolate: accession no MN854653, South Korea).

Phylogenetic relationships among 325 TSWV isolates were inferred based on partial NSs gene sequences. Nucleotide sequences of the NSs gene were aligned using ClustalW in MEGA 11 software (Tamura et al. 2021). An unrooted

phylogenetic tree was constructed using the Neighbour-Joining (NJ) method, with the Tamura-Nei model (Tamura and Nei 1993) applied as the substitution parameter and uniform rates of complete deletion for gaps in the partial NSs gene region. Phylogenetic data obtained using the algorithms and methods of Mega 11 software (Tamura et al. 2021) were transferred to the iTOL (Interactive Tree Of Life) V.6 online software (Letunic and Bork 2024) for re-evaluation and visualization. In addition, 1000 bootstrap was applied to increase the reliability values of the branches of the obtained clusters.

### 2.2. Haplotype network analyses

Haplotype networks were constructed at the geographic level to illustrate the genetic variation in the aligned NSs gene sequences of TSWV. The isolates were classified based on their geographic origins: the Asian population (n=22) (South Korea and China), the American population (n=15) (U.S.A. and Mexico), the Eastern European population (n=41) (Serbia, Croatia, Slovenia, Bulgaria, and Hungary), the Euro-Mediterranean population (n=243) (Türkiye, France, Spain, Italy, U.K., Germany, Netherlands, and Algeria), and the African population (n=3) (South Africa). Haplotype data for the partial NSs gene of TSWV were generated and analyzed using DnaSP v6.12.03 (Rozas et al. 2017). The haplotype networks were constructed using the Median Joining (MJ) algorithm (Bandelt et al. 1999) and visualized using PopART software (<http://popart.otago.ac.nz>) (Leigh and Bryant 2015).

### 2.3. Analyses of molecular variance (AMOVA)

Molecular variance analysis (AMOVA) (Excoffier et al. 1992) was performed to estimate the effects of genotype distributions on the total variation of TSWV isolates based on the partial NSs gene. Nucleotide sequence data for the NSs gene region from a total of 325 TSWV isolates were compiled to form the dataset. The analyses were conducted using Arlequin version 3.5.2.2 software (Excoffier and Lischer 2010).

## 3. Results

### 3.1. Phylogenetic inferences

Phylogenetic analyses examining the molecular evolutionary relationships among geographic populations revealed that the 325 TSWV isolates were grouped into two major clades. In our study, these clades were designated as Clade I and Clade II (Figure 1).

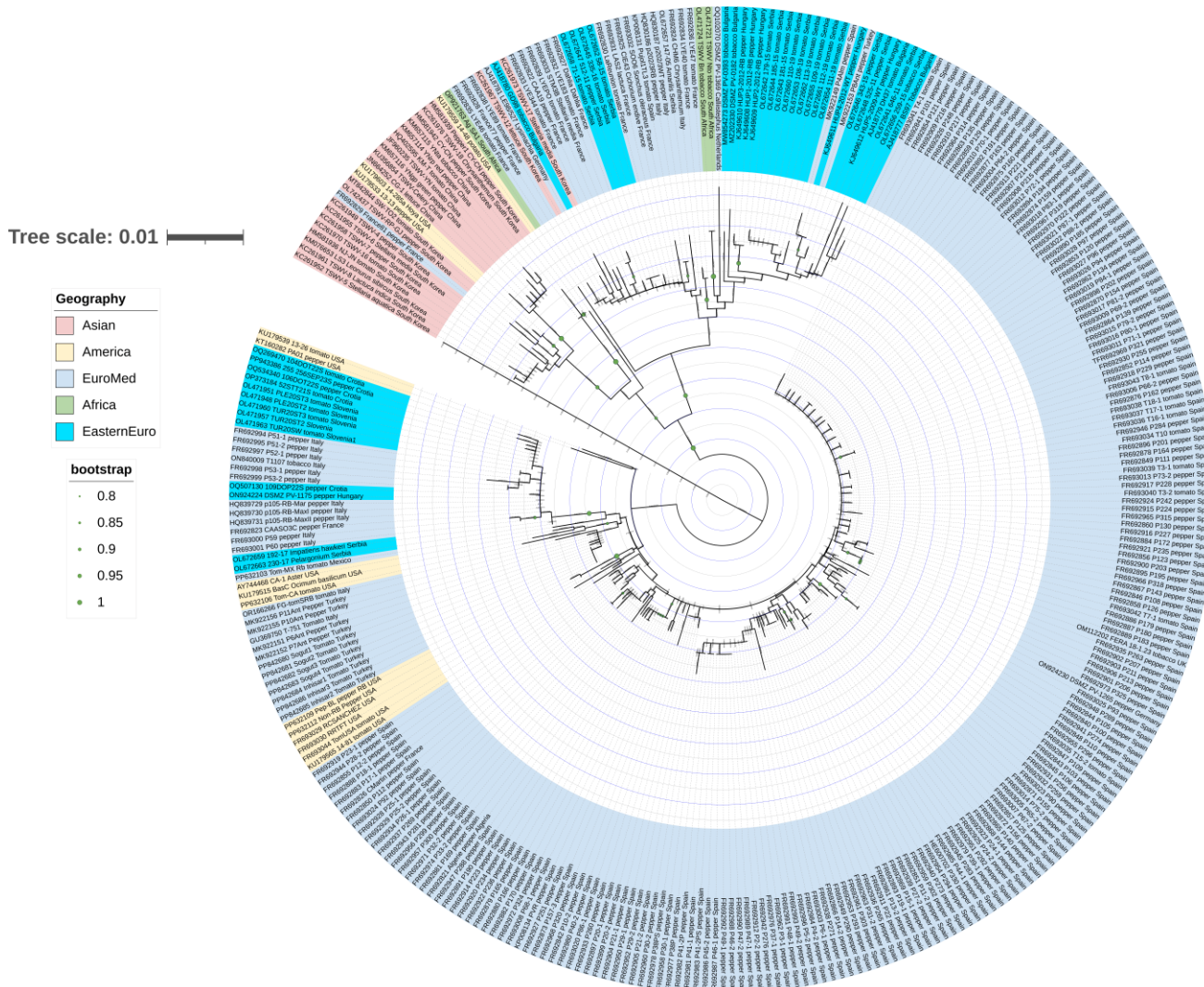


**Fig. 1** Phylogenetic tree based on partial NSs gene of the TSWV (n=325 isolates)

Clade I comprised a total of 255 isolates, including 11 from the America, 13 from Eastern Europe, and 221 from the Europe-Mediterranean region. Notably, no isolates from Asia or Africa were present in Clade I. In contrast, Clade II consisted of 80 TSWV NSs gene isolates, including 22 from Asia, 3 from Africa, 3 from the Americas, 28 from Eastern Europe, and 24 from the Europe-Mediterranean region. Additionally, while the Türkiye isolate P8Ant (GenBank accession number MK922153) clustered within Clade I, the other Türkiye isolates were also found in Clade I. Specifically, the seven TSWV isolates obtained from project no. 2022-01.BŞEÜ.06-02, along with four TSWV isolates from Antalya recorded in GenBank, clustered within the same subclade, showing a close relationship with each other and one isolate from Italy. The phylogenetic tree showed that in general, isolates obtained locally clustered more closely with each other.

**3.2. Haplotype Network Results**

The haplotype network analysis of the partial NSs gene region from 325 TSWV isolates illustrated distinct clustering patterns based on geographic origins (Figure 2). The 22 Asian isolates had 17 haplotypes, while the 243 Europe-Mediterranean isolates had 123 haplotypes.

Additionally, the 15 American isolates corresponded to 15 distinct haplotypes, the 3 African isolates formed 2 haplotypes, and the 41 Eastern European isolates were had 27 haplotypes. However, the most distinct and common haplotypes originated from isolates obtained from Spain. The Europe-Mediterranean isolates (in pink) form the largest and most diverse group, indicating a higher level of genetic diversity within this region. Conversely, isolates from Asia (green) and Africa (light blue) show more distinct and isolated clusters, reflecting limited gene flow between these regions and others. The isolates from the Americas (yellow) and Eastern Europe (blue) are distributed across smaller clusters, suggesting a moderate degree of genetic differentiation.

**3.3. Results of molecular variance analysis (AMOVA) among geographical populations**

The AMOVA results for the partial NSs gene region of TSWV revealed that 36.49% of the total genetic variation is attributed to differences among populations ( $\Phi_{ST} = 0.36491$ ,  $p < 0.001$ ), indicating significant genetic differentiation between the defined geographic populations (Asian, Euro-Med, America, Africa, and Eastern Europe) (Table 1).

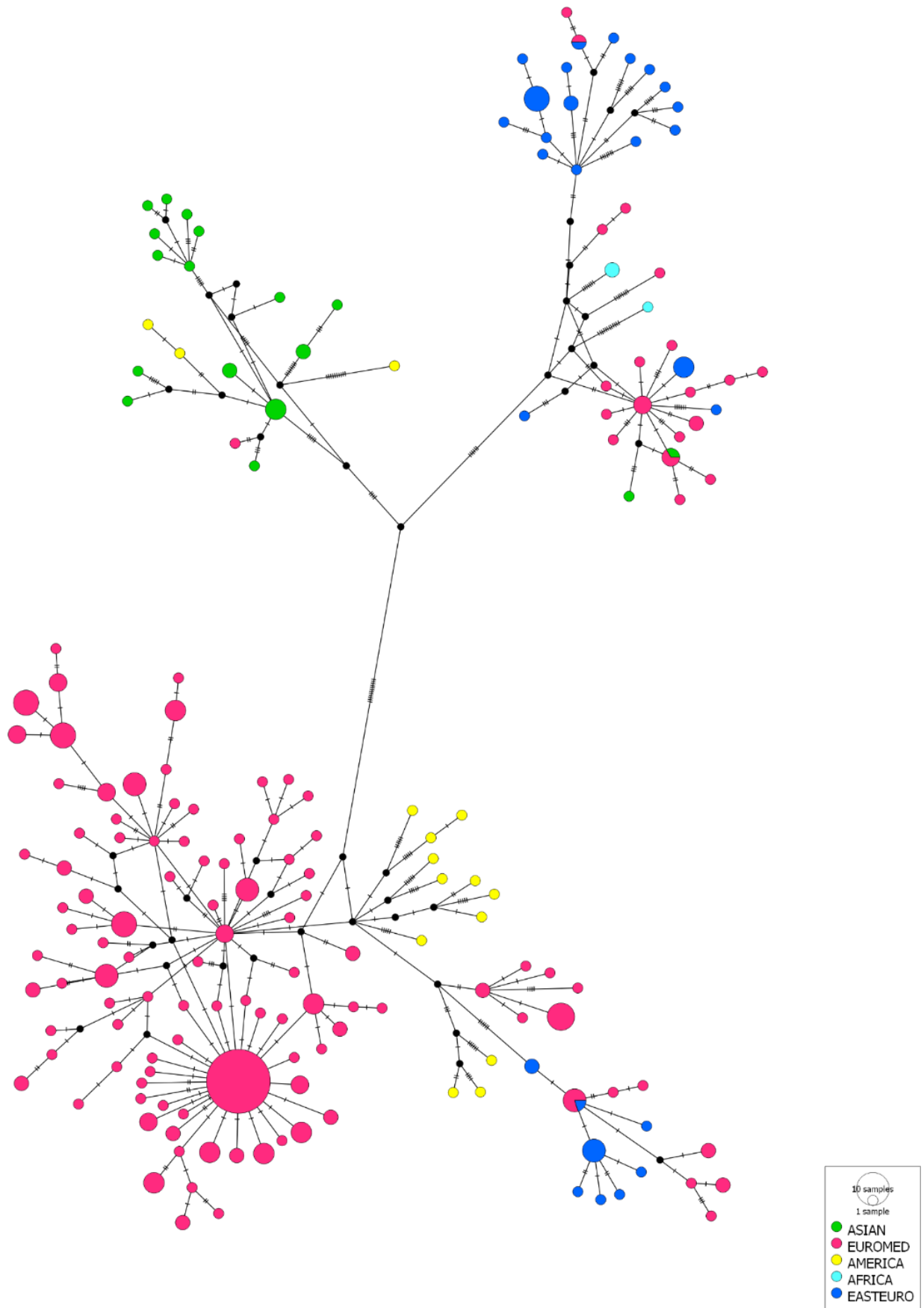


**Fig. 1** Network analysis of TSWV partial NSs haplotypes. The colour of each node represents different geographical populations and allele types. Green: Asian, Pink: Euro-Med, Yellow: American, Light blue: Africa, and Blue: Eastern Europe populations

**Table 1** Molecular variance results obtained among and within five different geographical populations consisting of NSs isolates of TSWV

Population definition	Source of variation	Sum of squares	Variance components	Percentage variation	$\Phi_{ST}$ and p-value
Partial NSs gene region	Among populations	421165.597	63.952	36.49098	$\Phi_{ST}=0.36491$ P< 0.001
	Within populations	31935505.329	111.302	63.50902	
Pop1: Asian					
Pop2: Euro-Med					
Pop3: America					
Pop4: Africa					
Pop5: Eastern-Euro					
Total		32356670.926	175.254		

Significance (1000 permutations):  $\Phi_{ST}$ : Pr(random value > observed  $\Phi_{ST}$ ) < 0.001

The remaining 63.51% of the variation was found within populations, highlighting the substantial genetic diversity present within each region. These results demonstrate that both inter-population and intra-population genetic variations contribute to the overall genetic structure of the TSWV NSs gene.

#### 4. Discussion

TSWV is one of the most economically destructive plant pathogens globally, with its rapid evolution and adaptation to various hosts and environments presenting major challenges for agriculture and disease management worldwide. Given the virus's extensive genetic diversity and adaptability, the development of resistant cultivars through genetic breeding has become crucial in mitigating crop losses. Breeding efforts that focus on enhancing resistance to TSWV in economically important crops, such as tomatoes, are essential for reducing the virus's spread and ensuring sustainable agricultural production in affected regions. Therefore, in this study, phylogenetic, haplotype network and molecular variance analyses were performed to understand the genetic diversity of the NSs gene of TSWV, which is responsible for breaking plant resistance genes, at the geographical level and to contribute to future studies. Population genetic studies are being conducted to understand the epidemiological cycle, evolutionary processes, host-vector interactions, genetic diversity and many factors related to evolutionary dynamics of plant viruses (Zelyüt and Ertunç 2021; Karanfil et al. 2023; Santosa et al. 2023; Güller et al. 2023). In addition, population dynamics have been reported from some studies for different gene regions of TSWV (Abadkhah et al. 2018; Morca et al. 2022; Usta et al. 2023). Here, NSs gene region isolates of TSWV were clustered in a geographical hierarchy and examined comprehensively.

NSs, identified as the suppressor protein of the host plant's gene silencing mechanism, plays a pivotal role in overcoming plant resistance as an avirulence (avr) factor

(De Ronde et al. 2013). Recent studies have provided detailed insights into how various domains of the NSs protein contribute to its gene silencing suppression function and its role as an avr factor (Du et al. 2020). Margaria et al. (2014) reported that while the NSs protein is not required for TSWV acquisition by thrip larvae, it is essential for its abundant accumulation in adults, which is necessary for successful virus transmission. TSWV resistance isolates are further categorized into resistance-inducing (RI) isolates, which trigger a hypersensitive response in resistant cultivars, and resistance-breaking (RB) isolates, which can overcome host resistance (Peiró et al. 2014; Turina et al. 2016). Thus, analyses conducted in other studies to determine isolates capable of breaking host resistance genes and the phylogenetic relationships of other isolates revealed the existence of 2 phylogroups for the NSs gene (Almásí et al. 2015). In this study, the topology of the phylogenetic tree constructed with 325 isolates was similar to the tree topology reported by Almási et al. (2015). Similarly, the data indicating that isolates that breaking-resistance genes did not show a separate clustering showed the same results in our study. However, one of the most important findings regarding the phylogenetic tree is that the clustering of the isolates is mostly due to geographical origin. Almási et al. (2015) reported similar results for pepper TSWV isolates. Herein, network analyses indicates the presence of geographically structured genetic diversity within TSWV populations. The central positions of certain haplotypes suggest that these may be ancestral or more widespread genotypes, particularly within the Europe-Mediterranean region. Meanwhile, the separation of Asian and African isolates into distinct clusters could indicate localized evolution, potentially driven by region-specific selection pressures or vector dynamics. These results align with the broader geographic distribution of the virus and its vector, *F. occidentalis*, which is known to contribute to the global spread and genetic diversification of TSWV. In addition, the knowledge that TSWV is also transmitted by pepper and

tomato seeds, as reported in another study, may contribute significantly to these findings (Jones 1944; Wang et al. 2022).

The AMOVA results for the partial NSs gene region of TSWV indicate that 36.49% of the total genetic variation is explained by differences among the five geographic populations (Asian, EuroMed, America, Africa, and Eastern Europe), with a highly significant  $\Phi_{ST}$  value of 0.36491 ( $p < 0.001$ ) (Table 1). This substantial inter-population variation suggests strong genetic differentiation among these regions, likely driven by limited gene flow and the localized evolution of TSWV in different parts of the world. This geographic structuring could be influenced by factors such as regional differences in host plants, climatic conditions, or the distribution of the primary vector, *F. occidentalis*. In contrast, 63.51% of the genetic variation occurs within populations, highlighting considerable genetic diversity at the regional level. The high level of intra-population variation suggests that TSWV isolates within each geographic group are still undergoing genetic diversification, possibly due to frequent recombination events, natural selection, or adaptation to local environmental conditions. These findings underscore the complex population structure of TSWV, with both geographic isolation and local evolutionary forces contributing to its genetic diversity. The significant  $\Phi_{ST}$  value further suggests that these regional populations are evolving independently, which has important implications for understanding the spread and management of TSWV on a global scale.

## 5. Conclusion

This study offers important insights into the genetic diversity and population structure of TSWV by analyzing the NSs gene across 325 isolates from around the world. The findings demonstrate significant geographic structuring, with notable differentiation among populations from Asia, Africa, the Americas, Eastern Europe, and the Euro-Mediterranean region. The phylogenetic and haplotype network analyses reveal that this structuring is largely driven by geographic origin rather than resistance-breaking capacity, suggesting localized evolution influenced by regional environmental conditions and vector dynamics. The substantial inter-population variation, as indicated by the AMOVA results, further highlights the independent evolution of TSWV populations across different regions. At the same time, the high level of intra-population genetic diversity emphasizes the ongoing diversification of TSWV within these regions. These results underscore the importance of considering both geographic isolation and local evolutionary pressures in the global management and control of TSWV. Future research should continue to explore the role of genetic recombination, natural selection, and host-vector interactions in shaping the virus's evolution, particularly with regard to the development of resistant cultivars and effective disease management strategies.

## Acknowledgements

This study was supported by a grant from Bilecik Şeyh Edebali University, The Scientific Research Coordination Unit, Project number: 2022-01.BŞEÜ.06-02.

**Authors' contributions:** F.R.Z. planned and carried out the study. F.R.Z and A.K. wrote the final version of the article.

## Conflict of interest disclosure:

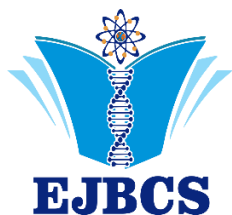
The authors state there is no competing interest.

## References

- Abadkhah M, Koolivand D, Eini O. 2018. A new distinct clade for Iranian Tomato spotted wilt virus isolates based on the polymerase, nucleocapsid, and non-structural genes. *Plant Pathol J.* 34:514.
- Almási A, Csilléry G, Csömör Z, et al. 2015. Phylogenetic analysis of Tomato spotted wilt virus (TSWV) NSs protein demonstrates the isolated emergence of resistance-breaking strains in pepper. *Virus Genes.* 50:71–78.
- Bandelt HJ, Forster P, Röhl A. 1999. Median-joining networks for inferring intraspecific phylogenies. *Mol Biol Evol.* 16:37-48. doi: 10.1093/oxfordjournals.molbev.a026036.
- De Haan P, Kormelink R, de Oliveira Resende R, van Poelwijk F, Peters D, Goldbach R. 1991. Tomato spotted wilt virus L RNA encodes a putative RNA polymerase. *J Gen Virol.* 71:2207–2216.
- De Ronde D, Butterbach P, Lohuis D, Hedil M, Van Lent JW, Kormelink R. 2013. Tsw gene-based resistance is triggered by a functional RNA silencing suppressor protein of the Tomato spotted wilt virus. *Mol Plant Pathol.* 14:405–415. doi: 10.1111/mpp.12016
- Du J, Song XY, Shi XB, Tang X, Chen JB, Zhang ZH, Chen G, Zhang Z, Zhou XG, Liu Y, Zhang DY. 2020. NSs, the Silencing Suppressor of Tomato Spotted Wilt Orthotospovirus, Interferes With JA-Regulated Host Terpenoids Expression to Attract *Frankliniella occidentalis*. *Front Microbiol.* 11:590451. doi: 10.3389/fmicb.2020.590451.
- Excoffier L, Smouse PE, Quattro JM. 1992. Analysis of molecular variance inferred from metric distances among DNA haplotypes: application to human mitochondrial DNA restriction data. *Genetics.* 131:479-491.
- Excoffier L, Lischer HE. 2010. Arlequin suite ver 3.5: a new series of programs to perform population genetics analyses under Linux and Windows. *Mol Ecol Resour.* 10:564-567.
- Francki RIB, Hatta T. 1981. Tomato spotted wilt virus. In: Kurstak E, ed. *Handbook of Plant Virus Infections and Comparative Diagnosis.* Amsterdam: Elsevier/North Holland Biomedical Press. 492–511.
- Guo Y, Liu B, Ding Z, Li G, Liu M, Zhu D, Sun Y, Dong S, Lou Z. 2017. Distinct mechanism for the formation of the ribonucleoprotein complex of Tomato spotted wilt virus. *J Virol.* 91:e00892-17.
- Gupta R, Kwon SY, Kim ST. 2018 An insight into the tomato spotted wilt virus (TSWV), tomato and thrips interaction. *Plant Biotechnol Rep.* 12:157–163.
- Güller A, Usta M, Randa-Zelyüt F. 2023. Genetic diversity and population structure of tomato brown rugose fruit virus (ToBRFV) variants from Antalya province, Turkey. *Notulae Botanicae Horti Agrobotanici Cluj-Napoca.* 51:13356-13356.
- Jones L. 1944. Streak and mosaic of *Cineraria*. *Phytopathology.* 34:941–953.

- Kamran A, Li Y, Zhang W, Jiao Y, Farooq T, Wang Y, Liu D, Jiang L, Shen L, Wang F, Yang J. 2024. Insights into the genetic variability and evolutionary dynamics of tomato spotted wilt orthotospovirus in China. *BMC Genomics*. 8:40. doi: 10.1186/s12864-023-09951-9.
- Karanfil A, Randa-Zelyüt F, Korkmaz S. 2023. Population structure and genetic diversity of tobacco mild green mosaic virus variants in Western Anatolia of Turkey. *Physiol Mol Plant Pathol*. 125:102008.
- Leigh JW, Bryant D. 2015. POPART: full-feature software for haplotype network construction. *Methods Ecol Evol*. 6:9.
- Letunic I, Bork P. 2024. Interactive Tree of Life (iTOL) v6: recent updates to the phylogenetic tree display and annotation tool. *Nucleic Acids Res*. gkae268. doi: 10.1093/nar/gkae268
- Margaria P, Bosco L, Vallino M, Ciuffo M, Mautino GC, Tavella L, Turina M. 2014. The NSs protein of tomato spotted wilt virus is required for persistent infection and transmission by *Frankliniella occidentalis*. *J Virol*. 88:5788-802. doi: 10.1128/JVI.00079-14.
- Morca AF, Çelik A, Coşkan S, Santosa AI, Akbaş B. 2022. Population analysis on tomato spotted wilt virus isolates inducing various symptoms on tomato, pepper, and *Chenopodium album* in Turkey. *Physiol Mol Plant Pathol*. 118:101786.
- Nagata T, Inoue-Nagata AK, Prins M, Goldbach R, Peters D. 2000. Impeded thrips transmission of defective Tomato spotted wilt virus isolates. *Phytopathology*. 90:454-459.
- Ocampo TO, Peralta SMG, Bacheller N, Uiterwaal S, Knapp A, Hennen A, Ochoa-Martinez DL, Garcia-Ruiz H. 2016. Antiviral RNA silencing suppression activity of Tomato spotted wilt virus NSs protein. *Genet Mol Res*. 15:15028625.
- Oetting RD. 1991. The effect of host species and different plant components on thrips feeding and development. In: Hsu TH, Lawson HR (eds) *Virus-Thrips-Plant Interaction of Tomato Spotted Wilt Virus*. United States Department Agriculture Research and Service. Maryland, pp 15-20.
- Peiró A, Cañizares MC, Rubio L, López C, Moriones E, et al. 2014. The movement protein (NSm) of tomato spotted wilt virus is the avirulence determinant in the tomato Sw-5 gene-based resistance. *Mol Plant Pathol*. 15:802-813. <https://doi.org/10.1111/mpp.12142>
- Prins M, Goldbach R. 1998 The emerging problem of tospovirus infection and nonconventional methods of control. *Trends Microbiol*. 6:31-35
- Reitz SR, Gao Y, Kirk WDJ, Hoddle MS, Leiss KA, Funderburk JE. 2020. Invasion Biology, Ecology, and management of Western Flower Thrips. *Annu Rev Entomol*. 65:17-37.
- Rozas J, Ferrer-Mata A, Sánchez-DelBarrio JC, Guirao-Rico S, Librado P, Ramos-Onsins SE, Sánchez-Gracia A. 2017. DnaSP 6: DNA sequence polymorphism analysis of large data sets. *Mol Biol Evol*. 34:3299-3302.
- Santosa AI, Randa-Zelyüt F, Karanfil A, et al. 2023. Phylogenetic and diversity analyses revealed that leek yellow stripe virus population consists of three types: S, L, and N. *Virus Genes*. 59:121-131.
- Snippe M, Borst JW, Goldbach R, Kormelink R. 2007. Tomato spotted wilt virus Gc and N proteins interact in vivo. *Virology*. 357:115-123.
- Tamura K, Nei M. 1993. Estimation of the number of nucleotide substitutions in the control region of mitochondrial DNA in humans and chimpanzees. *Mol Biol Evol*. 10:512-526.
- Tamura K, Stecher G, Kumar S. 2021. MEGA11: molecular evolutionary genetics analysis version 11. *Mol Biol Evol*. 38:3022-3027.
- Turina M, Tavella L, Ciuffo M. 2012. Tospoviruses in the Mediterranean area. *Advances in Virus Research*. 84:403-437.
- Turina M, Kormelink R, Resende RO. 2016. Resistance to tospoviruses in vegetable crops: epidemiological and molecular aspects. *Annu Rev Phytopathol*. 54: 347-371. <https://doi.org/10.1146/annurev-phyto-080615-095843>
- Usta M, Güller A, Demirel S, Korkmaz G, Kurt Z. 2023. New insights into tomato spotted wilt orthotospovirus TSWV infections in Türkiye Molecular detection phylogenetic analysis and in silico docking study, *Not Bot Horti Agrobot Cluj-Napoca*. 51:1-22.
- Wang H, Wu X, Huang X, Wei S, Lu Z, Ye J. 2022. Seed Transmission of Tomato Spotted Wilt Orthotospovirus in Peppers. *Viruses*. 14:1873. doi: 10.3390/v14091873.
- Whitfield AE, Kumar NKK, Rotenberg D, Ullman DE, Wyman EA, Zietlow C, Willis DK, German TL (2008) A soluble form of the Tomato spotted wilt virus (TSWV) glycoprotein G(N) (G(N)-S) inhibits transmission of TSWV by *Frankliniella occidentalis*. *Phytopathology*. 98:45-50.
- Zelyüt FR, Ertunç F. 2021. Population genetic analysis of lettuce big-vein disease viruses and their vector fungi *Olpidium virulentus* in Ankara province, Turkey. *Physiol Mol Plant Pathol*. 113:101593.





## Impact of growth medium components on absorbance-viable cell count correlation and cell surface area of *Cereibacter sphaeroides* O.U.001

Kader Çakır , Gökhan Kars 

\*Necmettin Erbakan University, Faculty of Science, Department of Molecular Biology and Genetics, Konya, Turkey

\*Corresponding author : [gkars@erbakan.edu.tr](mailto:gkars@erbakan.edu.tr)  
Orcid No: <https://orcid.org/0000-0002-2507-2305>

Received : 15/07/2024  
Accepted : 07/11/2024

To Cite / Atıf için: Çakır K, Kars G. 2024. Impact of growth medium components on absorbance-viable cell count correlation and cell surface area of *Cereibacter sphaeroides* O.U.001. Eurasian J Bio Chem Sci, 7(2):132-138 <https://doi.org/10.46239/ejbs.1516661>

**Abstract:** Today different methods are used in microbiology laboratories to monitor the growth and development of bacteria. Optical density measurement is one of the most preferred methods as being fast, practical and low cost. On the other hand, it cannot differentiate between living and non-living cells in the culture. Moreover, alteration in cell size may lead to the variations in the measurements. As a result, optical density measurements alone may cause wrong experimental results. Therefore, it is necessary to determine the absorbance-living cell number relationship for each specific culture condition. In this study, *Cereibacter sphaeroides* O.U.001 was cultured under four different culture conditions regarding the type of carbon and nitrogen sources (Malate/Glutamate, Molasses/Glutamate, Malate/N<sub>2</sub> and Acetate/Glutamate) and the effect of medium composition on cell size and absorbance-viable cell count relationship was investigated. Equations were obtained from curves drawn as optical density (x-axis) against CFU/mL (y-axis). Field emission scanning electron microscope was used to observe the effects of medium compositions on the size of *Cereibacter sphaeroides* O.U.001. It was revealed that the composition of the medium affected the absorbance-number of living cells relationship. Furthermore, it was evidenced that the size of the cells was changed significantly upon changing the medium composition. To conclude, it is advised that before performing experiments in which the cell numbers are significant, a comparative calibration curve for optical density measurement-the living cell number relationship should be established for more accurate results.

**Keywords:** *Cereibacter sphaeroides*, CFU/mL, FE-SEM, Viable Cell Count

© EJBCS. All rights reserved.

### 1. Introduction

The purple non-sulfur (PNS) photosynthetic bacteria are versatile group of organisms that can grow as photoheterotrophs, photoautotrophs or chemoheterotrophs. They can switch from one mode to another depending on the environmental conditions. PNS bacteria have important morphological, biochemical, and metabolic properties, as well. Thanks to their wide range of metabolic properties, they are able to cope with different physiological or environmental conditions (Basak and Das 2007; Madigan and Jung 2009; McEwan 1994). PNS bacteria, which are widely distributed in nature, are found in mud, wastewater, lake water and pool water. Representatives of this group of bacteria are *Cereibacter sphaeroides* (recently renamed from *Rhodobacter sphaeroides*), *Rhodobacter capsulatus*, *Rhodospirillum rubrum* and *Rhodopseudomonas palustris* (Kars and Alparslan 2013; Myung et al. 2004).

*Cereibacter sphaeroides*, which is a gram-negative bacterium, has the ability to adapt and grow in variety of environmental conditions (Vermeglio and Joliot 1999). It has been used in the laboratories for many years for basic studies like photosynthesis, respiration, CO<sub>2</sub> and N<sub>2</sub> fixation (Kars and Gündüz 2010). Moreover, *C. sphaeroides* is a biotechnologically versatile microorganism capable of producing many biotechnologically valuable chemicals like hydrogen (Kars and Alparslan 2013), 5-aminolevulinic acid (5-ALA) (Sasaki et al. 1990), polyhydroxybutyrate (PHB) (Lee et al. 2020), B12 and Coenzyme Q10 (Sasaki et al. 2005). The type and amount of carbon and nitrogen sources are determinative for the biotechnological product that *C. sphaeroides* can produce (Basak and Das 2007). For instance, hydrogen could only be produced under anaerobic conditions preferentially using fixed nitrogen sources like glutamate (Danış et al. 2022). Ammonia can also be used but its concentration needs to be below 2 mM (Akköse et al.



2009). PHB, for instance, could favorable be produced under high carbon to nitrogen ratios (Akpınar 2023). *C. sphaeroides* is an excellent model organism for studying nitrogen fixation, as well (Joshi and Tabita 1996). In PNS bacteria including the *C. sphaeroides*, the conversion of nitrogen gas to ammonia is catalyzed by the enzyme nitrogenase which is activated under diazotrophic conditions (under the atmosphere of nitrogen gas and in the absence of ammonia) in the absence of oxygen (Kars and Gündüz 2010). Under these conditions, the nitrogenase enzyme can convert free nitrogen gas into ammonia and then use it for cellular metabolism. The nitrogenase enzyme is known to be directly linked to the production of hydrogen. If the culture is devoid of free nitrogen gas, the nitrogenase enzyme can catalyze the conversion of protons into molecular hydrogen under anaerobic conditions in the light.

Since *C. sphaeroides* is a model bacterium for many basic metabolic activities and used as a chassis for the production of many high value-added products, it has been cultivated under different physiological conditions using various types of carbon and nitrogen sources. In these studies, starting with the correct number of cells is of great importance to get high quality data. Spectrophotometric optical density (OD) measurement at 600 nm or 660 nm is one of the mostly preferred and common methods in these studies. One of the most important reasons for the preference of spectrophotometric measurement, which is often used in laboratories to monitor the growth and development of bacteria, is that it is less time consuming and practical. Studies are being conducted by assuming that the optical density (OD) is completely proportional to the number of cells (Stevenson et al. 2016). However, this method does not directly measure viable cell number, but rather measures the turbidity of the cultures which contain both live and death cells (Beal et al. 2020; Sutton 2011). It was stated that environmental factors like temperature, water activity and pH influence the relationship between OD measurement and viable cell count (Francois et al. 2005). For example, Jorgensen et al. demonstrated that high osmotic stress resulted in elongation of *L. monocytogenes* (Jorgensen et al. 1995). Consequently, this morphological change affected the OD measurement-viable cell count relationship. The OD values do not mean the number of cells. This is because the capacity of bacteria to multiply varies with each different environment where they are found. Although this situation is already known to most researchers, it is ignored due the simplicity of the spectrophotometric measurement. However, ignoring the fact that the relation between OD values and live cell number depends on the culture conditions may lead to false results during the microbiological studies. Especially in sensitive techniques such as polymerase chain reaction (PCR), RNA-Seq and microarray, the result is strongly dependent on the initial cell number. In these techniques, live cells are generally preferred to obtain reliable and high-quality data, as they preserve the integrity of nucleic acids, allowing for the complete and accurate analysis of the desired genetic material. When working with dead cells, however, the degradation of DNA and RNA is likely, which can lead to incomplete or erroneous data. If the use of dead cells is

unavoidable, special care should be taken during sample preparation to maintain nucleic acid stability and minimize degradation (Nkuipou-Kenfack et al. 2013). Although quantification and adjustment of the initial amount of RNA or DNA help to avoid false results, starting with an equal number of cells for each experimental group would be more meaningful. Furthermore, in some other biotechnological studies, the experiments are being conducted by just starting with the cultures with similar OD values to equalize conditions without further considerations.

In this study, absorbance-viable cell number relationship of *C. sphaeroides* under four different culture conditions regarding the type of carbon and nitrogen sources (Malate/Glutamate, Molasses/Glutamate, Malate/N<sub>2</sub> and Acetate/Glutamate) was investigated. The sizes of the cells were also measured by a field emission scanning electron microscope (FE-SEM) under the same conditions to see if culture conditions have any effects on the morphology of the cells.

## 2. Materials and Method

### 2.1. Microorganism media and culture conditions

*Cereibacter sphaeroies* O.U.001 (DMS 5864) was used in this study. Four different growth media were prepared based on carbon and nitrogen content (Malate/Glutamate, Molasses/Glutamate, Malate/N<sub>2</sub> and Acetate/Glutamate) to investigate absorbance-viable cell count relationship of *C. sphaeroides*. The media contents are shown in Table 1.

**Table 1.** Media components designed regarding the carbon and nitrogen sources

Medium number	Carbon source	Nitrogen source
1	Malate (15 mM)	Glutamate (2 mM)
2	Molasses (28 g/L)	Glutamate (2 mM)
3	Malate (15 mM)	N <sub>2</sub> gas
4	Acetate (40 mM)	Glutamate (2 mM)

The first medium is a minimal medium often used for cultivation of *C. sphaeroides* and is called as Biebl and Pfenning minimal medium (Biebl and Pfenning 1981) medium, which uses malate (15 mM) as a carbon source and glutamate (2 mM) as a nitrogen source, was considered as a control group because it meets the requirements of bacteria at a minimum or basal level. It specifically allows the growth of PNS bacteria. In the second medium, sugar beet molasses obtained from a sugar factory (Konya Şeker, Konya, Türkiye) was used as the carbon source. Sugar beet molasses, which is obtained as a by-product in the process of sugar production, is one of the most economical carbon sources to grow bacteria (Bae and Shoda 2004). Raw molasses contains approximately 48-50% sugars, 1-3% nitrogen, a variety of organic acids (including malic, succinic, fumaric, lactic, acetic, propionic, and formic acids), as well as essential elements such as potassium, sodium, magnesium, calcium, aluminum, zinc, copper, nickel, cobalt, manganese, chromium, and boron, along

with various vitamins. This rich composition positively affects bacterial growth, allowing the bacteria to reach very high cell densities (Kars and Alparslan 2013). Molasses was pre-processed before use due to its complex content. After diluting the molasses with distilled water, it was centrifuged at 9000 rpm for 20 minutes. Then, the supernatant was passed through the 0.22  $\mu\text{m}$  filter to be ready for use. As the third medium, a nitrogen-fixing environment was designed. In this case, malate (15 mM) was used as carbon source and nitrogen gas was used as nitrogen source. The liquid culture was flushed with nitrogen gas for 3 min so that the bioreactor became anaerobic and saturated with the nitrogen gas at the same time (Sert 2022). The remaining content of the medium was the same as the others. In the final medium, acetate (40 mM) and glutamate (2 mM) were chosen as carbon and nitrogen source, respectively. Acetate is especially preferred in the PHB production processes since acetate catabolism uses the same pathway with PHB production metabolism in *C. sphaeroides* (Kars and Gündüz 2010). Thus, significant amounts of PHB can be formed. Acetate is accordingly chosen as a carbon source, and it was included in the study to see if PHB accumulation inside the cell leads the deviations in absorbances.

The main elements for each medium are  $\text{MgSO}_4 \cdot 7\text{H}_2\text{O}$  (0.2 g/L),  $\text{CaCl}_2 \cdot 2\text{H}_2\text{O}$  (0.05 g/L) and  $\text{NaCl}$  (0.4 g/L).  $\text{KH}_2\text{PO}_4$  (0.5 g/L) was used as buffer. In addition, trace element, iron sulfate and vitamin solutions were put into the media as documented earlier (Kars and Ceylan 2019). Initial pH of the medium was fixed to 6.9. After sterilization, the media were transferred to 100 mL sterile glass penicillin bottles. Then, they were inoculated by 10 % (v/v) with freshly grown cultures. Argon gas was passed through the medium to provide anaerobic conditions, if needed. To set nitrogen-fixing condition, nitrogen gas was passed through the bottles for 3 minutes instead of argon gas. The light energy was provided by an incandescent lamp (100 W) which was placed at a distance of 30-40 cm. The bioreactors were kept in incubator at 29 °C (Danış et al. 2022).

## 2.2. Growth curves and cell counting method

In order to compare the absorbance values with the number of living cells, spread plate technique was used (Koch 2006). Simultaneous cell counting and OD measurements were performed to find the number of living cells corresponding to the OD values. The OD values of the samples were measured using a spectrophotometer (Agilent, Cary 60 UV-Vis) at a wavelength of 660 nm. After the first absorbance value was taken at the zeroth hour ( $t=0$ ), the subsequent measurements were made at 24-hour intervals. After the initial absorbance value was taken at the zeroth hour ( $t=0$ ), subsequent measurements were made at 24-hour intervals based on previous studies (Sert 2022). For the spectrophotometric measurements above 1, the samples were diluted and then the results were multiplied by the dilution factor to get the exact OD value. The measurements were performed at least twice and then standard error of the mean (SEM) values for each time point were calculated. At the end,  $\text{OD}_{660}$  nm versus time (h) graphs were drawn. In parallel to OD measurements, culture samples were spread onto the agar plates after several dilutions and bacterial

colonies formed on petri dishes were counted. Due to the challenges of converting Molasses-Glutamate and Malate- $\text{N}_2$  gas liquid media to solid media, all cultures were grown on Malate-Glutamate (BP) agar plates for counting. For the total number of bacteria, the number of colonies as colony forming unit (CFU) was calculated according to the equation (Equation 1) (Koch 2006) given below and then graphs were created. The process was repeated at 24-hour intervals. Finally,  $\text{OD}_{660}$  nm versus CFU/mL graphs were drawn.

$$\frac{\text{CFU}}{\text{mL}} = \text{number of colonies} \times \text{dilution factor} \times \frac{1}{\text{volume transferred to petri dishes (mL)}} \quad (\text{Equation 1})$$

## 2.3. FE-SEM analyses and measurement of cell surface area

Size and morphology of *C. sphaeroides* O.U.001 were examined by a field emission scanning electron microscope (Hitachi SU 1510). To ensure that the morphological structures of the cells were not disrupted, no chemical treatments were applied, and direct FE-SEM images were obtained from *C. sphaeroides* O.U.001 grown in all media until it reached the logarithmic phase. For this purpose, liquid samples of *C. sphaeroides* O.U.001 were collected into Eppendorf tubes and centrifuged at 7000 rpm for 5 minutes. The supernatant was discarded, and the pellet was dissolved in 1 mL of sterile distilled water. 5  $\mu\text{L}$  of cell suspension was placed onto platform (stab). Sample platforms were kept in an incubator at 50 °C for 10 minutes to dry the cells. To ensure the necessary conductivity without compromising the morphological structure of the sample, it was coated with iridium at a thickness of 4.15 nm. (Zheng et al. 2017; Sert 2022). The FE-SEM images of bacteria were then used for the measurement of cell surface area by ImageJ image analysis program (Schneider et al. 2012). For this, ten bacterial cells were selected randomly (N:10) in each of the four groups and the surface area of them were calculated using the image analysis program. Then, one-way ANOVA was performed to see if growth media have any influence on the size of bacteria.

## 3. Results

### 3.1. Growth curves under different culture conditions

The growth of bacteria was followed by measuring the absorbances of the cultures by a spectrophotometer at 660 nm. At the time of inoculation, the time was taken as zero and then OD measurements were done at 24-hour intervals. Afterwards, these data were used to draw the growth curves as shown in Figure 1. The highest OD value obtained in each growth media was different from each other. For instance, the highest OD value (4.62) was achieved in Molasses/Glutamate media while the lowest value (1.39) was obtained in Malate/Glutamate medium. The cells attained an OD value of 2.70 in Acetate/Glutamate medium. In the case of Malate/ $\text{N}_2$  medium, the highest OD value of the culture was 2.39. In this medium design, carbon source was malate, but the nitrogen source was molecular nitrogen different from the others. In this experimental setup,

nitrogen fixation conditions were set so that the effect of nitrogen fixation on the growth profile was assessed. The OD value achieved in this medium was still higher than that obtained in Malate/Glutamate minimal medium.

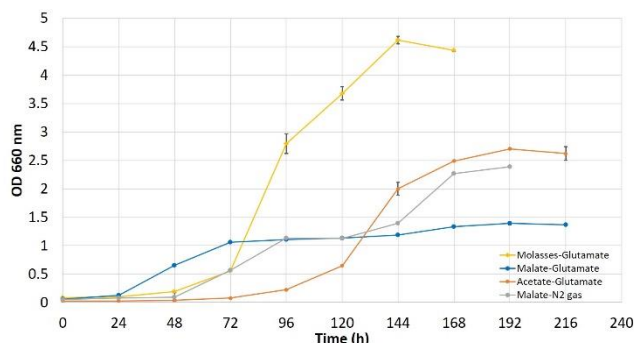


**Figure 1.** The growth of *C. sphaeroides* in Molasses/Glutamate, Malate/Glutamate, Acetate/Glutamate and Malate/N<sub>2</sub> media

### 3.2. Absorbance-viable cell count relationship

This section of the study looked at the link between *C. sphaeroides* O.U.001's absorbance and viable cell count in various conditions. A graph (Figure 2) was obtained, with absorbance (OD660 nm) on the x-axis and viable cell number (CFU/mL) on the y-axis. The graph illustrates how there were notable variations in the quantity of live cells with identical OD values. When the equations in the graph were used, an OD value of 1 corresponded to  $5.06 \times 10^8$ ,  $8.2 \times 10^8$ ,  $4.2 \times 10^8$ , and  $4.6 \times 10^8$  CFU/mL in Malate/Glutamate, Malate/N<sub>2</sub>, Acetate/Glutamate and Molasses/Glutamate media, respectively. When compared to others, the highest value for viable cells per milliliter of culture was achieved in that where nitrogen source was

supplied as molecular N<sub>2</sub>. On the other hand, when acetate was used as the carbon source, the smallest value for viable cell count per milliliter of culture was achieved.

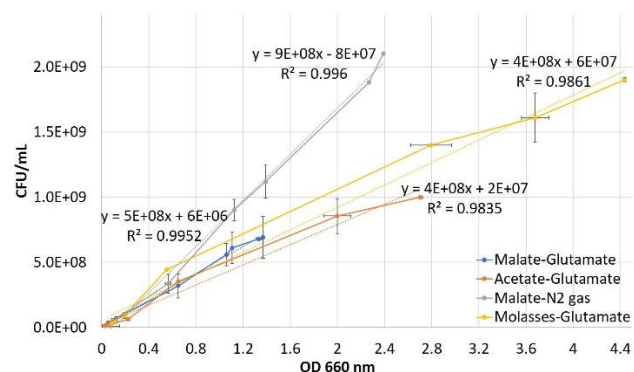


**Figure 2.** Absorbance-viable cell count relationship of *C. sphaeroides* O.U.001. Error bars indicate standard error of the mean

### 3.3. Field emission scanning electron microscope analyses and measurement of cell size

Field Emission Scanning Electron Microscopy (FE-SEM) was used to visualize the changes in the cell morphology of *C. sphaeroides* growing under different culture conditions. Moreover, the FE-SEM images (Figure 3) were used to measure cell sizes using ImageJ image analysis program (Schneider et al. 2012). In order not to give rise to any deformities in the cell structure, fixatives were not used. Cells were only treated with distilled water before FE-SEM analyses. No distinctive differences in cell morphologies were observed upon examining FE-SEM images (Figure 3). Further analyses with higher magnification might help to unveil the detailed morphological structures in the future studies.

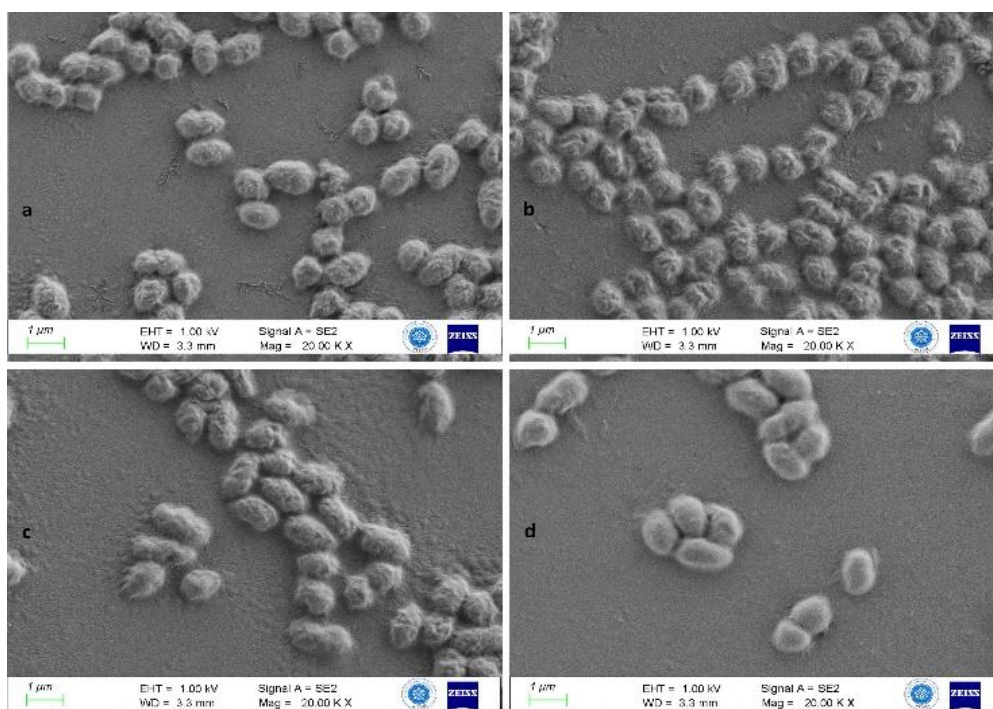


**Figure 3.** FE-SEM images of *C. sphaeroides* grown in Malate-Glutamate (a), Molasses-Glutamate (b), Malate-N<sub>2</sub> (c) and Acetate-Glutamate media (d)

FE-SEM images of *C. sphaeroides* grown in different growth media were used to analyze cell surface area (Figure 4). Surface area measurements of the cells in each growth media and subsequent one-way ANOVA analysis revealed that there was a statistically significant difference in test scores between at least two groups ( $F(2, 36) = 3.777$ ,  $p = 0.019$ ). Tukey's test for multiple comparisons found that mean surface areas were significantly different between the growth media Malate/Glutamate and Acetate/Glutamate ( $p = .031$ , 95% C.I. =  $[-.34637, -.01243]$ ) and Molasses/Glutamate and Acetate/Glutamate ( $p = .043$ , 95% C.I. =  $[-.33797, -.00403]$ ). There was no statistically significant difference between the other media ( $p > .05$ ).

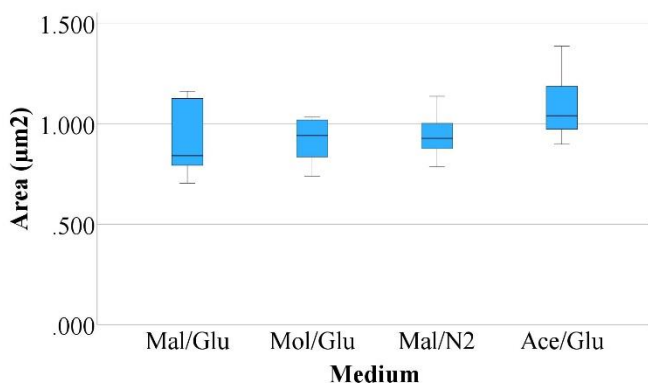


**Figure 4.** Cell surface area of *C. sphaeroides* grown in different media

#### 4. Discussion

When working with microorganisms, assessing growth is often crucial, and the most commonly used method for measuring growth/growth inhibition is absorbance measurement (Gabrielson et al. 2002). However, it is incorrect to directly relate absorbance values (OD) to live cell number without taking into account the physiological state of the medium, the type of microorganism, and the metabolic products produced. In this study, it was found that the OD value-viable cell count relationship of bacteria grown under different physiological conditions varied significantly.

The growth profiles changed depending on the culture conditions used. For example, the maximum OD value (4.62) was obtained in Molasses/Glutamate media (Figure 1), whereas the lowest (1.39) was obtained in Malate/Glutamate medium (Figure 1). This result was very plausible and reasonable when considering the composition of the medium. The highest cell density was obtained in the medium having the richest composition (Molasses/Glutamate) while the lowest cell density was obtained in the medium with minimal composition (Malate/Glutamate). The result was also consistent with previous findings. In a previous study, the highest cell density for *C. sphaeroides* O.U.001 ( $OD_{660}$ : 9.26, 4.54 g cdw/L) was reported to be obtained when using molasses as substrate (Kars and Alparslan 2020). This might be due to the fact that sugar beet molasses has a very rich composition, and it includes around 50% sucrose by weight. Moreover, several types of organic acids and elements were

found to be present in molasses (Kars and Alparslan 2013). In the study conducted by Palmonari et al. (2020) the detailed chemical composition of molasses includes sugars, elements, and vitamins, as well as nitrogen sources (such as protein and nitrate). Therefore, it is believed that the highest growth values of *C. sphaeroides* in molasses medium may be attributed to other nitrogen sources. It has been concluded that additional nitrogen sources likely enhance growth and significantly support bacterial development. Molasses is not only a rich substrate but also a cheap carbon source when compared to other commercially available sources. Thus, it is frequently used as a substrate in microbiology studies. Unlike molasses, the Malate/Glutamate medium which was named as minimal medium supported the cell growth at the basal level. As a result, obtaining the lowest cell density while utilizing malate/glutamate medium is highly likely and predictable. This medium, named as Bieble and Pfennig minimal medium, selectively allows the growth of PNS bacteria so that it has specific uses. For instance, *Escherichia coli* strains cannot grow in this minimal medium so that it can be used to select single recombinant *C. sphaeroides* after conjugation in site directed mutagenesis studies (Kars et al. 2008).

In the Acetate/Glutamate medium, the cells reached an OD value of 2.70 (Figure 1). The acetate assimilation pathway differs among bacterial species. Regarding acetate assimilation pathways in PNS bacteria, glyoxylate cycle, citramalate cycle and ethylmalonyl-CoA pathways were declared to exist (Kars and Gündüz 2010). *C. sphaeroides* lacks isocitrate lyase, the enzyme that provides the renewal of C4 acids in glyoxylate cycle. However, studies indicated that another acetate assimilation pathway called as ethylmalonyl-CoA (EMC) was operating in *C. sphaeroides* to metabolize acetate (Kars and Gündüz 2010; Shimizu et al. 2019). This pathway is linked to the production of PHB. Thus, acetate is known to positively affect the production of PHB. In the experiments, it was observed that acetate sufficiently supported the growth of *C. sphaeroides* so that the cells attained considerably high cell density. It is also highly probable that excess amount of acetate was stored in the form of PHB granules in the bacterial cells. The stored PHB granules can then be used as carbon sources and may cause late arrival to the stationary phase as witnesses in this study. The maximum OD value of the culture in the Malate/N<sub>2</sub> media was 2.39 (Figure 1). Malate served as the carbon supply and molecular nitrogen served as the nitrogen source in this particular medium design. The nitrogen fixation settings in this experiment were chosen to evaluate the impact of nitrogen fixation on the growth profile. Even with this medium, the OD value was greater than in the Malate/Glutamate minimum media. Consequently, it was discovered that nitrogen fixation promoted bacterial growth more effectively than glutamate, suggesting that nitrogen gas was a superior nitrogen source to glutamate.

When the association between the absorbance and viable cell count of *C. sphaeroides* O.U.001 in various medium was examined, significant variations in the quantity of live cells with identical OD values were observed, as the graph



illustrates (Figure 2). These variations might result from each cell's unique capacity to absorb light depending on the growth conditions. The ability of cells to absorb light can be influenced by a variety of factors including pigments, internal membrane architecture, granules, and the types of metabolites found inside the cells. For example, when anaerobic conditions are met, a photosynthetic intracytoplasmic membrane (ICM) system forms in the cell (Kars and Gündüz 2010). This internal structure is required for the light reactions of photosynthesis since it houses the photosynthetic machinery that contains carotenoids and bacteriochlorophylls. Owing to the presence of carotenoids and bacteriochlorophylls, these bacteria may display distinct light absorption characteristics. Furthermore, the cells convert excess carbon sources into PHB granules for later use when they are provided with a high amount of carbon source with limited amount of nitrogen or elements. Changes in the cells' ability to absorb light may also result from presence of such granules. Additionally, the growth medium's characteristics might have an impact on the cultures' ability to absorb light. This is particularly true when employing vibrant growth media, such as molasses made from sugar beets. These feedstocks' vibrant colors or particles invariably change the culture's capacity to absorb light. Consequently, the aforementioned discussions should be considered to understand the fluctuations in the absorbance-viable cell number relation of a bacterium under various physiological settings.

Field Emission Scanning Electron Microscopy (FE-SEM) was used to visualize changes in cell morphology of *C. sphaeroides* growing under different conditions. Cell sizes were measured using ImageJ image analysis program. No distinctive differences were observed in cell morphologies, but further analyses with higher magnification could reveal detailed structures. Surface area measurements showed a statistically significant difference in test scores between at least two groups, with significant differences between growth media Malate/Glutamate and Acetate/Glutamate and Molasses/Glutamate and Acetate/Glutamate. Similar to polyhydroxybutyrate biosynthesis, *C. sphaeroides*'s acetate assimilation mechanism follows the ethylmalonyl-CoA pathway. Stated differently, PHB synthesis is a necessary consequence of using acetate as the carbon source. As a result, in the Acetate/Glutamate medium, acetate stimulates the growth of PHB granules inside the cell, allowing the cells to attain a much larger surface area. This might be the reason why the cells in the Acetate/Glutamate medium had the largest surface area.

## 5. Conclusion

Bacterial cell cultures progress through distinct life stages, namely the lag phase, log phase, stationary phase, and death phase. To track this progression over time, the conventional method employed is spectrophotometric measurement. When using a spectrophotometer for measurement, the absorbance value is influenced not only by the cells but also by the composition of secretory substances and the properties of the growth medium, including its color. Consequently, the relationship between absorbance and the number of living cells varies depending on the specific

environment. Furthermore, cells exhibit distinct metabolic activities and produce different metabolites in various conditions, which can also impact absorbance values. Metabolites and bacterial structures resulting from diverse metabolic activities, such as membrane folds formed under photosynthetic conditions, are believed to influence absorbance. Physiological conditions not only determine the relationship between absorbance and viable cell count but can also lead to variations in cell size. As a result of this study, it was proved that cell surface area of *C. sphaeroides* varied significantly upon changing growth media.

In conclusion, despite the inherent limitations of spectrophotometric measurements due to variations in culture conditions, this method can still be useful following adequate control and calibration of the procedure. It is advisable to establish calibration protocols that compare absorbance with viable cell counts before utilizing a spectrophotometer to measure the density of cell suspensions. Once these calibration protocols are tailored to specific culture conditions, spectrophotometric studies can be conducted.

## Acknowledgements

This study was supported by TÜBİTAK 2209-A research project support program.

**Authors' contributions:** KÇ performed the experimental studies and prepared the draft of the manuscript. GK managed the project, performed the experimental studies, made the analyses and prepared the manuscript.

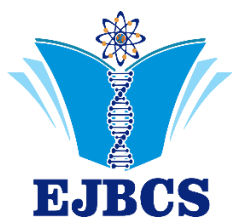
## Conflict of interest disclosure

There is no conflict of interest.

## References

- Akköse S, Gündüz U, Yücel M, Eroğlu I. 2009. Effects of ammonium ion, acetate and aerobic conditions on hydrogen production and expression levels of nitrogenase genes in *Rhodobacter sphaeroides* O.U.001. Int J Hydrogen Energy. 34:8818-8827.
- Akpınar BN. 2023. Asetat ortamında büyütilen *Cereibacter sphaeroides* O.U. 001, *Rhodospseudomonas palustris* 7850 ve *Cupriavidus necator* H16 ile polihidroksibütirat (PHB) üretimi ve üretilen polimerlerin karakterizasyonu. N. E. Ü. Fen Bilimleri Enstitüsü, MSc Thesis.
- Bae S, Shoda M. 2004. Bacterial cellulose production by fed-batch fermentation in molasses medium. Biotechnol Prog. 20:1366-1371.
- Basak N, Das D. 2007. The prospect of purple non-sulfur (PNS) photosynthetic bacteria for hydrogen production: The present state of the art. World J Microbiol Biotechnol. 23:31-42.
- Beal J, Farny NG, Haddock-Angelli T, Selvarajah V, Baldwin GS, Buckley-Taylor R, Gershater M, Kiga D, Marken J, Sanchania V, Sison A, Workman CT. 2020. Robust estimation of bacterial cell count from optical density. Commun Biol. 3:512.
- Biebl H, Pfennig N. 1981. Isolation of Members of the Family Rhodospirillaceae. In: Starr MP et al (eds.) The prokaryotes: a handbook on habitats, isolation, and identification of bacteria, Springer Berlin Heidelberg, Berlin.
- Danış K, Bingöl BN, Kars G. 2022. Production of biological hydrogen and bacterial carotenoids with *Rhodobacter sphaeroides* O.U.001 in a biorefinery concept. Eurasian J Bio Chem Sci. 5:56-61.

- Francois K, Devlignere F, Standaert AR, Greeraerd AH, Cools I, Van Impe JF, Debevere J. 2005. Environmental factors influencing the relationship between optical density and cell count for *Listeria monocytogenes*. *J Appl Microbiol*. 99:1503-1515.
- Gabrielson J, Hart M, Jarelöv A, Kühn I, McKenzie D, Möllby R. 2002. Evaluation of redox indicators and the use of digital scanners and spectrophotometer for quantification of microbial growth in microplates. *J Microbiol Methods*. 50:63-73.
- Jorgensen F, Stephens PJ, Knochel S. 1995. The effect of osmotic shock and subsequent adaptation on the thermotolerance and cell morphology of *Listeria monocytogenes*. *J Appl Bacteriol*. 79:274-281.
- Joshi HM, Tabita FR. 1996. A global two component signal transduction system that integrates the control of photosynthesis, carbon dioxide assimilation, and nitrogen fixation. *Proc Natl Acad Sci*. 93:14515-14520.
- Kars G, Alparslan Ü. 2013. Valorization of sugar beet molasses for the production of biohydrogen and 5-aminolevulinic acid by *Rhodobacter sphaeroides* O.U.001 in a biorefinery concept. *Int J Hydrogen Energy*. 38:14488-14494.
- Kars G, Alparslan Ü. 2020. Evaluation of high concentrations of sugar beet molasses as substrate for hydrogen and 5-aminolevulinic acid productions. *Int J Adv Eng Pure Sci*. 32:398-404.
- Kars G, Ceylan A. 2019. Hydrogen generation by *Rhodobacter sphaeroides* O.U.001 using pretreated waste barley. *Cumhur Sci J*. 40:414-423.
- Kars G, Gündüz U. 2010. Towards a super H<sub>2</sub> producer: Improvements in photofermentative biohydrogen production by genetic manipulations. *Int J Hydrogen Energy*. 35:6646-6656.
- Kars G, Gündüz U, Rakhely G, Yücel M, Eroğlu I, Kovacs KL. 2008. Improved hydrogen production by uptake hydrogenase deficient mutant strain of *Rhodobacter sphaeroides* O.U.001. *Int J Hydrogen Energy*. 33:3056-3060.
- Koch AL. 2006. Growth. In: Reddy CA et al. (eds.) *Methods for General and Molecular Microbiology*. American Society for Microbiology.
- Lee YR, Nur Fitriana H, Lee SY, Kim MS, Moon M, Lee WH, Lee JS, Lee S. 2020. Molecular profiling and optimization studies for growth and PHB production conditions in *Rhodobacter sphaeroides*. *Energies*. 13:6471.
- Madigan MT, Jung DO. 2009. An overview of purple bacteria: systematics, physiology, and habitats. In: Hunter et al (eds.) *The purple phototrophic bacteria*, Springer, Dordrecht.
- McEwan AG. 1994. Photosynthetic electron transport and anaerobic metabolism in purple non-sulfur phototrophic bacteria. *A Van Leeuw J Microb*. 66:151-164.
- Myung KK, Choi KM, Yin CR, Lee KY, Im WT, Ju HL, Lee ST. 2004. Odorous swine wastewater treatment by purple non-sulfur bacteria, *Rhodopseudomonas palustris*, isolated from eutrophicated ponds. *Biotechnol Lett*. 26:819-822.
- Nkuipou-Kenfack E, Engel H, Fakih S, Nocker A. 2013. Improving efficiency of viability-PCR for selective detection of live cells. *J Microbiol Methods*. 93:20-24.
- Palmonari A, Cavallini D, Sniffen CJ, Fernandes L, Holder P, Fagioli L, Fusaro I, Biagi G, Formigon A, Mammi L. 2020. Characterization of molasses chemical composition. *J Dairy Sci*. 103:6244-6249.
- Sasaki K, Tanaka T, Nishizawa Y, Hayashi M. 1990. Production of a herbicide, 5-aminolevulinic acid, by *Rhodobacter sphaeroides* using the effluent of swine waste from an anaerobic digester. *Appl Microbiol Biotechnol*. 32:727-731.
- Sasaki K, Watanabe M, Suda Y, Ishizuka A, Noparatnaraporn N. 2005. Applications of photosynthetic bacteria for medical fields. *J Biosci Bioeng*. 100:481-488.
- Schneider C, Rasband WS, Eliceiri KW. 2012. NIH Image to ImageJ: 25 years of image analysis. *Nat Methods*. 9:671-675.
- Sert M. 2022. Diazotrofik koşullarda çoğaltılan *Rhodobacter sphaeroides* O.U 001 ile hidrojen üretimi ve Nifh gen ifade analizi. N.E.Ü. Fen Bilimleri Enstitüsü, MSc Thesis.
- Shimizu T, Teramoto H, Inui M. 2019. Introduction of glyoxylate bypass increases hydrogen gas yield from acetate and l-glutamate in *Rhodobacter sphaeroides*. *Appl Environ Microbiol*. 85:1-17.
- Stevenson K, McVey AF, Clark IBN, Swain PS, Pilizota T. 2016. General calibration of microbial growth in microplate readers. *BioRxiv*. 6:32888.
- Sutton S. 2011. *Microbiology Topics*. Measurement of microbial cells by optical density. *J Valid Technol*. 17:46-49.
- Vermeglio A, Joliot P. 1999. The photosynthetic apparatus of *Rhodobacter sphaeroides*. *Trends Microbiol*. 7:435-440.
- Zheng Y, Cosgrove DJ, Ning G. 2017. High-resolution field emission scanning electron microscopy (FESEM) imaging of cellulose microfibril organization in plant primary cell walls. *Microsc Microanal*. 23:1048-1054.



## Investigation of the effects of lycorine and galanthamine extracted from *Galanthus elwesii* on viral and parasitic targets: An *in-silico* analysis and DFT Study

Melek Gul<sup>1\*</sup>, Ebru Batı Ay<sup>2</sup>

<sup>1</sup>Amasya University, Science-Art Faculty, Department of Chemistry, Amasya, Türkiye.

<sup>2</sup>Amasya University, Suluova Vocational School, Department of Plant and Animal Production, Amasya, Turkey.

\*Corresponding author : [melek.gul@amasya.edu.tr](mailto:melek.gul@amasya.edu.tr)

Orcid No: <https://orcid.org/0000-0002-0037-1202>

Received :22/09/2024

Accepted :24/11/2024

**To Cite / Atf için:** Gul M, Batı Ay E. 2024. Investigation of the effects of lycorine and galanthamine extracted from *Galanthus elwesii* on viral and parasitic targets: An *in-silico* analysis and DFT Study. Eurasian J Bio Chem Sci, 7(2):139-150 <https://doi.org/10.46239/ejbs.1554370>

**Abstract:** In this study, Density Functional Theory (DFT), ADME property analysis, and molecular docking simulations were employed to evaluate the electronic structure, antiviral potential, and antiparasitic effects of lycorine and galanthamine, two alkaloids extracted from *Galanthus elwesii*. We conducted a comprehensive study to assess the antiviral and antiparasitic potential of lycorine and galanthamine, two alkaloids whose biosynthetic production was significantly increased by zinc supplementation. DFT calculations revealed that lycorine has a lower  $E_{\text{gap}}$  than galanthamine, suggesting higher reactivity and lower stability, enhancing its potential as a drug candidate. Pharmacokinetic profiling indicated that galanthamine (TPSA: 41.93 Å<sup>2</sup>, logP: 0.797) has a lower total polar surface area (TPSA) and higher lipophilicity (logP) compared to lycorine (TPSA: 62.16 Å<sup>2</sup>, logP: -0.268), indicating that galanthamine may possess superior absorption and permeability characteristics. ADME analysis also identified galanthamine with a lower AMES toxicity score, implying reduced mutagenic risk. A total of nine target proteins, representing viral and parasitic diseases Zika virus, malaria, leishmaniasis, and dengue, were chosen for molecular docking. Molecular docking studies demonstrated that lycorine exhibited superior binding interactions (-8.76 kcal/mol), particularly against Leishmania, and displayed stronger binding affinity across all selected target proteins. Despite galanthamine's lower toxicity profile, lycorine's enhanced reactivity and stronger binding properties suggest its higher efficacy as a therapeutic candidate based on DFT and molecular docking results, while galanthamine shows potential based on its favorable ADME profile.

**Keywords:** Lycorine, Galanthamine, Zinc Supplementation, ADMET, Antiviral, Molecular Docking

© EJBCS. All rights reserved.

### 1. Introduction

Turkey occupies a significant position in the global context of plant diversity and richness, serving as a critical reservoir of various plant species. Among the diverse flora, bulbous tuberous plants, commonly called geophytes, represent a vital component of this biodiversity. According to the TUBIVES database, Turkey is home to an impressive array of 816 geophyte taxa, distributed across 73 genera and 11 families. The geographical distribution of these plants is notably concentrated in regions such as the Southwestern Aegean, the Black Sea Region, the Mediterranean Region, and the Taurus Mountains (Anonim 2015; Şekeroğlu et al. 2012).

The species of the Amaryllidaceae family, in which the snowdrop is included, contain alkaloids such as nivalin, galanthamine, tazettin and lycorine, which number up to 150 and are called Amaryllidaceae alkaloids (Ay et al. 2018; Bozkurt et al. 2021). Galanthamine and lycorine exhibit

anti-inflammatory (Kang et al. 2012), anti-cancer (Cimmino et al. 2017; Ying et al. 2017), anti-bacterial, anti-malarial, acetylcholinesterase and butyrylcholinesterase inhibitor (Pesaresi et al. 2022) properties. Lycorine is also known for its potential to affect SARS-CoV-2 infection due to its antiviral activity (Jin et al. 2021), while galanthamine is used in the treatment of Alzheimer's disease and other neurological disorders (Kaur et al. 2022; Pesaresi et al. 2022).

To enhance alkaloid production in selected plant species, zinc was utilized as a nutritional supplement during the growth phase, aiming to stimulate alkaloid biosynthesis. Research indicates that zinc plays a crucial role in plant metabolism and can influence the accumulation of secondary metabolites, including alkaloids. For instance, studies have shown that the presence of zinc can enhance the expression of genes involved in alkaloid biosynthesis pathways, thereby increasing the overall alkaloid content in plants (Sun et al. 2018; Zhang et al. 2020).



Viral and parasitic diseases are significant public health concerns worldwide, as they can lead to severe morbidity and mortality. Zika virus, malaria, leishmaniasis, and dengue are significant infectious diseases that pose substantial public health challenges, particularly in tropical and subtropical regions (Waggoner et al. 2016). Zika virus, primarily transmitted by *Aedes* mosquitoes, is notorious for its association with severe birth defects, such as microcephaly, when contracted during pregnancy. Malaria, caused by *Plasmodium* parasites and transmitted through *Anopheles* mosquitoes, remains a leading cause of morbidity and mortality (Fernando et al. 2013), particularly in sub-Saharan Africa, with the World Health Organization (WHO) estimating approximately 627,000 deaths globally in 2020 (Girard et al. 2020; Subhadra, et al. 2021). Leishmaniasis, transmitted by sandflies and caused by protozoan parasites of the genus *Leishmania*, is prevalent in the Middle East, South Asia, and South America, manifesting in forms that can be fatal if untreated. Dengue fever, caused by the dengue virus and also transmitted by *Aedes* mosquitoes, has seen a dramatic rise in incidence, with an estimated 390 million infections annually and approximately 20,000 deaths each year from severe forms (Ramirez-Jimenez et al. 2013). Addressing these diseases is crucial for their direct health impacts and socio-economic consequences, as they strain healthcare systems and hinder economic development. Dengue fever, classified as the most significant mosquito-borne viral disease, has increased tenfold in incidence over the past three decades, affecting over 100 countries (Ravilala et al. 2018). Similarly, malaria continues to contribute to high rates of child mortality in endemic regions. The emergence and re-emergence of these diseases are linked to climate change, urbanization, and increased human-animal interactions, necessitating comprehensive strategies for prevention, control, and treatment to mitigate their impact on global health.

This study aims to enhance the biosynthesis of galanthamine and lycorine alkaloids in *Galanthus elwesii* Hook through zinc supplementation. This approach aims to increase the production of these bioactive compounds, which have demonstrated antiviral and antiparasitic properties. To further investigate their potential therapeutic applications, molecular docking studies and assessments of physicochemical and pharmacokinetic properties (ADMET) will be conducted.

## 2. Materials and Method

A field experiment was carried out in Suluova, Amasya, Turkey, during the 2018-2019 growing seasons on a previously cultivated field. Bulbs of *G. elwesii* with a diameter exceeding 4 cm, procured from commercial sources, were used as planting material. The experimental design was a randomized complete block design with three replications. Three zinc sulfate ( $ZnSO_4$ ) rates (2.5, 5, and 10 kg/da) were applied.

### 2.1. Extraction method

At the end of the drying process, the roots and bulbs were macerated. The methanol was then evaporated by rotary evaporation and the extracts were obtained. After the

methanol was evaporated from the rotary evaporator, the crude extract obtained was acidified with 10%  $CH_3COOH$  (pH 2-3). The resulting extract was extracted with chloroform to remove oils, waxes, etc. other than alkaloids. The remaining extract was basicised with 25%  $NH_3$  until pH 8-9 to release the alkaloids in the extract and the resulting phase was extracted with chloroform.

### 2.2. Determination of Alkaloid Components by HPLC

HPLC working conditions and gradient elution program were used to quantitatively determine the alkaloid compounds of the extracted plants. The components in the samples were determined according to the retention times of the components in the system. For the quantification, firstly, the standards were taken as single readings and their retention times were determined. Then, mix. solutions of the standards at different concentrations were prepared and it was determined whether galantamine and lycorine caused a change in the retention times. Calibration curves were generated from the mix. solutions, and the amount was calculated.

High-Pressure Liquid Chromatography (HPLC) analysis conditions are given below:

Instrument: Shimadzu Prominence Modular LC20A HPLC; Column oven CTO-10AS VP; Column Used Intersil ODS 3, 5 $\mu$ m 4,6x250 mm; Mobile phase: 95% TFA-water / 5% acetonitrile; Detector: SPD-M20A.

### 2.3. Statistical Analysis

The data obtained were evaluated using the JUMP statistical package program. The Duncan test was used to check the significance of the differences between the means.

### 2.4. Theoretical Details and In-silico Methods

The theoretical investigations of galanthamine and lycorine were conducted using the Gaussian 09 software package and the GaussView 5.0 molecular visualization tool (Frisch et al., 2009). Gaussian 09 is a widely recognized computational chemistry software that facilitates the modeling of molecular systems using quantum mechanical principles. In our study, geometric optimization of the compounds was achieved through Density Functional Theory (DFT), employing Becke's (1988) Three-Parameter Hybrid Functional in conjunction with the Lee, Yang, and Parr (1988) correlation (B3LYP) method. This hybrid functional is well-regarded for its balance of accuracy and computational efficiency in predicting molecular geometries and electronic properties. We utilized the 6-311G(d,p) basis set for our calculations, which is commonly employed in DFT studies as it provides a good compromise between computational cost and accuracy. Including polarization functions (the 'd' in 6-311G(d,p)) is particularly important for accurately describing the electronic environment of the molecules under investigation, ensuring that our results are robust and reliable under ground state conditions in the gas phase.

For the assessment of ADMET (Absorption, Distribution, Metabolism, Excretion, and Toxicity) properties, we utilized the ADMET Lab platform, which is a user-friendly web-based tool that provides predictions of ADMET properties using a multitask graph attention framework. This platform covers various endpoints, including physicochemical properties, ADME characteristics, and toxicity assessments (Xiong et al., 2021). ADMET Lab employs various predictive models that have been validated against experimental data, enhancing the reliability of the predictions. The specific models used in our analysis include those for predicting solubility, permeability, and metabolic stability, which are critical for evaluating the pharmacokinetic profiles of the compounds. The integrated databases within ADMET Lab ensure that the predictions are based on reliable and precise data. Furthermore, the tool utilizes machine learning algorithms trained on extensive datasets, which significantly enhances the accuracy of the predictions. We ensured that the parameters and settings were appropriately configured to reflect the chemical nature of the compounds we were investigating. The tool is accessible online at: <https://admetlab3.scbdd.com/>.

The 3D structures of the malaria food vacuole function (PDB:1YVB), apicoplast maintenance (PDB:2QG8), mitochondrial activity (PDB:4PLT), and lipid biosynthesis (PDB:4ZCR), zika virus, proteins like the Zika virus protease (PDB:5H6V) and NS5 protein (PDB:5TFR), dengue virus NS2B/NS3 Protease (PDB: 2FOM), for leishmania Trypanothione Reductase from Leishmania infantum (PDB:2JK6), and Leishmania mexicana arginase (PDB: 4ITY) were obtained from the RCSB PDB database. Using AutoDock Tools 1.5.6, water molecules were removed, proteins were isolated, nonpolar hydrogens were added, Gasteiger charges were computed, and the structures were saved in PDBQT format. The PubChem database provided the 2D structures of alkaloid candidate compounds named lycorine and galanthamine, which were converted to PDBQT format via Chem3D for docking.

**Table 1** Molecular docking active site coordinates of target proteins

	Dimension Grid Box	Grid Box
<b>1YVB</b>	70.21*-38.10*-84.35	40*60*40
<b>2FOM</b>	5.56*-22.04*2.45	40*40*40
<b>2JK6</b>	19.83*42.98*-2.05	60*60*60
<b>2QG8</b>	5.38*38.00*15.02	40*40*40
<b>4ITY</b>	13.66*14.59*-5.85	60*60*60
<b>4PLT</b>	-1.47*48.30*42.11	40*40*40
<b>4ZCR</b>	13.04*-55.22*255.38	40*40*40
<b>5H6V</b>	-8.20*10.59*-17.25	40*40*40
<b>5TFR</b>	30.03*-40.47*-10.19	40*40*40

The binding site was defined by the ligand coordinates in the target protein complex and tabulated in Table 1. Ligands were modeled as flexible, while the receptor remained rigid. AutoDock 1.1.2 generated 20

conformations per ligand-receptor complex, and the conformation with the highest binding affinity was selected for further analysis. Discovery Studio was used to visualize the docking results.

### 3. Results

The predominant family of bulbous plants in Turkey are Amaryllidaceae, Liliaceae, and Iridaceae, esteemed for their ecological roles and ornamental value (Arslan et al., 2008). In Turkey, the bulbs and tubers of geophytes are harvested from their natural environments and subsequently exported as ornamental plants, thereby playing a significant role in both local and international horticultural markets. However, this practice has raised critical conservation issues, as certain species are increasingly threatened with extinction due to over-collection and habitat degradation (Batı Ay, 2019). Particularly concerning are several species within the genus *Galanthus*, commonly referred to as snowdrops, which have been classified as endangered or vulnerable. These species hold specific conservation statuses, including Critically Endangered (CR), Endangered (EN), and Vulnerable (VU), as documented in the Red Book of Plants of Turkey.

The results of the HPLC study on the effects of zinc supplementation on lycorine and galanthamine reveal significant differences in their flowering and ripening periods. For lycorine, increasing zinc doses resulted in a flowering period of 7.74 kg/da at 2.5 kg/da, which decreased to 2.65 kg/da at 5 kg/da, and then increased to 4.56 kg/da at 10 kg/da, indicating a complex response to zinc levels. In contrast, galanthamine showed a more consistent increase in flowering period with zinc doses, starting at 11.53 kg/da for 2.5 kg/da and peaking at 21.61 kg/da for 5 kg/da, before dropping to 5.76 kg/da at 10 kg/da.

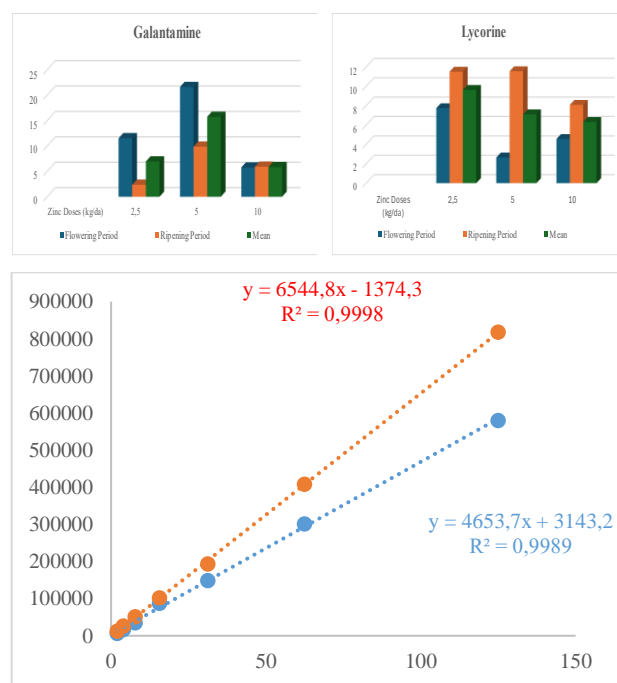


**Fig. 1** Effects of zinc supplementation on the flowering and ripening periods of lycorine (blue), and galanthamine (red)

These findings suggest that zinc plays a crucial role in the biosynthesis of alkaloids in both plant species, potentially influencing their growth and development, which may have implications for their therapeutic efficacy and yield in medicinal applications (Figure 1).

Zinc was added as a nutritional supplement during the growth phase to increase the concentration of alkaloids in the selected plant species. The addition of zinc supports plant growth and promotes the activity of specific transcription factors that regulate alkaloid biosynthesis (Deng et al. 2018). Furthermore, the interaction between zinc and other nutrients can lead to synergistic effects that further enhance alkaloid production (Kamran et al. 2017). This approach underscores the importance of optimizing nutrient management in agricultural practice secondary metabolites, such as alkaloids, which have significant pharmacological properties and economic value.

Density Functional Theory (DFT)-based calculations play a crucial role in drug design by offering a detailed understanding of the electronic properties and reactivity of pharmacophoric groups. This knowledge is essential for optimizing the efficacy and safety of therapeutic agents. These calculations allow researchers to predict how potential drug candidates interact with biological targets, facilitating the identification of compounds with desirable pharmacokinetic and pharmacodynamic properties.

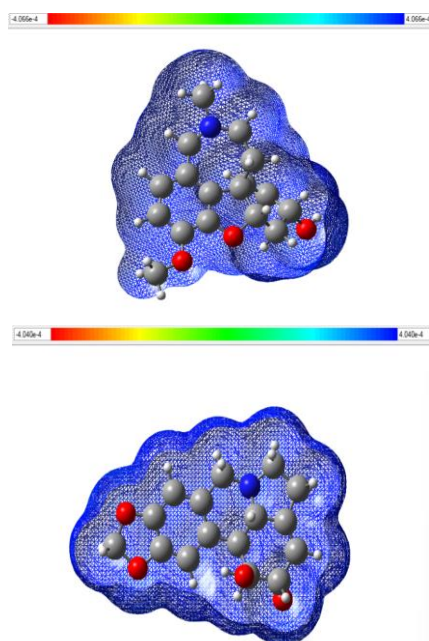


**Fig. 2** Electron density map results of the galanthamine and lycorine

For instance, studies have demonstrated that DFT can be employed to analyze the molecular interactions and binding affinities of alkaloids, which are known for their diverse biological activities, including antiviral and antiparasitic effects (Painter et al. 2013, Flores-Holgún et al. 2019). Moreover, integrating DFT calculations with molecular docking studies enhances the understanding of how specific structural features of alkaloids contribute to their biological activity. This approach enables the identification of key pharmacophoric elements that can be further optimized to

improve drug-like properties, such as solubility, permeability, and metabolic stability, as assessed through ADMET (Absorption, Distribution, Metabolism, Excretion, and Toxicity) analysis (Frau & Flores-Holgún, 2019; Flores-Holgún et al. 2019). Consequently, DFT-based methodologies are invaluable in rationalizing novel therapeutic agents targeting viral and parasitic diseases, ultimately leading to the development of more effective and safer pharmaceuticals.

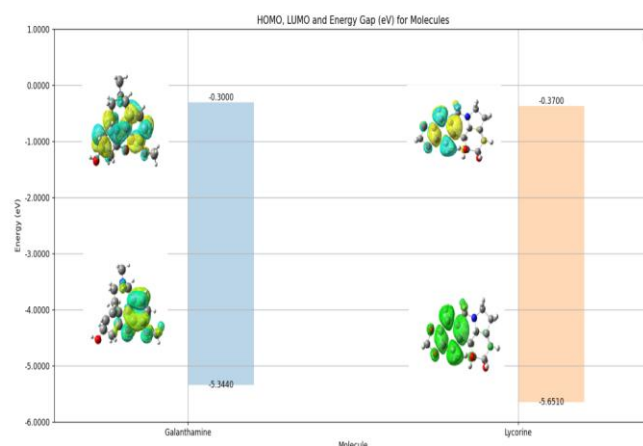


**Fig. 3** FMO of galanthamine, and lycorine

To calculate the global reactivity values for galanthamine and lycorine based on their frontier molecular orbital (FMO) energies, we can utilize the energy gap ( $E_{\text{gap}}$ ) derived from density functional theory (DFT) calculations via with the Gaussian 09 W package and GaussView 5.0 programmes (Dennington et al. 2009; Frisch et al. 2009). The energy gap is defined as the difference between the lowest unoccupied molecular orbital (LUMO) energy and the highest occupied molecular orbital (HOMO) energy (Khaled et al., 2022). This energy gap can be used to derive important global reactivity parameters such as electron affinity (EA), electronegativity ( $\chi$ ), chemical hardness ( $\eta$ ), and chemical softness ( $S$ ), which provide insights into the stability and reactivity of these alkaloids (Khelifaoui et al. 2020). The calculated HOMO and LUMO energies for galanthamine and lycorine (Figure 3) offer valuable information about their reactivity profiles, with the data indicating that lycorine has a smaller energy gap ( $E_{\text{gap}}$ ) of 5.282 eV compared to galanthamine's  $E_{\text{gap}}$  of 5.314 eV. This smaller  $E_{\text{gap}}$  for lycorine suggests higher reactivity and lower stability, which may enhance its potential as a drug candidate.

The ADMET profiles obtained for galanthamine and lycorine reveal important pharmacokinetic and toxicity characteristics critical for their potential therapeutic applications (Figure 4). In the radar chart, the green color represents the minimum values a drug candidate can have, while the blue color indicates the possible maximum values. The yellow color represents the values for the selected alkaloids. The TPSA, logP, logS, hydrogen bond donor and acceptor numbers, and ring numbers for AAAS and AAAC alkaloids fall within the maximum and minimum ranges. However, the logD (octanol/water distribution) values for these alkaloids are lower than the minimum threshold.

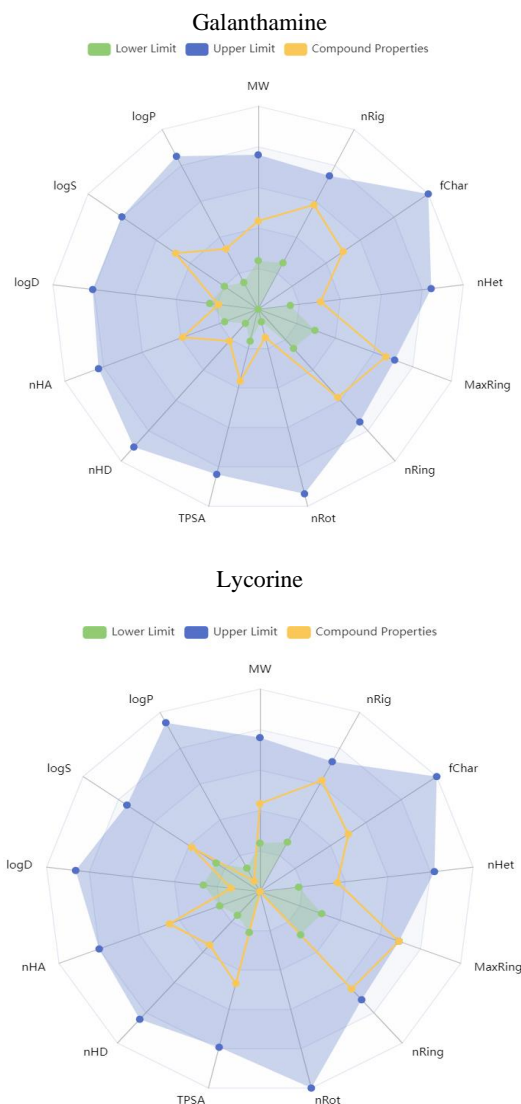


**Fig. 4** Radar view of the pharmacokinetic properties

Galanthamine, with a TPSA of 41.93 Å<sup>2</sup> and a logP of 0.797, demonstrates favorable absorption and permeability, while its CL<sub>plasma</sub> of 6.176 ml/min/kg indicates moderate clearance. In contrast, lycorine exhibits a higher TPSA of 62.16 Å<sup>2</sup> and a lower logP of -0.268, suggesting differences in their distribution and solubility profiles. In terms of metabolic interactions, galanthamine is identified as a CYP2C19 substrate, whereas lycorine acts as a CYP2D6 inhibitor, which could influence their pharmacokinetic behavior and drug-drug interactions.

The half-life (T<sub>1/2</sub>) of galanthamine is significantly longer at 5.088 hours compared to lycorine's 2.987 hours, suggesting that galanthamine may provide more sustained therapeutic effects. Additionally, while both compounds show potential for drug-induced liver injury (DILI) and carcinogenicity, lycorine has a higher AMES toxicity score, indicating a greater risk of mutagenicity compared to galanthamine (Table 2).

In the molecular docking analysis for malaria, the binding affinities of galanthamine and lycorine were evaluated against the food vacuole protein (PDB: 1YVB; Wang, et al.,

2006), with galanthamine exhibiting a binding energy of -6.09 kcal/mol and lycorine showing a stronger binding energy of -6.54 kcal/mol.

Both compounds formed hydrogen bonds with the amino acid residues MET(oa) and TYR(OC) for galanthamine, while lycorine interacted with SER111 and MET(OA), highlighting their distinct binding profiles; additionally, both compounds demonstrated  $\pi$ -alkyl interactions with PRO113, suggesting a favorable interaction with the target protein that may enhance their potential as therapeutic agents against malaria.

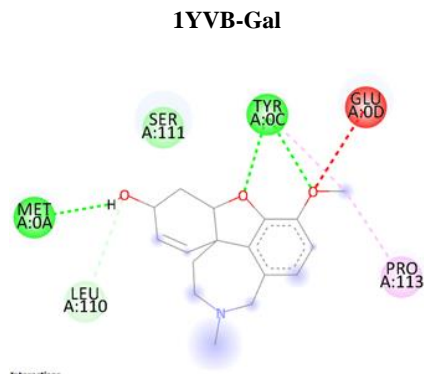
**Table 2** Some ADMET parameters of the galanthamine (GAL) and lycorine (LYC)

	GAL	LYC	Limit value
TPSA	41.93	62.16	Opt:0-140
logP	0.797	-0.268	0-3
logS	-1.855	-2.767	-4
QED	0.801	0.69	Drug-likeness score >0.67
Caco-2 Permeability	-4.313	-5.148	<-5.15
F50%	0.1	0.1	50% bioavailability
PPB	21.3%	64.15	Plasma protein binding <90%
BBB	0.9	0.9	Blood brain barrier
CYP2C19 substrate	0.7-0.9	-	-
CYP2D6 inhibitor	-	0.9-1	-
CL <sub>plasma</sub>	6.176	6.257	5-15 ml/min/kg moderate
T <sub>1/2</sub>	5.088	2.987	>4 short half-life drug 4-8 intermediate
AMES Toxicity	0.559	0.778	0 (-) 1(+)
DILI	0.461	0.426	Drug induced liver injury 0 (-) 1(+)
Carcinogenicity	0.726	0.817	0 (-) 1(+)
hERG Blockers	0.358	0.209	IC <sub>50</sub> <10 $\mu$ M

The interaction of galanthamine and lycorine with the acyl carrier protein synthase, which is essential (Figure 5) for the function of acyl carrier proteins in covalently binding nascent fatty acids during biosynthesis, was assessed using molecular docking studies. The Protein Data Bank entry PDB 2QG8 was utilized for this analysis (Nguyen, et al. 2022). The binding energies obtained were -5.29 kcal/mol for galanthamine and -4.98 kcal/mol for lycorine, indicating relatively low binding affinities. Given these values, it can be concluded that the interaction between these alkaloids and the acyl carrier protein synthase is insufficient to suggest an active role, thereby indicating that galanthamine and lycorine are unlikely to be effective in targeting this protein for therapeutic purposes.

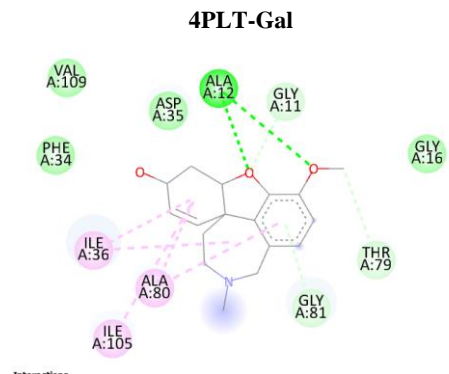
The molecular docking analysis of dihydroorotate dehydrogenase, a crucial druggable target in the mitochondria (PDB: 4PLT, Boucher, et al., 2014), highlights its significant role in malaria pathogenesis, particularly in electron transport and protein synthesis.





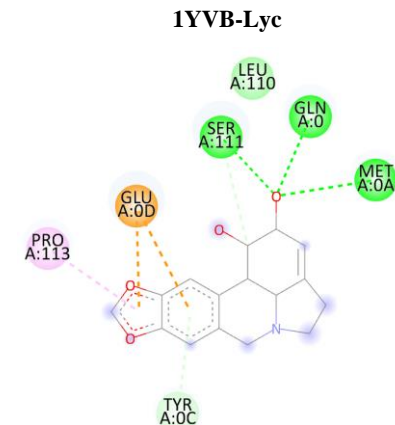
**Interactions**

- van der Waals
- Conventional Hydrogen Bond
- Carbon Hydrogen Bond
- Unfavorable Acceptor-Acceptor
- Alkyl
- Pi-Alkyl



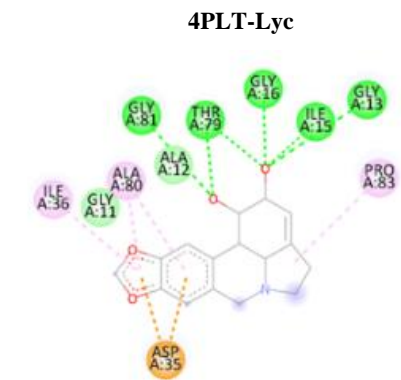
**Interactions**

- van der Waals
- Conventional Hydrogen Bond
- Carbon Hydrogen Bond
- Pi-Donor Hydrogen Bond
- Alkyl
- Pi-Alkyl

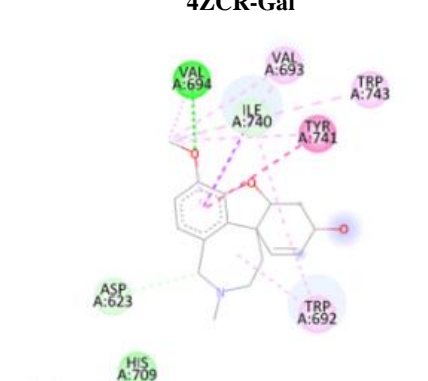


**Interactions**

- van der Waals
- Conventional Hydrogen Bond
- Carbon Hydrogen Bond
- Pi-Anion
- Pi-Donor Hydrogen Bond
- Pi-Alkyl

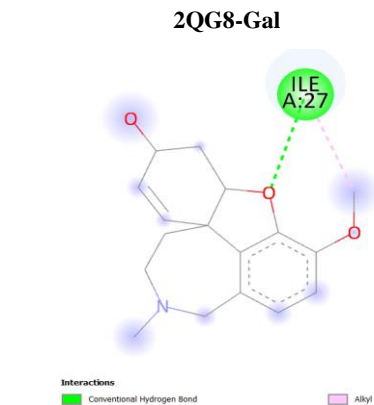


**4ZCR-Gal**



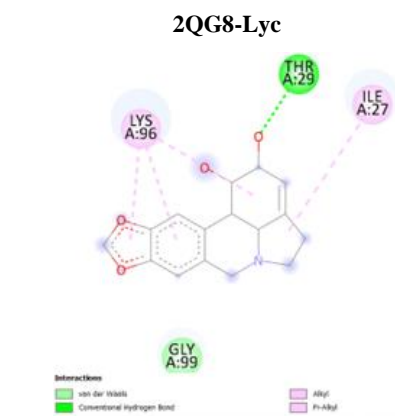
**Interactions**

- van der Waals
- Conventional Hydrogen Bond
- Carbon Hydrogen Bond
- Pi-Sigma
- Pi-H-T-Stack
- Alkyl
- Pi-Alkyl



**Interactions**

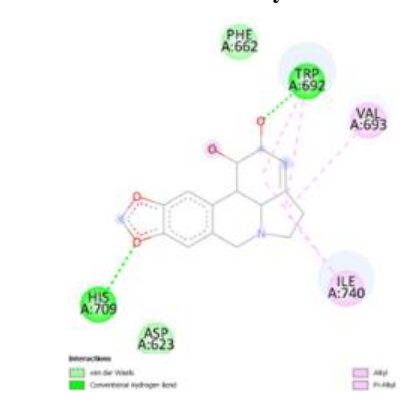
- Conventional Hydrogen Bond
- Alkyl



**Interactions**

- van der Waals
- Conventional Hydrogen Bond
- Alkyl
- Pi-Alkyl

**4ZCR-Lyc**



**Interactions**

- van der Waals
- Conventional Hydrogen Bond
- Alkyl
- Pi-Alkyl

**Fig. 5** 2D visualization of the related Malaria disease proteins with the galanthamine (Gal), and lycorine (Lyc) compounds

**Fig. 6** 2D visualization of the related Malaria disease proteins as PDB code 4PLT and 4ZCR with the galanthamine (Gal), and lycorine (Lyc) compounds

Lycorine exhibits a notably stronger binding affinity to this target, suggesting its potential as an effective therapeutic agent. This enhanced binding is supported by the electron density map from Gaussian calculations, confirming the structural compatibility of lycorine with the target protein. Additionally, key hydrogen bonds between lycorine and the residues Asn14, Ile15, and Asn127 were identified, indicating specific interactions that may enhance its efficacy in inhibiting the enzyme and disrupting malaria pathogenesis. The molecular docking analysis of dihydroorotate dehydrogenase, a crucial druggable target in the mitochondria (PDB: 4PLT, Boucher, et al., 2014), highlights its significant role in malaria pathogenesis, particularly in electron transport and protein synthesis. Lycorine exhibits a notably stronger binding affinity to this target, suggesting its potential as an effective therapeutic agent. This enhanced binding is supported by the electron density map from Gaussian calculations, confirming the structural compatibility of lycorine with the target protein. Additionally, key hydrogen bonds between lycorine and the residues Asn14, Ile15, and Asn127 were identified, indicating specific interactions that may enhance its efficacy in inhibiting the enzyme and disrupting malaria pathogenesis (Figure 6).

The molecular docking analysis targeting Plasmodium CCT, a crucial enzyme involved in malaria lipid biosynthesis, was conducted using the C-terminal catalytic domain of Plasmodium falciparum CTP:phosphocholine cytidyltransferase (PDB: 4ZCR, Guca, et al. 2018). The results indicated that lycorine engages in  $\pi$ -alkyl interactions with the phenanthridine moiety of its structure, while also forming hydrogen bonds with the oxygen atoms present in the diol and dioxolo regions. In contrast, galanthamine establishes hydrogen bonds with the substituted oxygen atoms in its benzofuran framework, alongside  $\pi$ -alkyl interactions with the azepine component of its structure. These distinct binding interactions suggest that both alkaloids may effectively inhibit Plasmodium CCT, thereby contributing to their potential as therapeutic agents against malaria.

The molecular docking results targeting Zika virus protease (PDB: 5H6V) (Li, et al. 2017), and NS5 protein (PDB: 5TFR) (Upadhyay, 2017), indicate that lycorine exhibits a significantly stronger binding affinity compared to galanthamine. Specifically, the active binding site for lycorine is identified as the phenanthridine-1,2-diol moiety, which facilitates effective interactions with the target proteins. In contrast, galanthamine's binding involves the nitrogen atom in the azepine ring, which participates in hydrogen bond formation (Figure 7). These findings suggest that lycorine may serve as a more promising candidate for the development of therapeutic agents against Zika virus, given its enhanced binding efficacy and the critical role of these proteins in the viral lifecycle.

We thoroughly examined the interactions of alkaloids with the Dengue Virus NS2B/NS3 protease (PDB: 2FOM), a critical target for dengue viral disease.

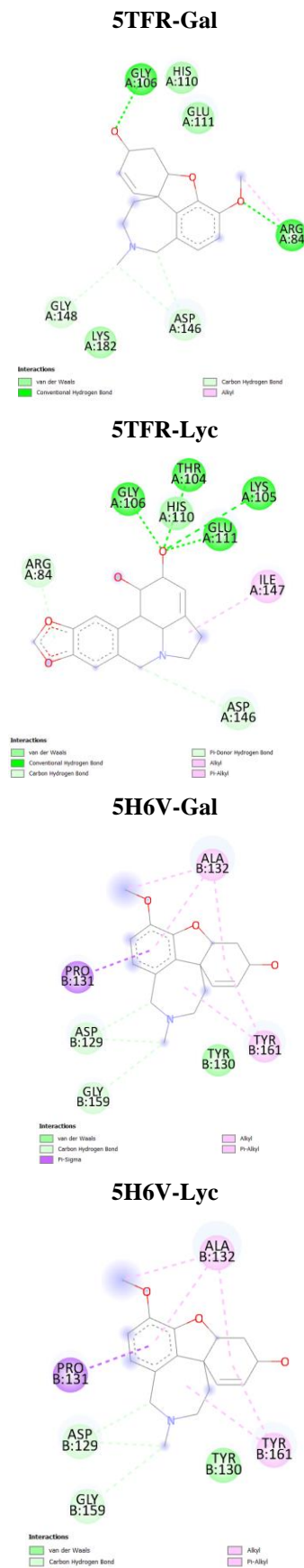


**Fig. 7** Binding interaction visualization of the Zika virus protease and NS5 protein with the galanthamine (left), and lycorine (right) compounds



Lycorine exhibited a binding energy of -7.76 kcal/mol, indicating a stronger affinity than galanthamine, which had a binding energy of -6.45 kcal/mol (Figure 8). Galanthamine formed hydrogen bonds with Lys74 through its benzofuran ring and Ala164 and Asn152 via its hydroxy substituent. In contrast, lycorine established hydrogen bonds with several residues, including Val146, Gly87, Trp83, Leu149, and Asn152, in addition to interacting with the oxygen atoms present in its molecular structure (Erbel, et al. 2006).

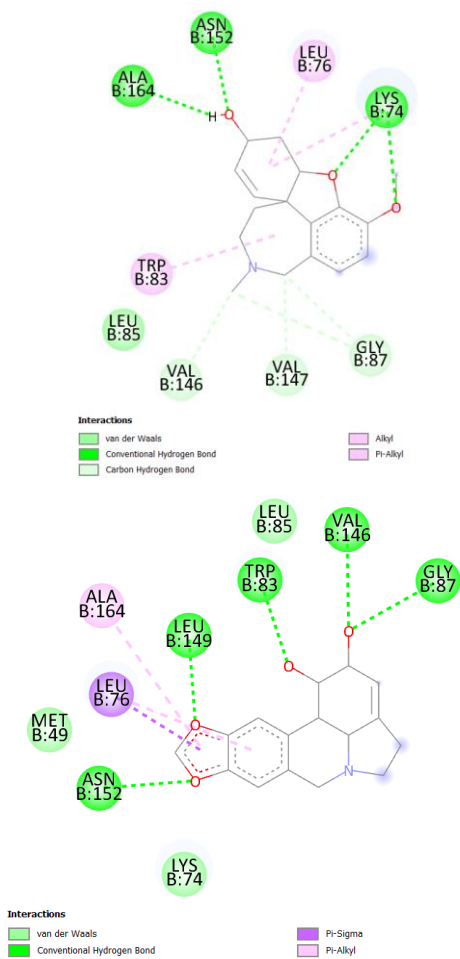


**Fig. 8** Binding interaction visualization of target protein 2FOM with the galanthamine (top), and lycorine (bottom) compounds

The molecular docking analysis targeting arginase from the parasitic protozoa *Leishmania*, specifically *Leishmania mexicana* (PDB: 4ITY), (D’Antonio, et al., 2013), highlights its potential as a drug target for the treatment of leishmaniasis. The results indicate that lycorine exhibits a binding energy of -7.45 kcal/mol, demonstrating a stronger affinity than galanthamine, which has a binding energy of -6.10 kcal/mol. Both compounds interact with the active site of the enzyme, with lycorine forming hydrogen bonds with key residues such as Asn14, Ile15, and Asn127.

In contrast, galanthamine's binding involves hydrogen bonding with the nitrogen atom in the azepine ring (Figure 9).

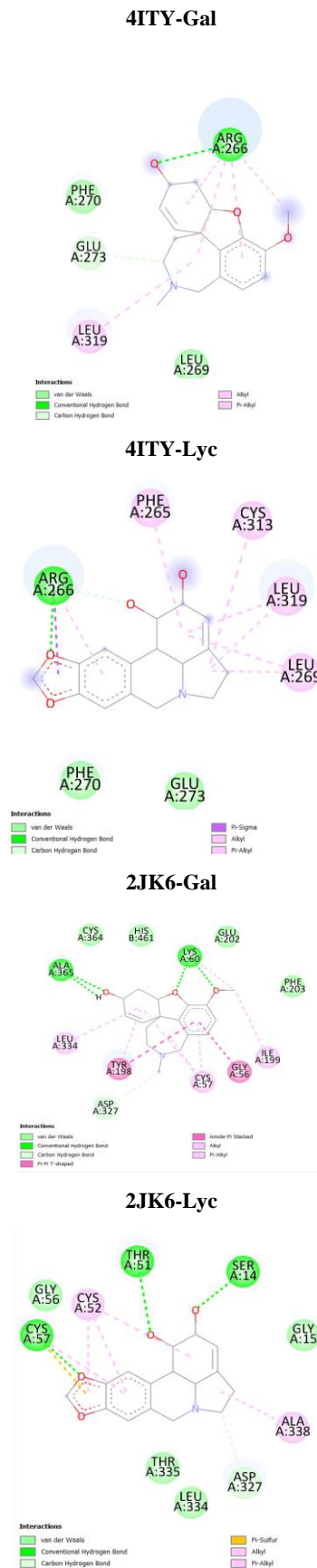


**Fig. 9** Binding interaction visualization of target protein 4ITY and 2JK6 with the galanthamine (left), and lycorine (right) compounds

These findings suggest that lycorine may be a more effective inhibitor of Leishmania arginase, potentially disrupting polyamine biosynthesis essential for the parasite's growth and survival. The final docking results for the structure of Trypanothione Reductase from Leishmania infantum, a human protozoan parasite belonging to the Trypanosomatidae family, indicate significant binding affinities for the selected compounds. The protein structure analyzed is PDB: 2JK6 (Baiocco, et al. 2009), which exhibited the highest binding energy values among the target proteins evaluated. Specifically, lycorine demonstrated a binding energy of -8.76 kcal/mol, while galanthamine showed a binding energy of -8.49 kcal/mol. These findings suggest that both compounds have strong potential as inhibitors of Trypanothione Reductase, which may contribute to their efficacy in treating leishmaniasis.

#### 4. Discussion

These results indicate that zinc as a nutritional supplement significantly enhances the concentration of alkaloids in selected plant species. This finding aligns with previous research demonstrating the role of zinc in promoting plant growth and its involvement in activating transcription factors that regulate alkaloid biosynthesis (Onyeonagu 2012). The synergistic effects observed when zinc is combined with other nutrients further emphasize the need to optimize nutrient management in agricultural practices to maximize the production of secondary metabolites, such as alkaloids, known for their pharmacological properties and economic significance (Helander et al. 2016).

**Table 3** Some global reactivity parameters of the alkaloids

	Galanthamine	Lycorine
HOMO(eV)	-5.344	-5.651
LUMO(eV)	-0.30	-0.370
E <sub>gap</sub>	5.314	5.282
(EA)*	0.30	0.370
( $\chi$ )*	2.687	3.010
( $\eta$ )*	2.657	2.641
(S)*	0.188	0.189

\* I; ionization potential ( $I = -E_{\text{HOMO}}$ ), A; electron affinity ( $A = -E_{\text{LUMO}}$ ),  $\chi$ ; electronegativity ( $\chi = (I + A)/2$ ),  $\eta$ ; chemical hardness ( $\eta = (I - A)/2$ ), S; chemical softness ( $S = 1/2\eta$ ).

The integration of Density Functional Theory (DFT) calculations in the analysis of alkaloids provides valuable understanding of their electronic properties and reactivity, which are crucial for drug design (Jain et al. 2023). Furthermore, lycorine exhibits higher electron affinity (0.370 eV) and chemical softness (0.189) relative to galanthamine, which has an electron affinity of 0.030 eV and a chemical softness of 0.188. These properties indicate that lycorine has a greater ability to accept electrons and a more favourable interaction profile with biological targets (Table 3). Consequently, these findings suggest that both compounds may be effective as drug candidates, with lycorine particularly well-positioned for further exploration in treating viral and parasitic diseases.

Additionally, the electrostatic potential maps generated from these calculations can elucidate the interaction sites

and binding affinities of these alkaloids, enhancing our understanding of their potential therapeutic applications.

The ADMET profiles of galanthamine and lycorine reveal significant pharmacokinetic and toxicity characteristics that are crucial for their potential therapeutic applications. Galanthamine demonstrates favorable absorption and permeability, with a TPSA of 41.93 Å<sup>2</sup> and a logP of 0.797, indicating its suitability for central nervous system (CNS) targeting, which is essential for its role as an acetylcholinesterase inhibitor in Alzheimer's disease treatment (Sancha et al., 2023). In contrast, lycorine presents a higher TPSA of 62.16 Å<sup>2</sup> and a lower logP of -0.268, suggesting challenges in its distribution and solubility profiles, which may limit its bioavailability (Bui, 2022). The pharmacokinetic parameters further differentiate the two compounds; galanthamine has a longer half-life (T<sub>1/2</sub>) of approximately 5.088 hours compared to lycorine's 2.987 hours, potentially allowing for more sustained therapeutic effects in clinical settings (Zhang et al., 2021).

The low AMES toxicity score of galanthamine indicates a reduced risk of mutagenic effects, thereby establishing a favorable safety profile for long-term administration (Shahid et al., 2016). This is particularly significant given the chronic nature of diseases such as Alzheimer's, which often necessitate prolonged therapeutic interventions, especially in vulnerable populations like the elderly. Consequently, this finding strongly supports the continued development of galanthamine as a therapeutic agent. Conversely, while lycorine has demonstrated promising anticancer efficacy, its toxicity profile warrants a comprehensive investigation (Ali et al., 2013). A thorough understanding of the underlying mechanisms of toxicity and the establishment of safe dosage ranges is imperative to ensure that the therapeutic benefits outweigh the potential adverse effects. In-depth investigations into the toxicity of lycorine using various in vitro and in vivo models can provide valuable insights into its safety profile and guide its development as a viable therapeutic option (Han et al., 2013).

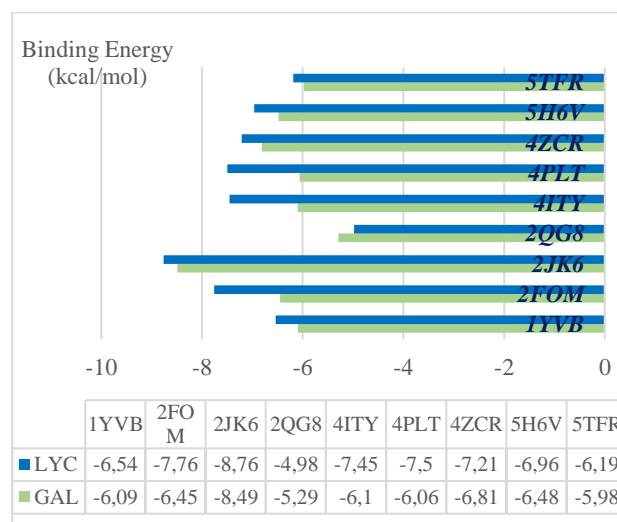


**Fig. 10** Comparison of binding affinities of GAL and LYC alkaloids across selected target proteins

In the context of drug discovery, computational methods such as molecular docking have become instrumental in predicting the binding interactions between potential inhibitors and their target enzymes. The results presented indicate the binding affinities of galanthamine and lycorine compounds to the title proteins related to Zika virus, malaria, leishmaniasis, and dengue as represented by the PDB code 1YVB, 2FOM, 2JK6, 2QG8, 4ITY, 4PLT, 4ZCR, 5H6V, 5TFR with negative values reflecting favourable binding interactions.

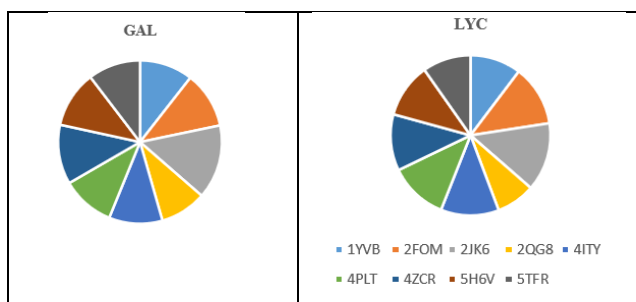


**Fig. 11** General aspect of the GAL, LYC against target proteins

When evaluating the binding affinities of the selected alkaloids, galanthamine (GAL) and lycorine (LYC), against the target proteins, GAL demonstrated a more favorable binding profile, specifically against the target protein 2QG8, which is the apicoplast is a vital organelle in the malaria parasite *Plasmodium falciparum*, playing a crucial role in various metabolic processes essential for the parasite's survival and development. However, for all other proteins, LYC exhibited stronger binding affinities (Figure 10). As depicted in Figure 11, among the target proteins analyzed, the best binding was observed for the protein with the PDB code 2JK6.

## 5. Conclusion

This study demonstrates that zinc supplementation significantly enhances alkaloid biosynthesis in *Galanthus elwesii*, with optimal zinc doses of 2.5 kg/da for lycorine and 5 kg/da for galanthamine. The molecular docking studies conducted on various targets relevant to malaria, leishmania, and viral diseases such as Zika and Dengue provide significant information about the binding affinities and potential therapeutic applications of the alkaloids lycorine and galanthamine. The DFT analysis indicates that lycorine possesses a smaller energy gap ( $E_{\text{gap}}$ ) of 5.282 eV compared to galanthamine's 5.314 eV, suggesting greater reactivity and potential as a therapeutic agent. While both alkaloids exhibit promising binding affinities, particularly to Trypanothione Reductase from *Leishmania infantum* (PDB: 2JK6), lycorine demonstrates superior binding energy of -8.76 kcal/mol, indicating its potential effectiveness against leishmaniasis. Conversely, galanthamine, with a longer half-life ( $T_{1/2}$ ) of 5.088 hours compared to lycorine's 2.987 hours, and favorable ADMET properties—such as a TPSA of 41.93 Å<sup>2</sup> and a logP of 0.797—remains a strong candidate for therapeutic applications, particularly in conditions requiring sustained effects. Overall, these findings underscore the therapeutic

promise of both alkaloids, warranting further investigation into their roles in treating viral and parasitic diseases.

## Acknowledgments

This research received no specific grant from funding agencies in the public, commercial, or not-for-profit sectors.

## Authors' contributions:

M.G: Writing – review & editing, Writing an original draft, Methodology, Investigation, Formal analysis, Data curation, Conceptualization. E.B.A: Writing – review & editing, Writing – original draft, Methodology, Investigation, Formal analysis, Data curation.

## Conflict of interest disclosure:

The authors confirm that there are no financial or personal relationships that could have influenced the research or findings presented in this paper.

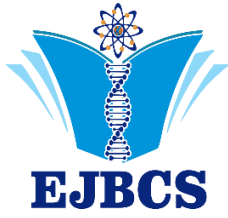
## References

- Anonim 2015. TUBİVES. <http://turkiyegeofitleri.com/Templates/Geofit%20Turleri.html> (Erişim: April 20)
- Ali SK, Hamed AR, Soltan MM, Hegazy UM, Elgorashi E, El-Garf IA, ... Hussein AA. 2013. In-vitro evaluation of selected egyptian traditional herbal medicines for treatment of alzheimer disease. *BMC Complement Altern Med.* 13(1).
- Arslan N, Sarıhan EO, İpek A. 2008. Farklı Soğan Kesme Yöntemlerinin *Fritillaria persica* L.'nın Bazı Özellikleri Üzerine Etkisi. *J Agr Sci-Tarım Bil.* 14(3): 246–250.
- Ay EB, Gül M, Açıkgöz MA, Yarılgöç T, Kara SM. 2018. Assessment of antioxidant activity of giant snowdrop (*Galanthus elwesii* Hook) extracts with their total phenol and flavonoid contents. *Indian J Pharm Educ Res.* 52:128–132.
- Baiocco P, Colotti G, Franceschini S, Ilari A. 2009. Molecular basis of antimony treatment in leishmaniasis. *J Med Chem.* 52(8): 2603-2612.
- Batu Ay E. 2019. Farklı Fosfor ve Çinko Dozları Uygulanan Kardelende (*Galanthus elwesii* Hook.) Fenolik Bileşikler, Alkaloit İçeriği ve Antioksidan Aktivitenin Bitki Organlarına ve Gelişme Dönemlerine Göre Değişimi. Doktora Tezi. Ordu Üniversitesi, Ordu, Türkiye.
- Becke AD. 1988. Density-functional exchange-energy approximation with correct asymptotic behavior. *Phys Rev A.* 38(6): 3098.
- Boucher JI, Jacobowitz JR, Beckett BC, Classen S, Theobald DL. 2014. An atomic-resolution view of neofunctionalization in the evolution of apicomplexan lactate dehydrogenases. *eLife.* 3: e02304.
- Bozkurt B, Kaya GI, Onur MA, Unver-Somer N. 2021. Chemo-profiling of some Turkish *Galanthus* L. (Amaryllidaceae) species and their anticholinesterase activity. *S Afr J Bot.* 136: 65–69.
- Bui TQ, Hai NTT, Van Chen T, Quy PT, Du L NH, Cuong TD, ... Nhung NTA. 2022. Theoretical study on inhibitability of some natural alkaloids against influenza virus hemagglutinin and sars-cov-2 main protease. *Vietnam J of Chem.* 60(4):502-517.
- Cimmino A, Masi M, Evidente M, Superchi S, Evidente A. 2017. Amaryllidaceae alkaloids: absolute configuration and biological activity. *Chirality.* 29: 486–499.
- D'Antonio EL, Ullman B, Roberts SC, Dixit UG, Wilson ME, Hai Y, Christianson DW. 2013. Crystal structure of arginase from *Leishmania mexicana* and implications for the inhibition of

- polyamine biosynthesis in parasitic infections. *Arch Biochem Biophys.* 535(2): 163-176.
- Deng X, Zhao L, Fang T, Xiong Y, Ogotu C, Yang D, ... Han Y. 2018. Investigation of benzyloisoquinoline alkaloid biosynthetic pathway and its transcriptional regulation in lotus. *Horticulture Research*, 5:(1).
- Dennington R, Keith T, Millam J. 2009. GaussView, version 5.
- Ekim T, Koyuncu M, Vural M, Duman H, Aytac Z, Adiguzel N. 2000. Türkiye Bitkileri Kırmızı Kitabı. Doğal Hayatı Koruma Derneği, Ankara.
- Erbel P, Schiering N, D'Arcy A, Renuis M, Kroemer M, Lim S. P., ... Hommel U. 2006. Structural basis for the activation of flaviviral NS3 proteases from dengue and West Nile virus. *Nat Struct Mol Biol.* 13(4):372-373.
- Fernando SD, Navaratne CJ, Galappaththy GNL, Abeyasinghe R, Silva N, Wickermasinghe R. 2013. The importance of accuracy in diagnosis of positive malaria cases in a country progressing towards malaria elimination. *J Global Infect Dis.* 5(4): 127.
- Flores-Holgún N, Frau J, Glossman-Mitnik D. 2019. Chemical-reactivity properties, drug likeness, and bioactivity scores of seragamides a-f anticancer marine peptides: conceptual density functional theory viewpoint. *Computation.* 7(3): 52.
- Frau J, Flores-Holgún N. 2019. Chemical reactivity theory and empirical bioactivity scores as computational peptidology alternative tools for the study of two anticancer peptides of marine origin. *Molecules.* 24(6):1115.
- Frisch MJ, Trucks, GWHB, Schlegel GE, Scuseria MA, Robb JR, Cheeseman G, Scalmani V, Barone GA, Petersson H, Nakatsuji X, Li M, Caricato A, Marenich J, Bloino BG, Janesko R, Gomperts B, Mennucci HP, Hratchian JV, Ortiz AF, Izmaylov JL, Sonnenberg D, Williams-Young F, Ding F, Lipparini F, Egidi J, Goings B, Peng A, Petrone T, Henderson D, Ranasinghe VG, Zakrzewski J, Gao N, Rega G, Zheng W, Liang M, Hada M, Ehara K, Toyota R, Fukuda J, Hasegawa M, Ishida T, Nakajima Y, Honda O, Kitao H, Nakai T, Vreven K, Throssell JA, Montgomery Jr JE, Peralta F, Ogliaro M, Bearpark JJ, Heyd E, Brothers KN, Kudin VN, Staroverov T, Keith R, Kobayashi J, Normand K, Raghavachari A, Rendell JC, Burant SS, Iyengar J, Tomasi M, Cossi JM, Millam M, Klene C, Adamo R, Cammi JW, Ochterski RL, Martin K, Morokuma O, Farkas JB, Foresman DJ, Fox Gaussian Inc, Wallingford CT, Revision C.01, 2009.
- Girard M, Nelson CP, Picot V, Gubler DJ. 2020. Arboviruses: a global public health threat. *Vaccine* 38(24): 3989-3994.
- Guca E, Nagy GN, Hajdú F, Marton L, Izrael R, Hoh F, ... Cerdan R. 2018. Structural determinants of the catalytic mechanism of Plasmodium CCT, a key enzyme of malaria lipid biosynthesis. *Scientific Reports.* 8(1): 11215.
- Han S, Chin Y, Choi YH. 2013. A new approach for pharmacokinetic studies of natural products: measurement of isoliquiritigenin levels in mice plasma, urine and feces using modified automated dosing/blood sampling system. *Biomed Chromatogr.* 27(6): 741-749.
- Helander M, Phillips T, Faeth S, Bush L, McCulley R, Saloniemi I, ... Saikkonen K. 2016. Alkaloid quantities in endophyte-infected tall fescue are affected by the plant-fungus combination and environment. *J Chem Ecol.* 42(2): 118-126.
- Jain P, Kumar A, Singh P, Kumari K, Bahadur I, Mohammad F, ... & Kaushik NK. 2023. Eutectic mixtures to enhance the solubility of active pharmaceutical ingredients: density functional theory and infrared spectroscopy approaches. *ChemistrySelect.* 8(25): 1-9.
- Jin YH, Min JS, Jeon S, Lee J, Kim S, Park T, Park D, Jang MS, Park CM, Song JH, Kim HY, Kwon S. 2021. Lycorine, a non-nucleoside RNA dependent RNA polymerase inhibitor, as potential treatment for emerging coronavirus infections. *Phytomedicine.* 86: 153440.
- Kamran S, Shahid I, Baig DN, Rizwan M, Malik KA, Mehnaz S. 2017. Contribution of zinc solubilizing bacteria in growth promotion and zinc content of wheat. *Front. Microbiol.* 8.
- Kaur H, Chahal S, Jha P, Lekhak MM, Shekhawat MS, Naidoo D, Arencibia AD, Ochatt SJ, Kumar V. 2022. Harnessing plant biotechnology-based strategies for in vitro galanthamine (GAL) biosynthesis: a potent drug against Alzheimer's disease. *PCTOC.* 149.1: 81-103.
- Khaled D, Elshakre ME, Noamaan MA, Butt H, Fattah MM., Gaber DA. 2022. A computational qsar, molecular docking and in vitro cytotoxicity study of novel thiouracil-based drugs with anticancer activity against human-dna topoisomerase ii. *Int J Mol Sci.* 23(19): 11799.
- Khelfaoui H, Harkati D, Saleh BA. 2020. Molecular docking, molecular dynamics simulations and reactivity, studies on approved drugs library targeting ace2 and sars-cov-2 binding with ace2. *JBSD.* 39(18): 7246-7262.
- Kong CK, Low LE, Siew WS, Yap WH, Khaw KY, Ming LC, Mocan A, Goh BH, Goh PH. 2021. Biological activities of snowdrop (*Galanthus* spp., Family Amaryllidaceae). *Front Pharmacol.* 11: 552453
- Lee C, Yang W, Parr RG. 1988. Development of the Colle-Salvetti correlation-energy formula into a functional of the electron density. *Phys Rev B.* 37(2): 785.
- Li Y, Zhang Z, Phoo WW, Loh YR, Wang W, Liu S, ... Kang C. 2017. Structural dynamics of Zika virus NS2B-NS3 protease binding to dipeptide inhibitors. *Structure.* 25(8): 1242-1250.
- Nguyen PTV, Nguyen GLT, Dinh OT, Duong CQ, Nguyen LH, Truong TN. 2022. In search of suitable protein targets for anti-malarial and anti-dengue drug discovery. *Journal of Molecular Structure.* 1256: 132520.
- Onyeonagu, C. 2012. Anti-nutrient components of guinea grass (*panicum maximum*) under different nitrogen fertilizer application rates and cutting management. *Afr J Biotechnol.* 11(9):2236-2240.
- Painter P P, Pemberton RP, Wong BM, Ho KC, Tantillo DJ. 2013. The viability of nitron-alkene (3 + 2) cycloadditions in alkaloid biosynthesis. *The Journal of Organic Chemistry,* 79(1): 432-435.
- Pesaresi A, Lamba D, Vezenkov L, Tsekova D, Lozanov V. 2022. Kinetic and structural studies on the inhibition of acetylcholinesterase and butyrylcholinesterase by a series of multitarget-directed galanthamine-peptide derivatives. *Chem Biol Interact.* 365: 110092
- Ramirez-Jimenez R, Zarate-Nahon EA, Alvarado-Moreno MS, Sánchez-Casas R, Laguna-Aguilar M, Sanchez-Rodriguez OS, ... Fernández-Salas I. 2013. Risks of dengue secondary infective biting associated withaedes aegypti in home environments in monterrey, mexico. *Southwestern Entomologist,* 38(1): 99-108.
- Ravilala VK, Ahmed S, Vanka MK, Rajesh S. 2018. Comparison of clinical profile between plasmodium vivax and plasmodium falciparum malaria in children in tertiary care hospital. *Int J Contemp Pediatr.* 5(4); 1294.
- Sancha SAR, Szemerédi N, Spengler G, Ferreira MJU 2023. Lycorine carbamate derivatives for reversing p-glycoprotein-mediated multidrug resistance in human colon adenocarcinoma cells. *Int J Mol Sci.* 24(3):2061.
- Shahid M, Takamiya M, Stegmaier J, Middel V, Gradl M, Klüver N, ... Strähle U. 2016. Zebrafish biosensor for toxicant induced muscle hyperactivity. *Sci Rep.* 6(1).
- Subhadra S, Sabat J, Dwibedi B, Panda S, Mandal MC, Rath S, ... Turuk J. 2021. Prevalence and trend of emerging and re-emerging arboviral infections in the state of odisha. *VirusDisease,* 32(3): 504-510.

- Sun B, Tian Y, Zhang F, Chen Q, Zhang Y, Wang X, ... Tang H. 2018. Variations of alkaloid accumulation and gene transcription in *Nicotiana tabacum*. *Biomolecules*. 8(4): 114. <https://doi.org/10.3390/biom8040114>
- Semerdjieva I, Sidjimova B, Yankova-Tsvetkova E, Kostova M., Zheljazkov, VD. 2019. Study on *Galanthus* species in the Bulgarian flora. *Heliyon*. 5: e03021. <https://doi.org/10.1016/j.heliyon.2019>.
- Şekeroğlu N, Aydın K, Gözüaçık HG, Kulak M. 2012. Kilis ilinde yetişen geofitler. *Türk Bilimsel Derlemeler Dergisi*, 6(1):199-201.
- Upadhyay AK, Cyr M, Longenecker K, Tripathi R, Sun C, Kempf DJ. 2017. Crystal structure of full-length Zika virus NS5 protein reveals a conformation similar to Japanese encephalitis virus NS5. *Acta Crystallogr Sect F Struct Biol Cryst Commun*. 73(3): 116-122.
- Wang SX, Pandey KC, Somoza JR, Sijwali PS, Kortemme T, Brinen LS, ... McKerrow JH. 2006. Structural basis for unique mechanisms of folding and hemoglobin binding by a malarial protease. *PNAS*. 103(31): 11503-11508.
- Waggoner JJ, Gresh L, Vargas MJ, Ballesteros G, Téllez Y, Soda K., ...Pinsky BA. 2016. Viremia and clinical presentation in Nicaraguan patients infected with Zika virus, Chikungunya virus, and dengue virus. *CID*. 63(12): 1584-1590.
- Xiong G, Wu Z, Yi J, Fu L, Yang Z, Hsieh C, ... Cao D. 2021. ADMETlab 2.0: an integrated online platform for accurate and comprehensive predictions of ADMET properties. *Nucleic acids research*. 49(W1): W5-W14.
- Ying X, Huang A, Xing Y, Lan L, Yi Z, He P. 2017. Lycorine inhibits breast cancer growth and metastasis via inducing apoptosis and blocking Src/FAK-involved pathway. *Sci. China Life Sci*. 60: 417-428.
- Yüzbaşıoğlu S. 2008. The development of non-detriment findings for *Galanthus elwesii* Hook. f., in Turkey. NDF Workshop Case Studies, Mexico, 1-13.
- Yüzbaşıoğlu S. 2012. Morphological variations of *Galanthus elwesii* in Turkey and difficulties on identification. *Boccone* 24: 335-339.
- Yüzbaşıoğlu E, Dalyan E. 2017. Effects of plant growth regulators and activated charcoal on in vitro formation of bulblet in snowdrop (*Galanthus woronowii*).
- Zhang W, Yang J, Chen Y, Xue R, Mao Z, Lu W, ... Jiang Y. 2021. Lycorine hydrochloride suppresses stress-induced premature cellular senescence by stabilizing the genome of human cells. *Aging Cell* 20(2).
- Zhang Y, Kang Y, Xie H, Wang Y, Li Y, Huang J. 2020. Comparative transcriptome analysis reveals candidate genes involved in isoquinoline alkaloid biosynthesis in *Stephania tetrandra*. *Planta Med*. 86(17): 1258-1268.





## Sorafenib ve Yalancı portakal ekstresi kombinasyonunun A549 hücre hatları üzerindeki *in vitro* sitotoksik ve antioksidan aktivitesi

Deniz Altun Çolak<sup>1\*</sup>, Heval Kaya<sup>2</sup>, Tuğba Atıcı<sup>3</sup>

<sup>1</sup>Erzincan Binali Yıldırım Üniversitesi, Fen Edebiyat Fakültesi, Biyoloji Bölümü, Erzincan, Türkiye

<sup>2</sup>Erzincan Binali Yıldırım Üniversitesi, Fen Bilimleri Enstitüsü, Erzincan, Türkiye

<sup>3</sup>Milli Eğitim Bakanlığı, Erzincan, Türkiye

\*Corresponding author: [daltun@erzincan.edu.tr](mailto:daltun@erzincan.edu.tr)  
Orcid No: <https://orcid.org/0000-0002-3576-0355>

Received : 03/10/2024  
Accepted : 28/11/2024

**To Cite / Atf için:** Altun Çolak D, Kaya H, Atıcı T. 2024. Sorafenib ve Yalancı portakal ekstresi kombinasyonunun A549 hücre hatları üzerindeki *in vitro* sitotoksik ve antioksidan aktivitesi. Eurasian J Bio Chem Sci, 7(2):151-156. <https://doi.org/10.46239/ejbc.1560686>

**Özet:** Akciğer kanseri, dünya genelinde kansere bağlı ölümlerin önde gelen nedenidir. Özellikle akciğer kanseri hücrelerine özgü, etkili ve güvenli yeni terapötik stratejilerin geliştirilmesi kanser araştırmalarında bir önceliktir. Bu çalışma, A549 insan akciğer kanseri hücre hatlarında sorafenib ve Yalancı portakal olarak bilinen *Maclura pomifera* ekstresi kombinasyonunun sitotoksik ve antioksidan etkilerini araştırmaktadır. Bir multikinaz inhibitörü olan sorafenib, çeşitli kanser türlerinin tedavisinde umut verici sonuçlar göstermiştir. Ancak, kanser hücreleri tarafından geliştirilen direnç ve yan etkiler nedeniyle terapötik potansiyeli sınırlı kalmaktadır. Özellikle Yalancı portakal gibi bitkilerden elde edilen doğal özler, önemli antioksidan özellik gösterir ve geleneksel kemoterapi ilaçlarının etkinliğini artırıp toksisitesini azaltabilir. A549 insan akciğer kanseri hücre hatları sorafenib, Yalancı portakal ekstresi ve bunların kombinasyonunun çeşitli konsantrasyonları ile muamele edilmiştir. Hücre canlılığı MTT testi ile değerlendirilirken, toplam oksidan durumu (TOS) ve toplam antioksidan durumu (TAS) seviyeleri ölçülmüştür. Sorafenib ve Yalancı portakal ekstresi kombinasyonu, tek başına sorafenib tedavisine kıyasla hücre canlılığında önemli bir azalma göstermiştir. Ayrıca, kombinasyon tedavisi toplam oksidan seviyelerinde önemli bir düşüşe yol açarak antioksidan aktivitenin arttığını göstermiştir. Bu çalışmanın bulguları, sorafenib ve Yalancı portakal ekstresi kombinasyonunun A549 insan akciğer kanseri hücre hatlarında güçlü sitotoksik ve antioksidan etkiler sergilediğini göstermektedir. Bu kombinasyon tedavisi, akciğer kanseri tedavisinde daha etkili ve daha güvenli bir alternatif olma potansiyeline sahiptir ve daha ileri *in vivo* çalışmalar ve klinik denemeler gerektirmektedir.

**Anahtar Kelimeler:** Akciğer kanseri, Sorafenib, *Maclura pomifera*, Sitotoksisite, Antioksidan, A549 hücre hatları

### *The cytotoxic and antioxidant effects of sorafenib and osage orange extract combination in A549 cell lines*

**Abstract:** Lung cancer is the leading cause of cancer-related deaths worldwide. Developing new therapeutic strategies that are effective, safe, and specific for lung cancer cells is a priority in cancer research. This study investigates the cytotoxic and antioxidant effects of a combination of sorafenib and *Maclura pomifera* extract, known as Osage orange, in A549 human lung cancer cell lines. Sorafenib, a multikinase inhibitor, has shown promising results in the treatment of various types of cancer. However, its therapeutic potential remains limited due to side effects and resistance developed by cancer cells. Natural extracts, especially those obtained from plants such as Osage orange, show significant antioxidant properties and may improve the efficacy and reduce the toxicity of conventional chemotherapy drugs. A549 human lung cancer cell lines were treated with various concentrations of sorafenib, Osage orange extract, and their combination. Cell viability was evaluated by MTT assay, while the levels of total oxidant status (TOS) and total antioxidant status (TAS) were measured. The combination of sorafenib and Osage orange extract demonstrated a significant decrease in cell viability compared to sorafenib treatment alone. In addition, the combination treatment significantly reduced total oxidant levels, indicating increased antioxidant activity. The findings of this study demonstrate that the combination of sorafenib and Osage orange extract exhibits potent cytotoxic and antioxidant effects in A549 human lung cancer cell lines. This combination therapy has the potential to be a more effective and safer alternative in the treatment of lung cancer, but further *in vivo* studies and clinical trials are required.

**Keywords:** Lung cancer, Sorafenib, *Maclura pomifera*, Cytotoxicity, Antioxidant, A549 cell lines



## 1. Giriş

Akciğer kanseri, tahminen 2 milyon tanı ve 1,8 milyon ölümle küresel kanser insidansı ve mortalitesinin önde gelen nedenidir. Akciğer tümörleri erkeklerde ve kadınlarda (sırasıyla prostat ve meme kanserinden sonra) ikinci en yaygın kanser teşhisidir (Thandra ve ark. 2021). Küçük hücreli akciğer karsinomu (KHAK) ve küçük hücreli dışı akciğer karsinomu (KHDAK) olmak üzere iki ana grupta sınıflandırılan akciğer kanserlerinde olgunların yaklaşık %80'i küçük hücreli dışı akciğer kanseri tanısı almıştır (Zheng, 2016). Radyoterapi, kemoterapi ve immünoterapi gibi yöntemler akciğer kanseri tedavisinde kullanılmakla birlikte bu tedaviler kanserli hücrelerle birlikte sağlıklı hücrelere de zarar verebilmektedir (Singh ve ark. 2018; Sung ve ark. 2021). Son yıllarda, protein kinazlar hücrel sinyal yollarının temel bileşenleri olarak öne çıkmış ve bu nedenle kanser tedavisinde ilaç geliştirme süreçlerinde en önemli hedeflerden biri haline gelmiştir. Apoptozu kolaylaştırma, anjiyogenezi azaltma ve tümör hücresi çoğalmasını baskılama yeteneğine sahip olan sorafenib çok hedefli bir ajandır ve insan küçük hücreli dışı akciğer kanseri dahil olmak üzere çeşitli tümör türlerine karşı güçlü antitümör etkilere sahip olduğu bildirilmiştir (Dal Lago ve ark. 2008; Zhang ve ark. 2013; Tang ve ark. 2020). Sorafenib tedavisine karşı gelişen direnç, kanser tedavisinde önemli bir sorun teşkil etmektedir. Direnç mekanizmaları arasında, ilaç hedeflerinde mutasyonlar, alternatif sinyal yollarının aktivasyonu ve ilaç metabolizmasında değişiklikler yer alır. Bu direnç mekanizmalarının anlaşılması, tedavi stratejilerinin optimize edilmesi ve yeni terapötik yaklaşımların geliştirilmesi açısından kritik öneme sahiptir (Chan ve ark. 2024). Sorafenib direnci, ilaç taşıma sistemlerinde meydana gelen değişiklikler, metabolize edici enzimlerdeki genetik polimorfizmler ve DNA onarımı, apoptoz ve otoliz gibi hücrel süreçlerin yeniden yönlendirilmesiyle ilişkilidir (Cabral ve ark. 2020). Bu mekanizmaların anlaşılması, tedavi stratejilerinin optimize edilmesi ve yeni terapötik yaklaşımların geliştirilmesi açısından büyük önem taşımaktadır. Bu direncin üstesinden gelmek için, sorafenib ile kombine tedavi seçenekleri veya yeni hedeflere yönelik ilaçların geliştirilmesi gereklidir (Zhao ve ark. 2023). Günümüzdeki tedavi yöntemlerinin olumsuz yanları nedeniyle, alternatif tedavi stratejilerine yönelik araştırmalar son yıllarda büyük bir ivme kazanmıştır. Özellikle, bitki ekstraktlarının kullanıldığı bitkisel terapi teknikleri, son yıllarda ilgi gören tedavi yöntemleri arasında ön plana çıkmaktadır (Mukherjee ve ark. 2001; Solowey ve ark. 2014). Halk arasında Yalancı portakal olarak bilinen *Maclura pomifera* (Rafin.) Schneid, Moraceae familyasına ait bir bitki olup bitkinin meyve, kabuk, yaprak, tohum ve köklerinin sahip olduğu fitokimyasal profili sebebiyle bilimsel çalışmalarda kullanılmaktadır (Smith ve ark. 1981; Filip ve ark. 2015; Filip ve ark. 2021). *M. pomifera* bileşenleri sitotoksik, antitümör, antibakteriyel, östrojenik, antifungal, antiviral ve antimalaral aktivitelere dahil olmak üzere çeşitli biyolojik aktivitelere sahiptir (Barnes ve ark. 1955; Kupeli ve ark. 2006; Lakornwong ve ark. 2022).

Bu çalışmada, farklı dozlarda *M. pomifera* bitkisine ait meyve ekstresi ve sorafenib kombinasyonunun insan akciğer kanser hücre hatları (A549) üzerindeki antisitotoksik ve antioksidan etkileri araştırılmıştır. Akciğer kanserinin sorafenibe duyarlılığını geliştirmek ve sorafenibin antitümör ve antioksidan aktivitesini iyileştirmek için etkili bir strateji olması bakımından *M. pomifera* bitkisine ait meyve ekstresi (MPME) ile sorafenib (SRB) birlikte kullanılmıştır. Sorafenib ve Yalancı portakal meyve ekstresinin kombinasyonunun akciğer hücre hatları üzerinde kullanımına ait literatüre rastlanmamış olması bu çalışmanın özgünlüğü açısından önemlidir.

## 2. Materyal ve Metot

### 2.1. A549 Hücre Kültürü

Çalışmada sorafenib ve Yalancı portakal ekstresi kombinasyonunun sitotoksik ve antioksidatif etkinliği A549 (ATCC- HB-8065) insan akciğer kanser hücre hatlarında *in vitro* olarak araştırılmıştır. Hücreler %10 FBS ve %1 penisilin-streptomisin ile desteklenmiş Roswell Park Memorial Institute (RPMI)-1640 ortamında CO<sub>2</sub> inkübatöründe %5 CO<sub>2</sub> ve 37°C sıcaklık altında nemlendirilmiş bir atmosferde büyütülmüştür. Hücreler yapışık tek tabakalar halinde büyütülmüş ve dönüşümlü olarak her gün beslenmiş ve hücreler yaklaşık %80 konfluensiye ulaştığında pasajlanmıştır.

### 2.2. Stok Çözeltilerin Hazırlanması

Birçok farklı kanser türünde etkili bir çoklu kinaz inhibitörü olup kimyasal formülü C<sub>21</sub>H<sub>16</sub>ClF<sub>3</sub>N<sub>4</sub>O<sub>3</sub> olan sorafenibin (SRB, Sigma- Aldrich) %50 inhibisyon konsantrasyonu (IC<sub>50</sub>) olarak belirlenen 9,9 µM'lik (µmol/L) dozu kullanılmıştır. Çalışmada kullanılan Eskişehir ilinden 2016 yılında toplanıp kurutulan *Maclura pomifera* (Rafin.) bitki örnekleri manyetik öğütücü ile toz haline getirilmiştir. 10 g alınan bitki örneği 100 mL %70'lik metanol kullanılarak oda sıcaklığında bir gece bekletilmiş ve süzildükten sonra evaporasyon işlemine alınmıştır. *Maclura pomifera* bitkisinin meyvelerine ait özütten (MPME) 50, 100 ve 200 µg/mL çalışma dozları hazırlanarak +4°C'de saklanmıştır.

### 2.3. Hücre Sayımı ve MTT Analizi

MTT analizi öncesinde, flaskların %80'ini kaplamış hücreler tripsinize edilmiştir. 96 kuyucuklu plaklara 10<sup>4</sup> canlı hücre/kuyucuk şeklinde Trypan mavisi ile canlılıkları belirlenen hücrelerden ekim yapılmış ve 24 saat inkübasyona bırakılmıştır. Süre sonunda hücreler SRB, MPME ve SRB+MPME uygulama gruplarını oluşturacak şekilde SRB (9,9 µM) ile MPME'nin seçilen üç farklı dozuna (50; 100; 200 µg/mL) 24, 48 ve 72 saat süre ile maruz bırakılmıştır. Süre sonunda hücrelerin canlılığını ve proliferasyonunu ölçmek için MTT Hücre Proliferasyon Kiti (Roche Applied Science) kullanılmıştır. MTT (3-(4,5-dimetiltiazol-2-il)-2,5-difeniltetrazolyum bromür), sarı renkli bir tetrazolyum tuzudur. Bu tuz, canlı hücrelerde bulunan mitokondriyal dehidrogenaz enzimleri tarafından metabolize edilerek formazan adı verilen mor renkli bir ürüne dönüştürülür. Canlı hücrelerin metabolik aktivitesi, MTT'nin indirgenmesiyle ölçülür. Hücreler ne kadar aktifse, o kadar çok MTT indirgenir ve daha fazla mor

formazan kristalleri oluşur. MTT Hücre Proliferasyon Kiti prosedürü takip edilerek her bir kuyucuktaki hücrelerin 570 nm'de absorbans değerleri Biotek ELISA mikropilaka kullanılarak belirlenmiştir. Hücrelerin % canlılık değerleri, absorbans değerleri kullanılarak aşağıdaki formüle göre belirlenmiştir.

Hücre canlılığı (%) = (Tedavi edilen hücrelerin absorbansı / Kontrol hücrelerinin absorbansı) × 100

#### 2.4. Total Oksidan Aktivite ve Total Antioksidan Kapasite Analizi

6 kuyucuklu plaklara  $5 \times 10^4$  canlı hücre/kuyucuk şeklinde Trypan mavisi ile canlılıkları belirlenen hücrelerden ekim yapılmış ve 24 saat inkübe edilmiştir. Süre sonunda hücreler aynı dozlarda SRB, MPME ve SRB+MPME ile muamele edilmiş hücrelerde gözlenen olası toksik etkinin antioksidan sistemlerin down regülasyonu ile ilişkili olup olmadığını belirlemek için yapılan biyokimyasal analizler için Rel Assay Diagnostics firmasına ait Total Oxidant Status (TOS) Assay Kit ve Total Antioxidant Status (TAS) Assay Kit kullanılmıştır. TOS/TAS oranını ifade eden oksidatif stres indeksi (OSI) de hesaplanmıştır. Spektrofotometrik ölçümler TOS için 530 nm ve TAS için 660 nm dalga boyunda yapılmıştır.

#### 2.5. İstatiksel Analizler

IBM SPSS Statistics software (SPSS v.22) hazır paket programı kullanılarak verilerin istatistiksel analizi için gerçekleştirilmiştir. Üç kez tekrarlanan uygulamalarda SRB, MPME ve SRB+MPME dozlarının sitotoksikite ve oksidatif parametre verileri değerlendirilirken istatistiksel anlamlılık değeri  $p < 0,001$  olarak kabul edilmiştir.

### 3. Bulgular

#### 3.1. A549 Hücre Hattı İçin $IC_{50}$ Değerlerinin Belirlenmesi

Çalışmada kullanılan sorafenib (SRB) ile *Maclura pomifera* (Yalancı portakal) ekstresinin (MPME) A549 hücre hattı üzerinde ayrı ayrı ve kombine bir şekilde sitotoksik etkisini belirlemek üzere uygulanan MTT analizi sonucunda belirlenen  $IC_{50}$  değerleri Tablo 1'de verilmiştir.

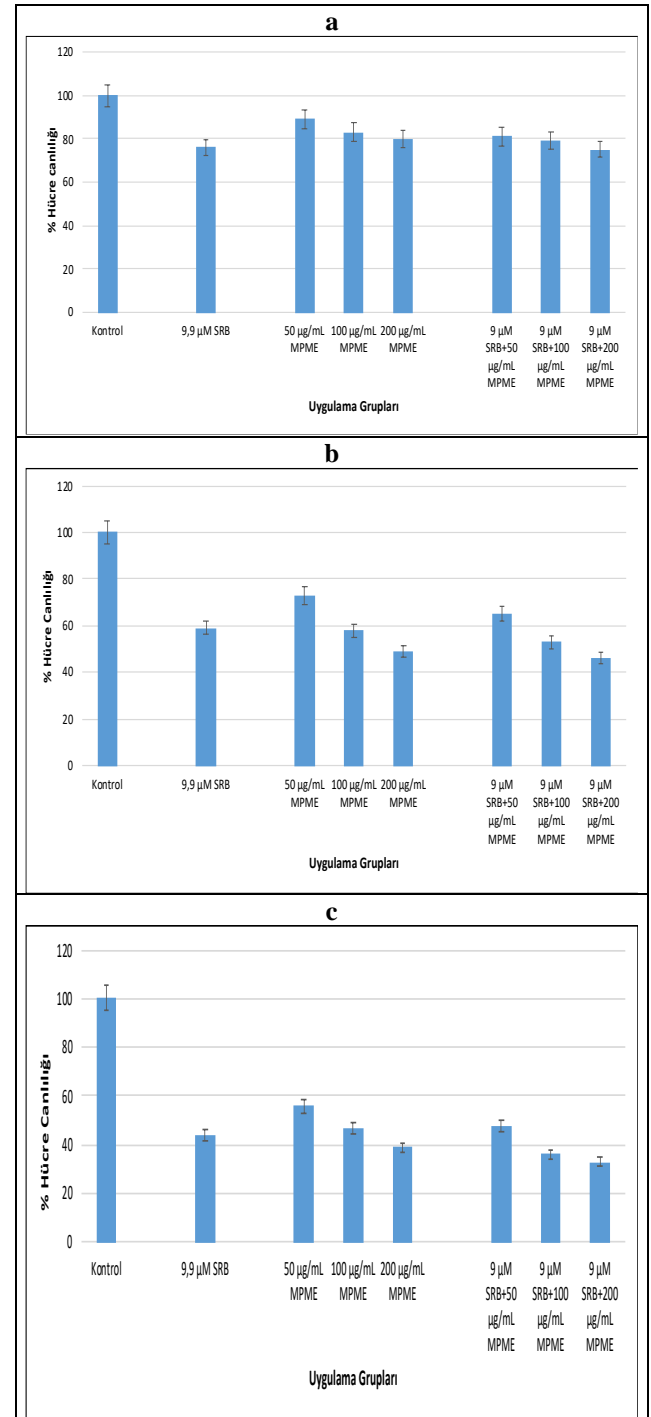
**Tablo 1.** A549 hatlarına SRB ve MPME uygulaması sonunda 24, 48 ve 72 saatleri için  $IC_{50}$  değerleri

Doz ( $\mu$ M)		$IC_{50}$	
Süre	Hücre	Sorafenib (SRB)	<i>M. pomifera</i> ekstresi (MPME)
24h	A549	>9,9 $\mu$ M	>200 $\mu$ g/mL
48h	A549	>9,9 $\mu$ M	183±0,01 $\mu$ g/mL
72h	A549	4,9±1,27 $\mu$ M	89±0,12 $\mu$ g/mL

#### 3.2. A549 Hücre Hattı İçin MTT Test Bulguları

Belirlenen konsantrasyon değerleri ile 24 saat inkübasyonun ardından yapılan canlılık belirlemelerinin sonuçları Şekil 1a'da gösterilmektedir. A549 hücre hattında 24 saat boyunca SRB (9,9  $\mu$ M) bileşiğinin tek başına

uygulanması sonucunda hücre canlılık oranı  $76 \pm 0,01$  olarak gözlenmiştir. Bu sonuç kontrole göre istatistiksel olarak anlamlıdır ( $p < 0,001$ ).



**Şekil 1.** A549 hücrelerinde a) 24 saatlik b) 48 saatlik ve c) 72 saatlik sitotoksitenin belirlenmesi

A549 hücre hattında 24 saat boyunca MPME'nin artan dozlarında (50; 100 ve 200  $\mu$ g/mL) tek başına uygulanması sonrası gözlenen canlılık oranları ise sırasıyla  $89,23 \pm 0,15$ ;  $83,12 \pm 0,24$ ;  $80,42 \pm 1,28$ 'dir. Tüm dozlarda gözlenen canlılık oranları kontrole göre istatistiksel olarak önemlidir ( $p < 0,001$ ). A549 hücre hattında 24 saatlik SRB+MPME kombinasyon uygulamaları (9,9  $\mu$ M SRB+50  $\mu$ g/mL MPME, 9,9  $\mu$ M

SRB+100 µg/mL MPME ve 9,9 µM SRB+200 µg/mL MPME) sonucu belirlenen canlılık oranları sırasıyla %81,4±0,75; %79,76±0,12; %75,13±1,01 şeklinde olup gözlenen canlılık oranları tüm dozlarda kontrol grubuna göre istatistiksel olarak anlamlıdır (p<0,001).

A549 hücre hattında 48 saat boyunca SRB (9,9 µM) bileşiminin tek başına uygulanması sonucunda hücre canlılık oranı %59,17±0,56'dır (Şekil 1b). Bu sonuç kontrole göre istatistiksel açıdan anlamlıdır (p<0,001). A549 hücre hattında 48 saat boyunca MPME'nin artan dozlarda (50; 100 ve 200 µg/mL) tek başına uygulanması sonrası elde edilen canlılık oranları ise sırasıyla %73,47±0,24; %58,14±0,6; %49,24±1,01 olup gözlenen canlılık oranları tüm dozlarda kontrol grubuna göre istatistiksel açıdan önemlidir (p<0,001).

A549 hücre hattında 48 saatlik SRB+MPME kombinasyon uygulamaları (9,9 µM SRB+50 µg/mL MPME, 9,9 µM SRB+100 µg/mL MPME ve 9,9 µM SRB+200 µg/mL MPME) sonucu canlılık oranları sırasıyla %65,48±0,14; %53,14±0,8; %46,35±1,25'dir ve gözlenen bu oranlar tüm dozlarda kontrole göre istatistiksel açıdan anlamlıdır (p<0,001). A549 hücre hattında 72 saatlik SRB (9,9 µM) bileşiminin tek başına uygulanması sonucu hücre canlılık oranı %44,10±0,23'e çıkmıştır (Şekil 1c). Bu sonuç kontrole kıyasla istatistiksel olarak önemlidir (p<0,001). A549 hücre hattında 72 saatlik MPME'nin artan dozlarda (50; 100 ve 200 µg/mL) tek başına uygulanmasıyla elde edilen canlılık oranları ise sırasıyla %56,11±0,25; %47,70±0,02; %39,50±0,30 olup tüm dozlarda gözlenen bu oranlar kontrol grubuna göre istatistiksel açıdan anlamlıdır (p<0,001).

### 3.3. Oksidatif Parametre Bulguları

A549 hücrelerinde SRB+MPME kombinasyonunun toplam oksidan kapasitesi (TOS), toplam antioksidan kapasitesi (TAS) ve toplam oksidatif stres indeksleri (OSI) Şekil 2'de gösterilmiştir. Elde edilen verilere göre SRB+MPME uygulama gruplarında SRB'nin tek başına kullanıldığı gruba göre TAS değerlerini artırıp TOS değerlerinde belirgin bir düşüşe yol açması artan antioksidan aktiviteyi işaret etmiştir. Oksidatif parametre değerleri bakımından kontrole göre gözlenen bu farklılıklar istatistiksel olarak anlamlı bulunmuştur (p<0,001).

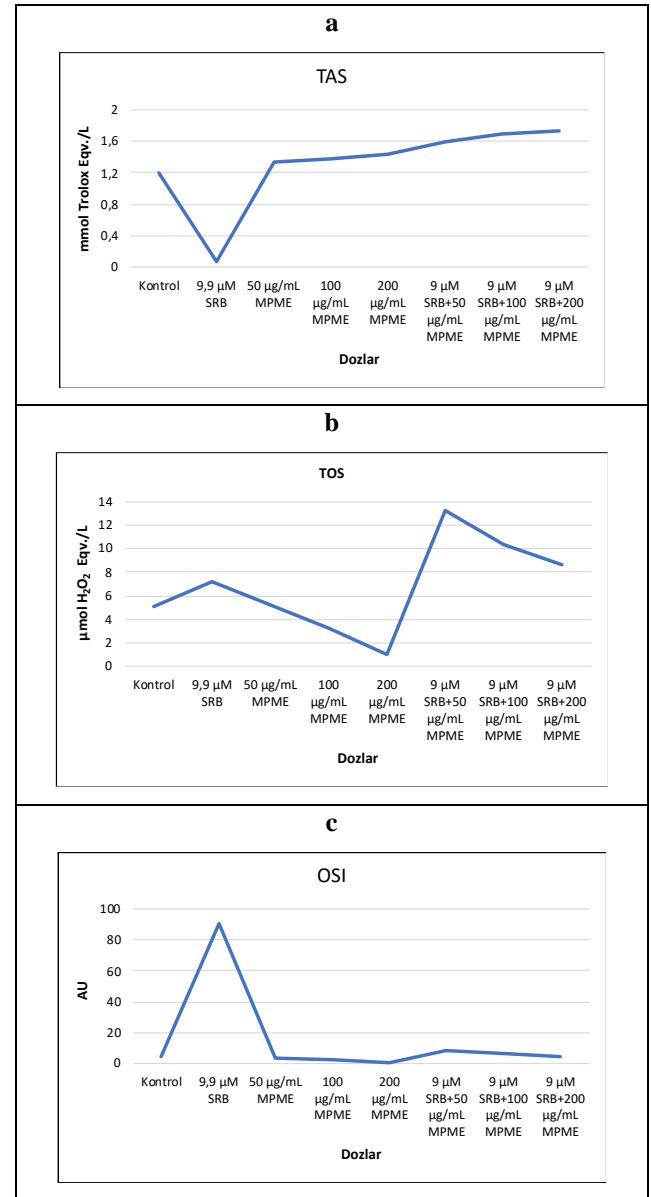
### 4. Tartışma

Akciğer kanseri hücrelerinin metastatik ilerlemesindeki farklı hedefler arasında çok seviyeli çapraz reaksiyonlar tanımlanmıştır ve bir hedefin baskılanması, diğerlerinin tümör hücreleri için immün kaçış moleküler mekanizmaları olarak hareket etmesine izin verir (Jiang ve ark. 2017). İki veya daha fazla antikanser ajandan oluşan kombinasyon tedavisinin, tek hedefli ajanlara kıyasla tümör ilerlemesini engellemede daha etkili olduğu düşünülmektedir (Li ve ark. 2013).

Reseptör tirozin kinazlar kanser gelişiminde önemli rol oynar ve spesifik terapötik yaklaşımlar için etkili hedefler sunar. Birçok çalışma, çoklu kinaz inhibitörü ve güçlü bir antikanser etkisi gösteren yeni bir oral bis-aril üre bileşiği

olan sorafenibin, protein kinazları hedefleyerek tümör büyümesini engelleyebileceğini öne sürmektedir (Jane ve ark. 2006; Zhang ve ark. 2012).

Sorafenib tedavisinin olumsuz yan etkileri nedeniyle, yeni terapötik stratejiler sorafenib tedavisinin kritik kusurlarını iyileştirmek için sorafenibin doğal ilaçlarla birleştirilmesine odaklanmıştır (Smit ve ark. 2010). Bir bitki flavonu olan apigeninin, kromozomal sapmalar ve mikronükleus, reaktif oksijen türleri (ROS) ve reaktif nitrojen türleri (RNS), oksidatif ve DNA hasarı, lipid peroksidasyonu ve hepatorenal hasarlarda artış ve antioksidan enzimlerde azalma ile karakterize genetik, oksidatif ve doku hasarlarına neden olan sorafenib ile kombine edilerek Swiss albino fareleri üzerinde yapılan bir çalışmada sorafenib kaynaklı toksisiteye karşı koruyucu etkileri olduğu ve yan etkilerini azaltmak ve etkinliğini artırmak için sorafenib ile kombine edilebileceğini göstermektedir (Singh ve ark. 2022).



Şekil 2. A549 hücre hattında SRB+MPME kombinasyonunun oksidatif stres parametre verileri a) TAS b) TOS c) OSI

At kestanesi tohumlarından elde edilen pentasiklik bir triterpene olan escin ile sorafenib kombinasyonunun A549 and NCIH460 akciğer kanseri hücrelerinin G0/G1 fazında geç apoptozu indüklemek için otofajiyi sinerjik olarak inhibe ettiği bildirilmiştir (Hussain ve ark. 2023). Kurkuminin polimerik nanopartikül formülasyonu olan NanoCurcumin, insan hepatoselüler karsinom modellerinde tümör büyümesini ve akciğer metastazlarını etkili bir şekilde inhibe ederek klinik gelişim için potansiyel sunmakta, ayrıca sorafenib ile kombinasyon halinde tümör büyümesini ve metastazı engellemektedir (Hu ve ark. 2015). Sentetik sorafenib, poli (laktik-ko-glikolik asit) ve doğal kurkumini birleştiren bir nanoformülün, küçük hücreli olmayan akciğer kanseri A549 hücre hatlarında önemli apoptozu indükleyebileceğini ve büyümeyi inhibe edebileceği ifade edilmiştir (El-Hamawi ve ark. 2023). Quercetin'in, EGFR C797S mutasyonunu barındıran küçük hücreli dışı akciğer kanseri hücrelerinde tümör büyümesini etkili bir şekilde inhibe ederek üçüncü nesil tirozin kinaz inhibitörlerine karşı kazanılmış direnç için potansiyel bir tedavi görevi gördüğü vurgulanmıştır (Huang ve ark. 2021). Benzer şekilde, bufalin ile kombinasyon halinde sorafenibin NCI-H292 insan küçük hücreli olmayan akciğer kanseri hücrelerinde tek başına sorafenib veya bufalin tedavisinden daha güçlü sitotoksik etki ve hücre apoptozu gösterdiği belirtilmiştir (Kuo ve ark. 2022). Başka bir çalışmada, erastin ve sorafenib ile temsil edilen ferroptoz indükleyicileri, ilerlemiş küçük hücreli dışı akciğer karsinomlu hastaların sağkalımına fayda sağladığı veya hatta sisplatin bazlı çok kürlü kemoterapi tedavisinin başarısızlığını takiben KDDAK tedavisi için yeni bir bakış açısı sağladığı bildirilmiştir (Li ve ark. 2020). Yine,  $\beta$ -iyonon ve sorafenibin antioksidan etkiler, sinyal yollarının modülasyonu ve ilaç direncinin üstesinden gelme gibi çeşitli mekanizmalar yoluyla hepatoselüler karsinoma karşı potansiyel kemoterapötik etkilere sahip olduğunu gösteren literatür mevcuttur (Abd-Elbaset ve ark. 2020).

Bu çalışmada, sorafenib ve *Maclura pomifera* (Yalancı portakal) meyve ekstresinin düşük dozlarda ve kısa süreli kombinasyon halinde uygulanmasının, tümör hücrelerinin canlılığını tek başına kullanılan dozlardan daha etkili bir şekilde azaltmasının ve antioksidan aktivite göstermesinin literatürle uyumlu olduğu görülmektedir.

## 5. Sonuç

Sonuç olarak, bu çalışma, sorafenib ve Yalancı portakal (*Maclura pomifera*) meyve ekstresinin A549 akciğer kanseri hücre hatları üzerinde belirgin sitotoksik ve antioksidan etkiler gösterdiğini ortaya koymuştur. Kombinasyon tedavisi, sorafenibin tek başına kullanımına kıyasla hücre canlılığını daha etkili bir şekilde azaltmış ve oksidatif stres seviyelerini belirgin biçimde düşürerek antioksidan aktiviteyi artırmıştır. Bu bulgular, sorafenib ile Yalancı portakal ekstresi kombinasyonunun akciğer kanseri tedavisinde daha etkili ve güvenilir bir seçenek olabileceğini öne sürmektedir. Bununla birlikte, bu sonuçların geçerliliğini desteklemek için daha fazla *in vivo* araştırma ve klinik çalışmalar gereklidir.

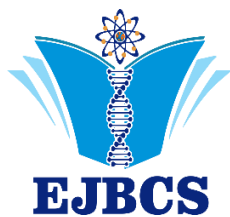
**Yazarların katkıları:** HK: Verileri topladı ve analiz etti, makalenin ilk taslağını yazdı ve son versiyonunu hazırladı. TA: Verileri topladı ve analiz etti, şekilleri çizdi, ilk taslağı yazdı. DAÇ: Projeyi tasarladı, verileri topladı ve analiz etti, ilk taslağı ve makalenin son versiyonunu gözden geçirdi.

**Çıkar çatışması beyanı:** Tüm yazarlar herhangi bir çıkar çatışması olmadığını beyan eder.

## Kaynaklar

- Abd-Elbaset M, Mansour AM, Ahmed OM, Abo-Youssef AM. 2020. The potential chemotherapeutic effect of  $\beta$ -ionone and/or sorafenib against hepatocellular carcinoma via its antioxidant effect, PPAR- $\gamma$ , FOXO-1, Ki-67, Bax, and Bcl-2 signaling pathways. *Naunyn Schmiedebergs Arch.* 393:1611-1624
- Barnes RA, Gerber NN. 1955. The Antifungal Agent from Osage Orange Wood. *J Am Chem.Soc.* 77(12):3259-3262
- Cabral LKD, Tiribelli C, Sukowati CHC. 2020. Sorafenib resistance in hepatocellular carcinoma: The relevance of genetic heterogeneity. *Cancers (Basel).* 12(6):1576
- Chan YT, Wu J, Lu Y, Li Q, Feng Z, Xu L, Yuan H, Xing T, Zhang C, Tan HY, Feng Y, Wang N. 2024. Loss of lncRNA LINC01056 leads to sorafenib resistance in HCC. *Mol Cancer.* 23:74
- Dal Lago L, D'Hondt V, Awada A. 2008. Selected combination therapy with sorafenib: A review of clinical data and perspectives in advanced solid tumors. *Oncologist.* 13(8):845-858
- El-Hamawi O, Eldin ZE, Abdel-Moneim A, Zanaty MI, El-Shahawy AA. 2023. A nanoformula comprising three entities in one design: Synthetic Sorafenib-loaded poly(lactic-co-glycolic acid) conjugated with natural curcumin induces a distinct intrinsic apoptosis pathway versus non-small cell lung cancer A549 cell lines. <https://www.researchsquare.com/article/rs-2824510/v1>. Accessed 21 Sept 2024.
- Filip S, Djarmati Z, Lisichkov K, Csanadi J, Jankov RM. 2015. Isolation and characterization of *Maclura (Maclura pomifera)* extracts obtained by supercritical fluid extraction. *Industrial Crops and Products.* 76:995-1000
- Filip S, Đurović S, Blagojević S, Tomić A, Ranitović A, Gašić U, Zeković Z. 2021. Chemical composition and antimicrobial activity of Osage orange (*Maclura pomifera*) leaf extracts. *Arch Pharm.* 354(2):2000195
- Hu B, Sun D, Sun C, Sun Y, Sun H, Zhu Q, Yang X, Gao Y, Tang W, Fan J, Maitra A, Anders R, Xu Y. 2015. A polymeric nanoparticle formulation of curcumin in combination with sorafenib synergistically inhibits tumor growth and metastasis in an orthotopic model of human hepatocellular carcinoma. *Biochem Biophys Res Commun.* 468(4): 525-532
- Huang KY, Wang TH, Chen CC, Leu YL, Li HJ, Jhong CL, Chen CY. 2021. Growth suppression in lung cancer cells harboring EGFR-C797S mutation by quercetin. *Biomolecules.* 11(9):1271
- Hussain Y, Singh J, Meena A, Sinha RA, Luqman S. 2023. Escin enhanced the efficacy of sorafenib by autophagy-mediated apoptosis in lung cancer cells. *Phytother Res.* 37(10):4819-4837
- Jane EP, Premkumar DR, Pollack IF. 2006. Coadministration of sorafenib with rottlerin potently inhibits cell proliferation and migration in human malignant glioma cells. *J Pharmacol Exp Ther.* 319(3):1070-1080
- Jiang S, Wang Q, Feng M, Li J, Guan Z, An D, Dong M, Peng Y, Kuerban K, Ye L. 2017. C2-ceramide enhances sorafenib-induced caspase-dependent apoptosis via PI3K/AKT/mTOR

- and Erk signaling pathways in HCC cells. *Appl Microbiol Biotechnol.* 101(4):1535-1546
- Kuo JY, Liao CL, Ma YS, Kuo CL, Chen JC, Huang YP, Chung JG. 2022. Combination treatment of sorafenib and bufalin induces apoptosis in NCI-H292 human lung cancer cells in vitro. *In Vivo.* 36(2):582-595
- Kupeli E, Orhan I, Toker G, Yesilada E. 2006. Anti-inflammatory and antinociceptive potential of *Maclura pomifera* (Rafin.) Schneider fruit extracts and its major isoflavonoids, scandenone and auricularin. *J Ethnopharmacol.* 107(2):169-174
- Lakornwong W, Kanokmedhakul K, Masranoi J, Tontapha S, Yahuafai J, Laphookhieo S, Kanokmedhakul S. 2022. Cytotoxic and antibacterial xanthenes from the roots of *Maclura cochinchinensis*. *Nat Prod Res.* 36(23): 6021-6030
- Li J, Pan YY, Zhang Y. 2013. Synergistic interaction between sorafenib and gemcitabine in EGFR-TKI-sensitive and EGFR-TKI-resistant human lung cancer cell lines. *Oncol Lett.* 5(2):440-446
- Li Y, Yan H, Xu X, Liu H, Wu C, Zhao L. 2020. Erastin/sorafenib induces cisplatin resistant non-small cell lung cancer cell ferroptosis through inhibition of the Nrf2/xCT pathway. *Oncol Lett.* 19(1):323-333
- Mukherjee AK, Basu S, Sarkar N, Ghosh AC. 2001. Advances in cancer therapy with plant-based natural products. *Curr Med Chem.* 8(12):1467-1486
- Singh, AK, Hennon M, Ma SJ, Demmy TL, Picone A, Dexter EU, Nwogu C, Attwood K, Tan W, Hermann GM, Fung-Kee-Fung S, Malhotra HK, Yendamuri S, Gomez-Suescun, JA. 2018. A pilot study of stereotactic body radiation therapy (SBRT) after surgery for stage III non-small cell lung cancer. *BMC Cancer.* 18:1183
- Singh D, Khan MA, Akhtar K, Arjmand F, Siddique HR. 2022. Apigenin alleviates cancer drug sorafenib-induced multiple toxic effects in Swiss albino mice via anti-oxidative stress. *Toxicol Appl Pharmacol.* 447:116072
- Smith JL, Perino JV. 1981. Osage orange (*Maclura pomifera*): History and economic uses. *Econ Bot.* 35(1):24-41
- Smit EF, Dingemans AMC, Thunnissen FB, Hochstenbach MM, van Suylen RJ, Postmus PE. 2010. Sorafenib in patients with advanced non-small cell lung cancer that harbor K-ras mutations: a brief report. *J Thorac Oncol.* 5(5): 719-720
- Solowey E, Lichtenstein M, Sallon S, Paavilainen H, Solowey E, Lorberboum-Galski H. 2014. Evaluating medicinal plants for anticancer activity. *Sci World J.* 2014(1): 721402.
- Sung H, Ferlay J, Siegel RL, Laversanne M, Soerjomataram I, Jemal A, Bray F. 2021. Global cancer statistics 2020: GLOBOCAN estimates of incidence and mortality worldwide for 36 cancers in 185 countries. *CA Cancer J Clin.* 71(3):209-249
- Tang W, Chen Z, Zhang W, Cheng Y, Zhang B, Wu F, Wang Q, Wang S, Rong D, Reiter FP, De Toni EN, Wang X. 2020. The mechanisms of sorafenib resistance in hepatocellular carcinoma: theoretical basis and therapeutic aspects. *Signal Transduct Target Ther.* 5(1):87
- Thandra KC, Barsouk A, Saginala K, Aluru JS, Barsouk A. 2021. Epidemiology of lung cancer. *Contemp Oncol/ Współcz Onkol.* 25(1):45-52
- Zhang Y, Zhang B, Zhang A, Zhao Y, Zhao J, Liu J, Rao Z. 2012. Synergistic growth inhibition by sorafenib and vitamin K2 in human hepatocellular carcinoma cells. *Clin.* 67:1093-1099
- Zhang J, Chen YL, Ji G, Fang W, Gao Z, Liu Y, Gao F. 2013. Sorafenib inhibits epithelial-mesenchymal transition through an epigenetic-based mechanism in human lung epithelial cells. *PLoS One.* 8(5):e64954.
- Zhao J, Lin E, Bai Z, Jia Y, Wang B, Dai Y, ZhuoW, Zeng G, Liu X, Cai C, Li P, Zou B Li J. (2023). Cancer-associated fibroblasts induce sorafenib resistance of hepatocellular carcinoma cells through CXCL12/FOLR1. *BMC Cancer.* 23(1): 1198.
- Zheng M. 2016. Classification and pathology of lung cancer. *Surg Oncol Clin.* 25(3):447-468.



## A hypothetical study on the structural properties of limonene compounds using semi-empirical (PM3) method with arguslab software

Özlem İşcan\* 

\*Bartın University, Rectorate, Project and Technology Office General Coordination, Bartın, Türkiye

\*Corresponding author : [oiscan@bartin.edu.tr](mailto:oiscan@bartin.edu.tr)  
Orcid No: <https://orcid.org/0000-0003-3282-1121>

Received : 30/08/2024  
Accepted : 12/12/2024

To Cite / Atıf için: İşcan Ö. 2024. A hypothetical study on the structural properties of limonene compounds using semi-empirical (PM3) method with arguslab software. Eurasian J Bio Chem Sci, 7(2):157-164 <https://doi.org/10.46239/ejbc.1558302>

**Abstract:** Limonene, in its racemic form (+/-), is a naturally occurring cyclic monoterpene and the primary component of citrus peel oil, known for its chemopreventive (cancer-preventive) and antitumor properties. Conformational analysis and geometric optimization of specific limonene derivatives (limonene, carvone, and 4-Methyl-beta-methylenecyclohex-3-en-1-ethyl acetate) were initially performed using ArgusLab 4.0.1 software with PM3 semi-empirical quantum mechanical calculations. Geometries, geometric, and thermodynamic parameters of the compounds were obtained based on their most stable conformations. The geometry energies of the compounds were found to be 62.2637567520 au, -52.6142315455 au, and -84.0390055928 au, respectively. The optimized compounds' HOMO-LUMO frontier orbital energies, molecular electrostatic potential (MEP), solvent surface distribution, UV spectrum values, ZDO and Mulliken charges, as well as dipole moment values, were also calculated using ArgusLab 4.0.1 software.

**Keywords:** ArgusLab, Limonene, Carvone, PM3, HOMO-LUMO, UV

### *Arguslab yazılımı ile yarı-empirik (PM3) metodu kullanılarak limonen bileşiklerinin yapısal özellikleri üzerine hipotetik bir çalışma*

**Özet:** Limonen, rasemik formda (+/-), doğal olarak oluşan bir döngüsel monotermen olup, turuncuğil kabuğu yağının birincil bileşenidir ve kemopreventif (kanseri önleyici) ve antitümör özellikleriyle bilinir. Belirli limonen bileşiklerinin (limonene, karvon ve 4-Metil-beta-metilen sikloheks-3-en-1-etil asetat) ilk olarak, konformasyon analizi ve geometrik optimizasyonu, ArgusLab 4.0.1 yazılımında PM3 yarı-empirik kuantum mekanik hesaplamaları kullanılarak gerçekleştirilmiştir. Bileşiklerin en kararlı yapıları kullanılarak geometrileri, geometrik ve termodinamik parametreleri elde edilmiştir. Bileşiklerin geometri enerjileri sırasıyla 62.2637567520 au, -52.6142315455 au, ve -84.0390055928 au, bulunmuştur. Optimizasyonu yapılan bileşiklerin HOMO-LUMO sınır orbital enerjileri, moleküler elektrostatik potansiyeli (MEP), çözücü yüzey dağılımı, UV spektrumu değerleri ZDO ve Mulliken yükleri ve dipol moment değeri de ArgusLab 4.0.1 yazılımıyla hesaplanmıştır.

**Anahtar Kelimeler:** ArgusLab, Limonen, Karvon, PM3, HOMO-LUMO, UV

## 1. Introduction

ArgusLab is a widely used software in molecular modeling and computational chemistry, supporting various semi-empirical methods to study the electronic properties of molecular structures (Thompson 2004). Through molecular orbital calculations and energy minimization processes, it has the potential to provide insights into the electronic transitions of organic molecules. These electronic transitions, particularly in molecules excited by light absorption in the UV-Vis region, are associated with

transitions from the ground electronic state ( $S_0$ ) to the excited state ( $S_1$ ), and are typically dependent on the HOMO-LUMO energy gap (Mortimer 2000). ArgusLab, a computational chemistry software, is commonly used for molecular modelling and drug design, particularly in ligand-receptor interactions. The program provides a graphical user interface (GUI) for building and visualising molecules, running molecular mechanics calculations, and performing semi-empirical quantum chemistry simulations (Laxmi 2014; Ikpeazu and Otuokere 2017; İşcan 2023). PM3 (Parametric Method 3) is a semi-empirical quantum



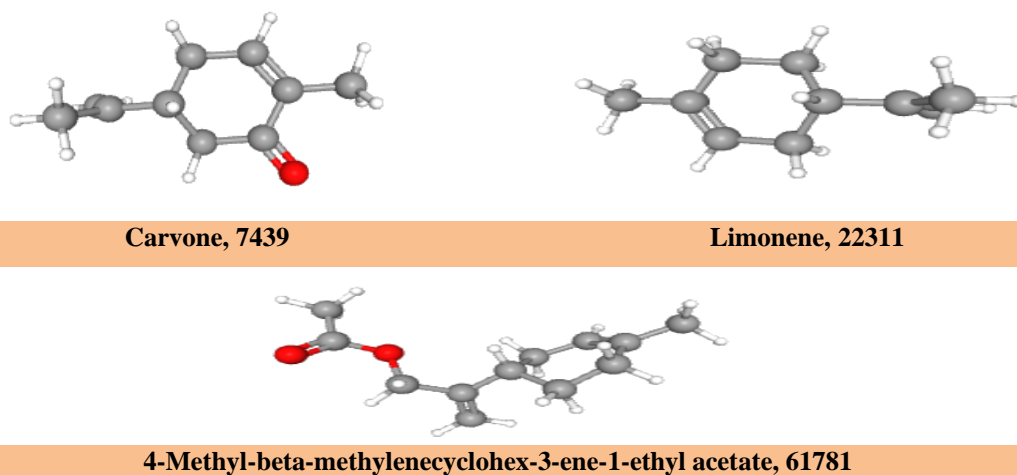


**Fig. 1** The names of the compounds and their PubChem ID numbers

chemistry method for studying molecular structures. It was developed to calculate the electronic structure of molecules and is mainly applied to organic molecules for determining energy levels, binding energies, and molecular orbital analyses (Laxmi 2016). DFT calculations for (R)-limonene and (S)-limonene revealed that the HOMO-LUMO energy gaps are 6.679 eV and 6.705 eV, respectively, and that UV absorption is associated with transitions from HOMO to LUMO, indicating that the two enantiomers exhibit comparable reactivity and stability (EL Quafy et al. 2021). The 2D representations of the compounds obtained from PubChem are shown in Fig. 1.

## 2. Materials and Method

ArgusLab software was employed on a Windows-based computer for all conformational analysis and geometry optimization research. Advances in computing have enabled numerous tools for model building, structure minimization, and molecular representation (Martin 1998; Cruciani et al. 1998; Dunn and Hopfinger 1998). After generating the compound's structure with ArgusLab, the semi-empirical Parametric Method 3 (PM3) parameterization was used to complete the minimization process (Dewar et al. 1985; James and Stewart 1989). The minimum potential energy was calculated using the

geometry convergence function in ArgusLab software. The generated surfaces were designed to illustrate properties of both the ground state and excited states, including orbitals, electron densities, spin densities, and electrostatic potentials (ESP). Grid data were also produced to create molecular orbital surfaces, which depict the molecular orbitals and map the electrostatic potential onto the electron density surface. The geometry convergence map was utilized to determine the minimum potential energy of limonene derivatives (Thomson 1994, 1995, 1996). Finally, the solvent-accessible surface and UV-visible spectra were generated using the ArgusLab software.

## 3. Results and Discussion

Using the ArgusLab program with the PM3 method, geometry optimization, HOMO-LUMO, MEP (molecular electrostatic potential) energies, UV, and solvent-accessible surface area calculations were performed sequentially on the compounds. Tables 1, 2 and 3 provide the atomic input data for the computation above.

The minimum geometrical energy and SCF energy values calculated using ArgusLab 4.0's RHF/PM3 method are detailed in Tables 4, 5 and 6. Table 7 presents the final minimum geometrical energy and SCF energy values

**Table 1** Atomic coordinates of 7439 compound

Atoms No	x	y	z	Atoms No	x	y	z
<b>1O</b>	2.058974	1.907818	-0.208963	<b>14H</b>	-0.499955	2.034432	0.046527
<b>2C</b>	-0.901563	-0.071314	-0.32127	<b>15H</b>	-0.839892	-2.235162	-0.494763
<b>3C</b>	-0.098907	1.046649	0.347208	<b>16H</b>	-0.650306	-1.652885	1.166001
<b>4C</b>	-0.366369	-1.439868	0.11378	<b>17H</b>	1.530653	-2.545856	-0.024922
<b>5C</b>	-2.371389	0.05708	-0.011295	<b>18H</b>	-2.988732	1.157925	-1.73915
<b>6C</b>	1.375139	0.923327	0.001594	<b>19H</b>	-3.168828	-0.600755	-1.884998
<b>7C</b>	1.113644	-1.530508	0.001868	<b>20H</b>	-4.319363	0.330788	-0.908441
<b>8C</b>	1.9255	-0.46404	-0.047952	<b>21H</b>	3.711691	-1.668344	-0.194286
<b>9C</b>	-3.261803	0.24575	-1.190597	<b>22H</b>	3.904055	-0.149202	0.701324
<b>10C</b>	3.401657	-0.615646	-0.156851	<b>23H</b>	3.775796	-0.123568	-1.065066
<b>11C</b>	-2.854127	0.008122	1.230245	<b>24H</b>	-3.91346	0.101883	1.452822
<b>12H</b>	-0.760971	0.020803	-1.427418	<b>25H</b>	-2.22442	-0.12661	2.106436
<b>13H</b>	-0.206026	0.998182	1.450167				

**Table 2** Atomic coordinates of 22311 compound

Atoms number	x	y	z	Atoms number	x	y	z
1C	0.719	-0.043	-0.366	14H	0.347	2.043	-0.748
2C	0.042	-1.208	0.353	15H	0.333	1.665	0.967
3C	0.038	1.284	-0.018	16H	-1.936	-1.968	0.697
4C	-1.441	-1.299	-0.017	17H	-1.54	-1.757	-1.009
5C	-2.14	0.038	-0.038	18H	-2.0	2.14	-0.019
6C	-1.46	1.197	-0.022	19H	-3.979	-0.542	-0.97
7C	2.167	0.006	0.013	20H	-4.078	1.001	-0.11
8C	-3.639	-0.002	-0.08	21H	-4.031	-0.511	0.807
9C	3.15	-0.17	-1.107	22H	3.007	-1.142	-1.59
10C	2.563	0.197	1.28	23H	3.016	0.617	-1.857
11H	0.624	-0.208	-1.448	24H	4.187	-0.122	-0.757
12H	0.113	-1.096	1.444	25H	3.617	0.23	1.536
13H	0.532	-2.158	0.105	26H	1.861	0.323	2.097

**Table 3** Atomic coordinates of 61781 compound

Atoms number	x	y	z	Atoms number	x	y	z
1O	-2.287	-0.291	0.224	17H	1.245	1.531	-1.819
2O	-4.259	-0.195	-0.976	18H	0.509	-0.872	1.665
3C	0.597	0.416	-0.064	19H	1.368	0.628	1.986
4C	1.675	1.12	-0.896	20H	3.659	0.751	-1.626
5C	1.21	-0.148	1.228	21H	2.491	-0.489	-2.083
6C	2.812	0.16	-1.258	22H	2.89	-1.454	1.827
7C	3.256	-0.713	-0.112	23H	-2.643	1.719	-0.053
8C	-0.542	1.341	0.244	24H	-1.825	0.899	-1.401
9C	2.53	-0.831	1.013	25H	4.802	-2.07	0.564
10C	-1.889	0.965	-0.308	26H	5.372	-0.733	-0.445
11C	4.552	-1.444	-0.299	27H	4.496	-2.095	-1.178
12C	-0.364	2.462	0.959	28H	-1.193	3.13	1.169
13C	-3.502	-0.758	-0.196	29H	0.605	2.751	1.351
14C	-3.788	-2.084	0.442	30H	-3.822	-1.972	1.528
15H	0.225	-0.431	-0.659	31H	-3.021	-2.807	0.153
16H	2.101	1.968	-0.344	32H	-4.76	-2.45	0.098

**Table 4** SCF is performed by computing SCF using a single electron matrix. (for 7439).

Cycle	Energy (au)	Difference	Cycle	Energy (au)	Difference	Cycle	Energy (au)	Difference
1	-28.421599		15	-61.618344575	-0.94631	29	-62.26375675	-1.71912e-09
2	-42.042046254	-13.6204	16	-62.184404656	-0.56606	30	-62.263756751	-8.38327e-10
3	-35.39518615	6.64686	17	-62.263291329	-0.0788867	31	-62.263756752	-4.1905e-10
4	-48.633214241	-13.238	18	-62.263682109	-0.00039078	32	-62.263756752	-2.1214e-10
5	-49.287915631	-0.654701	19	-62.263741203	-5.90934e-05	33	-62.263756752	-1.08344e-10
6	-48.939737512	0.348178	20	-62.263751879	-1.06761e-05	34	-62.263756752	-5.28075e-11
7	-50.153658701	-1.21392	21	-62.263755358	-3.47896e-06	35	-62.263756752	-3.10365e-11
8	-51.518937971	-1.36528	22	-62.263756196	-8.3808e-07	36	-62.263756752	-1.54614e-11
9	-52.886295528	-1.36736	23	-62.26375656	-3.64217e-07	37	-62.263756752	-8.35598e-12
10	-53.336277249	-0.449982	24	-62.263756675	-1.14928e-07	38	-62.263756752	-2.67164e-12
11	-54.270082974	-0.933806	25	-62.263756719	-4.39574e-08	39	-62.263756752	-2.38742e-12
12	-55.344065994	-1.07398	26	-62.263756737	-1.80694e-08	40	-62.263756752	-1.98952e-12
13	-57.801898402	-2.45783	27	-62.263756745	-7.88867e-09	41	-62.263756752	-4.54747e-13
14	-60.672034561	-2.87014	28	-62.263756749	-3.61348e-09	42	-62.263756752	-1.13687e-13

**Table 5** SCF is performed by computing SCF using a single electron matrix. (for 22311).

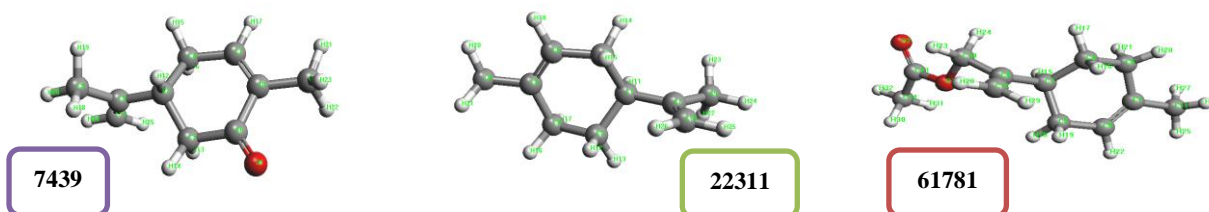
Cycle	Energy (au)	Difference	Cycle	Energy (au)	Difference	Cycle	Energy (au)	Difference
1	-21.768358		12	-52.614096137	-0.000848019	23	-52.614231545	-8.82039e-10
2	-33.511036521	-11.7427	13	-52.614182752	-8.66152e-05	24	-52.614231545	-2.72507e-10
3	-33.687344085	-0.176308	14	-52.614219586	-3.68342e-05	25	-52.614231545	-1.21929e-10
4	-40.157009475	-6.46967	15	-52.614227839	-8.25274e-06	26	-52.614231545	-3.7403e-11
5	-42.170399431	-2.01339	16	-52.614230464	-2.62523e-06	27	-52.614231545	-1.37561e-11
6	-43.695639593	-1.52524	17	-52.614231212	-7.47557e-07	28	-52.614231546	-5.11591e-12
7	-46.555932456	-2.86029	18	-52.61423144	-2.28267e-07	29	-52.614231546	-2.27374e-12
8	-51.301611257	-4.74568	19	-52.614231512	-7.13664e-08	30	-52.614231546	-4.54747e-13
9	-52.388557151	-1.08695	20	-52.614231534	-2.2776e-08	31	-52.614231546	-3.97904e-13
10	-52.594216425	-0.205659	21	-52.614231541	-7.01203e-09	32	-52.614231546	5.68434e-14
11	-52.613248118	-0.0190317	22	-52.614231544	-2.75202e-09			

**Table 6** SCF is performed by computing SCF using a single electron matrix. (for 61781).

Cycle	Energy (au)	Difference	Cycle	Energy (au)	Difference	Cycle	Energy (au)	Difference
1	-35.146201		16	-83.944417148	-0.576523	30	-84.039005592	-1.39846e-09
2	-56.182071326	-21.0359	17	-84.034575127	-0.090158	31	-84.039005593	-5.06247e-10
3	-50.861912527	5.32016	18	-84.03877621	-0.00420108	32	-84.039005593	-1.74964e-10
4	-60.508370615	-9.64646	19	-84.038930063	-0.000153853	33	-84.039005593	-7.57154e-11
5	-65.780687604	-5.27232	20	-84.038980106	-5.00423e-05	34	-84.039005593	-2.4329e-11
6	-68.604417017	-2.82373	21	-84.038997209	-1.71035e-05	35	-84.039005593	-9.89075e-12
7	-71.524265504	-2.91985	22	-84.039002699	-5.48981e-06	36	-84.039005593	-3.41061e-12
8	-73.109617973	-1.58535	23	-84.039004582	-1.8826e-06	37	-84.039005593	-1.13687e-12
9	-72.822269136	0.287349	24	-84.039005212	-6.30205e-07	38	-84.039005593	-1.59162e-12
10	-71.184165227	1.6381	25	-84.039005462	-2.49744e-07	39	-84.039005593	3.41061e-13
11	-71.084101598	0.100064	26	-84.039005546	-8.44531e-08	40	-84.039005593	9.09495e-13
12	-72.712369973	-1.62827	27	-84.039005576	-3.00626e-08	41	-84.039005593	-3.41061e-13
13	-74.735430973	-2.02306	28	-84.039005587	-1.07466e-08	42	-84.039005593	-9.09495e-13
14	-79.976575556	-5.24114	29	-84.039005591	-3.87865e-09	43	-84.039005593	0.0
15	-83.367893881	-3.39132						

**Table 7** compounds' final minimum geometrical energy and SCF energy values.

Compound Number	7439	22311	61781
Final SCF Energy	-62.2637567520 au	-52.6142315455 au	-84.0390055928 au
Final SCF Energy	-39071.1325 kcal/mol	-33015.9585 kcal/mol	-52735.3198 kcal/mol

**Fig. 2** Optimized structures of the compound

**Table 8.** Ground State Dipole (debye)

Comp. Number	X	Y	Z	length
7439	-1.74523919	-2.42399485	0.30117895	3.00205257
22311	-0.06869694	-0.19994140	-0.22845694	0.31126902
61781	1.12243970	-0.65112639	1.28898502	1.82902128

The geometry of the compounds was optimized using the PM3 method in the ArgusLab program. The optimized structures of the compounds are presented in Fig. 2. These structures represent the lowest energy configurations, providing insight into the molecular geometry and interactions within the compounds.

Mulliken and ZDO (Zero Differential Overlap) atomic charges are two essential approaches used to calculate the distribution of charges on atoms in molecular systems. Mulliken charges are based on the distribution of molecular orbitals across atoms to calculate charges. While the Mulliken method offers a simple and understandable approach to calculating atomic charges, it can sometimes lead to non-physical results, such as negative charges (Mulliken 1955). On the other hand, ZDO atomic charges stand out as a more suitable method, particularly for larger and more complex systems. ZDO simplifies the calculation process by neglecting differences in integrals, thus yielding more balanced results (Foster 1980). These methods are frequently used tools for researchers looking to analyse molecular charge distribution in quantum chemistry.

**Table 9** List of Mulliken and ZDO Atomic Charges of 7439 by using ArgusLab software

Atoms No	ZDO Atomic Charges	Mulliken Atomic Charges	Atoms No	ZDO Atomic Charges	Mulliken Atomic Charges
1O	-0.3143	-0.3251	14H	0.0824	0.1607
2C	-0.029	-0.1011	15H	0.0642	0.1378
3C	-0.1528	-0.3097	16H	0.0701	0.1412
4C	-0.0747	-0.2150	17H	0.1026	0.1894
5C	-0.1157	-0.1278	18H	0.0489	0.1166
6C	0.3220	0.3506	19H	0.0465	0.1136
7C	-0.0843	-0.1721	20H	0.0452	0.1128
8C	-0.1903	-0.2154	21H	0.0391	0.1051
9C	-0.0706	-0.2670	22H	0.0524	0.1225
10C	-0.0571	-0.2534	23H	0.0573	0.1286
11C	-0.1654	-0.3290	24H	0.0876	0.1729
12H	0.0734	0.1476	25H	0.0850	0.1664
13H	0.0776	0.1499			

**Table 10** List of Mulliken and ZDO Atomic Charges of 22311 by using ArgusLab software

Atoms No	ZDO Atomic Charges	Mulliken Atomic Charges	Atoms No	ZDO Atomic Charges	Mulliken Atomic Charges
1C	-0.0389	-0.1099	14H	0.0550	0.1266
2C	-0.0952	-0.2344	15H	0.0618	0.1319
3C	-0.0553	-0.1917	16H	0.0544	0.1250
4C	-0.0499	-0.1862	17H	0.0549	0.1239
5C	-0.1294	-0.1408	18H	0.0999	0.1866
6C	-0.1497	-0.2380	19H	0.0427	0.1097
7C	-0.1124	-0.1237	20H	0.0412	0.1076
8C	-0.0643	-0.2586	21H	0.0438	0.1103
9C	-0.0692	-0.2657	22H	0.0456	0.1125
10C	-0.1718	-0.3361	23H	0.0457	0.1128
11H	0.0690	0.1414	24H	0.0423	0.1093
12H	0.0571	0.1269	25H	0.0841	0.1686
13H	0.0524	0.1243	26H	0.0861	0.1678

**Table 11** List of Mulliken and ZDO Atomic Charges of 61781 by using ArgusLab software

Atoms No	ZDO Atomic Charges	Mulliken Atomic Charges	Atoms No	ZDO Atomic Charges	Mulliken Atomic Charges
1O	-0.2671	-0.2773	17H	0.0520	0.1237
2O	-0.3811	-0.3956	18H	0.0598	0.1330
3C	-0.0332	-0.1048	19H	0.0599	0.1289
4C	-0.0959	-0.2351	20H	0.0551	0.1258
5C	-0.0554	-0.1918	21H	0.0556	0.1246
6C	-0.0494	-0.1858	22H	0.1003	0.1871
7C	-0.1296	-0.1410	23H	0.0499	0.1204
8C	-0.1341	-0.1498	24H	0.0534	0.1236
9C	-0.1498	-0.2382	25H	0.0414	0.1078
10C	0.1186	-0.0144	26H	0.0440	0.1107
11C	-0.0646	-0.2590	27H	0.0430	0.1100
12C	-0.1349	-0.2986	28H	0.0848	0.1696
13C	0.3694	0.3976	29H	0.0867	0.1685
14C	-0.1143	-0.339	30H	0.0684	0.1412
15H	0.0736	0.1481	31H	0.0684	0.1407
16H	0.0557	0.1255	32H	0.0692	0.1442

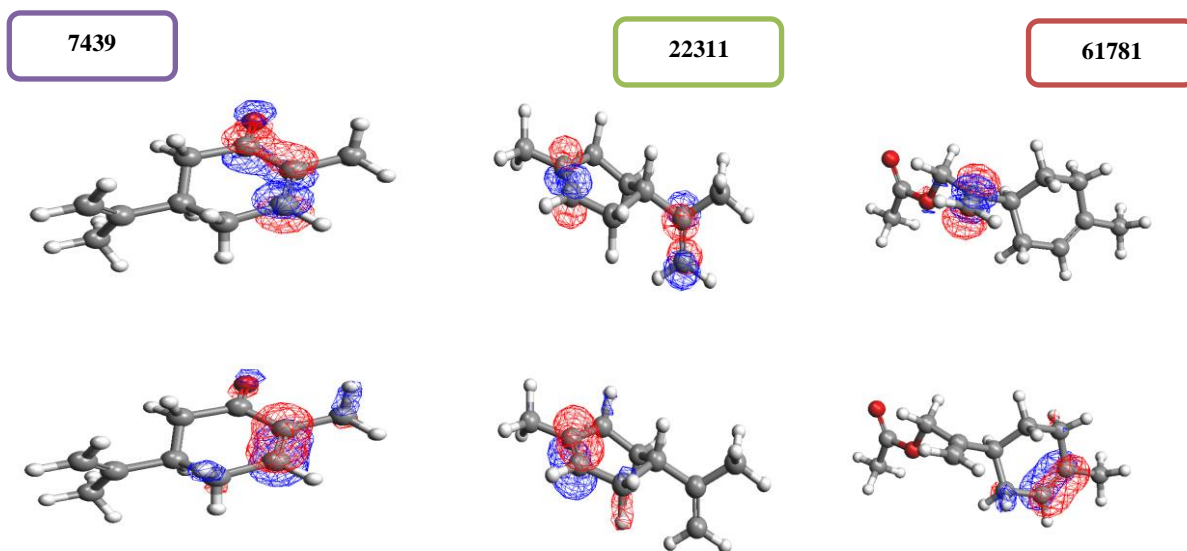


Fig. 3 Visualise the HOMO (a) and LUMO(b) of Compounds; blue shows positive and red shows negative.

**ELECTRON DENSITY**

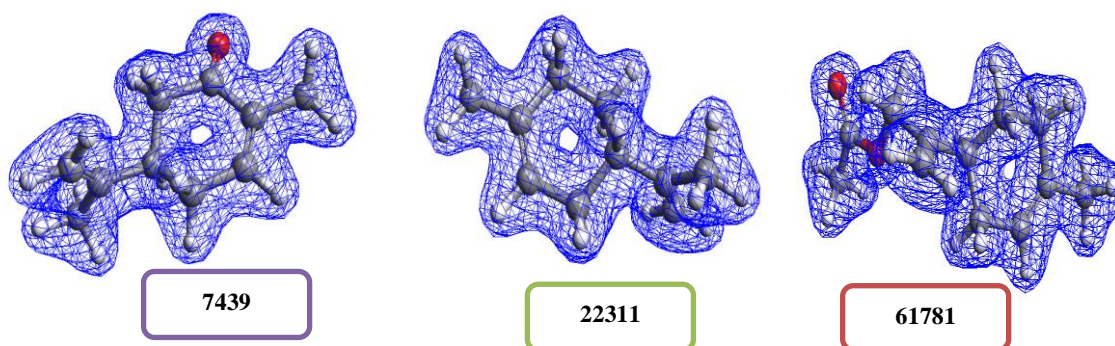


Fig. 4 Electron density representation of compounds

The HOMO-LUMO representations of limonene compound derivatives are shown in Fig. 3. The electron density of limonene compound derivatives is shown in Fig. 4.

An ESP-mapped density surface can illustrate areas within a molecule more susceptible to nucleophilic or electrophilic attack. These surfaces are valuable for qualitative interpretations, highlighting regions where chemical reactivity is likely, as seen in Fig. 5. A colour spectrum ranging between -0.0200 and +0.17 has been used.

**Solvent accesibe surface**

Solvent Accessible Surface" (SAS) refers to the external surface of a molecule that can interact with solvent molecules. This concept is typically used to study biomolecules' structural and functional properties, such as proteins, and plays a critical role in determining a molecule's interactions with solvents (Richard 1977). SAS calculates how much of a large molecule, like a protein, is accessible to solvent molecules (e.g., water), making it an essential parameter in biological processes. The solvent

accessible surface of the compounds, calculated using ArgusLab, is shown in Fig. 6.

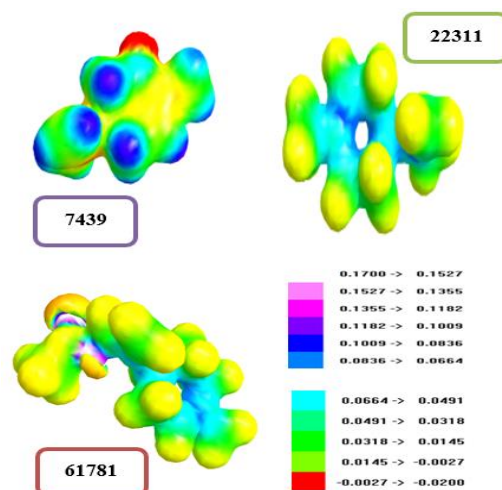


Fig. 5 shows a potential electrostatic map of the terminal molecule produced by applying the Mulliken charges with the scale of compounds



Compounds like limonene derivatives, which are aliphatic hydrocarbons, typically exhibit low UV absorption in UV-visible spectroscopy because they do not contain strong chromophore groups, such as conjugated double bonds. Limonene's UV absorption has been reported to occur mainly between 190–220 nm. This range is typical for simple aliphatic hydrocarbons and is generally attributed to  $\pi \rightarrow \pi^*$  transitions (Śmiałek et al. 2012).

Fig. 7 presents limonene derivative compounds' UV/visible electronic absorption spectrum. In the spectrum, intense peaks are observed at 174.1, 183.5, and 171.3 nm, while relatively low-intensity peaks appear at 228.5, 173.7, and 178.3 nm, representing the strength of the transitions of the compound. These values differ from experimental results by approximately 20–30 nm for all peaks, reflecting the challenges in accurately predicting the absorption spectra of these compounds with the currently available computational methods. Since the compounds do not possess UV-active

aromatic rings or large conjugation systems, the absorption peak observed in UV spectra is typically weak.

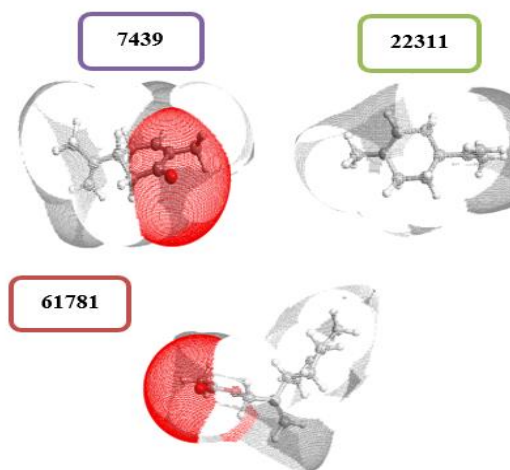


Fig. 6 Solvent-accessible surface of compounds

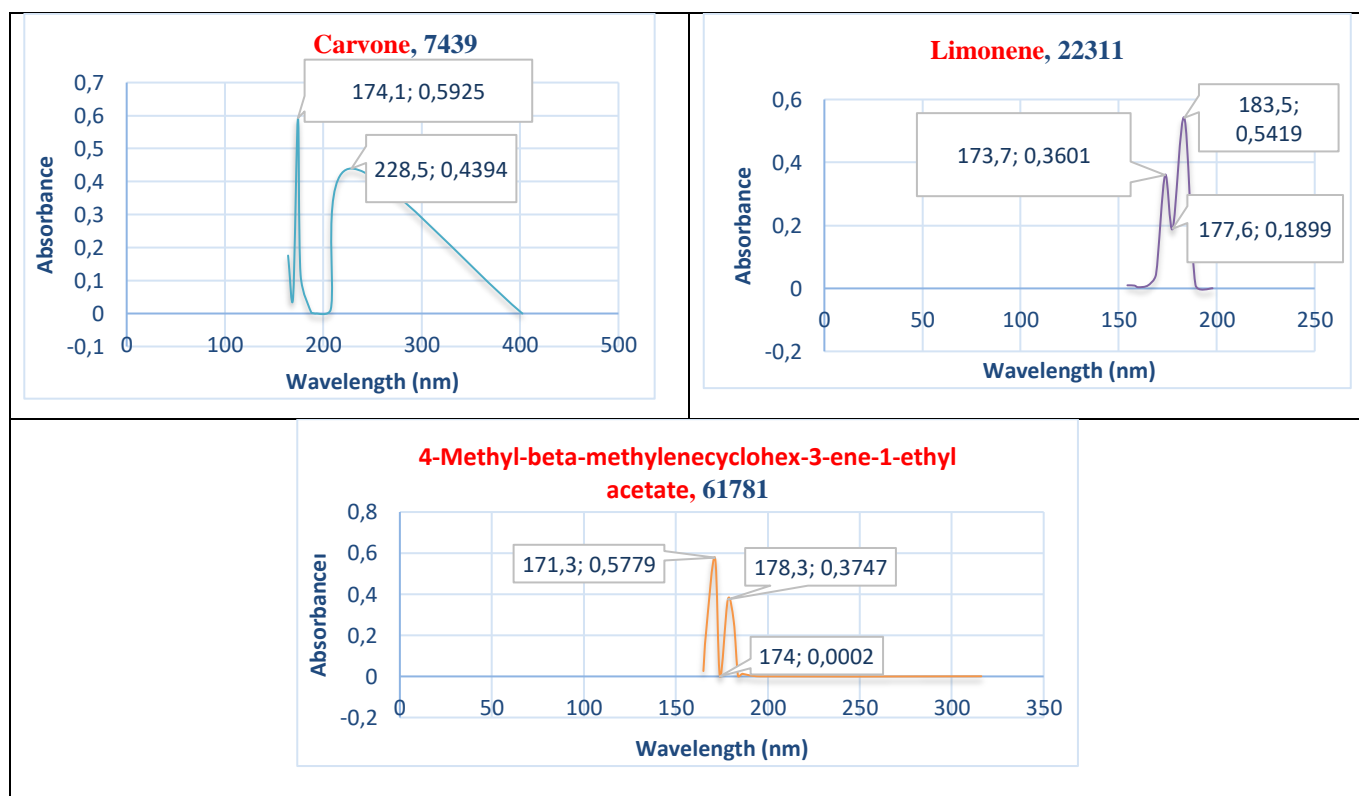


Fig. 7 Electronic absorption spectrum of the compounds

#### 4. Conclusion

It has been observed that the ArgusLab program has a very user-friendly interface and completes calculations in a very short time. In this research study, we included some calculation tasks that can be performed using ArgusLab and observed that the results are stable. Using the ArgusLab software, the lowest energy favorable conformations of limonene compound derivatives were found to be -62.2637567520 au, -52.6142315455 au, and -

84.0390055928 au, respectively. The lowest energy conformations were employed in molecular modeling calculations after the geometric variables related to compounds were finally fully optimized for the compound. The calculated thermodynamic parameter, dipole moment, Mulliken and ZDO Atomic Charge, and optimized geometry were all well within the computational results' accuracy range. The  $\Delta E$  values for the compounds numbered 7439, 22311, and 61781 are calculated as -



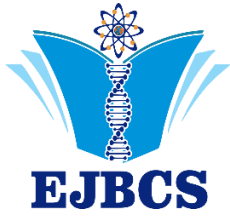
0.005155, -0.382305, and -0.038150, respectively, based on their eigenvalues. Compound 22311, with the largest  $\Delta E_{\Delta E}$ , exhibits the highest reactivity, while compound 7439, with the smallest  $\Delta E_{\Delta E}$ , indicates greater stability and lower reactivity, positioning 61781 as intermediate between the two. Azure A and Hyamine, with their narrow HOMO-LUMO energy gaps and active sites revealed through Mulliken charges, demonstrate the importance of computational models in understanding electronic structures for various applications (Özkır et al. 2012, 2013). The compound numbered 7439 appears to have a smaller solvent-accessible surface, indicating a more compact structure or fewer hydrophilic regions exposed to the solvent. In contrast, the compounds numbered 22311 and 61781 possess larger solvent-accessible surfaces, suggesting that their surface characteristics include a higher number of polar or nonpolar regions. This distinction may influence the hydrophilic and hydrophobic properties of the

compounds, as well as their interaction potential with solvents and solubility profiles.

In conclusion, the UV/visible electronic absorption spectrum of limonene derivative compounds, as presented in this study, demonstrates low-intensity peaks, consistent with the characteristics of aliphatic hydrocarbons that lack strong chromophores or large conjugation systems. The observed peaks at 174.1, 183.5, and 171.3 nm, along with weaker peaks at 228.5, 173.7, and 178.3 nm, correspond to  $\pi \rightarrow \pi^*$  transitions typical for such compounds. The discrepancies of approximately 20–30 nm between the computational and experimental results highlight the limitations of current computational methods in accurately predicting UV absorption spectra for limonene derivatives. These findings underline the need for further refinement of computational models to enhance the accuracy of spectral predictions for non-aromatic, non-conjugated systems.

## References

- Cruciani G, Clementi S, Pastor M. 1998. Golpe guided region selection. *Perspectives in Drug Discovery and Design*. 12-14(16): 71-86.
- Dewar MJS, Zoobisch EG, Healy EF, Stewart JJP. 1985. AM1: A new general purpose quantum mechanical molecular model. *J Am Chem Soc*. 107: 3902-3910.
- Dunn III, Hopfinger AJ. 1998. *Drug Discovery*, Kluwer Academic Publishers. Chapter 12, pp.167-182.
- EL Ouafy, H., EL Ouafy, T., Oubenali, M., EL Haimouti, A., Gamouh, A., & Mbarki, M. (2021). Analysis of the Chemical Reactivity of Limonene by the Functional Density Theory Method Using Global Descriptors. *Journal of Chemical Health Risks*, 11(2), 213-221.
- Foster, JP, Weinhold F. 1980. Natural hybrid orbitals. *J Am Chem Soc*. 102(24), 7211-7218. doi: 10.1021/ja00544a007.
- Ikpeazu OV, Otuokere IE, Igwe KK. 2017. Molecular geometry optimization and frontier molecular orbitals of luminal Na-K-Cl cotransporter (NKCC2) Inhibitor, 5-(aminosulfonyl)-4-chloro-2-[(2-furylmethyl) amino] benzoic acid, furosemide. *J. Environ Life Sci* 2(1), 29-33.
- İşcan Ö. 2023. A Insilico Study on Structural aspects of Caffeine by ArgusLab 4 software. *Journal of Physical Chemistry and Functional Materials*. 6(2):138-144. doi.org/10.54565/jphcfum.1402117.
- Laxmi K. 2014. *Scientia Research Library*. *J Appl Chem*. 2(1): 92-101.
- Laxmi K. 2016. A Hypothetical Study on Structural aspects of Indole-3-carbinol (I3C) by Hyperchem and Arguslab 4 software. *Int Journal of Engineering Research and Applications*. 6(1): 17-24.
- Martin YC. 1998. *Perspective in drug discovery and design*. Springer Publisher, 12th Volume, pp.3- 23.
- Mortimer RG. 2000. *Physical chemistry*. Academic Press.
- Mulliken RS. 1955. Electronic Population Analysis on LCAO–MO Molecular Wave Functions. I. *J Chem Phys* 23(10): 1833-1840. doi: 10.1063/1.1740588.
- Özkır, D., Kayakırılmaz, K., Bayol, E., Gürten, A. A., & Kandemirli, F. (2012). The inhibition effect of Azure A on mild steel in 1 M HCl. A complete study: Adsorption, temperature, duration and quantum chemical aspects. *Corrosion Science*, 56, 143-152.
- Özkır, D., Bayol, E., Gürten, A., Sürme, Y., & Kandemirli, F. (2013). Effect of hyamine on electrochemical behaviour of brass alloy in HNO<sub>3</sub> solution. *Chemical Papers*, 67(2), 202-212.
- Richards FM. 1977. Areas, volumes, packing, and protein structure. *Annu Rev Biophys*, 6(1): 151-176.
- Smialek MA, Hubin-Franskin MJ, Delwiche J, Duflo D, Mason NJ, Vronning-Hoffmann, SALV P, Limao-Vieira P. (2012). Limonene: electronic state spectroscopy by high-resolution vacuum ultraviolet photoabsorption, electron scattering, He (I) photoelectron spectroscopy and ab initio calculations. *Phys Chem Chem Phys*. 14(6), 2056-2064.
- Stewart JJP. 1989. *Comp. Chem.*, 10, 209-220 and 221-264, 1989.
- Thompson MA, Glendening ED, Feller D. 1994. The nature of K<sup>+</sup>/crown ether interactions: A hybrid quantum mechanical-molecular mechanical study. *J Phys Chem*. 98(41):10465-10476.
- Thompson MA, Gregory K, Schenter J. 1995. *Phys Chem*, 99:6374-6386.
- Thompson MA. 1996. QM/MMpol: A consistent model for solute/solvent polarization. Application to the aqueous solvation and spectroscopy of formaldehyde, acetaldehyde, and acetone. *J Phys Chem*. 100(34): 14492-14507.
- Thompson MA. 2004. Molecular docking using ArgusLab, an efficient shape-based search algorithm and the AScoring function. ACS meeting Philadelphia 172:CINF 42, PA.



## Synthesis of waste pineapple peel cellulose based hydrogels and aerogels

Oğuzhan Şimşek<sup>1</sup> , Burcu Okutucu<sup>2\*</sup> 

<sup>1</sup>Dokuz Eylül University, Institute of Health Sciences, Balçova, Türkiye

<sup>2</sup>Ege University, Faculty of Science, Biochemistry Department, Bornova, Türkiye

\*Corresponding author: [burcu.okutucu@ege.edu.tr](mailto:burcu.okutucu@ege.edu.tr)  
Orcid No: <https://orcid.org/0000-0002-0907-4175>

Received : 04/11/2024  
Accepted : 21/12/2024

To Cite / Atf için: Şimşek O, Okutucu B. 2024. Synthesis of waste pineapple peel cellulose based hydrogels and aerogels. Eurasian J Bio Chem Sci, 7(2):165-170 <https://doi.org/10.46239/ejbc.1576204>

**Abstract:** Aerogels were one of the groups of nanoporous materials with superior physicochemical properties. Their unique physical, chemical, and mechanical properties make aerogels as promising candidates for different applications including drug delivery, tissue engineering, medical implantable devices, biotechnology and wastewater treatments. The organic (silica) and inorganic (biopolymers) compounds can be used to synthesize aerogels. Cellulose found the most abundant in world was one of these biopolymers. Cellulose has properties such as biocompatibility, recyclability, excellent mechanical strength, adjustable optical appearance, thermostabilizing, non-toxicity make to prefer in aerogel studies. In this study, pineapple peel waste cellulose was used to synthesize aerogel. To obtain cellulose hydrogels cellulose and carboxymethyl cellulose (monomers) were mixed with epichlorohydrin (cross-linker). Alcolgels (by solvent exchange) and aerogels (by freeze-thaw) was synthesized from obtained hydrogels. The characterization studies water adsorption capacity and transparency tests were performed waste based hydrogel and aerogels.

**Keywords:** Bioaerogel, waste-based cellulose, pineapple peel, adsorption capacity

### *Atık ananas kabuğu selülozu temelli hidrojellerin ve aerojellerin sentezlenmesi*

**Özet:** Aerojeller, eşsiz fizikokimyasal özelliklere sahip nanoporöz malzeme gruplarından birisidir. Eşsiz fiziksel, kimyasal ve mekanik özellikleri aerojelleri; ilaç taşınımı, doku mühendisliği, implant medikal cihazlar, biyoteknoloji ve atık su arıtmaları gibi farklı uygulamalar için umut verici adaylar haline getirir. Aerojel sentezinde inorganik (silika) ve organik bileşikler (biyopolimerler) kullanılabilir. Dünyada en çok bulunan selüloz bu biyopolimerlerden birisidir. Selüloz, biyoyoumluluk, geri dönüştürülebilirlik, üstün mekanik kuvvet, ayarlanabilir optik görünüm, termostabilizasyon, toksik olmaması gibi özelliklerinden dolayı aerojel çalışmalarında tercih edilmektedir. Bu çalışmada ananas kabuğu atığı selülozu aerojel sentezinde kullanılmıştır. Selüloz hidrojellerini elde etmek için selüloz ve karboksimetil selüloz (monomerler) epiklorohidrin (çapraz bağlayıcı) ile karıştırılmıştır. Elde edilen hidrojellerden, alkojeller (solvent değişimi ile) ve aerojeller (dondurma-çözme ile) sentezlenmiştir. Atık selülozdan hazırlanan hidrojel ve aerojellerin karakterizasyonu için su adsorpsiyon kapasitesi ve saydamlık testi yapılmıştır.

**Anahtar Kelimeler:** Biyoaerogel, atık bazlı selüloz, ananas kabuğu, adsorpsiyon kapasitesi

### 1. Introduction

Aerogels were porous solid materials have unique properties such as bulk density, high porosity, large surface area. They had many different application areas; food industry, pharmaceutical, air filtration, wastewater treatment, dye adsorption, thermal insulation. (Azimi et al. 2024; Chen et al. 2022; Do et al. 2020; Ganesamoorthy et al. 2021; Groult et al. 2022; Gu et al. 2022; Guastaferrro et al. 2021; Ihsanullah et al. 2022; McNeil et al. 2022; Sanchez et al. 2023; Sozcu et al. 2024; Sun et al. 2022). Depending

on the nature of the initial precursors, aerogels were classified as inorganic, organic and hybrid. Inorganic aerogels were based on metals, oxides and silica. The organic aerogels were based on synthetic polymers (polystyrenes, polyurethanes, poly alcohols, polyacrylates) or natural biopolymers (protein, carbohydrates, pectins, mucilage) (He at al. 2023; Meti et al. 2022; Tafreshi et al. 2022; Wei et al. 2022). The waste based aerogels, generally had natural biopolymer precursor also known as bioaerogels. The biowaste that constitute the lignocellulosic

mass were excellent bioaerogel precursors (renewable, cheap). The lignocellulosic mass could be agricultural, food or fruit wastes (He et al. 2023; Joshi et al. 2023; Abdul Khalil et al. 2020). The components of lignocellulosic biomass were cellulose, hemicellulose and lignin. Cellulose had increasing interest in hydrogel/ aerogel areas due to its biocompatibility, thermal stability, renewability, biodegradability and non-toxicity (Joshi et al. 2022; Abdul Khalil et al. 2020; Al Abdallah et al. 2024; Chang et al. 2010a; Budtova 2019; Jianan et al. 1996; Li et al. 2024; Long et al. 2018)

The pineapple or *Ananas comosus*, a member of *Bromeliaceae* family and was grown in many parts of world. It is eaten as preserved or fresh fruit. Also, it was used jams, concentrates and juices. Since 60% of pineapple fruits can be eaten, the 40 % of parts were as wastes. The pineapple wastes were leaves, peels, roots and farm stems (Nath et al. 2023). Conversion of biomass wastes as a sustainable resource into bioaerogels was a new and innovative process. By this way utilizing biomass and wastes reduced environmental problems (Asim et al. 2019; Partow et al. 2022). Also, the properties of biomass waste (biodegradability, non-toxicity), make bioaerogel as an eco-friendlier material compared with silica based inorganic aerogels (Mazrouei-Sebdani et al. 2021). For this aim, we used free of charge pineapple peel waste as a cellulose was a source of bioaerogel

While synthesizing cellulose aerogel, the biggest problem was the solubility of cellulose. The chemical structure (high crystallized form, robust inter and intra molecular hydrogen bonds-high number hydroxyl groups) make cellulose insoluble in water. There were many solutions of this problem, but most of them included specific and toxic chemicals (Chang et al. 2010b). The eco-friendly choice for this dissolution problem was blending cellulose with cellulose derivatives such as carboxymethyl cellulose (CMC), ethyl cellulose (EHC), hydroxyethyl cellulose (HEC), hydroxypropyl cellulose (HPC). The carboxymethyl cellulose exhibited great potential for using this aim. Because, CMC had good water solubility, biocompatibility, biodegradability and sensitivity to pH or ionic strength. (Chang and Zhang 2011). After blending with carboxymethyl cellulose, cellulose became more soluble.

In this study, we converted pineapple peel wastes into cellulose based aerogels. For modifying and to solve the dissolution problem of cellulose we blended waste cellulose with CMC in sodium hydroxide/ urea. The cellulose hydrogels crosslinked with epichlorohydrin (ECH). To convert hydrogel to alcogel and then aerogel, we studied a multistage solvent exchange (ethanol) and freeze-drying process. The water adsorption studies and swelling degree, transparency of hydrogels and aerogels were studied for characterization.

## 2. Materials and Method

The pineapple peels were taken from local market free of charge (waste). The sodium hydroxide, urea, carboxymethyl

cellulose, epichlorohydrin (ECH), hydrogen peroxide, potassium hydroxide, hydrochloric acid 37 %, ethanol 99.9 % were purchased from Sigma-Aldrich Chemical Co. Ltd. All other chemicals were analytical grade.

### 2.1. The isolation of cellulose from pineapple peel waste

The cellulose could be isolated from biomass via mechanical, disintegration, chemical treatment with alkaline solutions and biological treatments. In this study; the cellulose extraction from pineapple peel was carried out with potassium hydroxide (Dai et al. 2016). The pineapple peels were taken from local markets as waste (free of charge). Pineapple peels were cut into small pieces and dried at 50°C. Dried pineapple peels were ground in mortar (Retsch RH 100). 50 grams of dry pineapple peel was boiled for 2 hours at 80 ° C in 1L distilled water and filtered through filter paper. This process was repeated 3 times. Soluble fiber tissues were removed and filtered again. The residue was mixed with 5% hydrogen peroxide and stayed at 75 ° C for 4 hours (to remove the lignin) and filtered. The residue was washed until neutralized with 95% ethanol and distilled water. The sample was dried at 50 ° C for 16 hours. To remove hemicellulose, the pellet as mixed with 10% potassium hydroxide for 24 hours and filtered. The residue (cellulose) was washed until neutralized with 95% ethanol and water and dried.

### 2.2. Preparation of waste cellulose based hydrogel and aerogel

To obtain 3 % cellulose solution; the waste cellulose was dissolved in 6 % NaOH/ 4 % urea / 90 % distilled water by stirring 5 minutes and then stored at -20° C for two days. After two days, the solid was thawed and stirred at room temperature till a transparent cellulose solution was taken. 3 wt% CMC was dissolved in same solution (6 % NaOH/ 4 % urea / 90 % distilled water). The cellulose and CMC solutions were mixed different ratios (5:5: 6:4;8:2; 9:1) respectively. ECH was added to the cellulose/ CMC mixtures as cross-linker (0.1 % v/v) stirred at room temperature for 2 days to obtain a homogeneous solution, and then kept at room temperature for four days to get hydrogel forms. Hydrogels were washed with distilled water before next step.

The cellulose alcogels were prepared from hydrogels first replacing the water in the hydrogel with ethanol (EtOH) by multistage solvent exchange process. During the solvent exchange process, the hydrogels were soaked in 30; 50; 70; 100 (%) EtOH and 100 % EtOH for 5 days, where the ethanol was centrifuged and replaced fresh EtOH everyday to obtain alcogels. The alcogels were then soaked with 100 (%) EtOH for 2 hours and centrifuged. The alcogels were freeze-dried at -80° C for 4 days to obtain aerogel. The final product cellulose aerogels were stored at dry place (room temperature) for further experiments (Gan et al. 2017; Paksung et al. 2020; Paulauskiene et al. 2022; Wang et al. 2016).

## 2.3. Characterization Studies

### 2.3.1. Water adsorption studies

To calculate water adsorbing capacity of hydrogels and aerogels, the samples were immersed into distilled water to acquire different conditions such as pH, temperature and time. We studied different time effect on water adsorption of hydrogels and aerogels in this study.

The hydrogels and aerogels (constant weight) were immersed in distilled water for 15-30-45 min- 1h -2 h-4 h-6 h. The weight of each sample was measured (before and after immersed) and the percentage of water adsorption capacity (WAC %) was calculated according to Equation 1.

$$WAC(\%) = \frac{W_s - W_d}{W_d} * 100 \text{ (Eq. 1)}$$

Where  $W_d$  and  $W_s$  were the weights of the hydrogel and aerogel before and after immersion in respectively.

### 2.3.2. The transparency of the hydrogels and aerogels

The transparency of aerogels were determined by UV-Vis microplate spectrophotometer at a wavelength ranging from 200 to 1000 nm

## 3. Results and Discussion

### 3.1. The preparation of waste based cellulose aerogels

The cellulose aerogels had the advantages renewability, biocompatibility, biodegradability as cellulose. Also; the cellulose aerogels could be ecofriendly because their natural decomposition and also they can be studied at many different areas because of their stability in harsh conditions. The cellulose aerogels was studied by using waste cellulose plant or plant based materials (cotton, hemp, coconut, pineapple waste). Depending on source the extraction of cellulose involves pretreatment, post treatment and dissolution stages. The extraction methods can change the characteristics of cellulose (size, degree of polymerization, thermal stability, degree of hydroxylation) The quality of extracted cellulose effect also the performance of the cellulose aerogels (Nguyen et al. 2022; Liu et al. 2024; Long et al. 2018; Asim et al. 2019).

The plant cellulose fibers fills with lignin and hemicellulose penetrates the cellulose skeleton to form 3D structure via covalent and hydrogen bonds by using alkaline solutions (sodium or calcium hydroxide) (Mujtaba et al. 2023). To unform this stable compact structure, many deconstruction techniques can be used such as ball-milling, acidic fraction, alkaline fraction, etc. All techniques resulted the different form of cellulose (fibers, nanowhisker, particle). In this study we used alkaline process. The alkaline fraction process is done to deconstruct lignocellulosic form at a certain tempertaure and residence time. The advantages of this process removes lignin and breaking bonds between hemicellulose, retaining cellulose in solid fraction as cellulose fibers and can be ingrated other techniques which were related the solubility of cellulose (Liyange et al. 2021; Gan et al. 2017).

The extraction quality of waste cellulose effected the formation of hydrogel and the initial hydrogel characteristics (porosity, pore volume) were the results of cellulose extraction. The aerogel properties mostly depend on the hydrogel 3D form. However the surface area of aerogels only depends on drying method of aerogel while preparing. The different methods were existed for this aim; freeze-drying, supercritical drying (CO<sub>2</sub>, acetone, methanol or ethanol), ambient pressure drying, vacuum drying, and microwave drying. These methods were used to remove the existed solvent inside the pores of the hydrogel maintaining the porous structure. Because of its simplicity, environmentally friendly and cheap cost, freeze-drying technique was used for waste based cellulose aerogel in this study. Freeze- drying of cellulose hydrogels involved three stages. The first stage consisted of freezing the hydrogels into ice crystals leading the ordered structure. The critical point of freezing was the temperature, we optimized the temperature at -80°C. This temperature affected the structure of the ice formed in aerogel and the quality of the aerogel. Primary drying was performed to remove 95 % of water and secondary drying was performed to eliminate unfrozen water (Simon-Herrero et al. 2016).

According to our results (Fig 1.) the hydrogels lost almost 95 % of their weight after freeze- drying and ultra weight cellulose aerogels were got.



**Fig. 1** The different ratio of waste cellulose: CMC based hydrogels (a), alcogels (b) and aerogel (c) after freeze-drying

### 3.2. The results of characterization studies

#### 3.2.1. Water adsorption capacities of hydrogels and aerogels

To confirm environmental adaptation of hydrogel and aerogel the adsorption capacity was studied. The water adsorption capacity of waste cellulose: CMC (9:1; 8.2; 6:4; 5:5) hydrogels and aerogels were studied according to weight changing with time.

According to Figure 2; the water adsorption capacity of waste cellulose: CMC based hydrogels were reached adsorption equilibrium within 60 min and aerogels reached at 30 min. The different ratio of cellulose/ CMC did not affect the water adsorption capacity of hydrogels The adsorption capacity increased time by time. The reason of this could be surface and high pore size of aerogels. The adsorption capacity of aerogels increased significantly at first and then water filled the aerogels pores and adsorption reached saturation quickly. The strong hydrophilicity of aerogel surface absorbed the water completely. The percentage of changing weight of aerogels after water adsorption were 300-800 % of its weight whereas the percentage changing of weight for hydrogels were 20-100 % of its weight. The cellulose aerogel reached average 500% of water adsorption within 30 min. This suggested us

the cellulose aerogel had a fast water adsorption ability due to the high porosity and abundant hydrophilic groups (hydroxyl, carboxyl).

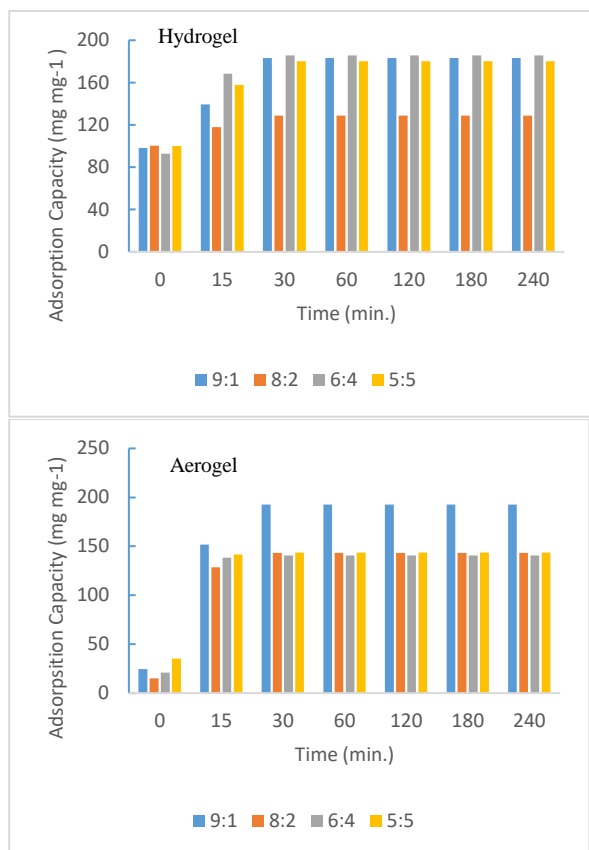


**Fig. 2** The adsorption capacity (mg mg<sup>-1</sup>) of waste cellulose: CMC (9:1; 8:2; 6:4; 5:5) based hydrogel and aerogel

### 3.2.2. The transparency of the cellulose hydrogels and aerogels

The UV-Vis transmission spectra of cellulose aerogels were given at Fig 2. According to the spectra results, our cellulose aerogels do not transmit light after 200-400nm, while cellulose hydrogel do not transmit light after 400-600 nm (Gan et al. 2017). The results shown that cellulose aerogels were more transparency than cellulose hydrogels.

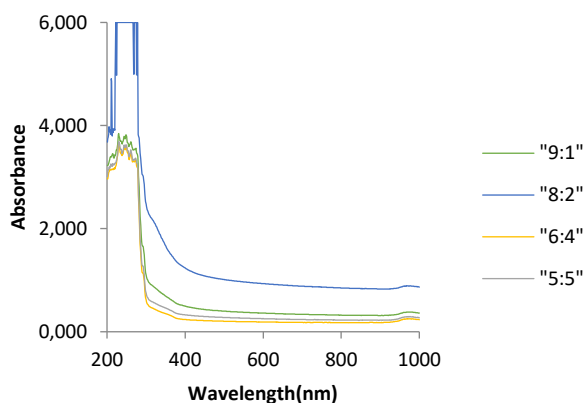


**Fig. 3** The UV-Vis spectra of different ratio of waste cellulose: CMC based aerogels

## 4. Conclusion

The waste pineapple cellulose require no harsh chemicals to make bioaerogels owing to their structural formability. The results were shown that bioaerogels kept several weeks at room temperature and did not seen any visible degradation. The important advance of this study was the simplicity of the bioaerogel preparation process. The prepared bioaerogel also distinguished itself through water adsorption capacities which were crucial for the potential applications such as the treatment and removal of metals/dyes/toxic compounds from wastewaters. The aerogel production in large scale faced problems involved toxic precursor compound and the sustainability of initial compounds. Bioaerogels overcome these problems by using raw materials (biomass-derived). So that using waste pineapple as the resource of bioaerogels is an alternative way of solving environmental pollution.

## Acknowledgements

This research did not receive any specific grant from university research center or company

## Authors' contributions:

OS: performed the analysis, obtaining data, editing; BO: editing, writing

## Conflict of interest disclosure:

The authors declare that there were no conflicts of interest in the realization of this research.

## References

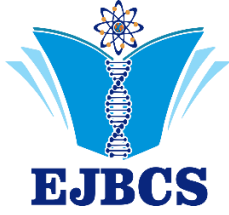
- Abdul Khalil HPS, Adnan AS, Yahya EB, Olaiya NG, Safrida S, Hossain S, Balakrishnan V, Gopakumar DA, Abdullah CK, Oyekanmi AA, Pasquini D. 2020. A Review on plant cellulose nanofibre-based aerogels for biomedical applications. *Polymers*. 12: 1759. doi:10.3390/polym12081759
- Al Abdallah H, Joy HJH, Abu-Jdayi B. 2024. Cellulose and nanocellulose aerogels, their preparation methods, and potential applications: a review. *Cellulose*. 31: 2001–2029. doi:10.1007/s10570-024-05743-w
- Asim N, Badiei M, Alghoul MA, Mohammad M, Fudholi A, Akhtaruzzaman Md, Amin N Sopian K. 2019. Biomass and Industrial Wastes as Resource Materials for AerogelPreparation: Opportunities, Challenges, and Research Directions. *Ind Eng Chem Res*. 58: 17621–17645. doi: 10.1021/acs.iecr.9b02661
- Azimi B, Sepahvand S, Ismaeilimoghadam S, Kargarzadeh H, Ashori A, Jonoobi M, Danti S. 2024. Application of cellulose-based materials as water purification filters; A state-of-the-art review. *J Environ Polym Degrad*. 32: 345–366. doi:10.1007/s10924-023-02989-6
- Budtova T. 2019. Cellulose II aerogels: a review. *Cellulose*. 26:81–121. doi: 10.1007/s10570-018-2189-1
- Chang C, Duan B, Cai J, Zhang L. 2010a. Superabsorbent hydrogels based on cellulose for smart swelling and controllable delivery. *Euro Polym J*. 46: 92–100. doi:10.1016/j.eurpolymj.2009.04.033
- Chang C, Zhang L, Zhou J, Zhang L, Kennedy JF. 2010b. Structure and properties of hydrogels prepared from cellulose in NaOH/urea aqueous solutions. *Carbohydr Polym*. 82 : 122–127. doi:10.1016/j.carbpol.2010.04.033



- Chang C, Zhang L. 2011. Cellulose-based hydrogels: Present status and application prospects. *Carbohydr Polym.* 84: 40–53 doi:10.1016/j.carbpol.2010.12.023
- Chen L, Jiang X, Qu N, Lu H, Xu J, Zhang Y, Li G. 2022. Selective adsorption and efficient degradation of oil pollution by microorganisms immobilized natural biomass aerogels with aligned channels. *Mater Today Sustain.* 19: 100208. Doi: 10.1016/j.mtsust.2022.100208
- Dai H, Huang H. 2016. Modified pineapple peel cellulose hydrogels embedded with sepia ink for effective removal of methylene blue *Carbohydr Polym.* 148: 1–10. Doi:10.1016/j.carbpol.2016.04.040
- Do NHA, Luu TP, Thai QB, Le DKN, Chau DQ, Nguyen ST, Le PK, Phan-Thien N, Hai M, Duong HM. 2020. Heat and sound insulation applications of pineapple aerogels from pineapple waste, *Mater Chem Phys.* 242: 122267. Doi: 10.1016/j.matchemphys.2019.122267
- Gan S, Zakaria S, Chia CH, Chen RS, Ellis AV, Kaco H. 2017. Highly porous regenerated cellulose hydrogel and aerogel prepared from hydrothermal synthesized cellulose carbamate. *PLoS ONE.* 12: e0173743. doi:10.1371/journal.pone.0173743
- Ganesamoorthy R, Vadivel VK, Kumar R, Kushwaha OS, Mamane H. 2021. Aerogels for water treatment: A review. *J Clean Prod* 329: 129713. doi: 10.1016/j.jclepro.2021.129713
- Ganesan K, Budtova T, Ratke L, Gurikov P, Baudron V, Preibisch I, Niemeyer P, Smirnova I, Milow B. 2018. Review on the production of polysaccharide aerogel particles. *Materials.* 11: 2144; doi:10.3390/ma11112144
- Groult S, Buwalda S, Budtova T. 2022. Tuning bio-aerogel properties for controlling drug delivery. Part 2: Cellulose-pectin composite aerogels. *Biomater Adv.* 135, 212732. doi:10.1016/j.bioadv.2022.212732
- Gu J, Fu R, Kang S, Yang X, Song Q, Miao C, Ma M, Wang Y, Sa H. 2022. Robust composite aerogel beads with pomegranate-like structure for water-based thermal insulation coating. *Constr Build Mater.* 341: 127722. doi: 10.1016/j.conbuildmat.2022.127722
- Guastaferrero M, Reverchon E, Baldino L. 2021. Polysaccharide-based aerogel production for biomedical applications: A comparative review. *Materials.* 14: 1631. doi:10.3390/ma14071631
- He ZJ, Chen K, Liu ZH, Li BZ, Yuan YJ. 2023. Valorizing renewable cellulose from lignocellulosic biomass toward functional products *J Clean Prod.* 414: 137708. doi: 10.1016/j.jclepro.2023.137708
- Ihsanullah I, Sajid M, Khan S, Bilal M. 2022. Aerogel-based adsorbents as emerging materials for the removal of heavy metals from water: Progress, challenges, and prospects. *Sep Purif Technol.* 291: 120923. doi:10.1016/j.seppur.2022.120923
- Jianan C, Shaoqiong Y, Jinyue R. 1996. A Study on the Preparation, Structure, and Properties of Microcrystalline Cellulose. *J Macromol Sci Chem A.* 33:1851-1862. doi:10.1080/10601329608011011
- Joshi P, Sharma OP, Ganguly SK, Srivastava M, Khatri OM. 2022. Fruit waste-derived cellulose and graphene-based aerogels: Plausible adsorption pathways for fast and efficient removal of organic dyes. *J Colloid Interfac Sci.* 608: 2870–2883. Doi:10.1016/j.jcis.2021.11.016
- Li X, Wan C, Tao T, Chai H, Huang Q, Chai Y, Wu Y. 2024. An overview of the development status and applications of cellulose-based functional materials. *Cellulose.* 31:61–99. doi: 10.1007/s10570-023-05616-8
- Liu L, Wang T, Li M, Gao Y, Zhang L. 2024. Carboxylated cellulose-based composite aerogel with double filling structure for sustained drug release. *Ind Crop Prod.* 210: 118126. doi: 10.1016/j.indcrop.2024.118126
- Liyanage S, Acharya S, Parajuli P, Shamshina JL, Abidi N. 2021. Production and surface modification of cellulose bioproducts. *Polym.* 13: 3433. doi:10.3390/polym13193433
- Long LY, Weng YX, Yu-Zhong Wang YZ. 2018. Cellulose Aerogels: Synthesis, applications, and prospects. *Polym.* 10: 623 doi:10.3390/polym10060623
- Mazrouei-Sebdani, Z., Begum, H., Schoenwald, S., Horoshenkov, K. V., Malfait, W. J. 2021. A review on silica aerogel-based materials for acoustic applications. *J Non-Cryst Solids.* 562: 120770. Doi: 10.1016/j.jnoncrystol.2021.120770
- McNeil SJ, Gupta H. 2022. Emerging applications of aerogels in textiles. *Polym Test.* 106: 107426. Doi: 10.1016/j.polymertesting.2021.107426
- Meti P, Mahadik DB, Lee KY, Wang Q, Kanamori K, Gong YD, Park HH. 2022. Overview of organic–inorganic hybrid silica aerogels: Progress and perspectives. *Mater Des.* 222: 111091. doi: 10.1016/j.mates.2022.111091
- Mujtaba M, Negi A, King AWT, Zare M, and J. Kuncova-Kallio J. 2023. Surface modifications of nanocellulose for drug delivery applications; a critical review. *Curr Opin Biomed Eng.* 28: 100475. doi 10.1016/j.cobme.2023.100475
- Nath PC, Ojha A, Debnath S, Neetu K, Mitra SBP, Sharma M, Sridhar K, Nayak PK. 2023. Recent advances in valorization of pineapple (*Ananas comosus*) processing waste and by-products: A step towards circular bioeconomy. *Trends Food Sci Tech.* 136: 100–111. doi: 10.1016/j.tifs.2023.04.008
- Nguyen PXT, Ho KH, Do NHN, Nguyen CTX, Nguyen HM, Tran KA, Le KA, Le PK. 2022. A comparative study on modification of aerogel-based biosorbents from coconut fibers for treatment of dye- and oil-contaminated water. *Mater Today Sustain.* 19:100175. doi.: 10.1016/j.mtsust.2022.100175
- Paksung N, Pfersich J, Arauzo PJ, Jung D, Kruse A. 2020. Structural effects of cellulose on hydrolysis and carbonization behavior during hydrothermal treatment. *ACS Omega.* 5: 12210-12223
- Partow AJ, Meng S, Wong AJ, Savin DA, Tong Z. 2022. Recyclable & highly porous organo-aerogel adsorbents from biowaste for organic contaminants' removal. *Sci Total Environ* 827: 154051. doi: 10.1016/j.scitotenv.2022.154051
- Paulauskiene T, Teresiute A, Uebe J, Tadzijevas A. 2022. Sustainable cross-linkers for the synthesis of cellulose-based aerogels: Research and Application, *J Mar Sci Eng.* 10:491. doi:10.3390/jmse10040491
- Sanchez LM, Hopkins AK, Espinosa E, Larrañet, E, Malinova D, McShane AN, Domínguez-Robles J, Rodríguez A. 2023. Antioxidant cellulose nanofibers/lignin-based aerogels: a potential material for biomedical applications. *Chem Biol Technol Agric.* 10: 72. doi: 10.1186/s40538-023-00438-z
- Simon-Herrero C, Caminero-Huertas S, Romero A, Valverde JL, Sanchez-Silva L. 2016. Effects of freeze-drying conditions on aerogel properties. *J Mater Sci* 51: 8977–8985. doi:10.1007/s10853-016-0148-5
- Sozcu S, Venkataraman M, Wiener J, Tomkova B, Militk J, Mahmood A. 2024. Incorporation of cellulose based aerogels into textile structures. *Mater.* 17, 27. doi:10.3390/ma17010027
- Sun M, Li C, JFeng J, Sun H, Sun M, Feng Y, Ji X, Han S, Feng J. 2022. Development of aerogels in solid-phase extraction and microextraction. *TrAC.* 146 : 116497. doi: 10.1016/j.trac.2021.116497
- Tafreshi OA, Mosanenzadeh SG, Karamikamkar, Saadatnia Z, Park CB, Naguib HE. 2022. A review on multifunctional aerogel fibers: processing, fabrication, functionalization, and applications. *Mater Today Chem.* 23: 100736, doi: 10.1016/j.mtchem.2021.100736
- Wang X, Zhang Y, Jiang H, Song Y, Zhou Z, Zhao H. 2016. Fabrication and characterization of nano-cellulose



- aerogels via supercritical CO<sub>2</sub> drying technology, *Mater Lett.* 183: 179-182. doi: 10.1016/j.matlet.2016.07.081
- Wei G, Zhang J, Usueli M, Zhang X, Liu B, Mezzenga R. 2022. Biomass vs inorganic and plastic-based aerogels: Structural design, functional tailoring, resource-efficient applications and sustainability analysis. *Prog Mater Sci.* 125: 100915. Doi: 10.1016/j.pmatsci.2021.100915
- Zhang J, Zhang H, Yan T, Fang Y, Huang Y, Tang J, He M. 2022. Low shrinkage, mechanically strong polymethylacrylimide aerogels with open-cell structure prepared by freeze-drying. *Polymer.* 245: 124705. doi:10.1016/j.polymer.2022.124705



## Effect of different azinphos-ethyl and azinphos-methyl concentrations on *Tetrademus obliquus* growth in culture conditions

Elif Neyran Soylu<sup>1</sup> , Bengü Temizel<sup>2\*</sup> 

<sup>1</sup>Giresun University, Faculty of Arts and Science, Department of Biology, Giresun, Turkey

<sup>2</sup>Giresun University, Central Research Laboratory Application and Research Center, Giresun, Turkey

\*Corresponding author : [bengu.temizel@gmail.com](mailto:bengu.temizel@gmail.com)  
Orcid No: <https://orcid.org/0000-0002-5217-3013>

Received : 11/10/2024  
Accepted : 23/12/2024

**To Cite / Atf için:** Soylu EN, Temizel B. 2024. Effect of different azinphos-ethyl and azinphos-methyl concentrations on *Tetrademus obliquus* growth in culture conditions. Eurasian J Bio Chem Sci, 7(2):171-177 <https://doi.org/10.46239/ejbc.1564696>

**Abstract:** Azinphos methyl (S-3,4-dihydro-4-oxo-1,2,3-benzotriazin-3-ylmethyl O,O-dimethyl phosphorodithioate) and Azinphos ethyl (S-3,4-dihydro-4 - oxo-1,2,3-benzotriazin-3-ylmethyl O,O-diethyl phosphorodithioate) are two phosphorus-containing pesticides. These pollutants are widely used as agricultural pesticides and acaricides and are used as broad-spectrum pesticides. It is assumed that these insecticides are carried out of the soil by rain, flood and snow water and pollute rivers, lakes and seawater. The aim of the study is to determine the effects of different concentrations of azinphos-ethyl and azinphos-methyl on the growth of green algae isolated from streams under culture conditions. The aim of this study was to determine the change in algal growth as a function of increasing the concentration of these pesticides in the algal cultures of *Tetrademus obliquus*. In addition, pH and conductivity measurements were carried out on the control group and on the cultures after dosing. In this study, based on the counts carried out in the cultures, it was found that the number of species has decreased over time, but there was no significant decrease.

**Keywords:** Algal growth, Azinphosethyl, Azinphosmethyl, stream, pesticide, greenalgae

### *Farklı azinfos-etil ve azinfos-metil konsantrasyonlarının Tetrademus obliquus'un kültür koşullarında büyümesi üzerindeki etkisi*

**Özet:** Azinfos metil (S-3,4-dihidro-4-okso-1,2,3-benzotriazin-3-ilmetil O,O-dimetil fosforoditiyoat) ve azinfos etil (S-3,4-dihidro-4 - okso-1, 2,3-benzotriazin-3-ilmetil O,O-dietil fosforoditiyoat) iki fosfor içeren pestisitlerdir. Bu kirleticiler tarımsal pestisit ve akarisit olarak yaygın olarak kullanılır, geniş spektrumlu pestisit olarak kullanılır. Bu insektisit yağmur, sel ve kar sularıyla topraktan sürüklenerek nehirleri, gölleri ve deniz sularını kirlettiği düşünülmektedir. Çalışmanın amacı, kültür koşulları altında akarsulardan izole edilen yeşil alglerin büyümesi üzerine farklı azinfos-etil ve azinfos-metil konsantrasyonlarının etkisini belirlemektir. Bu araştırma ile *Tetrademus obliquus* alg kültürlerinde bu pestisitlerin konsantrasyonunun artışına bağlı olarak alg büyümesinin değişimi belirlenmeye çalışılmıştır. Ayrıca çalışma sırasında kontrol grubu ve kültürlerin dozlama sonrası pH ve iletkenlik ölçümleri yapılmıştır. Bu çalışmada kültürlerde yapılan sayım sonucunda tür sayısının zamanla azaldığı ancak çok önemli bir düşüş olmadığı belirlenmiştir.

**Anahtar Kelimeler:** Alg büyümesi, Azinfosetil, Azinfosmetil, dere, pestisit, yeşil alg

## 1. Introduction

Various pesticides are widely used in agriculture to protect against all kinds of pests that reduce the yield of products and prevent their development. It is known that the pesticides used in these activities mix with irrigation or rainwater and run back into lakes or rivers, leading to the accumulation and death of living organisms at every stage of the food chain (Amdur et al. 1991).

Pesticides that pollute aquatic systems have serious ecological consequences such as the death of some aquatic organisms, the deterioration of species composition and the alteration of the ecosystem. Therefore, the study of the effects of pesticides on aquatic organisms is becoming increasingly important (Peterson et al. 1994).

Among the living groups in the aquatic environment that are most affected by the mixing of agricultural pesticides

with surface waters are the phytoplankton organisms that form the first step of the food chain. Microalgae are a widely used living group in pesticide bioassays to determine the effects of pollutants on ecosystems. Algae are sensitive to most pollutants and are used as bioassay organisms to determine the effects of chemical substances in the aquatic environment. There are many studies that have been conducted on microalgae to determine the toxic effects of herbicides and various industrial chemicals (Abdel-Hamid 1996, Djomo et al. 2004, Geyer et al. 1985, Lu et al. 2001, Ma et al. 2003, McFeters et al. 1983, Moreno-Garrido et al. 2001, Moreno-Garrido et al. 2003, Sáez et al. 2001, Sabater and Carrasco 2001, Sabater et al. 2002, Shehata et al. 1984, Soylu and Temizel 2023, Wong 2000).

Azinphosmethyl (S-3,4 - dihydro-4- oxo-1,2,3-benzotriazin-3-ylmethyl O,O-dimethylphosphorodithioate) and azinphos ethyl (S-3,4 - dihydro-4- oxo-1,2,3-benzotriazin-3-ylmethyl O,O-diethylphosphorodithioate) are two phosphorus containing pesticides. These pollutants are widely used as agricultural insecticides and acaricides, which are used as broad-spectrum pesticides. Like many other insecticides, these chemicals are compounds that are considered potential pollutants to surface and groundwater, even though they are used in agriculture worldwide. It is believed that these insecticides are washed out of the soil with rain, flood and snow water and pollute rivers, lakes and marine waters. The aim of the research is to determine the effects of pesticides on algae growth by applying different doses of pesticides to microalgae species to be isolated from streams.

The aim of this study is to show the effects of azinphos-methyl and azinphos-ethyl, insecticides used for agricultural purposes in the streams of Giresun province, on the phytoplanktonic algae species prevalent in the streams and to create a scientific database with the data obtained, which can be used for subsequent planning studies. In this study, new data will be obtained in this field by using organisms such as *Tetradesmus obliquus* (Turpin) Kütz. from the Chlorophyta division, which are dominant in the waters of our country.

Studies investigating the effects of pesticides on freshwater algae have mostly used green algae such as *Chlorella*, *Chlamydomonas* and *Scenedesmus* (Tadros et al. 1994). The aim of this study was to determine the toxic effects of azinphos ethyl and azinphos methyl on the microalgae *Tetradesmus obliquus* (Turpin) Kützing isolated from natural waters. The development of the species to be cultivated in cultures treated with 1 mg/l, 1.1 mg/l, 1.2 mg/l, 1.4 mg/l azinphos-methyl and in cultures treated with 0.1 mg/l, 0.5 mg/l, 1 mg/l, 1.5 mg/l, 2 mg/l azinphos-ethyl is compared with the development of the species in cultures without these pesticides. The determination of the toxic effects of these herbicides on the growth rate of *Tetradesmus obliquus* and the comparison of their toxic effects are of great importance for aquatic ecosystems. Repetition and continuity of such studies are very important to reveal the effects of pesticide

exposure on aquatic ecosystems and especially on algae (Öterler 2009).

## 2. Materials and Method

### 2.1. Description of the Research Area and Sampling Stations

Green algae were isolated and analysed from water samples taken from the Aksu stream in the province of Giresun in the eastern Black Sea region. The Aksu stream is about 60 km long and 100 m wide. Its average depth is about 3 metres. The map of the study area is shown in Figure 1.

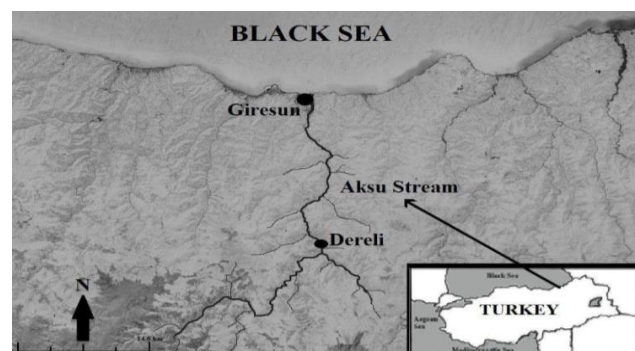


Fig. 1 Map of study area

### 2.2. Algological Features

#### 2.2.1. Sampling

Water samples were taken from the surface (0-20 cm) at the stations of the streams to be determined. To identify planktonic algae, 1-liter water samples were filtered through Whatman GF/A filter papers and preliminary preparations were made by scraping the algae collected on the surface of the filter paper with a coverslip and covering them in water or 10% glycerol solution. These preliminary preparations were examined under a research microscope and the algae identified. The works of Krammer and Lange-Bertalot, (1991a), Krammer and Lange-Bertalot, (1991b), Krammer and Lange-Bertalot, (1999a) and Krammer and Lange-Bertalot, (1999b) were used in the description of algae.

#### 2.2.2. Culture Conditions

The culture isolation was carried out in BG 11 medium from water samples from streams.

The algae were isolated and cultured from water samples from the Aksu stream. For the preservation of the cultures, the climate chamber was set to conditions suitable for algae (Hong et al. 2008, Lockert et al. 2006, Sabater and Carrosa 2001).

100 ml cultures were grown under defined climatic conditions (International Standard ISO-8692:1989) up to 4000-5000 cells/ml.

#### 2.2.3. Cell Count

The determination of the number of cells in a given volume is used for counting chambers. In our study, cell counts were performed with a Sedgewick-Rafter counting chamber. The Sedgewick-Rafter counting chamber

consists of a total of 1000 squares, 50 columns and 20 rows. The volume of each square is 1  $\mu$ l. The evaluation is carried out by random counting (LeGresley and McDermott 2010).

For the continuity of the algae cultures, 100 mL of culture medium was prepared in 250 mL bottles (ISO-8692 1989).

In the experiments, 4 different doses of azinphos-methyl (1 mg/l, 1.1 mg/l, 1.2 mg/l, 1.4 mg/l) and 5 different doses of azinphos-ethyl (0.1 mg/l, 0.5 mg/l, 1 mg/l, 1.5 mg/l, 2 mg/l) were applied to the algae cultivated in 100 ml flasks, which were prepared in accordance with similar studies (İbrahim et al. 2014, Öterler and Albay 2016).

The experiments were conducted in 2 different phases, which were initiated by treating the cultures with pesticides at predetermined concentrations approximately 5 days after entering the exponential growth phase. In the first phase, the cells of the pesticide-treated samples were counted with a Sedgewick-Rafter counting chamber after 0, 24, 48, 72 and 96 hours for 5 days. Subsequently, the spectrophotometric growth rates and absorbance values of the pesticide-treated samples were measured at 500, 665 and 750 nm wavelength and chlorophyll-*a* calculations were performed (Nusch 1980).

In addition, pH and conductivity measurements of the control group and the cultures after dosing were carried out during the study.

#### 2.2.4. Pesticide Analysis

For the species *Tetradesmus obliquus*, large quantities of precultures were established and their development regularly monitored. When the algal culture had reached a sufficient number of cells and entered the rapid growth phase (between days 15-21), 100 ml of the cell culture was divided into 250 ml vials under sterile conditions.

At 0 h, 20 ml of culture samples were taken from each experimental set under sterile conditions and the absorbance values were measured at 500, 665 and 750 nm to determine the spectral growth rates. The conductivity and pH were then measured and the cells counted. The chlorophyll values were measured the next day.

The experiments were carried out with doses according to the ISO 8692 and OECD 201 standards (ISO 8692, 2012; OECD, 2014) after 0 hours, 24 hours, 48 hours, 72 hours and 96 hours (ISO 8692, 2012; OECD, 2014).

### 3. Results

To determine the effects of Azinphos methyl and Azinphos ethyl on the growth of *Tetradesmus obliquus*, one of the green algae isolated from the Aksu stream, 1 mg/l, 1.1 mg/l, 1.2 mg/l, 1.4 mg/l Azinphos methyl and 0.1 mg/l, 0.5 mg/l, 1 mg/l, 1.5 mg/l, 2 mg/l Azinphos ethyl were used under culture conditions. In order to determine the effects of the pesticides added to the cultures, a comparison was made with the control group without pesticides. The aim of this study was to determine the change in algae growth in the cultures by increasing the concentrations of azinphos methyl and azinphos ethyl. As a result of the study, it was

found that the number of organisms did not decrease significantly by counting in the cultures, but the doses determined over time had a negative effect on algae growth.

At low pesticide applications, all pesticides induced the formation of chlorophyll-*a* and increased photosynthesis during the first 24 hours. However, there was no specific increase in absorbance and cell number measured spectrophotometrically over time. However, development slowed down after 48, 72 and 96 hours.

The pH and conductivity values of the samples were measured at 0 o'clock and the cells were counted. Then the remaining portion in the beaker was filtered through Whatman GF/C filter papers and chlorophyll-*a* determinations were performed by absorbance measurements at 500 nm, 680 nm and 750 nm wavelength. These measurements were repeated every day at the same time. The last measurement was taken at the 96th hour. Each dose was applied in 3 repetitions.

For azinphos-methyl, the lowest cell count in the cultures was determined at hour 0 with  $2.07 \times 10^6$  cells/ml at a dose of 1.4 mg/l. After 24 hours, the lowest cell count was determined to be  $2 \times 10^6$  cells/ml at a dose of 1.2 mg/l. After 48 hours, the lowest cell count was determined to be  $1.71 \times 10^6$  cells/ml at a dose of 1.4 mg/l. After 72 hours, the lowest cell count was determined to be  $1.48 \times 10^6$  cells/ml at a dose of 1 mg/l. Finally, after 96 hours, the lowest cell count was determined to be  $1.006 \times 10^6$  cells/ml at a dose of 1 mg/l (Figure 2).

In the second step, the same procedures were repeated for azinphos ethyl. The cultures that had reached the rapid growth phase (day 15-25) were divided into subcultures and 5 days after entering the exponential growth phase, 5 different doses of azinphos ethyl (0.1 mg/L, 0.5 mg/L, 1 mg/L, 1.5 mg/L and 2 mg/L) were applied to the cultures to determine the effect of the pesticide on algal growth.

For azinphos ethyl, the lowest cell count in cultures was determined after 0 hours with  $1.855 \times 10^6$  cells/ml at a dose of 0.5 mg/l. The lowest cell count after 24 hours was determined to be  $2.06 \times 10^6$  cells/ml at a dose of 1.5 mg/l. The lowest cell count after 48 hours was determined to be  $1.77 \times 10^6$  cells/ml at a dose of 1.5 mg/l. The lowest cell count after 72 hours was determined to be  $1.94 \times 10^6$  cells/mL in the control group. Finally, the lowest cell count after 96 hours was determined to be  $1.65 \times 10^6$  cells/mL at a dose of 1.4 mg/L (Figure 3). A decrease in the number of organisms was observed with increasing dose. A decrease in the number of organisms was observed particularly after the 24th hour when the dose was increased.

As a result of the experiments, the lowest pH value for azinphosethyl in the control group was measured at the beginning of the experiment (time 0) at 6.7, and the highest pH value was measured at a dose of 2 mg/l after 48 hours at 8.1 (Figure 5). The lowest pH value for azinphos-

methyl was measured at the beginning of the experiment (time 0) at a dose of 1.4 mg/l at 6.1, and the highest pH value was measured in the control group after 24 hours at 7.6 (Figure 4).

The lowest conductivity value ( $\mu\text{S}/\text{cm}$ ) for azinphosethyl was measured in the control group at the 24th hour with  $195 \mu\text{S}/\text{cm}$ ; the highest conductivity values were measured in the control group at the 96th hour and at a dose of 1 mg/l with  $285 \mu\text{S}/\text{cm}$  (Figure 7). For azinphos-methyl, the lowest conductivity value of  $1140 \mu\text{S}/\text{cm}$  was measured in the control group at the 48th hour, while the highest conductivity value of  $1955 \mu\text{S}/\text{cm}$  was measured at a dose of 1.1 mg/l at the 24th hour (Figure 6). It was found that the conductivity values generally did not vary greatly over time in all dose groups.

According to the test results, the highest chlorophyll-*a* for azinphos ethyl was measured at  $3.97 \mu\text{g}/\text{l}$  after 0 hours in the control group, and the lowest chlorophyll-*a* was measured at  $0.74 \mu\text{g}/\text{l}$  after 96 hours (Figure 9). The highest chlorophyll-*a* for azinphos-methyl in the control group was measured at  $0.78 \mu\text{g}/\text{l}$  after 0 hours; the lowest chlorophyll-*a* was measured at  $0.03 \mu\text{g}/\text{l}$  after 96 hours (Figure 8). As a result of our studies, it was found that chlorophyll-*a* levels in *Tetradesmus* cultures containing azinphos-ethyl increased in the first 24 hours at almost all doses and then decreased; while chlorophyll-*a* levels in *Tetradesmus* cultures containing azinphos-methyl increased in the first 48 hours at a dose of 1 mg/l and then decreased.

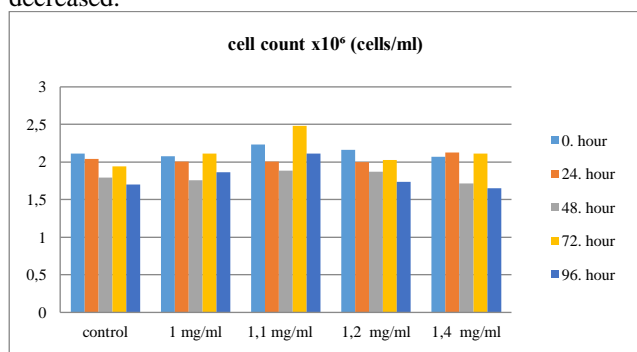


Fig. 2 Time-dependent change in the cell count, determined by counting in the control group and different doses of azinphos methyl

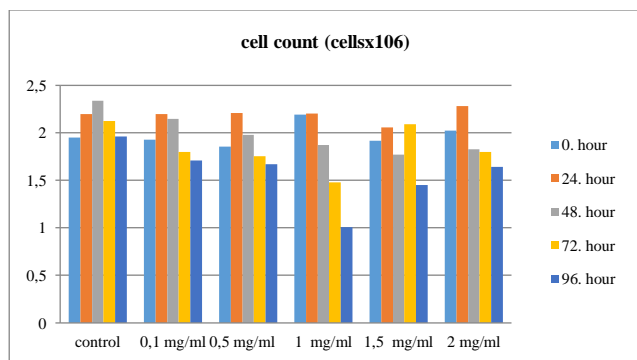


Fig. 3 Time-dependent change in the cell count, determined by counting in the control group and different doses of azinphos ethyl

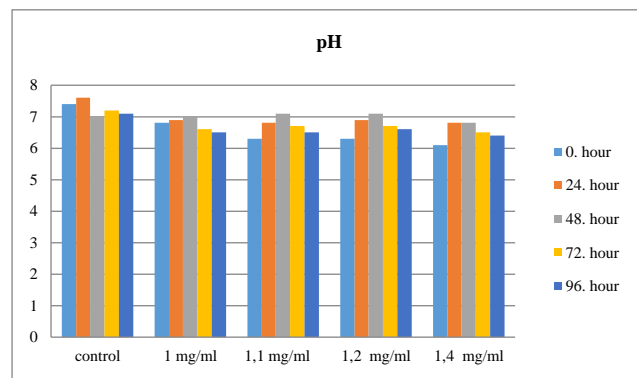


Fig. 4 pH change in the control group and different azinphos methyl doses

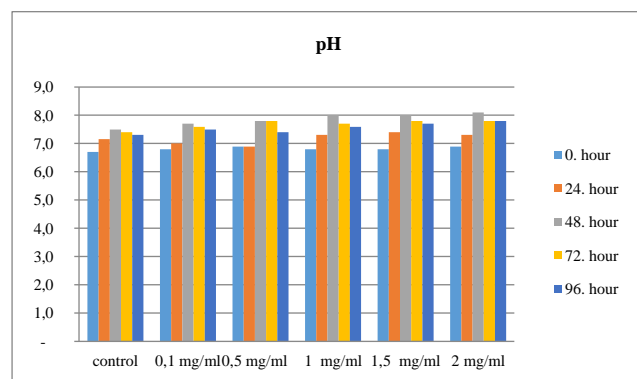


Fig. 5 pH change in the control group and different azinphos ethyl doses

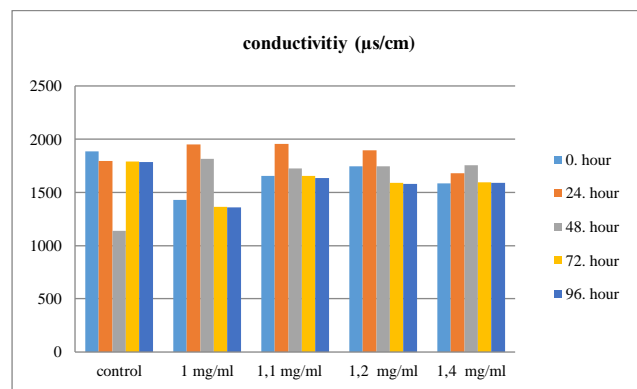


Fig. 6 Change in conductivity in the control group and different doses of azinphos methyl

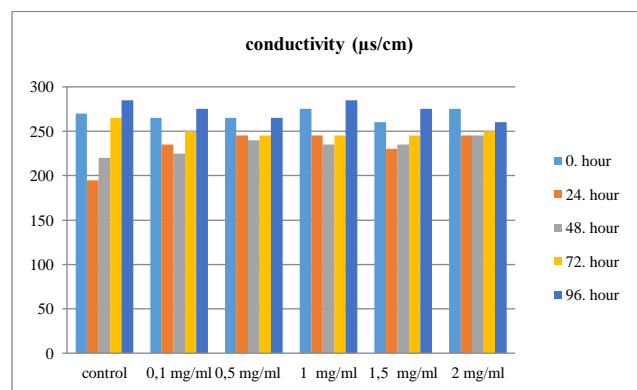
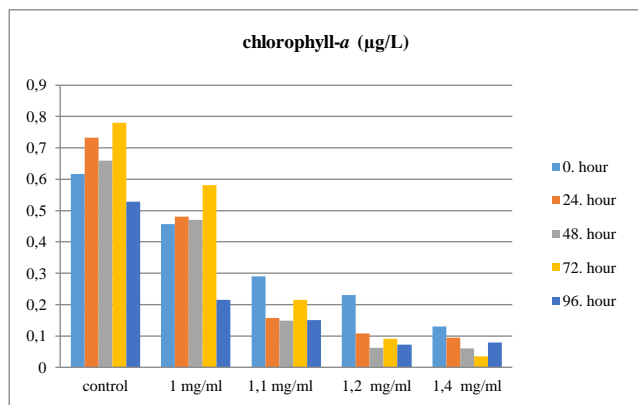
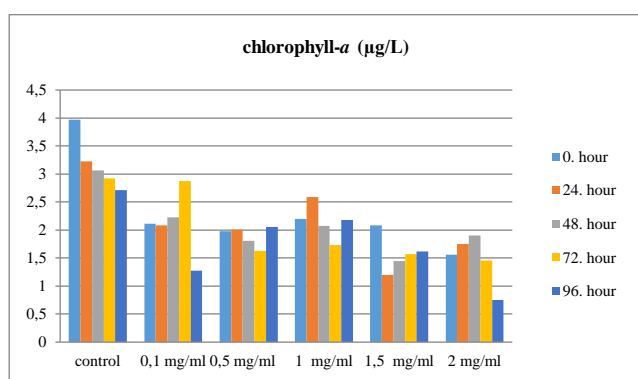


Fig. 7 Change in conductivity in the control group and different doses of azinphos ethyl



**Fig. 8** Change in chlorophyll-a in the control group and different doses of azinphos-methyl



**Fig. 9** Change in chlorophyll-a in the control group and different doses of azinphos-ethyl

#### 4. Discussion

Pesticides are substances that humans have used for many years to affect the environment, food sources and plants. A pesticide can be a chemical substance, a biological agent such as a virus or bacterium, an antimicrobial agent, a disinfectant, or another agent (Kaya 1996). The primary target of most herbicides used as pesticides against plant pests is the light reactions of photosynthesis. Therefore, herbicides used in agriculture interfere with the light reactions of photosynthesis. Chlorophyll is one of the most important photosynthetic pigments found in green algae. It is one of the most commonly used parameters for assessing the effects of pesticides on algal growth. Some herbicides inhibit photosynthesis and the synthesis of carotenoids. Some inhibit photosynthesis (Sikka and Pramer 1968), others inhibit fatty acid formation and thus cell division and growth (Couderchet and Boger 1993). Pesticides such as colchicine prevent chromosome segregation by inhibiting tubule formation (Fedtke 1982). As in similar studies, the chlorophyll-a content decreased over time in our experiments, as shown in Figure 8 and Figure 9 (Nie et al. 2002; Ou et al. 2003).

A small proportion (~0.1%) of the pesticides used for pest control reaches the target organism. The remainder enters the aquatic environment via leakage or surface runoff and poses a serious threat to other aquatic organisms. Many studies have shown that the accumulation of pesticides is also very harmful to non-target organisms (Baruah et al.

2024, Damalas and Eleftherohorinos 2011, Sanoja-López et al. 2023). Microalgae, which are primary producers and form the basis of the aquatic food web, are the most notable group among aquatic non-target organisms (Mofeed and Mosleh, 2013). They are responsible for about 60% of the total oxygen production in water (Castro et al. 2022) and play an important role in nutrient cycling (Sabater and Carrasco, 2001; Källqvist and Svenson, 2003). Pesticides that accumulate in algae can reach higher trophic levels through trophic interactions and accumulate toxins in the tissues of zooplankton and other herbivores that eat these algae (Meng et al. 2022).

Algae, which impair soil fertility and are the main food for fish in water bodies, are widespread in nature. The accumulation of pesticides in water, which are widely used worldwide, has a significant negative impact on algae. Any negative impact on the microalgae community can affect the structural balance of the entire ecosystem (Martinez et al. 2015, Villem, 2011). Therefore, it is very important to investigate the harmful effects of pollutants on microalgae (Neury-Ormanni et al. 2020). Recently, studies investigating the effects of pesticides on algal cultures have expanded. In their study investigating the effects of five different organophosphate pesticides on the growth of *Chlorella vulgaris*, a green microalgae, Öterler and Albay (2016) found that at a lower pesticide concentration, the pesticide degenerated like a nutrient and was taken up by the algal cells, whereupon the toxic effect of the pesticide limited the growth of the algae. In our study, the amount of algae increased for a while after the addition of the pesticide and then decreased (Figures 2 and 3). Therefore, this situation is parallel to our study as in many other studies.

In a similar study investigating the effects of Azinphos methyl and Azinphos ethyl on the growth of the marine green alga *Tetraselmis suecica*, it was found that these chemicals had an inhibitory effect on algal growth after 96 hours (Vagi et al. 2005). In another study investigating the time-dependent change in cell number in an Aphanizomenon aphanizomenoides culture to which azinphos ethyl was added, it was found that azinphos ethyl had a limiting effect on algal growth and caused a relative decrease by the end of 24 hours (Oğuz 2009).

#### 5. Conclusion

Changes in the community structure of algal species in the aquatic environment and the response of these species to environmental pollutants are very important for the ecosystem. Pesticide residues that accumulate in living organisms over time, even in very small amounts, have negative effects on living organisms and the environment.

Experiments have shown that pesticides cause structural changes in non-target organisms. Efforts should therefore be made to reduce the use of synthetic agrochemicals. Organic farming with the use of biopesticides/bioherbicides can help to reduce pesticide exposure.



In addition to biomonitoring, it is also very important to conduct research that provides early warning of pesticide contamination in aquatic systems. This and many other studies show that the accumulation of pesticides in water over time has a negative impact on algae growth. Although no rapid changes and declines can be observed, it is clear that the accumulation of pesticides over time has a negative impact on aquatic organisms. New projects should be developed to address the negative effects of pesticide use on the environment and human health, and water resources should be protected from pesticide pollution.

In order to predict future ecological scenarios, it is important to understand how pollutants affect algal communities and thus the aquatic ecosystem. Monitoring programs should be established to observe the long-term effects of pesticides on algal ecosystems, and how exposure to pesticides affects algal communities should be investigated. Knowledge of how different species interact and respond as a community will lead to a more comprehensive understanding of ecosystem dynamics, which will be of great benefit in the development of environmental policies. Knowing about the interaction between pesticides and microbial-algal communities can help us understand how ecosystems work more broadly.

Studies that consider the social and ecological aspects of pesticide use and understanding the relationships between ecological processes and human activities, as well as the use of sustainable and socially responsible pesticide management techniques, will further advance the sustainable management of aquatic ecosystems.

#### Acknowledgements

This paper was presented in 7th International Eurasian Conference on Biological and Chemical Sciences, 02-04 October 2024, Ankara-Türkiye and the authors would like to thank Giresun University Scientific Research Projects (BAP) unit for their contribution to this research (Project No: FEN-BAP-A-150219-07).

#### Authors' contributions:

ENS: Conceptualization, Funding acquisition, Investigation, Methodology, Project administration, Resources, Supervision, Visualization, Writing – original draft, Writing – review & editing.

BT: Conceptualization, Data curation, Investigation, Methodology, Visualization, Writing – original draft, Writing – review & editing.

#### Conflict of interest disclosure:

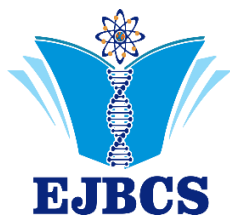
The authors declare that they have no known competing financial interests or personal relationships that could have appeared to influence the work reported in this paper.

#### References

Abdel-Hamid MI. 1996. Development and application of a simple procedure for the toxicity testing using immobilized algae. *Water Sci Technol.* 33(6): 129-138. doi:10.1016/0273-1223(96)00289-2

- Amdur MO, Doull J, Klassen CD. 1991. Casarett and Doull's toxicology: The basic science of poisons, Pergamon Press. New York 1033: 565-623.
- Baruah P, Srivastava A, Mishra Y, Chaurasia N. 2024. Modulation in growth, oxidative stress, photosynthesis, and morphology reveals higher toxicity of alpha-cypermethrin than chlorpyrifos towards a non-target green alga at high doses. *Environ Toxicol Pharmacol.* 106:104376. doi:10.1016/j.etap.2024.104376
- Couderchet M, Boger P. 1993. Chloroacetamide-induced reduction of fatty acid saturation. *Pestic Biochem Physiol.* 45: 91–97. doi:10.1006/pest.1993.1011
- Damalas CA, Eleftherohorinos IG. 2011. Pesticide exposure, safety issues, and risk assessment indicators. *Int. J. Environ. Res. Public Health.* 8(5):1402-1419. doi:10.3390/ijerph8051402
- Djomo JE, Dauta A, Ferrier V, Narbonne JF, Monkiedje A, Njine T, Garrigues P. 2004. Toxic effects of some major polyaromatic hydrocarbons found in crude oil and aquatic sediments on *Scenedesmus subspicatus*. *Water Res.* 38: 1817-1821. doi:10.1016/j.watres.2003.10.023
- Fedtko C. 1982. *Biochemistry and Physiology of Herbicide Action* Springer-Verlag, New York, NY, USA.
- Geyer H, Scheunert I, Korte F. 1985. The effects of organic environmental chemicals on the growth of the alga *Scenedesmus subspicatus*. *Chemosphere.* 14(9): 1355-1369. doi:10.1016/0045-6535(85)90156-0
- Hong Y, Hu HY, Li FM. 2008. Growth and physiological responses of freshwater green alga *Selenastrum capricornutum* to allelochemical ethyl 2-methyl acetoacetate (EMA) under different initial algal densities. *Pestic Biochem Physiol.* 90: 203-212. doi:10.1016/j.pestbp.2007.11.009
- Ibrahim WM, Karam MA, El-Shahat RM, Adway AA. 2014. Biodegradation and utilization of organophosphorus pesticide malathion by cyanobacteria. *Biomed Res Int.* 2014(1): 392682. doi:10.1155/2014/392682
- International Organisation for Standardisation. ISO-8692: 1989. Water quality- Freshwater algal growth inhibition test with *Scenedesmus subspicatus* and *Selenastrum capricornutum*, 95.99 (2004-09-22) www.İso.org.
- International Organisation for Standardisation. ISO 8692: 2012. Water quality-Algal growth inhibition test.
- International Organisation for Standardisation. ISO/DIS 14442. 2014. Water quality-Guidelines for algal growth inhibition tests with poorly soluble materials, volatile compounds, metals and waster water.
- Kaya S. 1996. Pesticides and the Major Problems They May Cause. Environment and Health Units Panel Notes. Ankara University, Faculty of Veterinary Medicine, Conference Hall. Ankara.
- Krammer K, Lange-Bertalot H. 1991a. Bacillariophyceae. 3. Teil: Centrales, Fragilariaceae, Eunotiaceae. In: Ettl H., Gerloff J., Heynig H. & Mollenhauer D. (Eds.) *Susswasserflora von Mitteleuropa Band 2/3.* Gustav Fischer Verlag: Stuttgart, Jena, 1-576.
- Krammer K, Lange-Bertalot H. 1991b. Bacillariophyceae. 4. Teil: Achnanthaceae Kritische Ergänzungen zu Navicula (Lineolatae) und Gomphonema, Gesamt literaturverzeichnis Teil: 1-4. In: Ettl H., Gerloff J., Heynig H. & Mollenhauer D. (Eds.) *Susswasserflora von Mitteleurope Band 2/4.* Gustav Fischer Verlag: Stutgard, Jena, 1-437.
- Krammer K, Lange-Bertalot H. 1999a. *Susswasserflora von Mitteleuropa. Bacillariophyceae.* Berlin: Spectrum Akademischer Verlag. Band 2/1, 1. Teil: Naviculaceae, 1-876.
- Krammer K, Lange-Bertalot H. 1999b. *Susswasserflora von Mitteleuropa. Bacillariophyceae.* Berlin: Spectrum

- Academischer Verlag. Band 2/2, 2. Teil: Bacillariaceae, Epithemiaceae, Surirellaceae, 1-610.
- LeGresley M, McDermott G. 2010. Counting chamber methods for quantitative phytoplankton analysis-haemocytometer, Palmer-Maloney cell and Sedgewick-Rafter cell. UNESCO (IOC manuals and guides), 55: 25-30.
- Lockert CK, Hoagland KD, Siegfried BD. 2006. Comparative sensitivity of Freshwater Algae to Atrazine. *Bull Environ Contam Toxicol*. 76:73-79. doi:10.1007/s00128-005-0891-9
- Lu G, Yuan X, Zhaon Y. 2001. QSAR study on the toxicity of substituted benzenes to the algae (*Scenedesmus obliquus*). *Chemosphere*. 44: 437- 440.
- Ma J, Lin F, Wang S, Xu L. 2003. Toxicity of 21 herbicides to the green algae *Scenedesmus quadricauda*. *Bull Environ Contam Toxicol*. 71: 594-601.
- McFeters GA, Bond PJ, Olson SB. 1983. A comparison of microbial bioassays for the detection of aquatic toxicants. *Water Res*. 17(12): 1757-1762. doi:10.1016/0043-1354(83)90197-5
- Moreno-Garrido I, Hampel M, Lubián LM, Blasco J. 2001. Marine microalgae toxicity test for linear alkyl benzene sulfonate (LAS) and alkyl phenol ethoxylate (APEO). *Fresenius J Anal Chem*. 371: 474-478.
- Moreno-Garrido I, Hampel M, Lubián LM, Blasco J. 2003. Marine benthic microalgae *Cylindrotheca closterium* (Ehrenberg) Lewin and Reimann (Bacillariophyceae) as a tool for measuring toxicity of linear alkyl benzene sulfonate in sediments. *Bull Environ Contam Toxicol*. 70: 242-247.
- Nie XP., Lan CY., Lin L., Huang MH. 2002. The effects of aroclor 1254 on the growth of *Chlorella pyrenoidosa* and *Scenedesmus obliquus*, *ACTA Scientiarum Naturalium Universitatis Sunyatseni*, 41,68-71.
- Nusch E. 1980. Comparison of different methods for Chlorophyll-*a* and phaeopigments determination. *Arch Hydrobiol Suppl*. 4: 14-36.
- Oğuz B. 2009. Effect of Pesticide Accumulation on Growth in Blue-Green Algae. Istanbul University, Institute of Science. Master Thesis.
- Ou XM, Lei MX, Huang MZ, Wang YL, Wang XG, Fan DF. 2003. Effects of novel sulfonylurea herbicide HNPC-(29908) on growth of green algae *Chlorella pyrenoidosa*, *Chinese Journal of Pesticide Science*, 5, 16-23.
- Öterler B. 2009. Toxicity of 5 different pesticides on the growth of 3 freshwater phytoplankton species (*Chlorella vulgaris* Berj. *Scenedesmus quadricauda* (Turpin) Breb. and *Cyclotella meneghiniana* Kütz.), Trakya University Faculty of Science, PhD Thesis, 1-121.
- Öterler B, Albay M. 2016. The effect of 5 organophosphate pesticides on the growth of *Chlorella vulgaris* Beyerinck [Beijerinck] 1890. *Int. J Res Stud Biosci*. 4: 26-33. doi:10.20431/2349-0365.0404003
- Peterson J, Zheng Y, Bender L, Myers A, Cerione R, Bender A. 1994. Interactions between the bud emergence proteins. Bem1p and Bem2p and Rho-type GTPases in yeast. *J Cell Biol*. 127(5): 1395-406. doi:10.1083/jcb.127.5.1395
- Sáez M, Gómez-Parra A, González-Mazo E. 2001. Bioconcentration of linear alkyl benzene sulfonates and their degradation intermediates in marine algae. *Fresenius J Anal Chem*. 371: 486-490. doi:10.1007/s002160101075
- Sabater C, Carrasco JM. 2001. Effects of pyridaphenthion on growth of five freshwater species of phytoplankton. A laboratory study *Chemosphere*. 44(8): 1775-1781. doi:10.1016/S0045-6535(00)00575-0
- Sabater C, Cuesta A, Carrasco R. 2002. Effects of bensulfuron-methyl and cino sulfuron on growth of four freshwater species of phytoplankton. *Chemosphere*. 46: 953-960. doi:10.1016/S0045-6535(01)00179-5
- Sanoja-López KA, Quiroz-Suárez KA, Dueñas-Rivadeneira AA, Maddela NR, Montenegro MC, Luque R, Rodríguez-Díaz JM. 2023. Polymeric membranes functionalized with nanomaterials (MP@ NMs): A review of advances in pesticide removal. *Environ Res*. 217:114776. doi:10.1016/j.envres.2022.114776
- Shehata SA, Aly OA, Farag H. 1984. Effects of bladex, etazine, dicryl and baylucide on growth of *Scenedesmus*. *Environ Int*. 10: 225-234. doi:10.1016/0160-4120(84)90239-3
- Sikka HC, Pramer D. 1968. Physiological effects of fluometuron on some unicellular algae. *Weed Sci*. 16: 296-299. doi:10.1017/S0043174500047184
- Soylu E, Temizel B. 2023. The Effects of Different Malathion Concentrations on Algal Growth in Cultural Conditions. *KFBD*. 13(4): 1510-1522. doi:10.31466/kfbd.1305969
- Tadros TF. 1994. Fundamental principles of emulsion rheology and their applications. *Colloids and Surfaces A: Physicochem Eng Asp*. 91: 39-55. doi:10.1016/0927-7757(93)02709-N
- Vagi M, Kostopoulou MN, Petsas AS, Laloussi ME, Rasouli C, Lekkas TD. 2005. Toxicity Of Organophosphorous Pesticides To The Marine Alga *Tetraselmis suecica*. *Global Nest J*. Vol 7: No 2, pp 222-227.
- Wong PK. 2000. Effects of 2,4-D, glyphosate and paraquat on growth, photosynthesis and chlorophyll-*a* synthesis of *Scenedesmus quadricauda* Berb. 614. *Chemosphere*. 41: 177-182. doi:10.1016/S0045-6535(99)00408-7



## An overview of leech saliva and cosmetic potential

Fatma Çoruk<sup>1</sup>, Sibel Kaymak<sup>1\*</sup>, Hüseyin Ayhan<sup>1,2</sup>, Nilüfer Vural<sup>1,3</sup>, Salih Mollahalioglu<sup>4</sup>

<sup>1</sup>Department of Traditional, Complementary and Integrative Medicine, Biotherapeutic Products Research and Development Program, Ankara Yıldırım Beyazıt University, Ankara, Türkiye

<sup>2</sup>Department of Medical Laboratory Techniques Program, Health Services Vocational School, University of Ankara Yıldırım Beyazıt, 06760, Çubuk, Ankara, Türkiye

<sup>3</sup>Department of Food Processing-Food Technology, Health Services Vocational School, University of Ankara Yıldırım Beyazıt, 06760, Çubuk, Ankara, Türkiye

<sup>4</sup>Department of Public Health, Faculty of Medicine, Ankara Yıldırım Beyazıt University, Ankara, Türkiye

\*Corresponding author : [sibelkaymak@aybu.edu.tr](mailto:sibelkaymak@aybu.edu.tr)

Orcid No: <https://orcid.org/0000-0002-6523-7637>

Received : 18/10/2024

Accepted : 12/12/2024

To Cite / Atf için: Çoruk F, Kaymak S, Ayhan H, Vural N, Mollahalioglu S. 2024. An overview of leech saliva and cosmetic potential. Eurasian J Bio Chem Sci, 7(2):178-185 <https://doi.org/10.46239/ejbc.1569164>

**Abstract:** The therapeutic benefits of leech secretion have been known for centuries, and the potential of this substance in modern cosmetics is now attracting increasing interest. Leech secretion contains various bioactive compounds, including enzymes, peptides, and proteins. The bioactive components found in leech saliva, including anticoagulants, growth factors, and antimicrobial peptides, are responsible for leech saliva's effectiveness in increasing skin hydration, reducing inflammation, and promoting wound healing. To utilize their potential, it is imperative to sift through the skin area. This study reviews the available literature and research studies on the chemical properties of leech saliva and its use in cosmetic formulations. It highlights the bioactive compounds, their potential mechanisms of action, and their efficacy in cosmetic applications. The sources consulted include peer-reviewed articles, clinical studies, and industry reports. Data from these studies are synthesized to provide a comprehensive overview of the current state of knowledge. The findings suggest that leech saliva has significant potential as an ingredient in cosmeceutical products and offers new benefits for skin rejuvenation and repair. The review highlights the need for further research to optimize extraction processes, ensure product safety, and investigate additional applications. By advancing our understanding of leech saliva's chemical properties and mechanisms, future studies may facilitate the development of innovative skincare solutions and increase the efficacy of cosmetic formulations.

**Keywords:** Leech, Leech saliva, Bioactive compounds, Cosmetic, Cosmeceutical

© EJBCS. All rights reserved.

### 1. Introduction

The use of leeches in medical practice is a practice that has persisted for centuries and across various civilisations. The word 'leech' is etymologically derived from the old English word 'leace' (doctor). The first known use of leeches as medicine dates back to ancient Egypt when leech drawings from 1567–1308 BC adorned the walls of a pharaoh's tomb belonging to the 18th dynasty. Galen (130–201 AD) created the idea of humoral sickness and utilized leeches for bloodletting, which helped explain why leech therapy is so popular today. Medical records from the Anglo-Saxon, Chinese, Arabic, Ancient Greek, and Roman eras all make frequent mention of leech therapy (Mory et al. 2000; Whitaker et al. 2004). In the medieval period, Arab physicians employed the use of leeches in the treatment of alopecia, dermatological conditions, postoperative and pain

relief, and joint diseases. Ibn Sina and Ibn Al-Quff provided a comprehensive account of medicinal leeches and were instrumental in distinguishing them from non-medical leeches (Alaama et al. 2024; Alharbi 2015). Furthermore, Ibn Sina (980-1037 AD) also documented the use of leeches for the treatment of certain dermatological conditions in his Canon of Medicine (Amani et al. 2020). For centuries, medicinal leeches have been employed in the treatment of a wide range of ailments, including eye diseases, malaria, typhoid, obesity, and skin disorders, among numerous other complications. It was also believed that leeches could be used to treat plague patients by eliminating the 'bad blood' in their bodies (Arabacı 2023; Sawyer 2013). In the late nineteenth century, Dr. John H. Haycraft's discovery of anticoagulants in leech head extract challenged the traditional belief that the benefits of leech therapy were

solely derived from bloodletting. Instead, he suggested that the real therapeutic benefit came from the substances injected into the patient's body by the leech (Haycraft 1883). Although the use of leeches for medical purposes declined in the early 20th century due to the development of precise theoretical bases for disease and treatment and the discovery of chemical drugs, leech therapy came back in the late 20th century, particularly in microsurgery and plastic surgery. The utilisation of leeches in medical applications has increased since the United States Food and Drug Administration (FDA) granted approval for the use of the medical leech *Hirudo medicinalis* as a medical device in plastic surgery in 2004 (Rados 2004).

Medical leeches (subclass Hirudinea) are hermaphroditic, ringed, amphibious animals belonging to the phylum Annelida. Some leeches are hematophagous, while others are carnivorous (Sawyer 1986). The bioactive substances present in the saliva of medicinal leech species, such as *Hirudo* sp., enable them to feed on and store blood, while also conferring therapeutic benefits to their hosts. Following the leech's bite, it must create a suction pathway (extracellular matrix degradation), inhibit adhesion and aggregation (antiplatelet activity), inhibit clotting (anticoagulant activity), increase blood flow, protect itself (antimicrobial activity) and avoid detection (analgesic and anti-inflammatory activity) (Sig et al. 2017).

The disturbance or absence of microcirculation represents a significant pathomechanism in numerous diseases, and as a result, leech therapy is employed in both traditional and complementary medicine for both therapeutic purposes and as an adjunct to treatment for a wide range of disorders. From a terminological perspective, hirudotherapy can be defined as an integrative treatment method in which medicinal leeches are applied to the body for therapeutic purposes. Currently, leeches have been used in the treatment of over twenty clinical conditions, including cardiovascular, musculoskeletal, plastic and reconstructive surgery, soft tissue injuries, and dental and skin diseases (Abdualkader et al. 2013; Ayhan and Mollahaliloğlu 2018). Of particular interest in recent years has been the investigation of the cosmetic applicability of hirudotherapy in dermatological diseases.

As the largest organ in the body, the skin serves as a physical barrier between the body and the external environment, and is involved in both physical and immunological processes. Furthermore, the skin, which is composed of hair and nails, performs additional functions such as the production of hormones and enzymes, maintenance of homeostasis, and regulation of body temperature (Xu et al. 2019). As the body's primary line of defense, the skin is frequently subjected to damage from external factors, which serves as the foundation for a multitude of related dermatological complications. As of today, over 3,000 dermatological diseases have been identified in the literature (Bickers et al. 2006). In comparison to conventional therapeutic and pharmacological treatments for dermatological conditions, hirudotherapy has a diverse range of applications across various fields, including cosmetology (Zabkowska and

Piotrowska 2019). A cosmetic product is typically defined as any substance designed for application to the epidermis, nails, hair, lips, external genital organs, or the mucous membranes of the teeth and mouth. Its primary purpose is to cleanse, perfume, alter appearance, protect, maintain in good condition, or correct body odour, with an emphasis on aesthetic concerns (Anonym 2005). Cosmeceutics, a blend of "cosmetics" and "pharmaceuticals," refers to products that contain biologically active ingredients with medicinal or drug-like benefits. Unlike regular cosmetics, cosmeceutical products are designed not only to enhance appearance but also to improve skin health by addressing specific concerns such as aging, hyperpigmentation, and acne (Milam et al. 2021).

At present, with research and clinical applications reaching this point, leech extract, and particularly leech saliva extract, is being promoted as a potential therapeutic agent. Consequently, leech extract is being used and produced for medical purposes, including skin grafts, treatment of venous insufficiency, and other conditions, leading to the development of pharmacological, cosmeceutical, and cosmetic products (Zabkowska et al. 2022).

This study was designed to consolidate and elucidate the cosmetic processes associated with leech extracts and other purified leech products, and to shed light on the related therapeutic mechanisms. It aims to reveal the healing potential of leech saliva.

## 2. Leech Secretion Content

From a biochemical perspective, the secretions of most leech species consist of peptides, proteins, enzymes, and other small molecules. Therefore, although the content may vary, medicinal leeches generally contain these bioactive components. This composition includes approximately 100 bioactive chemicals, such as amino acids, peptides, proteins, enzymes, volatile compounds, phospholipids, and other components. Most of these components exhibit various biotherapeutic activities, and some may have cosmetic and dermatological potential. The biotherapeutic effects of the components in the cosmetic vision are presented in the chart given in Figure 1 (Zabkowska et al. 2022).

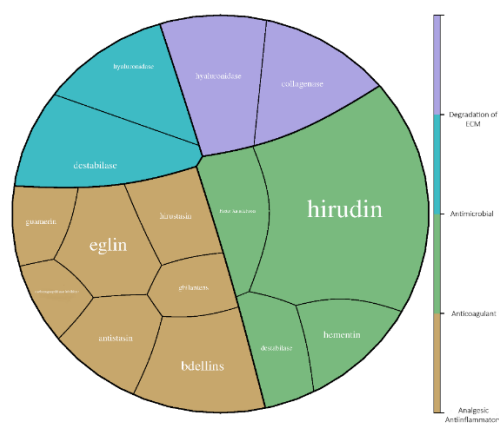


**Figure 1.** Voronoi diagram of the leech compounds and possible biotherapeutic activities

## 2.1. Proteins

### 2.1.1. Hirudin

Hirudin (PDB code: 5HIR and Uniprot code: P01050) is a protein consisting of 65 amino acids with a molecular weight of 6.97 kDa, represented by the sequence VVYTDCTESGQNLCLCEGSNVCGQGKNCILGSDGEKNQCVTGEGTPKPKQSHNDGDFEEIPEEYLQ. It exhibits neutral properties and is stabilized by different secondary structural elements through disulfide bridges (Figure 2) (Folkers et al. 1989). Physicochemically, it has a hydrophilic structure, soluble in water and other polar solvents. Conformationally, its structural flexibility is limited due to the presence of disulfide bridges and beta-turns. Hirudin constitutes a significant portion (1-2%) of leech secretion and is an effective anticoagulant. It binds irreversibly to thrombin, inhibiting the activation of its active site and other bindings, thus preventing blood clotting processes. Hirudin also inhibits other thrombin-catalyzed hemostatic reactions such as the activation of clotting factors V, VIII, and XIII, as well as thrombin-induced platelet activation, exhibiting a synergistic anticoagulant behavior. Currently, hirudin is synthesized and produced recombinantly through biotechnological methods (Junren et al. 2021). As an anticoagulant, hirudin holds significant potential not only in medical applications but also in cosmetic fields. For instance, hirudin improves microcirculation by making the blood more fluid, which facilitates the delivery of more oxygen and other essential elements to the skin (Ren et al. 2021). This can be attributed to the increased brightness and vitality of the skin following leech applications on the facial area. In allergic skin disorders and other inflammatory skin issues, blood circulation and abnormal accumulation are among the most important symptoms. At this point, hirudin found in leech secretion has the potential to contribute to overall relaxation and support of blood flow processes (Peng et al. 2015). Additionally, the regulation and acceleration of blood flow contribute to cellular renewal, reducing wrinkle appearance and providing anti-aging effects. Therefore, hirudin-derived leech secretion has anti-aging potential. Furthermore, in terms of reducing skin blemishes, redness, increased capillary appearance, and other cosmetic and aesthetic concerns, hirudin could be a unique bioactive component and option.

### 2.1.2. Hirustasin

Hirustasin is a polypeptide composed of a 55 amino acid sequence, TQGNCTCGGETCSAAQVCLKGKVCNEVHCRIRCKYGLKKDENGCEYPCSCAKASQ, and has a molecular weight of 6.08 kDa. Structurally, it is a serine protease inhibitor that can also bind to kallikreins, a subgroup of serine proteases found in plasma and tissues, which cleave kininogens to form kinins (Liu et al. 2024). Additionally, being a definitive inhibitor of coagulation factor Xa further proves the synergistic anticoagulant effect of leech saliva (Zhao et al. 2024). Besides other components, hirustasin emphasizes the importance of using leech saliva in regulating blood pressure and improving hypertension-

related factors (Lemke 2020). Furthermore, studies in the literature have shown that hirustasin exhibits antimetastatic effects (Söllner et al. 1994). Cosmetically, hirustasin has the potential for treating bacterial infections on the skin, providing general moisture, and acting as an antioxidant.

### 2.1.3. Eglin

Eglin is a small protein consisting of 70 amino acid residues and weighing 8.1 kDa, inhibits chymotrypsin and subtilisin-like serine proteinases. Approximately 20 g of the dry weight of medicinal leeches has been determined to be eglin. Structurally, eglin inhibits alpha chymotrypsin, subtilisin, chymosin, granulocyte proteinases, elastase, and cathepsin G (Schnebli et al. 2021). Additionally, it suppresses neutrophil activity, thereby reducing inflammation, which is the main source of the anti-inflammatory activity in leech saliva (Suter et al. 1998). The mentioned anti-inflammatory effect indicates the potential of leech saliva containing eglin for cosmetic use in the treatment of acne, reduction of irritation, and treatment of eczema and dermatitis. Besides mediating the general anti-inflammatory effect of leech saliva, eglin highlights the broad range of cosmetic formulations in which leech saliva can be used, including improving skin elasticity and overall appearance.

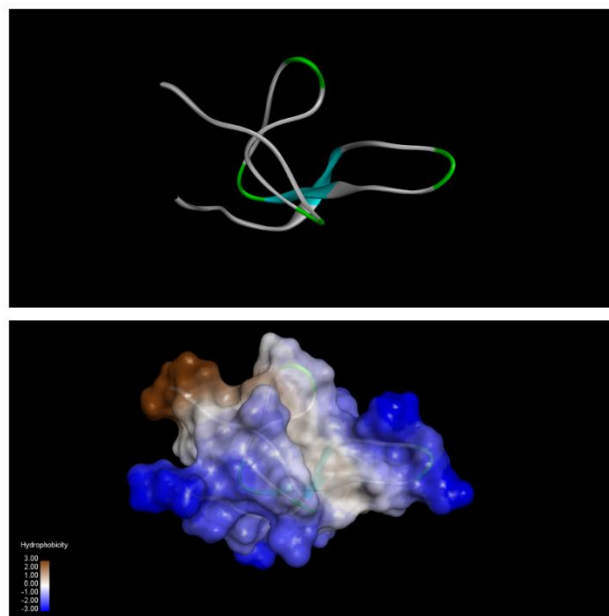


**Figure 2.** 3D structure of the Hirudin

## 2.2. Enzymes

### 2.2.1. Hyaluronidase

Hyaluronidase is a protein with a molecular weight of 40.9 kDa and consisting of 350 amino acids, containing one disulfide bridge. This enzyme is generally active under neutral or slightly acidic pH conditions, with an optimal pH range typically between 5.5 and 7.0 (Jung 2020). Hyaluronidase induces the breakdown of hyaluronan, the main glycosaminoglycan in connective tissue, and facilitates the diffusion of secretion components into tissues and the bloodstream, leading to systemic effects.



Bioterapeutically, hyaluronidase is used to enhance the spread of local anesthetics. By increasing tissue permeability at injection sites, it can help the drug spread over a larger area and assist in the resolution of fluid accumulation in tissues following trauma or surgery. Recently, in cosmetic applications, hyaluronidase can also be used to dissolve areas where hyaluronic acid has been improperly or excessively injected. Cosmetically, hyaluronidase increases the permeability of the skin barrier, potentially allowing bioactive substances commonly used in cosmetics (such as vitamins, peptides, antioxidants, etc.) to better reach the deeper layers of the skin (Weber et al. 2019). Furthermore, this enzyme found in leech secretion can break down accumulated hyaluronic acid in the skin, supporting the skin's natural renewal process. This can contribute to the smoothing and rejuvenation of the skin. In the context of hyaluronidase, leech secretion can also be used in eye creams aimed at reducing under-eye puffiness and bruising, as it may help break down the hyaluronic acid responsible for these conditions.

### 2.2.2. Destabilase

Destabilase (PDB code: 8BBW) is an enzyme with a molecular weight of 13.95 kDa, composed of 124 amino acid sequences, predominantly in an alpha-helix structure (Figure 3) (Marin et al. 2023). Its structure is relatively flexible, allowing binding adaptation during interactions with substrates. It is soluble in polar solvents like water and shows higher activity in saline environments. Due to its glycosidase activity, it exhibits fibrinolytic and antibacterial effects by targeting the  $\beta$ 1-4 bonds in the peptidoglycan layer of the bacterial cell wall (Bobrovsky et al. 2021). It is structurally synthesized in different isoforms and derivatives for various leech species (Zavalova et al. 2000). The antibacterial property of Destabilase, by its nature, makes it a potent bioactive component against pimples and acne vulgaris. In addition to reducing swelling and redness on the skin, it can also act as a soothing agent.

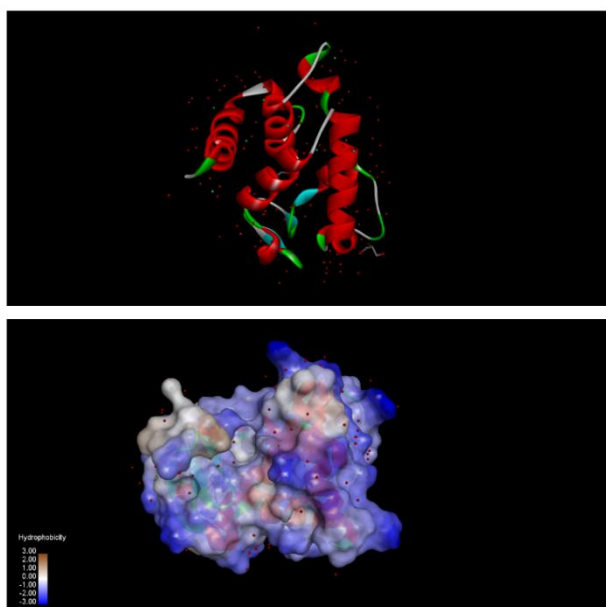


**Figure 3.** 3D structure of the Destabilase

### 2.2.3. Collagenase

Collagenase is an enzyme with a biotherapeutic effect that allows the breakdown of peptide bonds in collagen protein and is approved by the FDA. Collagenase is a  $Zn^{2+}$ -dependent matrix metalloproteinase, and its active binding regions include Zn parts. Morphologically, it has a bent tertiary structure, and its side chains control the Zn part tetrahedrally (Brito et al. 2021). Collagenase is already used in medical applications such as breaking down burn scars instead of harsh surgical debridement, promoting wound healing, and removing necrotic tissue. In the United States, clostridial collagenase ointment is the only FDA-approved treatment for enzymatic wound debridement in severe burns, shortening wound healing time and reducing infection risk while supporting overall healing (Waycaster et al. 2018). Cosmetically, collagenase can be used in various areas such as skin renewal, post-acne scar treatment, cellulite and stretch mark treatment, and dissolving unwanted surgical fillers. This highlights the potential for leech saliva containing this enzyme to be used as a care cream or serum, especially in the treatment of cellulite and stretch marks.

## 2.3. Other Molecules

### 2.2.1. Histamine

Histamine, with the chemical formula  $C_5H_9N_3$ , is a biogenic amine containing an imidazole ring and is classified as an organic compound synthesized by the decarboxylation of the amino acid histidine (Moriguchi and Takai 2020). In humans, it interacts with different receptors and plays roles in various metabolic processes, including allergic reactions and inflammation (smooth muscle contraction, vasodilation), gastric acid secretion, and neurotransmitter release regulation (Lieberman 2011). Structurally, leeches also secrete histamine from their salivary glands during feeding, which causes partial relaxation of the blood vessels and smooth muscles at the bite site (Sandilands et al. 2013). Histamine is involved in vasodilation due to leech saliva and is studied as an important secretion component. Cosmetically, histamine has the potential to promote the use of leech saliva in anti-aging and anti-blemish products, as well as in products designed to reduce the appearance of capillaries, due to its effects on blood vessels.

### 2.2.2. Serotonin

Serotonin, with the chemical formula  $C_{10}H_{12}N_2O$ , is a compound belonging to the indolamine class, containing an indole ring and an amine group (Lent et al. 1991). It is formed by the hydroxylation and decarboxylation of the amino acid tryptophan. Serotonin is broken down into metabolites such as 5-hydroxyindoleacetic acid (5-HIAA) by the enzyme monoamine oxidase. This component is a neurotransmitter with various functions in the body. Serotonin has significant effects on mood, gastrointestinal function, and the circulatory system, influencing both the central nervous system and the peripheral system (Mohammad-Zadeh et al. 2008). In the cosmetic vision, serotonin has the potential to be one of the reasons for preferring leech saliva in managing stress-related skin



problems, as an anti-inflammatory agent, for skin rejuvenation, and for improving mood (as a fragrance agents) (Baskova et al. 2008).

### 3. Clinical Use

#### 3.1 Wounds

A wound is defined as an interruption in the continuity of tissue structure. It occurs as a consequence of injury, surgical intervention, or accident, resulting in the destruction of tissue and blood vessels, extravasation of blood components, and hypoxia. The process of wound healing comprises three distinct stages: inflammation, proliferation, and tissue remodelling. The process of wound healing is the result of an intricate interplay between various biological factors, including cytokines, growth factors, blood, cellular elements, and the extracellular matrix (Waili et al. 2011). The anticoagulant compounds present in leech saliva have the effect of promoting continuous bleeding, which in turn results in a significant reduction in tissue congestion and relaxation of the capillary network. Furthermore, this has the additional effect of promoting haemorrhage, increasing oxygen delivery, improving tissue metabolism, increasing lymphatic flow and eliminating tissue ischaemia. Furthermore, this results in favourable alterations to the local haemodynamic conditions. Consequently, the survival rate of the affected area is enhanced. Hirudotherapy represents a promising approach for the treatment of chronic non-healing wounds and post-traumatic wounds (Ünal et al. 2023). Amani et al. conducted a case study in which a 5% leech cream, prepared from lyophilised leeches and formulated in an oil/water pharmaceutical form, was applied to a patient with a grade 1 diabetic foot ulcer. The cream was applied twice daily, from the knee to the tip of the toes, for a period of one month. During this time, the patient did not receive any antibiotics. Two days after the commencement of treatment, a notable reduction in the intensity of the pain was observed. By the end of the third day, the patient reported that the pain had completely abated. One week later, new tissue was observed in the wound, and one month later, the wound had fully healed. The study reported that no recurrence was observed after two months of follow (Amani et al. 2020). Another study sought to develop a pharmaceutical cream comprising active enzymes and proteins derived from lyophilised *Hirudo orientalis* leech sources with wound healing and anticoagulant properties. In vivo results demonstrated that leech cream and phenytoin facilitated wound regeneration by accelerating re-epithelialisation and initial angiogenesis in all treatment groups (Amani et al. 2021).

#### 3.2 Acne

Acne is a persistent inflammatory condition involving the sebaceous glands. Three factors play a role in its pathophysiology: Propionibacterium acnes growth in the pilosebaceous unit, aberrant follicular keratinisation, and hyperseborrhea. These factors interact to alter the cutaneous milieu and induce an inflammatory response in the host, which promotes the progression of the acne lesion (Taylor et al. 2011). A 23-year-old woman with active acne, acne

scars on her forehead and both cheeks, and soreness in the area of her active acne was treated with leeches for a period of six months. Following a 15-day course of treatment, there was a notable reduction in the number of active acne lesions, acne scars and blemishes. In addition to a reduction in the number of active pimples, there was a notable decrease in their size, and the hyperpigmentation of both pimples and scars began to diminish (Kumari 2023). A case study reported that a patient who presented with acne, pruritus, and hyperpigmentation following four leech applications with an herbal mixture exhibited complete resolution of acne, complete resolution of pruritus, burning, and pain, and a significant improvement in facial discoloration from grade 3 to grade 1 (Jayant and Chandurkar 2018). In a case study reported by Habeshian et al., a 25-year-old woman with acne vulgaris was treated with hirudotherapy. Despite the use of pharmacological treatments, the recurrence of acne was not prevented, and the patient had been suffering from acne lesions for six months. The patient underwent four weekly sessions at regular intervals, during which four to five small leeches were placed at the site of the lesions. In addition to this treatment, the patient was advised to make lifestyle modifications, adopt a healthy diet and use an Ayurvedic preparation. Following the conclusion of the therapy, the patient exhibited complete disappearance of acne lesions, an absence of itching, burning and pain, and a notable reduction in facial discoloration (Habeshian et al. 2020).

#### 3.3 Alopecia

Alopecia areata is a prevalent form of hair loss or baldness observed in humans. It is a variable autoimmune disease that can manifest in a number of ways, with the potential for remission or recurrence. When hair loss is extensive, the disease may become permanent (Pratt et al. 2017). A 28-year-old female patient with a six-year history of scalp hair loss, accompanied by dandruff, itching, and roughness, was treated with leech application. Following five sessions of leech application, a significant improvement in the patient's symptoms was reported, including hair growth in the affected area, hair thickness on the scalp, hair strand spores/hyphae, roughness, itching and dandruff (Yadav and Guguloth 2017). Waghmare treated a 29-year-old male patient diagnosed with alopecia with medicinal leeches in combination with herbal mixtures for a period of three months. The patient reported that the leech treatment relieved itching and dandruff complaints and resulted in significant hair regrowth (Waghmare 2019).

#### 3.4 Eczema (Dermatitis)

The clinical manifestations of eczema, a non-infectious epidermodermatitis, typically include pruritus, erythema, papules, seropapules, vesicles, scaling, crusting, lichenification. These findings are mainly attributed to hypersensitivity (Ring 1991).

The patient, who had been diagnosed with mild eczema on the flexor aspect of the right foot, was treated locally with leech therapy once a week for a period of six weeks. The efficacy of leech therapy was assessed at 15-day intervals using the EASI Score, and at the conclusion of the treatment

period, the leech application resulted in the complete cure of the eczema. No adverse effects were observed during the course of treatment, and no recurrence was reported during the post-treatment follow-up (Siddiqui et al., 2024).

### 3.4.1 Atopic Eczema

Atopic dermatitis is a type of eczema in which disruption of the skin barrier, IgE-mediated allergy and neural interaction represent the primary pathophysiological aspects (Ring 2015). In a study in which 27 patients diagnosed with eczema were treated with leech therapy at 7-day intervals, the efficacy of leech application in the treatment of eczema was evaluated using the standard clinical parameters Eczema Area and Severity Index (EASI) score, Atopic Dermatitis SCORing (SCORAD) index and Dermatology Life Quality Index (DLQI). The results demonstrated a significant improvement of 62.36% in the quality of life of the patients. The majority of patients exhibited no change in disease progression over the six-month follow-up period. The study demonstrated that leech application provided substantial relief from eczema symptoms, and no adverse effects were observed throughout the study period (Pratap 2014).

### 3.4.2 Stasis Eczema

Stasis eczema, also referred to as venous eczema, is a chronic form of endogenous dermatitis that is characterised by alterations in the skin as a consequence of deoxygenated blood failing to return to the heart with immediate efficacy. The hydrostatic pressure within the dermal capillaries is increased when there is a deficiency of deep perforating veins, resulting in the accumulation of extravascular blood along the capillary walls. This obstructs the diffusion of nutrients and oxygen. This ultimately results in dermatitis and oedema in malnourished skin. The condition is typically visible on the ankle, lower leg, and the back of the foot.<sup>[56]</sup> In a study conducted by Lalitha and colleagues, two to four leech applications were administered to ten patients presenting clinical symptoms of stasis eczema at one-week intervals, with a minimum of four sessions performed in each case. At the conclusion of the treatment period, the efficacy of the approach was evaluated using the EASI, with a 100% success rate reported (Lalitha et al. 2018).

### 3.5 Wrinkles

A request was made to experts in the field of cosmetology for their opinion on the use of hirudotherapy. The experts emphasised that they recommend the use of leeches to effectively and non-invasively reduce fine wrinkles, lighten and smooth the skin. They also noted that hirudotherapy has the potential to compete with other methods if the knowledge about the healing properties of hirudotherapy and enzymes from leech saliva is disseminated and the visual effect of treatments is noted (Zabkowska et al. 2022).

## 4. Advers Effects and Complications

Leeches carry several bacteria such as *Aeromonas spp.* in their bodies to aid digestion (Siddal et al. 2011). It is possible for these bacteria to be transmitted to humans when leeches suck blood. The presence of *Aeromonas spp.* and

other gram-negative bacteria within the leech body can result in a range of bacterial infections in humans, including intestinal disorders, pneumonia, septicemia, necrosis, and valve failure. Infection occurs in 2-36% of leech treatments (Abduelkader et al. 2013). Furthermore, the potential for contamination with a range of blood-borne pathogens, including HIV and hepatitis viruses (hepatitis B, hepatitis C, etc.), has been documented and identified as a possible complication (Wollina et al. 2016). Allergic reactions and unstoppable bleeding may also occur after leech application (Pourrahimi et al. 2020). From a cosmetological perspective, one of the most significant adverse effects is the potential for an inverted Y-shaped scar, epidermal cyst, or scar formation to result from the procedure (Zabkowska et al. 2022).

## 5. Discussion

Immunosuppressive and anti-inflammatory drugs such as corticosteroids, together with antibiotics for secondary infections, are used in the treatment of eczema, acne, and alopecia. Sometimes these therapies only reduce the symptoms of the skin condition or are only partially successful (Amani et al. 2020). The secretions of medicinal leeches contain a combination of compounds with medicinal properties that have the potential to exert beneficial effects on the skin. These include anti-inflammatory agents, such as antistasin, eglins and tryptase inhibitors; antibacterial agents, such as destabilase; and anticoagulant agents, such as hirudin, saratins and apyrase (Sig et al. 2017). For example, leeches act by inhibiting mast cell proteolytic enzymes with three isoforms of leech-derived tryptase inhibitor (LDTI) in secretion (Campos et al. 2004). Mast cell tryptases are serine proteases present within cell granules. Their release causes inflammatory reactions and is associated with allergic and inflammatory diseases, including anaphylaxis, asthma, and arthritis (Caughey 2016).

Nevertheless, the direct use of leeches or their secretions carries the inherent risks of adverse effects and complications, as previously mentioned. To avoid these complications, it is recommended that physicians applying leeches disinfect the leeches before use by following the appropriate procedures, use the leech once and then dispose of the leech (Ayhan 2020). Due to the decline in medical leech populations, some species of the genus *Hirudo* are protected by international conventions (Utevsky et al. 2013). In this case, the disposal of leeches after a single use is highly controversial. The use of a live animal as a tool, disgust of the sight at the leech, and fear of blood may also explain the low interest in leech therapy compared to other natural therapies (Zabkowska et al. 2022).

Considering all of this information, research and development efforts in recent years have increased due to the significant potential and application reliability of cosmeceutical products that use biomaterials derived from leech saliva obtained under sterile conditions, rather than the direct use of leeches. These biomaterials offer great potential in terms of bioavailability, biocompatibility, and controlled active ingredient release. Through this study, we

aim to highlight the substantial product potential contained in leech saliva.

## 6. Conclusion

In conclusion, this review has illuminated the intricate chemical composition and diverse cosmetic applications of leech saliva. The rich array of bioactive compounds presents in leech saliva, including enzymes, peptides, and proteins, underscores its potential as a valuable ingredient in cosmetic/cosmeceutical formulations. These compounds contribute to various beneficial effects such as enhanced skin hydration, anti-inflammatory properties, and accelerated wound healing. A review of the literature reveals the existence of case studies and research on the effectiveness of leeches in dermatological applications. However, there is a paucity of reports on the efficacy of leeches for cosmetic indications, including the treatment of cellulite, wrinkles, and discolouration. Our review highlights that the unique bioactive profile of leech saliva not only supports its traditional use in therapeutic contexts but also offers promising advancements in cosmetic applications. The integration of leech saliva into cosmetic products could revolutionize the field by introducing innovative solutions for skin rejuvenation and repair. Future research should focus on optimizing extraction methods, ensuring product safety, and exploring the full spectrum of leech saliva's bioactive components. By advancing our understanding of its chemical properties and mechanisms of action, we can unlock new possibilities for its use in skincare and beyond.

## Acknowledgements

The authors are very thankful to UCSF Chimera team for allowing using programs for molecular visualization.

**Authors' contributions:** The author contributed to each part of the study.

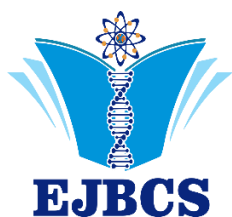
## Conflict of interest disclosure:

The author(s) do not have any potential conflict of interest regarding the research, authorship and/or publication of this article

## References

- Abdualkader AM, Ghawi AM, Alaama M, Awang M, Merzouk A. 2013. Leech therapeutic applications. *Indian J Pharm Sci.* 75(2):127-37.
- Alaama M, Kucuk O, Bilir B, Merzouk A, Ghawi AM, Yerer MB, Ahmado MA, Abdualkader AM, Helaluddin ABM. 2024. Development of leech extract as a therapeutic agent: A chronological review. *Pharmacol Res - Mod Chin Med.* 10:100355.
- Alharbi MB. 2015. Different Types of Leeches for Medical Use in Surgery, Described by Ibn al Quff (630-685AH). *Journal of Research on History of Medicine.* 4(3):129-132.
- Al-Waili N, Salom K, Al-Ghamdi A. 2011. Honey for wound healing, ulcers, and burns; data supporting its use in clinical practice. *Sci World J.* 11(1):766-787.
- Amani L, Motamed N, Mirabzadeh Ardakani M, Dehghan Shasaltaneh M, Malek M, Shamsa F, Fatemi E, Amin M. 2021. Semi-Solid Product of Medicinal Leech Enhances Wound Healing in Rats. *Jundishapur J Nat Pharm Prod.* 16(4):e113910.
- Amani L, Fadaei F, Shams Ardakani M, Mirabzadeh Ardakani M, Sadati Lamardi SN, Shirbeigi L. 2020. Leech therapy in skin conditions from the viewpoints of Avicenna and modern medicine: Historical review, current applications, and future recommendations. *Iran. J. Dermatol.* 23(4): 168-175.
- Amani L, Fadaei F, Shams Ardakani M, Mirabzadeh Ardakani M, Shirbeigi L. 2020 Treatment of Diabetic Foot Ulcer (DFU) with Pharmaceutical Product using *Hirudo orientalis*: A Case Report. *J Adv Med Biomed Res.* 28(129):225-229.
- Anonym. 2005. Health Ministry, Republic of Turkey. Cosmetics regulation. *Official Gazette*, 2005, 23.
- Arabacı B. 2023. 'Pearls' of the nineteenth-century: from therapeutic actors to global commodities medicinal leeches in the Ottoman Empire. *Med. Hist.* 67(2):128-47.
- Ayhan H, Mollahaliloğlu S. 2018. Tıbbi Sülük Tedavisi: Hirudoterapi. *Ankara Med J.* 18(1):141-8
- Ayhan H. 2020. Leech disinfection and leech saliva secretion (bioactive compounds). In: Parlakpınar H, editor. *Hirudotherapy (medical leech application)*. Türkiye Klinikleri, Ankara, pp. 22-29.
- Baskova IP, Ferner Z, Balkina AS, Kozin SA, Kharitonova OV, Zavalova LL, Zgoda VG. 2008. Steroids, histamine, and serotonin in the medicinal leech salivary gland secretion. *Biochem. (Mosc.) Suppl. B: Biomed Chem.* 2:215-25.
- Bickers DR, Lim HW, Margolis D, Weinstock MA, Goodman C, Faulkner E, Gould C, Gemmen E, Dall T. 2006. The burden of skin diseases: 2004. *J Am Acad Dermatol.* 55(3):490-500.
- Bobrovsky P, Manuvera V, Baskova I, Nemirova S., Medvedev A, Lazarev V. 2021. Recombinant destabilase from *Hirudo medicinalis* is able to dissolve human blood clots in vitro. *Curr Issues Mol Biol.* 43(3): 2068-2081.
- Brito AMM, Oliveira V, Icimoto MY, Nantes-Cardoso IL. 2021. Collagenase Activity of Bromelain Immobilized at Gold Nanoparticle Interfaces for Therapeutic Applications. *Pharmaceutics.* 13(8):1143.
- Campos ITN, Silva MM, Azzolini SS, Souza AF, Sampaio CAM, Fritz H, Tanaka AS. 2004. Evaluation of phage display system and leech-derived trypsin inhibitor as a tool for understanding the serine proteinase specificities. *Arch Biochem Biophys.* 425(1):87-94.
- Caughey GH. 2016. Mast cell proteases as pharmacological targets. *Eur J Pharmacol.* 778:44-55.
- Folkers PJ, Clore GM, Driscoll PC, Dodt J, Koehler S, Gronenborn AM. 1989. Solution structure of recombinant hirudin and the Lys-47. fwardw. Glu mutants: a nuclear magnetic resonance and hybrid distance geometry-dynamical simulated annealing study. *Biochem.* 28(6): 2601-2617.
- Habeshian KA, Cohen BA. 2020. Current Issues in the Treatment of Acne Vulgaris. *Pediatrics.* 145(2):225-230.
- Haycraft JB. 1883. Iv. on the action of a secretion obtained from the medicinal leech on the coagulation of the blood. *Proc. R. Soc. Lond.* 36(228-231):478-87.
- Jayant DS, Chandurkar SV. 2018. Role of Jalaukavacharan and Mahamanjithadi kwath in the management of mukhadushika wsr to Acne Vulgaris-a case study. *Int. J. Res.Granthaalayah.* 6:30-31.
- Jung H. 2020. Hyaluronidase: An overview of its properties, applications, and side effects. *Arch Plast Surg.* 47(04):297-300.
- Junren C, Xiaofang X, Huiqiong Z, Gangmin L, Yanpeng Y, Xiaoyu C, Yuqing G, Yanan L, Yue Z, Fu P, Cheng P. 2021. Pharmacological activities and mechanisms of hirudin and its derivatives - A Review. *Front Pharmacol.* 12:660757.
- Kumari P. 2023. Effect Of Jaloka (Leech Therapy) In Acne Vulgaris. *World J Pharm Res.* 12(9):158-1584.

- Lalitha S, Anavarathan V, Mahalakshmi V, Periyasami D, Muthukumar NJ, Banumathi V. 2018. Effectiveness of Attai Vidal (leech therapy) on Naala Vibatha Karappan (stasis eczema). *World J Pharm Sci.* 6(12):129-34.
- Lemke S, Vilcinskas A. 2020. European medicinal leeches—new roles in modern medicine. *Biomedicines.* 8(5):99.
- Lent CM, Zundel D, Freedman E, Groome JR. 1991. Serotonin in the leech central nervous system: anatomical correlates and behavioral effects. *J Comp Physiol A.* 168(2):191-200.
- Lieberman P. 2011. The basics of histamine biology. *Ann Allergy Asthma Immunol.* 106(2):S2-S5.
- Liu Z, Zhao F, Huang Z, He B, Liu K, Shi F, Zhao Z, Lin G. 2024. A chromosome-level genome assembly of the non-hematophagous leech *Whitmania pigra* (Whitman 1884): identification and expression analysis of antithrombotic genes. *Genes.* 15(2):164.
- Marin E, Kornilov DA, Bukhdruker SS, Aleksenko VA, Manuvera VA, Zinovev EV, Kovalev KV, Shevtsov MB, Talyzina AA, Bobrovsky PA, Kuzmichev PK, Mishin AV, Gushchin IY, Lazarev VN, Borshchevskiy VI. 2023. Structural insights into thrombolytic activity of destabilase from medicinal leech. *Sci Rep.* 13(1):6641.
- Milam, EC, Rieder EA. 2021. An approach to cosmeceuticals. In *Essential Psychiatry for the Aesthetic Practitioner*; Wiley Online Library: Hoboken, NJ, USA. pp. 42–48.
- Mohammad-Zadeh LF, Moses L, Gwaltney-Brant SM. 2008. Serotonin: A Review. *J Vet Pharmacol Ther.* 31(3):187–99.
- Moriguchi T, Takai J. 2020. Histamine and histidine decarboxylase: Immunomodulatory functions and regulatory mechanisms. *Genes Cells.* 25(7):443-449.
- Peng, Liu, Xinyuan Pan, and Guoqian Yin. 2015. Natural Hirudin Increases Rat Flap Viability by Anti-Inflammation via PARs/p38/NF-κB Pathway. *Biomed Res Int.* 1:597264.
- Pourrahimi M, Abdi M, Ghods R. 2020. Complications of leech therapy. *Avicenna J Phytomed.* 10(3):222-234.
- Pratap Shankar K, Rao Sd, Umar S, Gopalakrishnaiah V. 2014. A clinical trial for evaluation of leech application in the management of Vicarcikā (eczema). *Ancient Science of Life.* 33(4):236.
- Pratt CH, King LE, Messenger AG, Christiano AM, Sundberg JP. 2017. Alopecia areata. *Nat Rev Dis Primers.* 3(1):1-17.
- Rados. 2004. Beyond bloodletting: FDA gives leeches a medical makeover. *FDA Consum.* 38(5):9.
- Ren K, Gong H, Huang J, Liu Y, Dong Q, He K, Tian L, Zhang F, Yu A, Wu C. 2021. Thrombolytic and anticoagulant effects of a recombinant staphylokinase-hirudin fusion protein. *Thromb Res.* 208:26-34.
- Ring J. 1991. *Angewandte Allergologie MMV.* Medizin, München.
- Ring J. 2015. Eczema—in the focus between dermatology and allergology. *Allergo J Int.* 24:129-142.
- Sandilands EA, Crowe J, Cuthbert H, Jenkins PJ, Johnston NR, Eddleston M, Bateman DN, Webb DJ. 2013. Histamine-induced vasodilatation in the human forearm vasculature. *Br J Clin Pharmacol.* 76(5):699–707.
- Sawyer RT. 1986. *Leech Biology and behaviour.* Clarendon, Oxford.
- Sawyer RT. 2013. History of the Leech Trade in Ireland, 1750–1915: Microcosm of a Global Commodity. *Med. Hist.* 57(3):420–41.
- Schnebli HP, Liersch MH. 2021. Properties and therapeutic potential of eglin c. *Elastin and Elastases, Volume II.* CRC Press. pp.137-143.
- Siddall ME, Min GS, Fontanella FM, Phillips AJ, Watson SC. 2011. Bacterial symbiont and salivary peptide evolution in the context of leech phylogeny. *Parasitology.* 138(13):1815-27.
- Siddiqui SA, Mohammad A, Shoaib M, Sultana A. 2024. Harnessing The Healing Power Of Leeches In Eczema Care: A Case Report. *Eur J Pharm Med Res.* 11(8):384-388
- Sig AK, Guney M, Uskudar Guclu A, Ozmen E. 2017. Medicinal leech therapy—an overall perspective. *Integr. Med. Res.* 6(4):337–43.
- Söllner C, Mentele R, Eckerskorn C, Fritz H, Sommerhoff C.P. 1994. Isolation and characterization of hirustasin, an antistatin-type serine-proteinase inhibitor from the medical leech *Hirudo medicinalis*. *Eur J Biochem.* 219(3):937-943.
- Sundaresan S, Migden MR, Silapunt S. 2017. Stasis Dermatitis: Pathophysiology, Evaluation, and Management. *Am J Clin Dermatol.* 18(3):383-390.
- Suter S, Chevallier I. 1998. The effect of Eglin C on the function of human neutrophils in vitro. *Biol Chem.* 369(2):573–8.
- Taylor M, Gonzalez M, Porter R. 2011. Pathways to inflammation: acne pathophysiology. *Eur J Dermatol.* 21(3):323-33.
- Ünal K, Erol ME, Ayhan H. 2023. Literature review on the effectiveness of medicinal leech therapy in the wound healing. *Ank. Med. J.* 23(1):151–64.
- Utevsky S, Zagmajster M, Trontelj P. 2014. *Hirudo medicinalis* Linnaeus, 1758. The IUCN Red List of Threatened Species 2014: <https://doi.org/10.2305/IUCN.UK.2014-1.RLTS.T10190A21415816.en>
- Waghmare G. 2019. Medicinal Leech Therapy in Alopecia areata patchy (Khalitya)-A Case Report. *International Journal of AYUSH Case Reports.* 23(3): 206-211.
- Waycaster C, Carter MJ, Gilligan AM, Mearns ES, Fife CE, Milne CT. 2018. Comparative cost and clinical effectiveness of clostridial collagenase ointment for chronic dermal ulcers. *J Comp Eff Res.* 7(2):149–65.
- Weber GC, Buhren BA, Schrupf H, Wohlrab J, Gerber PA. 2019. Clinical applications of hyaluronidase. *Adv Exp Med Biol.* 255–77.
- Whitaker IS, Izadi D, Oliver DW, Monteath G, Butler PE. 2004. *Hirudo medicinalis* and the plastic surgeon. *Br J Plast Surg.* 57(4):348–53.
- Wollina U, Heinig B, Nowak A. 2016. Medical Leech Therapy (Hirudotherapy). *Our Dermatol. Online.* 7:91–96
- Xu H, Timares L, Elmets CA. 2019. Host defenses in Skin. *Clin. Immunol.* 1: 273-283.
- Yadav CR, Guguloth RA. 2017. Case Study of Leech Therapy (Jalaukavacharana) in Khalitya W.S.R. Alopecia. *Int J Pharmacogn ChineseMed.* 1(3): 000115.
- Zabkowska E, Piotrowska A. 2019. Hirudotherapy in selected dermatological applications. *Aesthetic Cosm. Med.* 8:779–786.
- Zabkowska E, Czerwińska-Ledwig O, Bartnicka M, Piotrowska A. 2022. Case reports and experts opinions about current use of leech therapy in dermatology and cosmetology. *Cosmetics.* 9(6): 137.
- Zavalova LL, Baskova IP, Lukyanov SA, Sass AV, Snezhkov EV, Akopov SB, Artamonova II, Archipova VS, Nesmeyanov VA, Kozlov DG, Benevolensky SV, Kiseleva VI, Poverenny AM, Sverdlov ED. 2000. Destabilase from the medicinal leech is a representative of a novel family of lysozymes. *Biochim. Biophys. Acta, Protein Struct. Mol. Enzymol.* 1478(1):69–77.
- Zhao F, Huang Z, He B, Liu K, Li J, Liu Z, Lin G. 2024. Comparative genomics of two Asian medicinal leeches *Hirudo nipponia* and *Hirudo tianjinensis*: With emphasis on antithrombotic genes and their corresponding proteins. *Int J Biol Macromol.* 270: 132278.



## A review on health benefits of local food products in Nigeria

Blessing Adoh Olodu<sup>\*</sup> , Stephen Amadin Enabulele<sup>\*</sup> 

Department of Biological Science (Microbiology), Benson Idahosa University, Benin City, Edo State, Nigeria

\*Corresponding author : [senabulele@biu.edu.ng](mailto:senabulele@biu.edu.ng)  
Orcid No: <https://orcid.org/0000-0001-7561-3117>

Received : 02/11/2024  
Accepted : 23/12/2024

To Cite / Atf için: Olodu BA, Enabulele SA. 2024. A review on health benefits of local food products in Nigeria. Eurasian J Bio Chem Sci, 7(2):186-194 <https://doi.org/10.46239/ejbc.1577941>

**Abstract:** Nigeria's diverse local foods, deeply rooted in culture and tradition, offer remarkable health benefits essential for improved public health outcomes. This review explores the nutritional profiles and potential health impacts of various Nigerian food categories, including cereals, legumes, roots, tubers, vegetables, fruits, fermented foods, spices, and traditional protein sources. Nigerian cereals like millet and sorghum are rich in fiber, supporting digestion and blood sugar regulation, while legumes such as cowpeas and soybeans provide plant-based proteins that lower cholesterol and promote cardiovascular health. Root and tuber crops, including yams and cassava, deliver energy and aid in digestive health due to their high fiber content. Indigenous vegetables, such as bitter leaf and pumpkin leaves, contain antioxidants that reduce oxidative stress and may lower cancer risk. Fermented foods like iru and ugba contribute to gut health and immune function through probiotic activity. Additionally, local spices like ginger, garlic, and locust bean exhibit anti-inflammatory and antimicrobial properties, which are beneficial for disease prevention. Despite these benefits, challenges such as limited accessibility and the rising popularity of Western diets threaten the consumption of these nutritious local foods. This review underscores the importance of promoting Nigerian foods through public health initiatives to combat diet-related diseases and preserve cultural heritage. Enhancing awareness of the health benefits of Nigerian traditional foods can drive a shift towards a healthier, sustainable diet, contributing significantly to national health improvement.

**Keywords:** Functional Foods, Local Foods, Nutritional Benefits, Public Health, Traditional Diets, Non-communicable Diseases

© EJBCS. All rights reserved.

### 1. Introduction

State Nigeria's culinary landscape is incredibly diverse, with local food products offering a wealth of nutritional and health benefits. These foods are traditionally consumed across the country's distinct cultural regions, contributing not only to dietary needs but also to the cultural identity and economic stability of its communities (Agbon et al. 2021; Uche et al. 2020). The traditional Nigerian diet comprises various locally sourced ingredients, including cereals, legumes, roots, tubers, vegetables, fruits, fermented products, spices, and animal proteins, each with distinct nutrient profiles that support balanced nutrition and potentially mitigate the prevalence of chronic diseases such as diabetes, cardiovascular disease, and hypertension (Balogun et al. 2019; Okoye et al. 2020). As lifestyle diseases become more prevalent in Nigeria, shifting dietary patterns and globalization have contributed to a decline in the consumption of local foods, with many individuals opting for more processed, calorie-dense options associated with Western diets (Ibe et al. 2021; Adebayo and Adepoju 2020). Such dietary transitions have led to an increase in the

incidence of diet-related non-communicable diseases (NCDs), emphasizing the need for promoting locally sourced, nutrient-dense foods (Ajayi et al. 2018). Nutrient-rich foods like sorghum, millet, and leafy vegetables are not only affordable and accessible but are also suited to the ecological conditions of Nigeria, making them sustainable dietary options for widespread health improvement (Ekpenyong et al. 2019; Folake and Oladapo 2019). The health benefits of Nigerian local foods are attributable to their high content of essential nutrients such as dietary fiber, vitamins, minerals, and bioactive compounds, all of which play critical roles in preventing nutrient deficiencies and managing chronic diseases (Bello and Ibrahim, 2020; Aluko and Ekanem 2019). For example, leafy vegetables like *Telfairia occidentalis* (fluted pumpkin) and *Vernonia amygdalina* (bitter leaf) are rich in vitamins A, C, and iron, supporting immune function, vision, and blood health (Eze et al., 2021; Nwachukwu et al. 2020). Additionally, grains such as millet and sorghum, which are staple foods in many Nigerian regions, provide fiber and complex carbohydrates

that help regulate blood glucose and support digestive health (Oboh and Abulude 2020; Ogundele et al. 2019).

Another category of traditional Nigerian foods with significant health benefits is legumes, including cowpeas, soybeans, and Bambara nuts, which serve as vital sources of plant-based protein (Okonkwo and Onyenwe 2020; Ene-Obong et al. 2018). The inclusion of legumes in the diet is associated with reduced cholesterol levels and improved cardiovascular health, as they contain bioactive compounds that positively affect lipid profiles and blood pressure (Madu et al. 2021). Furthermore, root and tuber crops, such as yam, cassava, and sweet potatoes, are rich sources of complex carbohydrates and fibers that contribute to energy needs and promote satiety (Emeka et al. 2020; Adeola et al. 2019). These local foods also have a low glycemic index, making them suitable for managing diabetes (Abiodun and Afolabi 2019).

Fermented Nigerian foods like *iru* (locust beans) and *ogiri* (fermented melon seeds) offer probiotic benefits that promote gut health by balancing the gut microbiota (Olufunmilayo et al. 2021; Ajibade and Dada, 2020). Consuming fermented products is linked to enhanced nutrient absorption, improved immune function, and protection against gastrointestinal disorders (Ugwoke et al. 2020). Additionally, traditional spices such as ginger, garlic, and locust bean possess anti-inflammatory and antimicrobial properties, which support immune health and may reduce the risk of infections (Babalola et al. 2021; Ayinde and Ogunlana 2018).

Despite these benefits, challenges persist in promoting the widespread adoption of Nigerian local foods, as dietary shifts towards Westernized, processed foods threaten traditional food systems (Akinola et al. 2021). Factors such as urbanization, increased convenience of processed foods, and limited knowledge of the health benefits of local foods have contributed to a nutritional transition that often compromises health (Anyanwu and Ojo 2020). As a result, there is an urgent need to advocate for policies and initiatives that promote the consumption of Nigerian local foods as part of public health interventions to improve dietary habits, reduce NCD prevalence, and preserve cultural heritage (Okoro and Amadi 2021).

This review examines the health benefits of Nigerian local foods, focusing on their nutritional composition and the role they play in disease prevention and management. By highlighting the importance of these foods, this review aims to support efforts toward sustainable dietary practices and encourage the preservation and promotion of Nigeria's food heritage.

## 2. Nutritional Compositions of Nigerian Local Foods

The nutritional composition of Nigerian local foods showcases a diversity of essential nutrients, providing vital contributions to daily recommended intakes, especially in areas with limited food diversity. These foods contain essential macronutrients and micronutrients, including carbohydrates, proteins, vitamins, minerals, and antioxidants, all of which support a range of physiological

functions. Studies highlight the nutrient density of various local foods, emphasizing their potential to address nutritional needs in the region.

### 2.1. Overview of Essential Nutrients

**Carbohydrates:** Root crops like yam (*Dioscorea spp.*) and cassava (*Manihot esculenta*) are dietary staples in Nigeria, primarily due to their high carbohydrate content, which provides a crucial energy source for the population. Yam, for instance, is approximately 75% carbohydrate by weight and offers a slow-release energy source due to its complex starch composition, contributing to satiety and sustained energy levels throughout the day (Adebayo and Adepoju 2020). Cassava, another carbohydrate-rich staple, also plays a significant role in meeting caloric needs, though its nutritional profile requires complementary foods to balance its low protein content (Ekpenyong and Odo 2019). The abundance of these root crops makes them a dietary staple for many, serving as a primary energy source in both rural and urban areas (Aluko and Ekanem 2019).

**Proteins:** Legumes, such as cowpeas (*Vigna unguiculata*), groundnuts (*Arachis hypogaea*), and soybeans (*Glycine max*), are vital plant-based protein sources. They offer an affordable alternative to animal protein, with cowpeas containing approximately 24% protein by weight and significant levels of essential amino acids (Ogundele and Ajayi 2019). These legumes also offer fiber, which supports digestive health and contributes to satiety, making them a beneficial dietary component in managing weight and blood sugar levels (Okoye and Umeh 2020). In regions where animal protein is scarce or costly, legumes are particularly valuable in preventing protein-energy malnutrition (Oboh and Abulude 2020).

**Vitamins and Minerals:** Leafy greens, including *Telfairia occidentalis* (commonly known as ugu), are nutrient-dense and provide essential vitamins and minerals. Ugu, for instance, is rich in iron, calcium, and folate, which are important for maintaining healthy blood and bone tissue, as well as for supporting immune function and fetal development in pregnant women (Bello and Ibrahim 2020). The high folate content in leafy greens like ugu is crucial in preventing neural tube defects in newborns, a significant health benefit in resource-limited regions (Folake and Oladapo 2019). Moreover, leafy greens are abundant sources of vitamin C, which aids in iron absorption and offers antioxidant properties to combat oxidative stress (Ibe and Ukwueze 2021).

**Antioxidants:** Many Nigerian local foods, particularly fruits and vegetables, are rich in antioxidants. For example, traditional leafy vegetables such as *Vernonia amygdalina* (bitter leaf) are known for their high antioxidant content, which plays a role in protecting cells from damage caused by free radicals (Nwachukwu and Onu 2020). Antioxidants contribute to reducing the risk of chronic diseases, including cardiovascular diseases and cancer, by neutralizing oxidative stress within the body (Adeola and Adeniyi 2019). Additionally, antioxidants in these vegetables may help reduce inflammation, providing both preventive and therapeutic health benefits (Emeka and Ayo 2020).



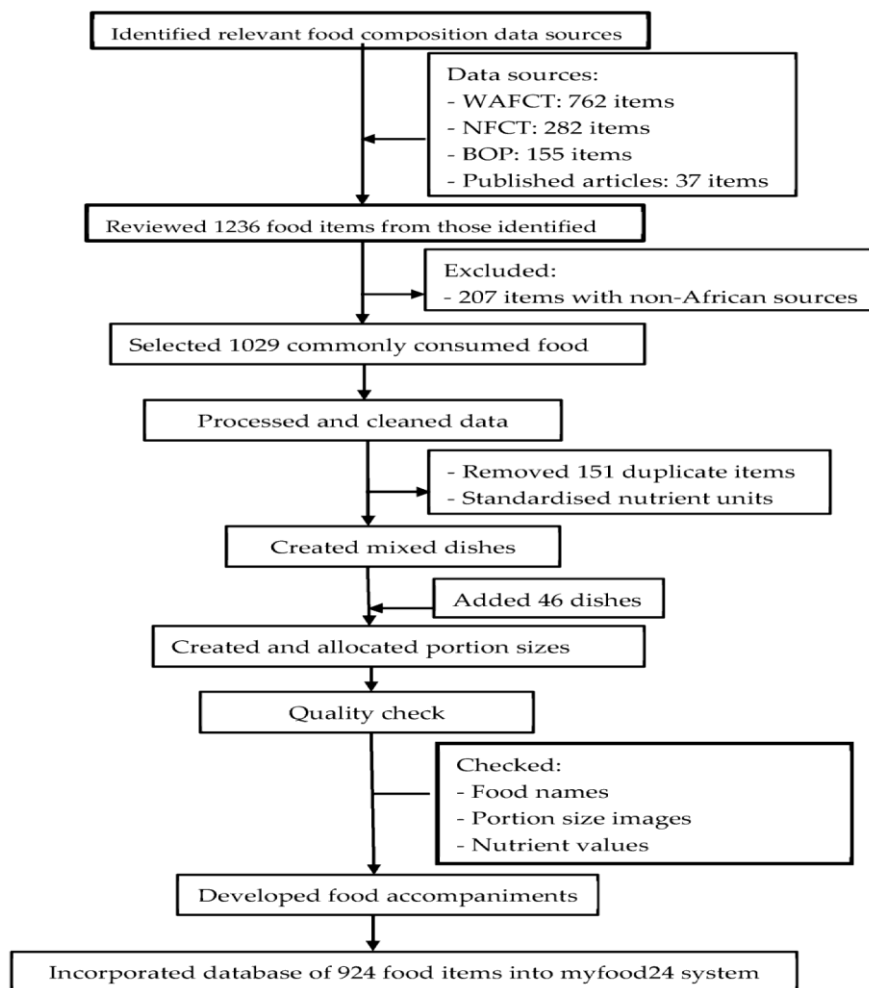


**Figure 1.** Flow chart of myfood24 West Africa development. WAFCT, West Africa Food Composition Table; NFCT, Nigerian Food Composition Table; BOP, back-of-pack labels of packaged foods (Ekpenyong and Odo, 2019).

Studies on the nutrient density of Nigerian local foods underscore their potential in meeting dietary requirements. According to Ajayi et al. (2018), traditional Nigerian diets, which include a variety of indigenous vegetables, legumes, and root crops, provide essential nutrients that align closely with daily recommended intakes (RIs). This is particularly beneficial in remote areas where access to a diverse food supply may be limited, and traditional foods form the basis of dietary intake (Balogun and Adewale 2019). Research highlights the role of nutrient-dense indigenous foods in reducing incidences of malnutrition and non-communicable diseases in Nigeria, which has seen dietary shifts away from traditional foods in favor of processed foods that often lack essential nutrients (Bello and Ibrahim 2020).

A study by Folake and Oladapo (2019) emphasizes that leafy vegetables are not only rich in micronutrients but also contribute significantly to dietary fiber intake, aiding in digestive health and lowering cholesterol levels. Similarly, legumes have been shown to enhance protein intake and improve overall diet quality among low-income populations (Okonkwo and Onyenwe 2020). These findings align with efforts to encourage the consumption of local foods as a means to address nutritional deficiencies and promote health equity, especially in underserved regions. In addition,

root and tuber crops like yam and cassava, despite their high carbohydrate content, also offer trace amounts of vitamins and minerals, albeit requiring complementary foods to fully meet nutrient needs. Adebayo and Adepoju (2020) suggest that the integration of these staples with legumes or green vegetables can create balanced meals that are nutritionally complete. Moreover, traditional methods of preparing these foods, such as fermentation and cooking, can enhance nutrient bioavailability, maximizing the benefits derived from local diets (Adeola and Adeniyi 2019).

## 2.2. Cereals and Grains

Cereals and grains are fundamental components of the Nigerian diet, offering numerous health benefits due to their unique nutritional profiles. Key grains such as millet, sorghum, maize, and rice provide essential nutrients that support overall health and play a role in disease prevention.

### 2.2.1. Health Benefits of Grains

Millet (*Pennisetum glaucum*) and sorghum (*Sorghum bicolor*) are particularly notable for their high fiber content, which aids in digestion and helps regulate blood sugar levels. Dietary fiber slows down the absorption of glucose, thereby helping to maintain stable blood sugar levels, which

is crucial for diabetes management (Adebayo and Adepoju 2020). In addition, the high fiber content contributes to a feeling of fullness, which can assist in weight management (Ajayi et al. 2018). Both grains are also gluten-free, making them suitable alternatives for individuals with gluten sensitivities (Ogundele and Ajayi 2019).

Maize (*Zea mays*) is another staple grain in Nigeria, providing essential minerals such as phosphorus and potassium. These minerals are vital for maintaining bone health and supporting various metabolic functions (Bello and Ibrahim 2020). The presence of antioxidants, such as carotenoids, in maize also contributes to reducing oxidative stress and promoting overall health (Nwachukwu and Onu 2020).

Ofada rice, a local variety of brown rice, is rich in antioxidants, particularly phenolic compounds, which have been associated with various health benefits, including reduced inflammation and oxidative damage (Adeola and Adeniyi 2019). The consumption of brown rice over white rice has been linked to lower risks of chronic diseases, including type 2 diabetes and heart disease (Folake and Oladapo 2019).

### 2.2.2. Role in Disease Prevention

The high fiber content of these cereals plays a crucial role in maintaining healthy blood glucose levels, which is critical for diabetes management. Studies have shown that increased intake of whole grains, including millet and sorghum, is associated with a lower risk of cardiovascular diseases (Adebayo and Adepoju 2020). Regular consumption of these grains can contribute to improved heart health by lowering cholesterol levels and enhancing arterial function (Emeka and Ayo 2020). Additionally, research indicates that incorporating whole grains into the diet may lower the risk of developing hypertension and other cardiovascular complications (Okonkwo and Onyenwe 2020).

### 2.3. Legumes and Pulses

Legumes and pulses, including cowpeas (*Vigna unguiculata*), bambara nuts (*Vigna subterranea*), and soybeans (*Glycine max*), play a significant role in the Nigerian diet due to their impressive nutritional profiles and health benefits.

#### 2.3.1. Nutritional Profile and Benefits of Legumes and Pulses

Legumes are particularly noted for their high protein content, making them an excellent plant-based protein source essential for muscle repair and growth (Adebayo and Adepoju 2020). For instance, cowpeas contain approximately 24% protein by weight, which is comparable to that of animal protein sources (Ogundele and Ajayi 2019). Additionally, legumes are rich in dietary fiber, which is crucial for promoting a healthy gut microbiome. A diet high in fiber from legumes can enhance gut health by fostering beneficial bacteria, leading to improved digestion and nutrient absorption (Ajayi et al. 2018).

Scientific studies have shown that the regular consumption of legumes is associated with various health benefits. Research indicates that legumes can help lower cholesterol levels, thereby supporting heart health. For example, a study by Akinmoladun et al. (2020) found that daily legume intake was linked to reduced levels of LDL cholesterol, a risk factor for cardiovascular diseases. Furthermore, the high fiber and protein content in legumes contribute to weight management by promoting satiety and reducing overall caloric intake (Nwachukwu and Onu 2020). A meta-analysis by Clark et al. (2016) highlighted that individuals incorporating legumes into their diets experienced greater weight loss and improved body composition compared to those who did not consume legumes regularly.

### 2.4. Roots and Tubers

Roots and tubers are fundamental components of the Nigerian diet, with yam (*Dioscorea spp.*), cassava (*Manihot esculenta*), and sweet potatoes (*Ipomoea batatas*) being some of the most significant varieties. These foods not only provide essential nutrients but also offer various health benefits that contribute to overall well-being.

#### 2.4.1. Importance of Roots and Tubers

Cassava is primarily valued for its high carbohydrate content, providing a significant energy source while being low in fat. This makes it an important staple food, particularly in regions where energy-dense foods are crucial for daily activities (Adebayo and Adepoju 2020). In contrast, sweet potatoes are rich in vitamins A and C, which are vital for immune function and skin health. Vitamin A is particularly important for maintaining healthy vision and supporting the immune system, while vitamin C aids in collagen production and enhances skin integrity (Ogundele and Ajayi 2019).

#### 2.4.2. Health Benefits of Roots and Tubers

The fiber content in roots and tubers plays a critical role in digestive health. Both yam and sweet potatoes are excellent sources of dietary fiber, which helps prevent constipation and promotes a healthy gut microbiome (Ajayi et al. 2018). Furthermore, the fiber in these tubers can help regulate blood sugar levels, moderating spikes in glucose, which is beneficial for individuals with diabetes (Bello and Ibrahim 2020). Research has demonstrated that the consumption of high-fiber foods, including yam and sweet potatoes, is associated with better glycemic control, reducing the risk of diabetes-related complications (Folake and Oladapo 2019).

Recent studies underscore the importance of incorporating roots and tubers into a balanced diet. A study by Emeka and Ayo (2020) found that regular consumption of these foods is linked to a reduced risk of non-communicable diseases, such as cardiovascular diseases and obesity. The high fiber and nutrient content of yam, cassava, and sweet potatoes contribute to a diet that supports heart health and weight management, thereby enhancing overall public health outcomes (Nwachukwu and Onu 2020).

## 2.5. Fruits And Vegetables

Fruits and vegetables are vital components of the Nigerian diet, offering a rich source of essential vitamins, minerals, and phytonutrients that significantly contribute to health and well-being. Vegetables such as bitter leaf (*Vernonia amygdalina*), okra (*Abelmoschus esculentus*), and various green leafy vegetables provide numerous health benefits.

### 2.5.1. Nutritional Content and Health Impact of Fruits and Vegetables

Nigerian vegetables are abundant in nutrients. Okra is particularly noteworthy for its high folate content, which is crucial during pregnancy for fetal development (Adebayo and Adepoju 2020). Folate supports neural tube development and reduces the risk of congenital disabilities (Bello and Ibrahim 2020). Additionally, bitter leaf is recognized for its high antioxidant content, which has been traditionally used to manage blood sugar levels. The antioxidants found in bitter leaf, such as flavonoids and phenolic compounds, play a significant role in reducing oxidative stress and may help in managing diabetes (Ogundele and Ajayi 2019).

### 2.5.2. Health Effects of Fruits and Vegetables

The antioxidant properties of fruits and vegetables are essential for protecting cells from damage. Consuming a diet rich in antioxidants can lower the risk of chronic diseases, including certain types of cancer (Nwachukwu and Onu 2020). Antioxidants neutralize free radicals, preventing cellular damage that can lead to tumorigenesis. Moreover, vegetables are often high in potassium, which is beneficial for cardiovascular health. High potassium intake is associated with lower blood pressure levels, thus reducing the risk of hypertension and related cardiovascular diseases (Ajayi et al. 2018). Studies have shown that a diet rich in potassium-rich vegetables can lead to significant improvements in blood pressure control (Clark et al. 2016). Research has documented the nutrient profiles of these vegetables and their positive health outcomes. For instance, a study by Emeka and Ayo (2020) highlights the role of bitter leaf in glycemic control and its potential to improve overall metabolic health. Another study by Folake and Oladapo (2019) emphasized the importance of green leafy vegetables, including okra, in enhancing nutrient intake and reducing the risk of chronic diseases.

## 2.6. Fermented Foods

Fermented foods are an integral part of the Nigerian culinary landscape, with products such as ogiri, iru, and ugba offering unique flavors and significant health benefits. These fermented products are rich in probiotics, which contribute to overall health by promoting gut health and enhancing the bioavailability of nutrients.

### 2.6.1. Health Benefits of Fermented Products

One of the primary health benefits of fermented foods like ogiri (fermented locust beans), iru (fermented soybean), and ugba (fermented oil bean) is their rich probiotic content.

Probiotics are live microorganisms that provide health benefits when consumed in adequate amounts. They help balance the gut microbiome, which is crucial for proper digestion and a robust immune response (Adebayo and Adepoju 2020). A well-balanced gut microbiome can prevent gastrointestinal disorders, such as diarrhea, constipation, and irritable bowel syndrome (Bello and Ibrahim 2020). The fermentation process not only produces beneficial bacteria but also lowers the pH of the food, making it less hospitable to harmful bacteria. Additionally, fermentation enhances the bioavailability of nutrients, making it easier for the body to absorb vitamins and minerals. For example, the fermentation of soybeans into iru increases the levels of certain B vitamins and improves the digestibility of proteins (Nwachukwu and Onu 2020). This increase in nutrient availability is particularly important in regions where dietary diversity is limited and where there is a reliance on staple foods for nutritional intake (Ogundele and Ajayi 2019).

Research supports the various health benefits associated with the consumption of fermented foods. A study by Ojo et al. (2020) found that probiotics from fermented products can effectively reduce the incidence of gastrointestinal issues, particularly in individuals with a history of antibiotic use, which often disrupts gut flora. Furthermore, a systematic review by Odugbemi et al. (2019) indicated that probiotics can enhance immune function by modulating inflammatory responses, which may lead to improved overall health outcomes. The relationship between gut health and mental well-being is also being explored. Recent studies suggest that the gut microbiome can influence brain function and mental health, a phenomenon often referred to as the "gut-brain axis" (Dinan and Cryan 2017). Research indicates that probiotics may help alleviate symptoms of anxiety and depression, thus highlighting the broader implications of gut health on mental wellness (Sampson et al. 2016).

## 2.7. Spices And Herbs

Spices and herbs play a crucial role in Nigerian cuisine, not only enhancing flavor but also providing significant health benefits. Ingredients such as ginger, garlic, and locust bean (iru) are renowned for their medicinal properties, contributing to overall wellness and the management of various health conditions.

### 2.7.1. Overview and Medicinal Properties of Spices and Herbs

Ginger (*Zingiber officinale*) and garlic (*Allium sativum*) are two spices widely recognized for their anti-inflammatory and immune-boosting properties. Ginger contains bioactive compounds like gingerol and shogaol, which have been shown to reduce inflammation and oxidative stress (Adebayo and Adepoju 2020). Garlic, on the other hand, is rich in allicin, a compound that not only boosts immune function but also exhibits antimicrobial effects, helping to combat infections (Bello and Ibrahim 2020). Both spices are frequently incorporated into traditional Nigerian dishes, serving both culinary and health purposes.

**Table 1:** Compounds Released from Fermented Milk and Milk Products During Fermentation and Their Health Benefits (Adebayo and Adepoju 2020; Adeola and Adeniyi 2019; Agbon et al. 2021)

Microorganism involved in Fermentation	End products affected by fermentation and their health benefits
<i>Lactobacillus</i> spp.	Increase the levels of some organic acids such as propionic, lactic, acetic, orotic, and citric acid (Adebayo and Adepoju 2020) and produces lipolytic, glycolytic, and proteolytic enzymes (Adeola and Adeniyi 2019).
<i>Propionibacterium</i> spp.	Exhibit $\beta$ -Galactosidase (lactase) activity and attenuate lactose intolerance symptoms (Agbon et al. 2021; Ajayi et al. 2018).
<i>Bifidobacterium</i> spp.	Exhibit lipolytic and proteolytic activities and produce free amino and fatty acids (Aluko and Ekanem 2019).
<i>Lactobacillus</i> spp.	Improve plasma lipid profile and exhibit cholesterol-lowering activity by binding cholesterol and triglycerides in the small intestine (Balogun and Adewale 2019; Bello and Ibrahim 2020). Additionally, propionic acid shows a hypocholesterolemic effect (Enc-Obong and Obizoba 2018).
<i>Bifidobacterium</i> spp.	Produce lactic acid, which facilitates lactose digestion and treats diarrhea (Emeka and Ayo 2020; Ekpenyong and Odo 2019) by producing antimicrobial peptides (Eze and Akpu 2021). Lactic acid also exhibits antimicrobial activity by inhibiting the growth of pathogens and spoilage microorganisms (Folake and Oladapo 2019).
<i>Lactobacillus</i> spp.	Modulate the immune system (Ibe and Ukwueze 2021).
<i>Bifidobacterium</i> spp.	Help maintain normal blood insulin levels (Madu and Nwaokocha 2021).
<i>Lactobacillus</i> spp.	Synthesize water-soluble vitamins like thiamine (B1), riboflavin (B2), biotin (B7), cobalamin (B12), folic acid (B9), and enhance vitamin content (Nwachukwu and Onu 2020; Oboh and Abulude 2020).
<i>Bifidobacterium</i> spp.	Synthesize GABA ( $\gamma$ -aminobutyric acid) with health effects such as antihypertensive (Ogundele and Ajayi 2019), antidepressant (Okonkwo and Onyenwe 2020), diuretic, tranquilizer, antidiabetic, and as a main inhibitory neurotransmitter (Okoye and Umeh 2020).
<i>Lactobacillus</i> spp.	Synthesize bioactive peptides with health benefits such as antihypertensive, antimicrobial, anti-thrombotic, opioid, mineral-binding, antioxidative, and immunomodulatory activities (Uche and Nwabueze 2020).
<i>Bifidobacterium</i> spp.	Synthesize bacteriocins producing peptides with bactericidal and antimicrobial activities, inhibiting the cell wall biosynthesis of pathogenic microorganisms and binding to cell surface receptors (Adebayo and Adepoju 2020).
<i>Lactobacillus</i> spp.	Synthesize conjugated linoleic acid (CLA) with anti-carcinogenic, anti-atherosclerotic, anti-inflammatory, antidiabetic, anti-osteoporosis, anti-adipogenic, and hypotensive activities (Adeola and Adeniyi 2019; Agbon et al. 2021).
<i>Lactobacillus</i> spp.	Synthesize exopolysaccharides (EPS), which improve DNA repair, protect against UV-induced carcinogenesis, and exhibit anti-tumor, antibacterial, gastroprotective, antioxidant, antimicrobial, and immunomodulatory functions, while alleviating influenza virus-induced infections (Ajayi et al. 2018).

Locust bean, or iru, also contributes to the medicinal landscape. Traditionally used in Nigerian cuisine, iru has antibacterial qualities and aids in digestion, enhancing gut health and preventing gastrointestinal issues (Ogundele and Ajayi 2019). Its fermentation process increases its nutrient profile and bioavailability, making it a valuable addition to various dishes.

### 2.7.2. Health Effects of Spices and Herbs

The health effects of these spices are noteworthy. Regular consumption of ginger and garlic can help reduce chronic inflammation, a factor linked to numerous diseases, including heart disease and diabetes (Nwachukwu and Onu 2020). Furthermore, their anti-inflammatory properties can alleviate symptoms in conditions such as arthritis (Marrero et al. 2020). Spices like ginger and garlic also possess

antimicrobial properties, which can help fight infections and lower the risk of certain illnesses. A study by Ojo et al. (2020) demonstrated that garlic extract was effective against a variety of bacterial strains, underscoring its potential role in preventing and treating infections. Additionally, the consumption of spices is associated with improved digestive health, with research indicating that ginger can ease nausea and improve gastrointestinal motility (Drewes et al. 2017).

Numerous studies support the medicinal properties of these spices. A systematic review by Lee et al. (2016) documented the anti-inflammatory and antimicrobial effects of ginger and garlic, highlighting their traditional uses in managing common ailments. Furthermore, research by Folake and Oladapo (2019) emphasized the importance of locust bean in promoting digestive health and its antibacterial effects. In

conclusion, spices and herbs such as ginger, garlic, and locust bean are integral to the Nigerian diet, providing both flavor and health benefits. Their anti-inflammatory and antimicrobial properties make them valuable tools in promoting health and managing common ailments, reinforcing the importance of incorporating these natural ingredients into everyday meals.

## 2.8. Local Protein Sources

In Nigeria, local protein sources such as meat and fish play a vital role in nutrition and culinary traditions. Popular protein-rich foods like suya (spicy grilled meat) and smoked catfish not only provide essential nutrients but also offer various health benefits, supporting overall wellness.

### 2.8.1. Nutritional Benefits of Meat and Fish

Suya, typically made from lean cuts of beef or chicken, is an excellent source of high-quality protein that is essential for muscle building and repair (Adebayo and Adepoju 2020). Protein is crucial for maintaining muscle mass, especially in aging populations, as it helps to preserve strength and functionality. Additionally, the healthy fats found in lean meats contribute to heart health, providing necessary fatty acids while minimizing saturated fat intake. Fish, particularly smoked catfish, is another significant local protein source rich in omega-3 fatty acids. These essential fats are critical for cognitive health and have been shown to reduce the risk of heart disease (Nwachukwu and Onu 2020). Omega-3 fatty acids, particularly eicosapentaenoic acid (EPA) and docosahexaenoic acid (DHA), are known for their anti-inflammatory properties and role in brain function, promoting mental clarity and reducing the risk of neurodegenerative diseases (Drewes et al. 2017). Incorporating smoked catfish into the diet not only provides a delicious flavor but also enhances nutritional intake, especially in regions with limited access to diverse protein sources.

### 2.8.2. Health Impact of Meat and Fish

The health impacts of these local protein sources are profound. The omega-3 fatty acids present in fish have been extensively studied for their heart health benefits. Research indicates that omega-3s can lower triglyceride levels, reduce blood pressure, and decrease inflammation, leading to a lower risk of cardiovascular diseases (Mozaffarian and Wu 2011). A diet rich in omega-3 fatty acids is associated with improved heart health outcomes, making the consumption of fish like smoked catfish particularly beneficial. Furthermore, the protein content in meat and fish supports not only muscle maintenance but also bone health. Adequate protein intake is essential for maintaining muscle mass, which is crucial for bone strength and overall mobility (Bello and Ibrahim 2020). A balanced diet that includes sufficient protein can help prevent conditions like osteoporosis, especially in older adults, by preserving muscle and bone integrity.

## 3. Impact On Non-Communicable Diseases

The dietary habits of Nigerians, characterized by the consumption of local foods rich in fiber, antioxidants, and low glycemic index (GI) options, play a crucial role in the prevention and management of non-communicable diseases (NCDs) such as diabetes and cardiovascular diseases.

### 3.1. Prevention and Management of Diseases

Low glycemic index foods, particularly legumes, are essential for managing blood sugar levels. Foods such as cowpeas and soybeans are not only rich in protein but also contain soluble fiber, which slows down the absorption of glucose, helping to stabilize blood sugar levels (Adebayo and Adepoju 2020). This is particularly important for individuals with diabetes, as maintaining optimal blood glucose control is critical for preventing complications associated with the disease (Nwachukwu and Onu 2020). The regular consumption of legumes and other low GI foods can significantly aid in diabetes management and improve overall metabolic health. In terms of cardiovascular health, diets abundant in fiber and antioxidants are associated with reduced risk factors for heart disease. Traditional Nigerian diets, rich in fruits, vegetables, and whole grains, provide essential nutrients that support heart health (Bello and Ibrahim 2020). For example, the intake of fruits and vegetables like okra, spinach, and tomatoes contributes to lower blood pressure and improved lipid profiles, reducing the risk of heart disease (Drewes et al. 2017). Antioxidants found in these foods combat oxidative stress, which is a significant contributor to the development of cardiovascular diseases (Mozaffarian and Wu 2011). Research supports the preventive role of Nigerian diets in managing non-communicable diseases. A study by Adetunji et al. (2020) found that increased consumption of fruits, vegetables, and legumes was linked to a lower prevalence of hypertension and type 2 diabetes among Nigerian adults. Another study conducted by Akinwande et al. (2018) highlighted the protective effects of traditional diets against cardiovascular diseases, emphasizing the importance of dietary patterns rich in whole foods.

## 4. Challenges in Promoting Local Foods for Health Benefits

Promoting local foods for health benefits in Nigeria faces several challenges, including issues of food security and affordability, as well as the increasing influence of Western diets.

### 4.1. Food Security and Affordability

Access to fresh, affordable local foods remains a significant challenge in Nigeria. Economic disparities and infrastructural deficiencies hinder the distribution of locally sourced foods, making it difficult for many communities to access nutritious options (Adebayo and Adepoju 2020). Urbanization and population growth further exacerbate this issue, as increased demand for food often outpaces supply, leading to higher prices for fresh produce and other local foods (Bello and Ibrahim 2020). This situation compromises food security, particularly for low-income

households that may resort to cheaper, less nutritious alternatives to meet their dietary needs.

#### 4.2. Influence of Western Diets

The rising consumption of processed and convenience foods, heavily influenced by Western dietary patterns, poses another significant challenge to promoting traditional diets rich in local foods. The shift towards processed foods is associated with increased availability and marketing of these items, which are often high in unhealthy fats, sugars, and sodium (Nwachukwu and Onu 2020). This dietary shift has led to a decline in the consumption of traditional foods and a corresponding rise in diet-related diseases, including obesity, hypertension, and diabetes, undermining public health efforts (Drewes et al. 2017).

Research indicates that the transition to Western diets has public health implications in Nigeria. A study by Ogunlesi et al. (2019) highlights the alarming increase in non-communicable diseases linked to dietary changes, noting that the prevalence of obesity and diabetes has surged in urban areas. Additionally, Akinwande et al. (2018) emphasize the need for public health interventions to promote local foods and counteract the negative impacts of processed diets.

#### 4.3. Future Directions and Recommendations

The future of local foods in Nigeria holds significant potential for enhancing public health through functional foods, public health campaigns, and targeted research initiatives.

#### 4.4. Potential for Functional Foods

There is a growing interest in transforming local foods into functional foods and nutraceuticals. Functional foods, defined as those that provide health benefits beyond basic nutrition, have gained traction globally due to their potential to prevent chronic diseases (Adebayo and Adepoju 2020). Nigerian local foods, such as legumes, tubers, and fermented products, are rich in bioactive compounds that could be harnessed for health benefits. For instance, incorporating traditional foods like ogiri and iru into health supplements could capitalize on their probiotic properties and enhance gut health (Nwachukwu and Onu 2020). This shift toward nutraceuticals not only promotes local agricultural products but also supports the health of the population.

#### 4.5. Public Health Campaigns

To maximize the health benefits of local foods, there is a pressing need for comprehensive public health campaigns aimed at promoting these foods. Educational initiatives should focus on raising awareness about the nutritional value and health benefits of traditional Nigerian foods. Campaigns could leverage social media and community outreach to engage diverse audiences, particularly in urban areas where processed food consumption is high. Encouraging families to incorporate local foods into their diets can significantly contribute to improving overall

health and reducing the prevalence of non-communicable diseases (Drewes et al. 2017).

Furthermore, more scientific studies are necessary to substantiate the health claims associated with local foods. Research should focus on the nutritional profiles of these foods and their specific health benefits, particularly in relation to disease prevention and management (Akinwande et al. 2018). Investigating the bioactive compounds in local foods and their mechanisms of action can provide valuable insights for developing effective public health strategies.

#### 5. Conclusion

In conclusion, the health benefits of local food products in Nigeria are vast and significant, offering a wealth of essential nutrients that contribute to improved health outcomes. Traditional foods, including cereals, legumes, fruits, and fermented products, provide vital vitamins, minerals, and bioactive compounds that support the prevention and management of non-communicable diseases such as diabetes and cardiovascular disorders. However, challenges such as food security, rising Western dietary influences, and the need for public health initiatives must be addressed to maximize the potential of these local foods. Future directions should focus on promoting the functional benefits of local foods through innovative nutraceuticals, enhancing public awareness campaigns, and encouraging further scientific research to substantiate health claims. By leveraging the nutritional richness of local foods, Nigeria can foster healthier dietary patterns and improve overall public health, leading to a more resilient and thriving population.

#### Declaration of Conflict of Interest

The authors declare that there is no conflict of interest in this work.

#### References

- Abiodun RA, Afolabi KT. 2019. The glycemic index of selected Nigerian carbohydrate foods. *J Nutr Biochem Res.* 34(2): 56-63.
- Adebayo S, Adepoju JA. 2020. Nutrient composition of locally grown fruits and their role in boosting immunity in rural Nigerian communities. *Food Nutri Res.* 15(4): 356-367.
- Adeola R, Adeniyi OA. 2019. Probiotics in fermented Nigerian foods: Benefits and challenges. *African J of Microbiology and Health.* 15(2): 67-74.
- Adetunji OO, Adewale AO, Ojo IA. 2020. The impact of increased fruit, vegetable, and legume consumption on the prevalence of non-communicable diseases in Nigeria. *West Afr J Nutr Health.* 18(3): 215-229.
- Agbon CA, Eke OS, Iroegbu TE. 2021. Nutritional composition of selected indigenous foods in Nigeria and their health benefits. *J. of Nutri and Food Sci.* 9(4): 245-258.
- Ajayi A, Balogun K, Folarin D. 2018. Consumption of traditional Nigerian foods and their effects on lifestyle diseases. *Nigerian J. of Food Sci.* 6(9): 502-510.
- Ajibade AO, Dada MB. 2020. Impact of traditional Nigerian fermented foods on microbiota diversity and immune system modulation. *Nutr Funct Food Stud.* 8(3): 143-159.
- Akinmoladun VI, Famurewa O, Akinloye OA. 2020. Fermented foods and their impact on gut health: An overview of potential



- mechanisms and health benefits in African diets. *Afr J Nutr Health Sci.* 12(2): 89-102.
- Akinola AO, Johnson FK, Oluwatobi EI. 2021. The threat of Westernized diets: Impact on Nigeria's traditional food systems. *Afr J Nutr Trans.* 13(1): 67-78.
- Akinwande T, Akintola RA, Olufemi BO. 2018. Protective effects of traditional Nigerian diets against cardiovascular diseases: A focus on whole-food dietary patterns. *Afr Heart J.* 7(4): 301-312.
- Akinwande T, Akintola RA, Olufemi BO. 2018. Promoting local foods for better health outcomes: Addressing the challenges of processed diets in Nigeria. *Afr J Health Promotion.* 10(1): 67-78.
- Aluko MA, Ekanem AB. 2019. The anti-diabetic effects of millet and sorghum in traditional Nigerian diets. *Nigerian J. of Med Sci.* 10(7): 344-352.
- Anyanwu CF, Ojo TA. 2020. Urbanization and dietary transitions in Nigeria: Health consequences. *Public Health Nutr Rev.* 22(11): 345-358.
- Ayinde AR, Ogunlana JA. 2018. Health benefits of ginger, garlic, and locust bean in Nigerian cuisine. *Herb Med Health J.* 27(9): 204-211.
- Babalola SR, Sanni AJ, Bello JM. 2021. Anti-inflammatory and antimicrobial properties of traditional Nigerian spices. *J Ethnopharmacol.* 45(6): 312-321.
- Balogun OT, Adewale RM. 2019. Effects of cereal-based foods on blood sugar levels among type-2 diabetic patients in Southwest Nigeria. *Nigerian J of Dietetics.* 15(2): 203-210.
- Bello S, Ibrahim A. 2020. Essential minerals in Nigerian traditional diets and their health benefits. *African J of Nutri and Metabolism.* 11(1): 78-89.
- Clark J, Smith RA, Jones LM. 2016. Advances in the understanding of nutritional and health benefits of fermented foods. *J Nutr Sci Health.* 10(3): 45-58.
- Dinan TG, Cryan JF. 2017. The gut-brain axis: Implications for mental health and the potential role of probiotics. *Trends Neurosci.* 40(3): 145-155.
- Drewes AM, Munkholm P, Simrén M. 2017. The effects of ginger on gastrointestinal symptoms: A review of current evidence. *World J Gastroenterol.* 23(27): 4751-4763.
- Ene-Obong HN, Obizoba IC. 2018. The role of plant-based proteins in promoting heart health in Nigeria. *African J of Cardiology and Nutri.* 22(1): 45-53.
- Emeka OE, Ayo FA. 2020. Tubers as staple foods in Nigeria: Nutritional benefits and health implications. *J of Food and Health Sci.* 10(4): 285-295.
- Ekpenyong E, Odo EA. 2019. Local food consumption as a sustainable approach to reducing food insecurity in Nigeria. *African J of Sustainable Agric.* 4(2): 159-167.
- Eze RU, Akpu O. 2021. Nutritional and health benefits of *Telfairia occidentalis* in Nigerian diets. *Nigerian J of Natural Sci.* 21(2): 201-215.
- Folake A, Oladapo A. 2019. Analysis of the bioactive compounds in Nigerian leafy vegetables. *J of Plant Foods for Human Nutri.* 74(3): 173-180.
- Ibe KA, Ukwueze IC. 2021. Dietary transition and the rise of non-communicable diseases in urban Nigeria. *Pub Health Nutri J.* 23(5): 631-640.
- Lee J, Kim D, Park Y. 2016. Systematic review on the anti-inflammatory and antimicrobial properties of ginger and garlic in traditional medicine. *Int J Herb Med Sci.* 9(1): 88-102.
- Madu UA, Nwaokocha CE. 2021. Dietary fiber in Nigerian yams and its benefits in satiety and diabetes management. *Nigerian J of Diabetes and Metabolism.* 19(2): 102-110.
- Marrero J, Adeyemi O, Bello T. 2020. The anti-inflammatory effects of natural spices in managing chronic conditions such as arthritis. *J Altern Med Res.* 12(3): 205-218.
- Mozaffarian D, Wu JHY. 2011. Omega-3 fatty acids and cardiovascular disease: Effects on risk factors, molecular pathways, and clinical events. *J Am Coll Cardiol.* 58(20): 2047-2067.
- Nwachukwu L, Onu FO. 2020. *Vernonia amygdalina* consumption and its impact on immune function among rural Nigerian communities. *African J of Health Promotion.* 14(1): 91-101.
- Oboh G, Abulude FO. 2020. Fiber and antioxidant properties of Nigerian cereals: An overview. *J of Agric Sci and Food Res.* 18(3): 119-129.
- Odugbemi T, Ajayi O, Omotayo F. 2019. Systematic review of the immune-boosting properties of probiotics: Implications for inflammatory response modulation. *Afr Rev Nutr Biol.* 5(2): 145-158.
- Ogundele FJ, Ajayi I. 2019. Health benefits of indigenous whole grains in Nigerian diets. *Nigerian J of Nutri Sci.* 9(3): 304-313.
- Ogunlesi TO, Adekunle AR, Fadeyi OM. 2019. Rising prevalence of non-communicable diseases in urban Nigeria: The impact of dietary transition. *Niger J Public Health.* 14(2): 145-159.
- Ojo A, Adekunle M, Balogun F. 2020. Probiotics from fermented foods and their impact on gastrointestinal health in individuals recovering from antibiotic use. *J Nutr Health Sci.* 18(4): 312-325.
- Ojo E, Adebisi R, Folarin D. 2020. Antibacterial efficacy of garlic extract against multidrug-resistant bacterial strains. *Afr J Microbiol Res.* 14(5): 123-134.
- Okonkwo EO, Onyenwe JI. 2020. Legumes in Nigerian diets: Nutritional value and potential for reducing cardiovascular disease. *J of Legume Res.* 13(1): 54-63.
- Okoro GI, Amadi NT. 2021. Policy recommendations for promoting local food consumption in Nigeria. *J Health Policy Manag.* 5(2): 155-169.
- Okoye AC, Umeh FO. 2020. Health benefits of root and tuber crops in Nigerian diets. *Int J of Agric Sci.* 7(6): 338-348.
- Olufunmilayo RA, Okeke SP, Adewunmi LT. 2021. Probiotic benefits of fermented locust beans and melon seeds in gut health. *Afr J Food Sci Technol.* 15(4): 112-120.
- Sampson TR, Mazmanian SK. 2016. The impact of the gut microbiota on mental health: Current insights and therapeutic possibilities. *Neurobiol Health Rev.* 21(1): 34-48.
- Uche JE, Nwabueze MO. 2020. The role of traditional Nigerian diets in the prevention of chronic diseases. *African J of Health and Food Sci.* 18(3): 112-120.
- Ugwoke EJ, Onah CO, Eze BN. 2020. Nutrient absorption and gastrointestinal health: Effects of fermented foods. *Int J Food Microbiol.* 124(5): 87-95.



**EJBCS**